Cobalt, Zinc, and Cadmium Tropocoronand Complexes

by

Linda H. Doerrer

B.A., Cornell University (1991)

Submitted to the Department of Chemistry

in partial fulfillment of the requirements for the

degree of Doctor of Philosophy

at the

Massachusetts Institute of Technology

February, 1997

©Massachusetts Institute of Technology 1997

Signature of Author_____

Certified by___

Accepted by___

Department of Chemistry

August 19, 1996

Stephen J. Lippard

Thesis Supervisor

Dietmar Seyferth

Chairman, Departmental Committee on Graduate Studies

This doctoral thesis has been examined by a Committee of the Department of Chemistry as follows:

Professor Dietmar Seyferth, Committee Chairman
Robert T. Haslam and Bradley Dewey Professor of Chemistry

Professor Stephen J. Lippard
Arthur Amos Noyes Professor of Chemistry

Professor Gregory C. Fu
Assistant Professor of Chemistry

Cobalt, Zinc, and Cadmium Tropocoronand Complexes

by

Linda H. Doerrer

Submitted to the Department of Chemistry on August 19, 1996, in partial fulfillment of the requirements for the Degree of Doctor of Philosophy.

Abstract.

Chapter 1. Tropocoronand Complexes and Macrocyclic Tuning.
    A general introduction to transition metal macrocyclic complexes with focus on tetraazamacrocycles is given. The chemistry of transition metal tropocoronand complexes is reviewed and presented as background for the questions addressed in this thesis.

Chapter 2. Zinc and Cadmium Tropocoronand Complexes.
    The four-coordinate [Zn(TC-n,m)], n + m = 7, 8, 9, 10, 12, and [Cd(TC-n,m)], n + m = 8, 9, 10, 12, complexes and the five-coordinate complex [Zn(py)(TC-3,3)] have been synthesized and characterized by ^{1}H-NMR and UV-vis spectroscopy as well as X-ray crystallography. The dihedral angle Θ at the metal center increases linearly as a function of the number of methylene linker units, n + m. The angles range from 35.5° in [Zn(TC-3,4)] to 84.4° in [Zn(TC-6,6)] and from 36.8° in [Cd(TC-4,4)] to 80° in [Cd(TC-6,6)]. For a given value of n + m, a larger dihedral angle is observed in the [M(TC-n,m)] complex with the smaller metal ion. The compounds [Cd(TC-4,4)] and [Zn(py)(TC-3,3)] demonstrate the newly-recognized tropocoronand ligand folding mode which results when the metal ion fit into the macrocycle hole is poor.

Chapter 3. Ligand Field Tuning in Cobalt Tropocoronand Complexes.
    The ligand field of [Co(TC-n,m)] complexes, n + m = 6, 8, 9, 10, 12 has been investigated with MO calculations, low-temperature EPR spectroscopy, and cyclic voltammetry. The macrocycle exhibits significant π-donation to the metal center such that the d_{xz}, not d_{z^2}, orbital is the HOMO for Co(I), Co(II), and Co(III) oxidation states in the pseudo-square-planar complexes. The d_{xz} is the HOMO in pseudo-tetrahedral Co(III) complexes, and the d_{xy} in pseudo-tetrahedral Co(II) and Co(I) complexes. Low-spin complexes [Co(TC-3,3)] and [Co(TC-4,4)] have rhombic EPR spectra and high-spin complexes [Co(TC-5,5)] and [Co(TC-6,6)] have axial spectra. The ligand twist generates a novel rhombic EPR spectrum for high-spin [Co(TC-4,5)]. The Co(III)/(II) $E_{1/2}$ values are finely tuned to higher potentials at higher Θ values

in steps of approximately 40 mV per additional methylene unit by the ligand. The Co(II)/(I) potentials are tuned similarly tuned to lower values for the larger macrocycles by 30 mV per methylene unit.

Chapter 4. Tuning of the Reactivity of Four-Coordinate Co(III)Tropocoronand Complexes by the Macrocycle Size

The first mononuclear cationic $Co^{III}X_4$ complexes, [Co(TC-3,3)]BPh$_4$, **2a**, [Co(TC-3,3)]BAr'$_4$, **2a'**, and [Co(TC-4,4)]BPh$_4$, **2b**, have been synthesized and structurally characterized. The dihedral angle of 41° in **2b** is the largest distortion from square planar yet observed in a $Co^{III}X_4$ complex. Electronic tuning of the ligand field in the [Co(TC-n,m)]X complexes causes **2b** to be inert to addition of a Lewis base under the same conditions in which **2a** binds THF to form [Co(THF)(TC-3,3)]BPh$_4$, **3**. The bent nitrosyl complexes [Co(NO)(TC-3,3)], **4a**, and [Co(NO)(TC-4,4)], **4b**, were synthesized from [Co(TC-n,m)] and NO and structurally characterized. Reaction of [Co(TC-n,m)]$^+$ with SC$_6$F$_5^-$ yielded the structurally characterized thiolate complexes [Co(SC$_6$F$_5$)(TC-3,3)], **5a**, and [Co(SC$_6$F$_5$)(TC-4,4)], **5b**. Compounds **4a** and **5a** have square-pyramidal geometry like **3** and all other structurally characterized [MX(TC-3,3)] complexes. Compounds **4b** and **5b** have trigonal bipyramidal geometry, formerly rare for Co(III), and **4b** is diamagnetic due to the strong antibonding π-interaction of the metal d-orbitals with the NO π* orbitals.

Thesis Supervisor: Stephen J. Lippard
Title: Arthur Amos Noyes Professor of Chemistry

This thesis is dedicated to my beloved grandfather

Stephen Hollis Ritchie Upson

Acknowledgments

The work presented in this thesis has been done in somewhat less than five years in the MIT chemistry department. It has been a time of tremendous intellectual and personal growth for me, much of which, ironically, is not reflected in this document. I have many people to thank and their contributions have helped me grow both as a chemist and as a human being.

There is no question that the central figure behind the development of this thesis is Steve Lippard. His indefatigable drive for good science coupled with his obsession with detail and breadth of knowledge have made working with him a very enriching and rewarding experience. He has made me a much better scientist by demanding precision in speech, writing, and thought, and by challenging my assumptions of what is possible. I thank him for his balance of constructive criticism and encouragement which have taught me great perseverance and patience. I also thank Steve for the incomparably talented and helpful group of people he has collected in his laboratory who have become my collaborators and friends.

Direct help with this thesis came from several people to whom I am indebted. The collection of EPR data was greatly aided by Shari Dunham, Andy Gelasco, Sonja Komar, Ann Valentine, and Joyce Whitehead. Alan Davison gave generously of his time in helping me to understand Co(II) EPR and use the EPRSIM program. Rene Lachicotte successfully modeled the CF_3 group disorder in compound **2a'**.

Scott Jaynes got me started in cobalt tropocoronand chemistry and taught me a great deal in his uniquely quiet, efficient, and competent way. Kingsley Taft guided me in my role of VAX system manager and showed me that hard work and ice hockey are quite compatible. Andrew Feig taught me a many, many little things and impressed me with his attention to detail, love of debate, and big heart. Jackie Acho has been a special friend who has encouraged me as her chemical younger sister and given me perspective. We share a love of teaching, country music, red wine, and good conversation and I am lucky to have worked with her.

My baymates have been continually helpful and supportive during my time at MIT. John Protasiewicz was a friendly and instructive labmate at Cornell and I was lucky to overlap with him again in Cambridge. Tomoaki Tanase is a superb chemist, a great teacher, and a wonderful man. Dietrich Steinhuebel is an underrated guy whom I have enjoyed knowing and have learned a lot from his quiet observations and deep-seated enthusiasm for what interests him.

To my labmate Dan LeCloux I offer special thanks for his friendship, conversations over beer, scathing but accurate criticism, and his keen chemical intellect. Laura Pence is a wonderful coworker and friend who taught me much about crystallography, made the VAX/CAD4 connection less of a burden, and continues to share excitement about teaching. I thank Mike Scott for sharing the joys and woes of a tropocoronand chemist and also teaching me about X-ray crystallography from reaction to ORTEP. I have had the pleasure of passing on some of my tropocoronand wisdom to two special people, Mairin Anderson who worked with me as an undergraduate, and Kathy Franz, who is now preparing to take over my bench. Kathy has made finishing up much easier by her patience with my stresses and her zeal as a student; she will go far.

I also want to thank Dave Coufal, Steve and Shari Dunham, Sofi Elmroth, Andy Gelasco, Susanna Herold, Sonja Komar-Panicucci, Rajesh Manchanda, Axel Masschelein, Uta Ohndorf, Lynn Rardin, Tong Ren, Tricia Takahara, Steve Watton, Ann Valentine, Joanne Yun, and Deborah Zamble. Working with people like you has made graduate school much more personally fulfilling than I could have imagined.

Sandy Gould has been a great friend since our very first week at MIT and I want her to know how much I appreciate and value our friendship. It is greater for all that has gone into it. Heidi Erlacher is one of the toughest people I know, and has heart and compassion to match. Our friendship has been cemented by rugby bruises and beer and I never want to be on the other side of the pitch from her. Andreja Bakac has taught me how to balance quality science with a greater perspective on scientists and life in general. Cindy Schauer has helped me to think more deeply about my work and focus on the important questions as well as how to answer them.

Outside the lab I have been supported and encouraged many people who don't understand chemistry, but have made an effort to understand why I like it. Melinda Cerny has always been ready to listen and offer her input. Jackie Simonis has more patience with, tolerance for, and understanding of people than I can fathom. Karen Cozzetto and Amy Tsui are physically far away but have never stopped letting me know that they are there. Carmen Platt has been a great penpal and a great friend for a long time. Aline Yu has known me forever and I am very lucky and happy that our friendship continues. I thank the MIT Women's Ice Hockey team for accepting a Floridian skating novice among them. The MIT

Women's Rugby team has been a tremendous source of fun, stress release, support, relaxation, and remarkable people. Keep on ruckin' and maulin'.

Jonathan Wilker has been my friend and coworker since our earliest days in the Lippard Lab and has also been a great apartment mate for the last four years. He is one of the coolest guys I know for his sense of humor, generous nature, and easy laugh. I also want to thank Larry Rozsynai for being a great roommate for four years with many interesting conversations, a little bit of hockey, and science, too. Most recently Doug Whittington has taken on the role of labmate and apartment mate with his typical friendly style.

My best friend in and out of lab for the last year, Maria Bautista, is a relative newcomer to MIT. She shares my enthusiasm for sports and music, for puttering around in the lab, and reading. She has helped me to develop a more unified vision of the chemistry in this thesis and bravely dug into Chapter 3 to help me understand what I wanted to say. I have learned a lot from her and hope our friendship and professional collaborations continue for a very long time.

My family have been invaluable to me in my life, and my time at MIT is no exception. I thank my adopted aunt and uncle Josephine and Harold Hart for welcoming me in their home and sharing many happy times together. My maternal grandfather has always supported my academic interests with his own enthusiasm for scholarship and ideas, and will continue to be a role model and an inspiration wherever I am. My sister Alex is also one of my best friends because we have many things in common and many differences; in the face of the latter she is always giving, supporting, understanding and fun to be with.

My parents deserve the most special thanks and recognition. They have always been supportive and understanding and encouraged me in whatever effort or interest I was drawn toward, regardless of how different from their own. Their own respect for scholarship and reading and gave me my love for books and learning. My father taught me to be forthright, honest, and to treat everybody as you would like to be treated because he believes that is right. My mother has taught me to try and look at everything from the other person's point of view, to be generous and considerate and almost everything I know about teaching, I learned from her. Whatever skills my professional training has instilled in me, the best of me is from them.

Table of Contents

List of Tables

Chapter 3.

Chapter 4.

List of Figures

Chapter 3.

Chapter 4.

Chapter 1

Tropocoronand Complexes and Macrocyclic Tuning

Macrocycles are a diverse family of compounds used by organic, inorganic, organometallic, materials, and biological chemists. The unifying and distinguishing features of macrocycles are an organic ring backbone with at least nine members and the presence of at least three heteroatoms suitable for metal binding sites.[1] Macrocyclic ligands have the ability to constrain and define the metal center geometry, limiting the size and relative orientation of substrates with which it may react. Moreover, the ligand field can be altered by a macrocycle to shift substantially the metal redox potentials for a given set of donor atoms. Reactivity of the metal with substrates, or of two substrates bound to the metal with each other, can also be dictated by the macrocycle. The earliest synthetic macrocycles, phthalocyanines, were discovered fortuitously in 1928 as a by-product of phthalimide synthesis from phthalic anhydride and ammonia in an iron vessel, as shown in eq 1. Formation of the unexpected product was apparent from an intense blue color in the reaction mixture. Phthalocyaninines have been subsequently investigated as dyes and as

$$ \text{phthalic anhydride} + NH_3 \xrightarrow{Fe^{3+}} \text{phthalocyanine} \qquad (1) $$
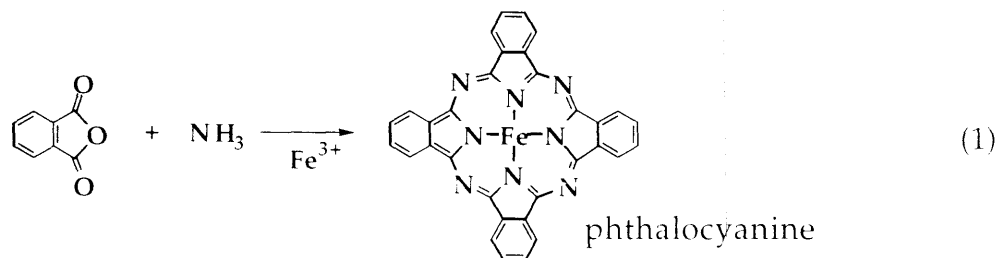
structural analogs of the biologically important porphyrins. Further work in macrocycle synthesis was minimal, however, until another serendipitous discovery. In 1960, Curtis[2] found that reaction of $[Ni(en)_3]^{2+}$ with dry acetone yielded a yellow, crystalline product which was exceptionally stable to boiling in acid or base. Subsequent characterization of the product[3] revealed a mixture of the isomeric nickel macrocyclic complexes, shown below. The presence of nickel is essential in

the template condensation of the terminal amines with the ketone to form
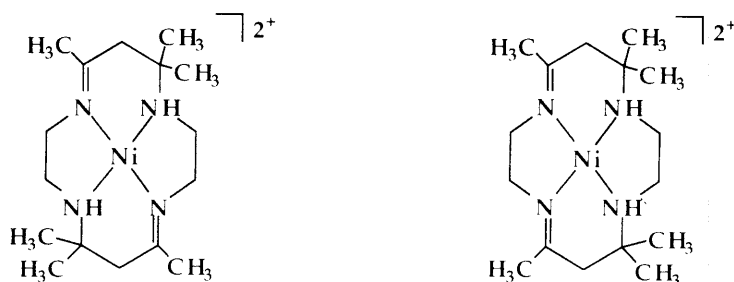
the four carbon-nitrogen linkages and close the macrocycle. Such tetraazamacrocycles with a highly reduced backbone, often called Curtis-type macrocycl became the cornerstone of both template-based macrocycle synthesis and related studies of transition metal-macrocyclic complexes themselves. The years since 1960 have witnessed a tremendous proliferation in the study of macrocycles, in both the syntheses of the macrocycles themselves and their metal complexes.[1,4]

Naturally occurring macrocyclic complexes have been studied with similar intensity and their reactions include transformations which are essential to life. Ionophores bind and encapsulate metal ions for transport across biological membranes.[5,6] Depsipeptides such as valinomycin and enniatin B are ionophores which kill cells by selectively binding potassium over sodium, altering the
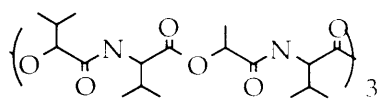
valinomycin
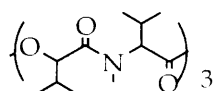
enniatin B
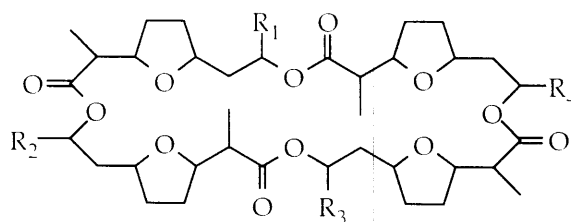
R=CH$_3$ nonactin

normal metal ion gradients and thereby interfering with normal cellular function. The macrotetrolides, such as nonactin, are also antibiotics and transport potassium preferentially to sodium through cellular membranes. The flexibility of these large rings, polyamide/esters in the depsipeptides and polyether/esters in the tetrolides, enables them to wrap completely around potassium and insulate its charge in a hydrophilic environment while exposing a hydrophobic surface to the protein-lipid bilayer of the cell membranes.

More rigid macrocyclic complexes in biology afford a broader range of functions than the flexible ionophores. Tetrapyrrole derivatives are the most common biological macrocycles, some of which are shown in Figure 1.1. Magnesium ion binds to a partially reduced porphyrin chromophore in chlorophyll, which absorbs light energy and converts it to electrons which are transferred through a series of cytochromes and ultimately oxidize water to O_2. The iron porphyrin unit known as heme is active in dioxygen transport and storage in hemoglobin and myoglobin, respectively. Hemes are also used in dioxygen activation for alkane functionalization in cytochrome P450 and in electron transfer in cytochrome c oxidase, which contains two iron porphyrin units. A highly reduced tetrapyrrole unit bound to nickel, called cofactor F430,[7] participates in the final step of methanogenesis in the enzyme methyl coenzyme M methylreductase. Methyl transfer is achieved through the intermediacy of methyl cobalamin, in which methyl is bound to cobalt in the corrin macrocycle.[8] The distinguishing feature of the corrin, in addition to the highly reduced backbone, is the missing methine unit between two pyrrole rings. Differences among the macrocycles in Figure 1.1 and their complexes, including choice of metal ion, degree of ligand saturation, sites and types of ligand derivatization, and other coordinating ligands are critical for their proper functioning in biology.[9]

One manner by which a macrocycle can control the reactivity of a metal center is illustrated by the porphyrin, a rigid molecule where the four pyrrolic nitrogens are forced to bind in one plane. The remaining two sites in an octahedral complex are thus required to be trans to one another. Some cis complexes are known in porphyrin chemistry, but they are rare.[10] In ligands such as tmtaa, shown in Figure 1.2 (i), the metal is forced out of the N_4 plane and the other two ligands are forced to bind in a cis configuration. Macrocycles have also been developed that bind two or more metals simultaneously.[11] This property can, in theory, allow two metals to bind the same substrate or each to bind a single substrate. The latter mode brings the two substrates together to react with greater facility than if the two metal ions were independent. Although the porphyrin and tmtaa ligand families can bind many different metal ions, the crown ethers developed by Pederson and coworkers are designed to bind selectively only one ion.[12] As with the biological ionophores mentioned above, 18-crown-6 binds potassium much more effectively than any other alkali metal ion. By adjusting the number of (CH_2CH_2O) repeats in crown ethers, lithium, sodium and alkaline earth metals can be specifically chelated.

Another important feature of macrocylic complexes is their enhanced thermodynamic stability and reduced kinetic lability compared to complexes of analogous acyclic ligands. Thermodynamically there are both entropic and enthalpic contributions to consider. Replacement of multiple ligands by one macrocycle clearly has a favorable entropic effect. Depending on the system and the equilibria present, the enthalpic contribution can be favorable or unfavorable, but the net result is that the macrocyclic complex is often formed preferentially over an acyclic analog. The reduced kinetic lability of macrocycles results from the difficulty in dissociating one donor atom in a molecule that is linked to several other donor atoms, all bound to the same metal center. Together these kinetic and thermodynamic factors have been termed the "macrocyclic effect".[13]

With the development of Curtis-type macrocycles and an understanding of their syntheses, rational techniques were used to generate macrocycles with specific ring numbers, chelate sizes, denticities, and donor atom types. Macrocycles with a wide variety of chalcogen and pnictogen donors have been prepared and complexed and their coordination chemistry has been extensively reviewed.[1,4] The remainder of this introduction focuses on polyazamacrocycles, the tetraazamacrocycles in particular. Tetraazamacrocycles have been described as providing "the ultimate in metal ion control".[14] Exploitation of this characteristic underlies much of the work in this thesis.

A nitrogen atom in a macrocycle can have a variety of bonding modes. With sp^3 hybridization, an amine nitrogen can bind to three carbon atoms, NR_3, or to two carbons and a hydrogen, NR_2H. The latter motif allows deprotonation of the nitrogen to form anionic NR_2^-, a stronger donor than neutral NR_3. Nitrogen can also exhibit sp^2 hybridization as an imine, R-N=R. The most important ramification of these differences in hybridization is that sp^3 nitrogens with only single bonds are more flexible than the sp^2 nitrogen atoms linked by double bonds and will provide more flexibility in their macrocycles. The directionality of nitrogen bonding is fixed in the latter, but much less so in the former. Macrocycles exist with all amine donors, all imine donors, and mixtures of the two as shown in Figure 1.2. The ligands depicted are only a small fraction of those known which, in turn, are only a fraction of those conceivable. Each methylene unit could be replaced by zero or two such units. Each C-H bond affords a potential substitution site and saturated C-C bonds could be oxidized. The ligands that have been studied are those of particular interest and synthetically accessible.

The goal of macrocyclic ligand design is to control precisely reactivity at a metal center. Toward this end, many different versions of a macrocycle type are examined. A common way of incrementally changing a macrocycle is to use α.ω-

diamines of varying length in the synthesis. The facile condensation of amines with ketones is often employed in both template and non-template syntheses. Some results of this approach are shown in Figure 1.3. The most common lengths of diamine used are those with two and three methylene units, forming five- and six-membered chelate rings, respectively. The well known stabilities of these ring sizes provide an important driving force for their formation in template syntheses.

The ligand systems explored to date have exposed several limitations. Ligand designs that restrict the length of α,ω-diamine chain narrow the range of geometries at the metal center that can be explored. Relying on template syntheses does not allow access to geometries or oxidation states that may be kinetic lly but not thermodynamically stable.

We now consider complexes of the tropocoronands, tetraazamacrocycles which are the subject of this thesis. As shown below, the ligand contains two seven-membered rings each having two nitrogen donor atoms. The aminotropone-

H$_2$TC-n,m, Tropocoronand Ligand
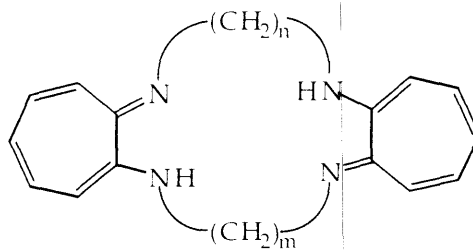
iminate rings are connected to one another through methylene linker chains of varying lengths, n and m. These lengths can be controlled independently in the direct synthesis as shown in Figure 1.4, affording the H$_2$TC-n,m family of ligands. No template synthesis has yet been successful for the preparation of these ligands. Ligands with n and m values from two to twelve have been synthesized,[15-17] and complexes with n and m ranging from three to seven have been made[7,15,17-29] with a variety of transition metals. Deprotonation of the macrocycle produces a dianionic

ligand formally having two amine and two imine nitrogen donors, similar to the porphyrin, tmtaa, and other ligands shown in Figure 1.2 (d-i).

Use of seven-membered rather than six-membered aromatic rings in the tropocoronand ligand distinguishes it from all other tetraazamacrocycles. Although the seven-membered ring is uncommon, the odd-membered ring is required to maintain a 10 e$^-$ conjugated system[30] including both the ring and the two nitrogen atoms, as shown below. With a six-membered ring, equivalent resonance structures delocalizing the electron density over both nitrogen atoms cannot be drawn. The aminotroponeiminate ring is also more strongly donating and more basic than the six-membered analog. As a result, aminotroponeiminate chelates are intensely colored, owing to ligand-to-metal charge transfer bands.

7-membered ring   6-membered ring
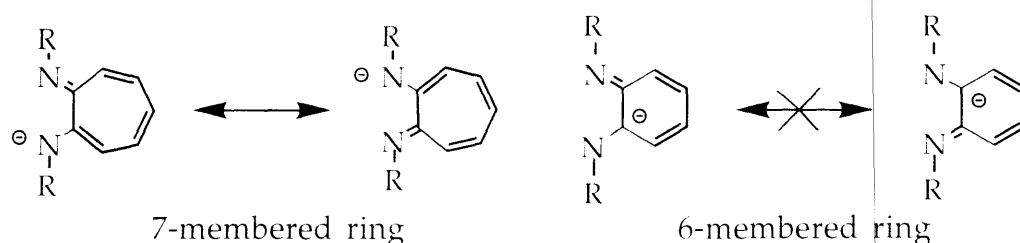
Prior to the synthesis of the first tropocoronand complex, coordination of the unlinked aminotroponeiminate (ati) ligands had been studied. The ati ring, which can be substituted on both nitrogen atoms, serves as a bidentate ligand, forming complexes with di- and trivalent metal ions, formulated as $[M^{II}(R_2ati)_2]$ and $[M^{III}(R_2ati)_3]$.[30-32] We briefly discuss these acyclic complexes since the differences
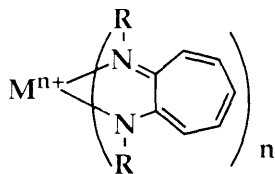
and similarities to tropocoronand complexes help to clarify some of the properties unique to the latter class of ligand. Reaction of divalent or trivalent metal ions or metal carbonyls with the dialkylaminotroponeiminates in the presence of base affords the neutral bis- or tris-chelate complexes. Many of these complexes, both

diamagnetic[31] and paramagnetic,[32] have been investigated by ^{1}H-NMR spectroscopy, solution state magnetics methods, and, in some cases, by X-ray crystallography.[33,34] All tris-chelates have octahedral geometries, whereas the bis-chelates have either square-planar or tetrahedral structures. The preference for square-planar versus tetrahedral geometry was dictated largely by the steric bulk of the R group on nitrogen, typically Me, Et, i-Bu, t-Bu, Ph or p-Tol. The bulkier ligands such as Ph_2ati formed only tetrahedral complexes, whereas the interconversion of square-planar and tetrahedral geometry was encountered for the Et_2ati and Me_2ati ligands, and in some cases was followed by ^{1}H-NMR methods. Only the smallest ligands could form tris-chelate complexes, which were too sterically congested with bulkier R groups.

The other feature of note in the chemistry of aminotroponeiminate chelates is the group of complexes which could not be synthesized with the acyclic ligands. Attempts to prepare $[M(Me_2ati)_2]$ for metals with a readily available trivalent oxidation state, including Cr, Fe, and Co, failed. Even under an inert atmosphere, the neutral tris-chelate complexes were obtained. A detailed mechanistic study was not undertaken but some evidence was presented for attack on a $[M(R_2ati)_2]$ complex by a third HR_2ati ligand.[31] The ready synthesis of square-planar, four-coordinate Co(II) complexes with the tropocoronand ligand,[23] however, indicates that the lower oxidation state is not incompatible with the donor properties of the chelate, but requires the additional stabilization of the macrocycle to prevent oxidation.

Investigation of the R_2ati chelates demonstrated that a wide variety of metals would form complexes with this ligand set, but some oxidation states and geometries could not be accessed. The remedy for this situation is the macrocyclic analog, the tropocoronand. Early work with aminotroponeiminates reported connection of two seven-membered rings with one equivalent of either hydrazine or phenylene diamine[30] to form an acyclic species, but no reactions of these ligands

with metals were reported. Synthesis of the complete macrocycles and their nickel complexes were first reported in 1983.[15] Since then, many more tropocoronand complexes have been characterized, the majority of which have been studied by X-ray crystallography. A large body of information now exists on the structures and coordination modes adopted by this family of ligands. In the overview that follows, the known complexes will be discussed according to their nuclearity, coordination number, metal center and auxiliary ligands. This summary is intended to highlight the unique structural features of tropocoronand complexes and some less well understood phenomena to be addressed in this thesis.

Mononuclear Tropocoronand Complexes.

Four-coordination. Like many new macrocyclic systems, the first tropocoronand ligands were complexed with air-stable Ni(II).[15,17] As mentioned earlier, the ligand is synthesized directly and then allowed react with nickel in the presence of a base. The series of mononuclear complexes [Ni(TC-n,m)] was prepared for n + m = (6, 8, 9, 10, 12) and structurally characterized.[18] The smallest ligand, TC-3,3, forms two five-membered rings with nickel from the aminotroponeiminate chelates and two six-membered rings enclosed by the aliphatic linker chains. These four rings with sp^2 hybridized nitrogen atoms afford a rigid macrocycle that enforces an essentially square-planar geometry at the metal center. The largest complex
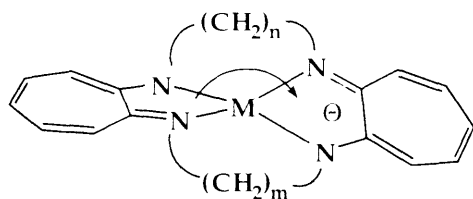
studied with nickel, [Ni(TC-6,6)], has a five-nine-five-nine ring set, producing an almost tetrahedral geometry. The geometry at the metal center can be measured by the dihedral angle, Θ, between the two five membered N-M-N chelate rings. When

$\Theta = 0°$, the complex is square-planar and when $\Theta = 90°$, it is tetrahedral. The dihedral angles for the [Ni(TC-n,m)] complexes are shown in Figure 1.5. In addition to spanning the extremes of four-coordinate geometry, this series of complexes also presents several intermediate values of Θ. It is important to note that the increase in Θ with (n + m) in Figure 1.5 is not monotonic, however. With the addition of only one methylene unit to the macrocycle in changing from [Ni(TC-4,5)] to [Ni(TC-5,5)], the dihedral angle increases by over 40°. This point will be discussed further shortly. In general, as the sum of methylene linker units, (n + m), increases, Θ also increases, reflecting a distortion of the metal geometry away from square-planar toward tetrahedral.

The driving force for this distortion comes from the aliphatic linker chains. For a given complex, [M(TC-n,m)], the M-N distance is fixed, and for any value of Θ the distance between the nitrogens on the ends of one chain is fixed. As the number of methylene units, n or m, increases, more carbon atoms are packed between the end carbons of each chain, the $C\alpha$ and $C\omega$ atoms, putting tremendous torsional strain on the methylene linker units. Increasing the $C\alpha$ to $C\omega$ distance releases this torsional strain by rotation of the seven-membered rings away from coplanarity. This rotation increases Θ and also increases the N-to-N distance for each chain, simultaneously maintaining the M-N distance and the integrity of the complex.

In addition to pure -CH_2- links, a tropocoronand with an oxygen atom in the chain, (CH_2CH_2-O-CH_2CH_2) was prepared and its nickel complex, [Ni(TC-2,O,2)],[18] structurally characterized. Recently a new four-coordinate nickel tropocoronand complex with another ligand derivative has been reported.[35] This ligand differs from the original one in that the γ positions on the aminotroponeiminate rings have been substituted with isopropyl groups. The structure of this nickel complex is quite similar to that of [Ni(TC-5,5)]. The average Ni-N distance in [Ni(TC-5,5)] is 1.949(2) Å versus 1.959(4) Å in the isopropyl-substituted derivative and the Θ values

in [Ni(TC-5,5)] is 70.1° versus 69.5°. The isopropyl groups exert a significant electronic effect, however. The original Ni(TC-5,5) complex is a deep red-brown
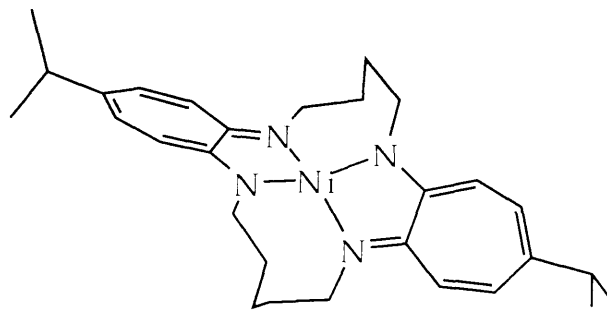
color but the isopropyl substituted complex had a dark blue-black color in CH_2Cl_2. No electronic spectra were reported for the latter.

A series of [Co(TC-n,m)] complexes with the original tropocoronand ligand, analogous to the Ni derivatives, were also synthesized and structurally characterized.[23] The geometry of the end members of the series were very similar to those from the nickel system and are also presented in Figure 1.5. For the TC-4,5 complexes, however, the Θ values in nickel and cobalt differ by 27°. The two series of complexes show abrupt increases in Θ, but at different values of (n + m), eight for cobalt and nine for nickel.

The cobalt and nickel complexes, also change their spin ground state as a function of the changes in geometry. The approximately square-planar complexes are low spin, S = 0 for Ni and S = 1/2 for Co, and the pseudo-tetrahedral complexes are high spin S = 1 for Ni and S = 3/2 for Co. These spin state changes, summarized in Table 1.1, correspond to the discontinuous changes in Θ as a function of the total methylene linker chain length, n + m. The [Co(TC-4,4)] complex has a dihedral angle of 31.8° and spin S = 1/2 but the [Co(TC-4,5)] complex has an angle of 58.7° and S = 3/2. The nickel spin state change occurs between the [Ni(TC-4,5)], Θ = 27.1° and S = 0, and the [Ni(TC-5,5)] complex, Θ = 70.1° and S = 1. In both cases, ligand field splitting energies favor the low spin electronic configuration for pseudo-square-planar geometries, and high spin for geometries closer to tetrahedral. The difference

between cobalt and nickel is the greater preference of d^7 Co(II) for tetrahedral over square-planar, whereas d^8 Ni(II) prefers square-planar over tetrahedral.[36,37] Thus [Co(TC-4,5)] is high spin and [Ni(TC-4,5)] is low spin. In the absence of a spin state transition, the change in dihedral angle should be continuous as a function of the number of methylene linker units. Such a trend occurs for the [Cu(TC-n,m)][19] tropocoronand complexes, the dihedral angles of which are also plotted in Figure 1.5.

Structural characterization of the [Cu(TC-n,m)] complexes revealed two interesting features. As just mentioned, the change in Θ versus (n + m) is linear since there is no spin state change. Secondly, the [Cu(TC-6,6)] complex could not be synthesized. Since tetrahedral Cu(II) complexes are well known, there must be some other incompatibility of Cu(II) with the TC-6,6 ligand. The ionic radius for tetrahedral Cu(II) is 0.71 Å,[27] slightly smaller than that of tetrahedral Co(II), 0.72 Å.[27] Perhaps the Cu(II) radius is just too small for "Cu(TC-6,6)" to be formed, the shorter Cu-N distance, and hence shorter $C\alpha$ to $C\omega$ distance, being incompatible with the large Θ value required for a [M(TC-6,6)] complex. Instead, the TC-6,6 ligand forms a variety of dinuclear copper complexes. The [Cu$_2$(μ-X)$_2$(TC-6,6)] complexes may be more stable than the unobserved [Co$_2$(μ-X)$_2$(TC-6,6)] because in four-coordinate square-planar geometries, Co(II) is less stable than Cu(II). A detailed investigation of the effect of transition metal size on the structure and stability of [M(TC-n,m)] complexes is presented in Chapter 2 of this thesis.

Recently mononuclear manganese tropocoronand complexes have also been prepared.[38] The complex [Mn(TC-6,6)] has a dihedral angle of 82° and an average Mn-N distance of 2.077(4) Å. The related [Mn(TC-5,5)] compound has a dihedral angle of 60° and an average Mn-N distance of 2.099(3) Å. The smaller dihedral angle Θ for the smaller macrocycle indicates that steric tuning of the ligand environment obtains here also.

In all four-coordinate mononuclear tropocoronand complexes, the tuning ability of the tropocoronand macrocycle is apparent. For Co, Ni, and Cu, complexes with geometries ranging from square-planar to tetrahedral have been obtained, and work is in progress for the [Mn(TC-n,m)] complexes with n + m < 10. Such tuning has not been observed with the acyclic R_2ati ligands, although tuning the geometry by tuning the R group steric bulk might be possible. In the absence of the macrocycle, some geometries cannot be stabilized, as in the case of Co(II) where no square-planar [Co(Me$_2$ati)$_2$] complex could be made whereas [Co(TC-3,3)] is readily synthesized.

Five-coordination. The ease of oxidation of Co to Co(III) makes five-coordinate [CoX(TC-n,m)] complexes readily accessible, allowing tropocoronand ligand tuning effects to be investigated for pentacoordinate species. Oxidation of pseudo-square-planar [Co(TC-n,m)] complexes in the presence of chloride ion produced a series of [CoCl(TC-n,m)] complexes.[21] Both [CoCl(TC-3,3)] and [CoCl(TC-3,4)] have square pyramidal geometries whereas [CoCl(TC-4,4)] is trigonal bipyramidal. This latter feature was highly unusual at the time, and further work with [CoL(TC-4,4)] complexes, discussed in Chapter 4, reveals this geometry to be routinely accessible. The difference in coordination geometry between square pyramidal [CoL(TC-4,4)] and trigonal bipyramidal [CoL(TC-4,4)] is dictated by the electronic nature of the fifth ligand, as further elaborated in Chapter 4.

Cobalt alkyl complexes were prepared by reaction of the [CoX(TC-n,m)] halides with metal alkyls or by reduction of the Co(II) species to Co(I) followed by addition of R^+.[22] All [CoR(TC-n,m)] complexes are square pyramidal, unlike the halides where both square pyramidal and trigonal bipyramidal geometries obtain. As in the case of the halides, the effects of only slight increases in the macrocycle size were significant. The Co(III) alkyl complexes are also subject to Co-C bond homolysis, but the rate is greater by a factor of ten at 40° C for [CoMe(TC-4,4)] than for [CoMe(TC-

3,3)]. The rate increase was attributed to greater strain in the larger macrocycle. Moreover, [CoMe(TC-4,4)] can insert CO to form the acyl complex, [Co(Ac)(TC-4,4)], but, under the same conditions, [CoMe(TC-3,3)] cannot. In this example, the greater flexibility of the larger macrocycle allows it to accommodate CO in a position cis to methyl for subsequent alkyl migration. The TC-3,3 ligand is rigidly planar and could only bind a sixth ligand trans to the fifth. With the tropocoronand ligand, small changes in the macrocycle can incrementally tune the geometry and hence the reactivity at the metal center.

The differences observed in the chemistry of (TC-6,6)$^{2-}$ with Co and Ni versus Cu showed th t the tropocoronand ligand is sensitive to changes in metal ion radius. This sensitivity is also seen in the tropocoronand chemistry of early first-row transition metals. Vanadium chlorides [VCl(TC-n,n)] have been synthesized for n = 4, 5, 6[39] and are trigonal bipyramidal in each case with chloride in an equatorial position, analogous to [CoCl(TC-4,4)].[21] Notably, five-coordinate square-pyramidal [VCl(TC-n,m)] complexes could not be synthesized from the smaller tropocoronand ligands, TC-3,3 or TC-3,4, under the same conditions. Terminal oxo complexes [V(O)(TC-n,m)] with square pyramidal geometry were obtained with these ligands, however.[39] This result suggests that, for TC-3,3 or TC-3,4, even with a slight displacement of V(III) out of the N_4 plane, this ion is too large to be accommodated. Oxidation of V(III) to V(IV) decreases the ionic radius from 0.78 Å to 0.67 Å[40] allowing the vanadium ion to coordinate to the macrocycle. The chloride ion in [VCl(TC-4,4)] can be substituted by either triflate or mesityl to form the [V(OTf)(TC-4,4)] and [V(mes)(TC-4,4)] complexes.[39] Trigonal bipyramidal geometries have been confirmed for both molecules by X-ray crystallography and preliminary data suggest that [VCl(TC-5,5)] reacts similarly to yield [V(OTf)(TC-5,5)].

The [CoX(TC-n,m)] complexes were prepared by oxidation of Co(II) to Co(III) and addition of a fifth ligand. Five-coordinate cationic alkyl complexes of Zr and Hf

have been prepared by removal of a ligand from parent six-coordinate complexes. When six-coordinate [M(CH$_2$Ph)$_2$(TC-3,3)] complexes, M = Zr, Hf , are treated with one equivalent of [Cp$_2$Fe]BPh$_4$, a benzyl ligand is oxidized to diphenylethane, affording the five-coordinate cation, [M(CH$_2$Ph)(TC-3,3)]$^+$. These cations are square pyramidal, like all known five-coordinate [MX(TC-3,3)] species, reflecting the rigidity of the TC-3,3 macrocycle.

Six-coordination. The ability of [CoMe(TC-4,4)] to insert CO and form an acyl led to the supposition that the TC-4,4 ligand can fold to accommodate two more ligands in cis positions in an octahedral geometry. Proof of this hypothesis was provided by the six-coordinate complex [Co(acac)(TC-4,4)].[41]

Metathesis reactions of the mononuclear vanadium tropocoronand halides [VCl(TC-4,4)] and [VCl(TC-5,5)] produced several five-coordinate complexes as discussed above. In contrast to the TC-4,4 case, the TC-5,5 system produced two octahedral vanadium centers.[39] Protonolysis of H$_2$TC-5,5 with [V(mes)$_3$(THF)$_3$] afforded [V(mes)(TC-5,5)]$_2$, in which each vanadium ion has four nitrogen donors from the tropocoronand ligand and two carbon atoms from each of two bridging aryl groups. A similar product, [V(OTf)(TC-6,6)]$_2$, was obtained from reaction of five-coordinate [VCl(TC-6,6)] with TMSOTf. These six-coordinate species again demonstrate the ability of the tropocoronand ligand to tune the geometry and coordination number of a metal center.

Numerous six-coordinate zirconium(IV) and hafnium(IV) tropocoronand complexes have also been prepared and the crystallographically characterized species are summarized in Table 1.2.[39] Addition of Li$_2$TC-n,m to MX$_4$(THF)$_2$ affords the [MX$_2$(TC-n,m)] dihalides and the dialkyls [MR$_2$(TC-n,m)] are accessible by reacting H$_2$TC-n,m with MR$_4$, R = CH$_2$Ph, CH$_2$SiMe$_3$. Treatment of the latter with two equivalents of [Cp$_2$Fe]OTf produced the triflate complexes [M(OTf)$_2$(TC-n,m)]. Adding one equivalent of [Cp$_2$Fe]BPh$_4$ to the bis(benzyl) complexes [M(CH$_2$Ph)$_2$(TC-

3,3)] produced the five-coordinate, monoaryl cations mentioned above. Mixed halide alkyl/aryl complexes could be made from the dialkyls by protonolysis of one alkyl/aryl with Me_3NHX. In some cases, protonation was found to be an alternate route to the dihalide. The alkyl can also be protonated by aniline, effectively replacing the alkyl with an amide.

Table 1.2 shows that the majority of the Zr(IV) and Hf(IV) complexes contain the TC-3,3 ligand. Previous work demonstrated that the TC-3,3 macrocycle consistently forms a rigid plane of four nitrogen donors. These Zr(IV) and Hf(IV) compounds reinforce this observation. For almost all the $[MX_2(TC-3,3)]$, M = Zr, Hf, complexes listed the geometry is rigorously trigonal prismatic in which the two non-macrocyclic ligands are consistently positioned above the two seven membered rings. The only exceptions to this rule are those complexes with two (CH_2SiMe_3) ligands, in which case the steric bulk of the tertiary trimethylsilyl moiety forces the groups away from the rings, toward the nitrogen atoms, distorting the metal center toward octahedral geometry. Interestingly, this distortion is not seen in the $[HfCl(CH_2CMe_3)(TC-3,3)]$ complex, suggesting that an electronic effect is also operative.

When the ligand size is increased, distortion away from the trigonal prismatic toward octahedral geometries is seen as demonstrated in the $[ZrCl_2(TC-n,m)]$, $[M(OTf)_2(TC-n,m)]$, $[Hf(CH_2Ph)_2(TC-n,m)]$ and $[M(CH_2SiMe_3)_2(TC-n,m)]$ series of complexes. It is notable that the bis(benzyl) compounds could not be synthesized from macrocycles having two linker chains with n or m > 3. Decomposition products consistent with attack on the linker chain by a benzyl group were obtained. Lack of such decomposition with the CH_2SiMe_3 ligand suggests that the metal center is much less electrophilic in this case than with the more weakly donating benzyl group. The stability of complexes with *either* n or m = 3, but not necessarily both,

implies that the structural rigidity imposed by the three-methylene linker chain prohibits C-H activation of the linker arms.

Eight-coordination. It is not surprising that tropocoronand complexes with coordination numbers greater than six are available with the second and third row congeners zirconium and hafnium. With both the TC-3,3 and TC-4,4 ligands the [M(TC-n,m)2] complexes of both Zr and Hf can be synthesized.[39]

Dinuclear Tropocoronand Complexes.

A dinuclear cobalt tropocoronand, [Co2(μ-OH)(μ-OAc)(TC-7,7)],[23] was prepared with the two bridging groups, one on each side of the macrocycle. The tropocoronand ligand is bent in a saddle conformation, with the acetate ligand on the convex side and the hydroxide more enclosed on the concave side of the macrocycle. This arrangement results in tetrahedral geometries for both metal ions.

Tetrahedral geometries are also seen in the new dinuclear nickel tropocoronand complex shown below.[42] In addition to the four nitrogen
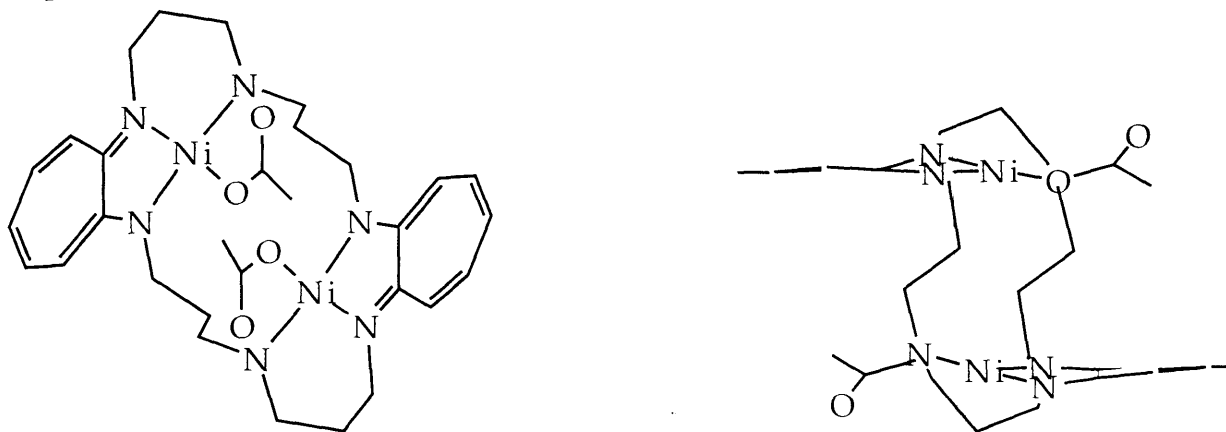
donors at the aminotroponeiminate ends of the macrocycle, the seven-atom long linker chains have nitrogen atoms incorporated in the center, each of which also coordinate to nickel. This complex is the first example of a heteroatom in a linker chain coordinating to the metal center, although heteroatoms have been included as in the [Ni(TC-2,O,2)] complex, vide supra. Charge neutrality is maintained at each nickel center by coordination of a monodentate acetate ligand. Because there are no

bridging ligands between the two nickel centers, other than the tropocoronand, the macrocycle is not constrained to the saddle geometry seen in $[Co_2(\mu\text{-OH})(\mu\text{-OAc})(TC\text{-}7,7)]$. Rather, the two seven-membered rings are held apart by the three methylene linkers between the linker and aminotroponeiminate nitrogen, as shown in the depictions above.

The slightly smaller size of Cu(II) versus Co(II) or Ni(II) leads to the stable dinuclear species, $[Cu_2(\mu\text{-OMe})(\mu\text{-OAc})(TC\text{-}6,6)]$[20], with a ligand having six- rather than seven-atom linker chains. Both bridging units are on the same side of the macrocycle, which is folded in a saddle conformation along a vector perpendicular to the Cu-Cu axis. This arrangement is in contrast to $[Co_2(\mu\text{-OH})(\mu\text{-OAc})(TC\text{-}7,7)]$ in which the acetate and hydroxide groups are on opposite sides. The result is square-planar Cu(II) centers, rather than tetrahedral. Copper(I) can also form dinuclear tropocoronand species with electron accepting ligands such as CO and alkynes. By generating the $[Cu_2(NCCH_3)_2(TC\text{-}n,m)]$ species in situ and then adding the appropriate ligand, dicopper carbonyl and alkyne complexes were synthesized. Trigonal copper centers on either side of the macrocycle were found in $[Cu_2(CO)_2(TC\text{-}5,5)]$ and $[Cu_2(CO)_2(TC\text{-}6,6)]$.[26] These carbonyl complexes have the same characteristic open structure seen in the absence of bridging ligands pictured above in $[Ni_2(OAc)_2(TC\text{-}3,NH,3)]$. Alkynes were found to bind to both metal centers in a $\mu_2\text{-}\eta^2\eta^2$ coordination mode in the complexes $[Cu_2(RCCR)(TC\text{-}6,6)]$ for R = Me, Ph, OAc, $EtCO_2$. The macrocycle is folded in a saddle configuration similar to $[Cu_2(\mu\text{-OMe})(\mu\text{-OAc})(TC\text{-}6,6)]$.

A dinuclear complex of hafnium, $[Hf(CH_2SiMe_3)_3]_2[TC\text{-}5,5]$, has also been made. This product resulted from treatment of $H_2TC\text{-}5,5$ with $Hf(CH_2SiMe_3)_4$ and is the result of the inability of the TC-5,5 ligand to distort further toward octahedral geometry than the TC-4,5 ligand in $[Hf(CH_2SiMe_3)_2(TC\text{-}4,5)]$. Such a distortion could

be unfavorable either from excessive torsional strain in the linker chains or steric clashes between the bulky R groups and the longer linker chains.

The last set of dinuclear complexes to be discussed were the first tropocoronand complexes of any kind to be synthesized with a second-row metal, namely rhodium.[29] Two dicarbonyl complexes with the stoichiometry [Rh$_2$(CO)$_4$(TC-5,5)] were prepared from [Rh(CO)$_2$Cl]$_2$ and Li$_2$TC-5,5. Two different isomers could be isolated from the reaction mixture. In the syn isomer, each rhodium atom has two terminal carbonyls and forms a square-planar geometry with the aminotroponeiminate ring and both metal centers residing on the same side of the macrocycle. In the anti isomer, the metal centers have the same coordination spheres but one is on each side of the macrocycle. Thus syn-[Rh$_2$(CO)$_4$(TC-5,5)] has the folded saddle geometry previously seen only in bridged complexes and anti-[Rh$_2$(CO)$_4$(TC-5,5)] has the open geometry more common for the unbridged dinuclear tropocoronand complexes.

Summary

The tropocoronand complexes described here demonstrate the tremendous versatility of this tetraazamacrocycle in both structure and reactivity. The geometric and steric constraints of each ligand drive geometric tuning at the metal center, but the final structure is also affected by metal ion size and ligand field preference, as well as the steric bulk, by electronic effects and by binding modes of additional ligands. Extensive use of crystallographic characterization has provided a detailed picture of the subtle combination of these effects on the tropocoronand metal complex geometry.

A summary of the geometric spectrum covered by tropocoronand complexes is presented in Figure 1.6. In four-coordinate mononuclear complexes, geometries from square-planar to tetrahedral can be accessed by changing the size of the

macrocycle. Square pyramidal or trigonal bipyramidal compounds can be made by changing the number of methylene linkers also in five-coordinate complexes in addition to the tuning effects due to the electronic nature of the fifth ligand. Six-coordinate geometries may be tuned from trigonal prismatic toward octahedral depending on both the length of the linker chains and the nature of the fifth and sixth ligands. Switching from mononuclear to dinuclear tropocoronand complexes is also accomplished by varying the (n + m) in the TC-n,m. Changing between the open and closed dinuclear geometries can be effected by thermal interconversion or modification of the acyclic ligands.

These results provide the background against which new areas have been explored in this thesis. Chapter 2 provides a detailed comparison of [Zn(TC-n,m)] versus [Cd(TC-n,m)] complexes, revealing the effect of changing the metal ion radius on the twist in four-coordinate tropocoronands. The electrochemical behavior of the [Zn(TC-n,m)] complexes has also been investigated to evaluate the redox stability of the coordinated tropocoronand ligand. In Chapter 3 cyclic voltammetric studies, EPR spectra, and molecular orbital calculations are used to investigate ligand electronic tuning of the [Co(TC-n,m)] complexes in detail. Chapter 4 describes several novel Co(III) tropocoronand complexes including the first mononuclear cationic, square-planar, four-coordinate Co(III) complex and the four-coordinate Co(III) complex with the largest distortion from planarity for $Co^{III}X_4$ complexes of any charge. Five-coordinate Co(III) nitrosyl and thiolate complexes are also discussed, including the first diamagnetic trigonal-bipyramidal cobalt nitrosyl complex with a bent nitrosyl group, and comparisons of these pseudo-halogens are made to the [CoCl(TC-n,m)] complexes synthesized previously. The results offer insight into some of the novel examples of reactivity previously seen and attributed to the unique features of the tropocoronand ligand in cobalt chemistry.

References.

(1)   Melson, G. A. *Coordination Chemistry of Macrocyclic Compounds*; Plenum Press: New York, 1979.

(2)   Curtis, N. F. *J. Chem. Soc.* **1960**, 4409-4413.

(3)   Curtis, N. F.; House, D. A. *Chem. Ind.* **1961**, 1708-1709.

(4)   Lindoy, L. F. *The Chemistry of Macrocyclic Ligand Complexes*; Cambridge University Press: New York, 1989.

(5)   Hilgenfeld, R.; Saenger, W. *Topics in Current Chem.* **1982**, *101*, 1-82.

(6)   Racker, E. *Acc. Chem. Res.* **1979**, *12*, 338-44.

(7)   Kolodziej, A. F. In *Progress In Inorganic Chemistry*; Karlin, K. D., Ed.; John Wiley & Sons, Inc.: New York, 1994; Vol. 41, pp 493-598.

(8)   Dolphin, D. *B12*; John Wiley & Sons, Inc.: New York, 1982; Vol. 1 and 2.

(9)   Lippard, S. J.; Berg, J. M. *Principles of Bioinorganic Chemistry*; University Science Books: Mill Valley, CA, 1994.

(10)   Dawson, D. Y.; Sanalang, J. C.; Arnold, J. C. *J. Am. Chem. Soc.* **1996**, *118*, 6082-6083.

(11)   Atkins, A. J.; Black, D.; Blake, A. J.; Marin-Becerra, A.; Parsons, S.; Ruiz-Ramirez, L.; Schroeder, M. *Chem. Commun.* **1996**, 457-464.

(12)   Pederson, C. J.; Frensdorff, H. K. *Angew. Chem., Int. Ed. Eng.* **1972**, *11*, 16-25.

(13)   Cabbiness, D. K.; Margerum, D. W. *J. Am. Chem. Soc.* **1969**, *91*, 6540-6541.

(14)   Goedken, V. L. In *Coordination Chemistry of Macrocyclic Compounds*; Melson, G. A., Ed.; Plenum Press: New York, 1979, pp 603-654.

(15)   Imajo, S.; Nakanishi, K.; Roberts, M.; Lippard, S. J.; Nozoe, T. *J. Am. Chem. Soc.* **1983**, *105*, 2071-2073.

(16)   Shindo, K.; Wakabayashi, H.; Ishikawa, S.; Nozoe, T. *Bull. Chem. Soc. Jpn.* **1993**, *66*, 2941-2948.

(17)   Zask, A.; Gonnella, N.; Nakanishi, K.; Turner, C. J.; Imajo, S.; Nozoe, T. *Inorg. Chem.* **1986**, *25*, 3400-3406.

(18)   Davis, W. M.; Roberts, M. M.; Zask, A.; Nakanishi, K.; Lippard, S. J. *J. Am. Chem. Soc.* **1985**, *107*, 3864-3870.

(19)   Davis, W. M.; Zask, A.; Nakanishi, K.; Lippard, S. J. *Inorg. Chem.* **1985**, *24*, 3737-3743.

(20)   Davis, W. M.; Lippard, S. J. *Inorg. Chem.* **1985**, *24*, 3688-3691.

(21)   Jaynes, B. S.; Ren, T.; Liu, S.; Lippard, S. J. *J. Am. Chem. Soc.* **1992**, *114*, 9670-9671.

(22)   Jaynes, B. S.; Ren, T.; Masschelein, A.; Lippard, S. J. *J. Am. Chem. Soc.* **1993**, *115*, 5589-5599.

(23)   Jaynes, B. S.; Doerrer, L. H.; Liu, S.; Lippard, S. J. *Inorg. Chem.* **1995**, *34*, 5735-5744.

(24)   Villacorta, G. M.; Gibson, D.; Williams, I. D.; Lippard, S. J. *J. Am. Chem. Soc.* **1985**, *107*, 6732-6734.

(25)   Villacorta, G. M.; Lippard, S. J. *Pure Appl. Chem.* **1986**, *58*, 1477-1484.

(26)   Villacorta, G. M.; Lippard, S. J. *Inorg. Chem.* **1987**, *26*, 3672-3676.

(27)   Villacorta, G. M.; Gibson, D.; Williams, I. D.; Whang, E.; Lippard, S. J. *Organometallics* **1987**, *6*, 2426-2431.

(28)   Villacorta, G. M.; Rao, C.-P.; Lippard, S. J. *J. Am. Chem. Soc.* **1988**, *110*, 3175-3182.

(29)   Villacorta, G. M.; Lippard, S. J. *Inorg. Chem.* **1988**, *27*, 144-149.

(30)   Brasen, W. H.; Holhquist, H. E.; Benson, R. E. *J. Am. Chem. Soc.* **1961**, *83*, 3125-3135.

(31)   McClellan, W. R.; Benson, R. E. *J. Am. Chem. Soc.* **1966**, *88*, 5165-5169.

(32)   Eaton, D. R.; McClellan, W. R.; Weiher, J. F. *Inorg. Chem.* **1968**, *7*, 2040-2046.

(33)   Laing, M. *A.C.A. (Summer)* **1976**, 76.

(34)   Bartlett, M.; Palenik, G. J. *J. Chem. Soc., Chem. Commun.* **1970**, 416-416.

(35)   Shindo, K.; Zhang, L.-C.; Wakabayashi, H.; Miyamae, H.; Ishikawa, S.; Nozoe, T. *Heterocycles* **1995**, *40*, 913-924.

(36)   Cotton, F. A.; Wilkinson, G. *Advanced Inorganic Chemistry*; 5th ed.; John Wiley & Sons, Inc.: New York, 1988.

(37)   Douglas, B. E.; McDaniel, D. H.; Alexander, J. J. *Concepts and Models of Inorganic Chemistry*; John Wiley & Sons, Inc.: New York, 1983.

(38)   Franz, K. J.; Lippard, S. J., unpublished results.

(39)   Scott, M. J.; Lippard, S. J., unpublished results.

(40)   Shannon, R. D. *Acta Cryst.* **1976**, *A32*, 751-767.

(41)   Jaynes, B. S. *thesis*; Jaynes, B. S., Ed.; Massachusetts Institute of Technology, 1992.

(42)   Shindo, K.; Wakabayashi, H.; Miyamae, H.; Ishikawa, S.; Nozoe, T. *Heterocycles* **1994**, *37*, 943-954.

Table 1.1. Dihedral Angles and Spin-States in [Co(TC-n,m)][a] and [Ni(TC-n,m)][b] Complexes.

	Co		Ni	
(n + m)	Θ	S	Θ	S
6	9.0	1/2	8.3	0
8	31.8	1/2	28.9	0
9	58.7	3/2	27.1	0
10	69.9	3/2	70.1	1
12	84.5	3/2	85.2	1

[a]Jaynes, B. S.; Doerrer, L. H.; Liu, S.; Lippard, S. J. *Inorg. Chem.* **1995**, *34*, 5735-5744.

[b]Davis, W. M.; Roberts, M. M.; Zask, A.; Nakanishi, K.; Lippard, S. J. *J. Am. Chem. Soc.* **1985**, *107*, 3864-3870.

Table 1.2. Six-Coordinate Zirconium and Hafnium Tropocoronand Complexes[a]

(TC-3,3)	(TC-3,4)	(TC-3,5)	(TC-4,4)	(TC-4,5)
$ZrCl_2$		HfI_2	$ZrCl_2$	
			$HfCl_2$	
$Zr(OTf)_2$			$Hf(OTf)_2$	
$Zr(CH_2SiMe_3)_2$	$Zr(CH_2SiMe_3)_2$	$Zr(CH_2SiMe_3)_2$		$Zr(CH_2SiMe_3)_2$
$Hf(CH_2SiMe_3)_2$	$Hf(CH_2SiMe_3)_2$	$Hf(CH_2SiMe_3)_2$		$Hf(CH_2SiMe_3)_2$
$Zr(CH_2Ph)_2$				
$Hf(CH_2Ph)_2$	$Hf(CH_2Ph)_2$	$Hf(CH_2Ph)_2$		
$ZrI(CH_2Ph)$				
$HfCl(CH_2CMe_3)$				
$Zr(HNCC_6H_4t-Bu)_2$				

[a]Scott, M. J.; Lippard, S. J. unpublished results, 1996

43
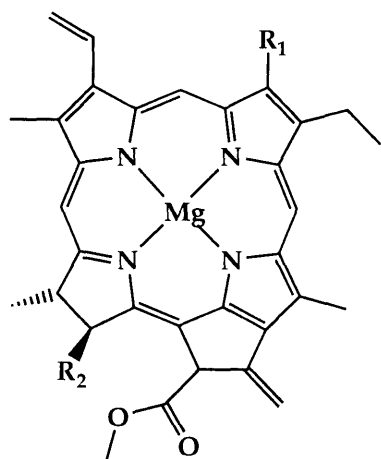
chlorophyll
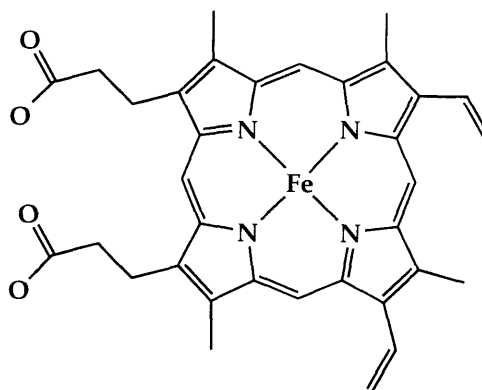
heme
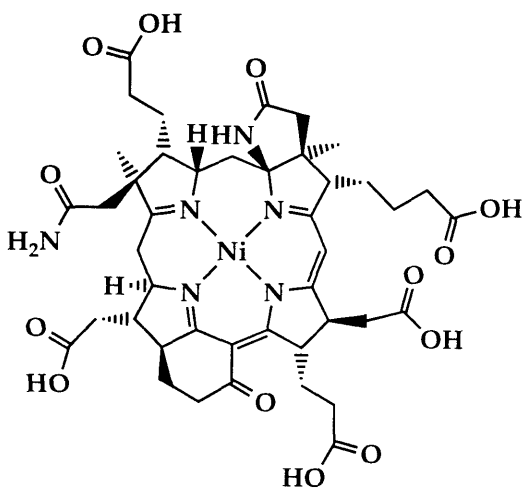
F430
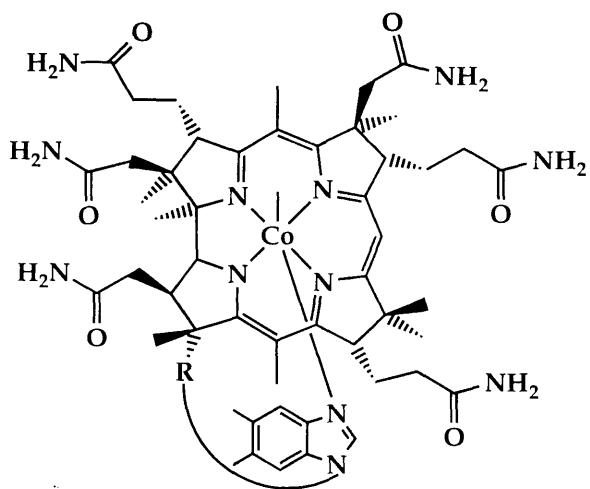
methyl cobalamin

Figure 1.1. Naturally occurring tetraazamacrocycles.

(a)

(b)

(c)

(d)

(e)

(f)

(g)

(h)

(i)

(j)

(k)

(l)
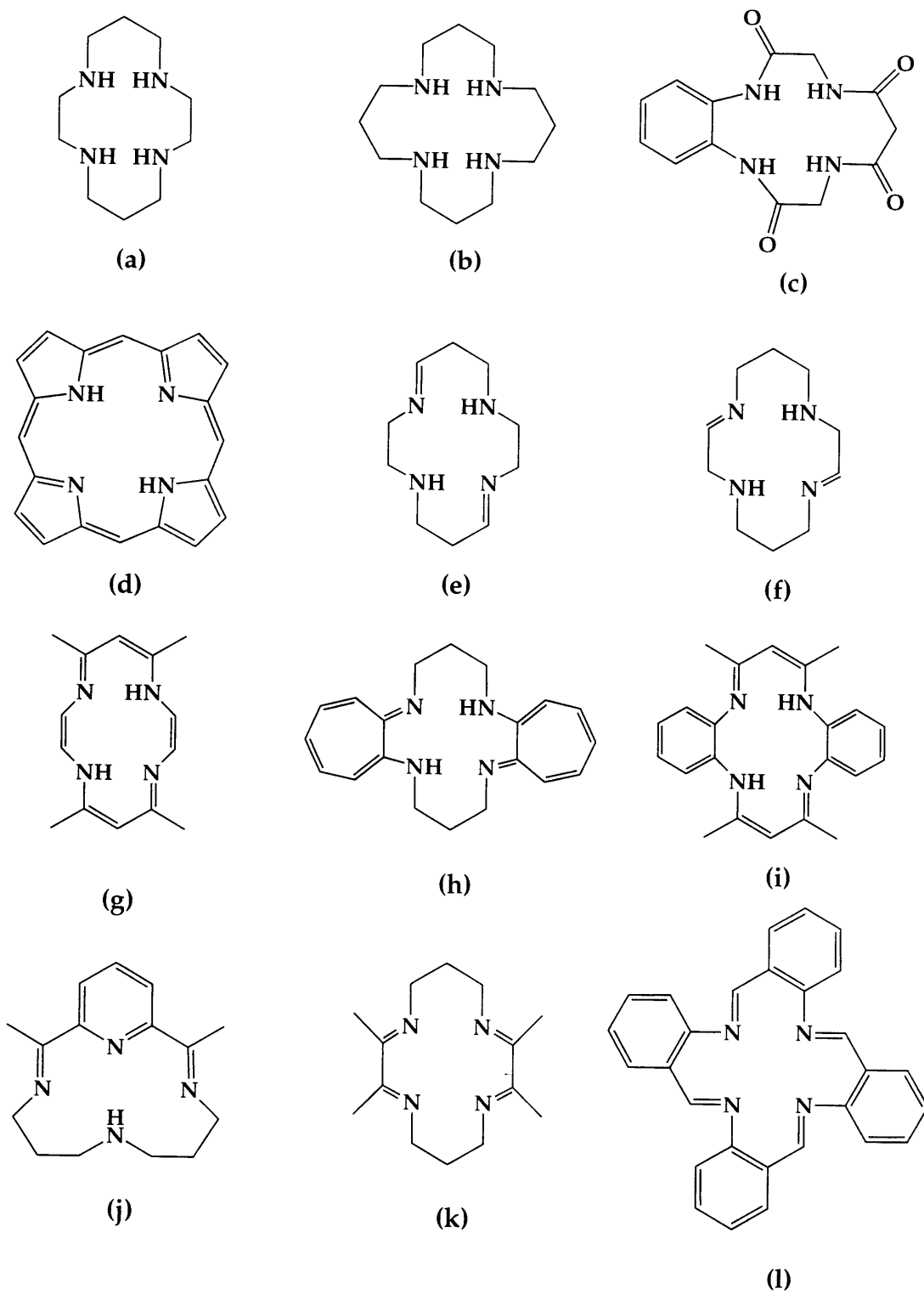
Figure 1.2. Examples of synthetic tetraazamacrocycles.
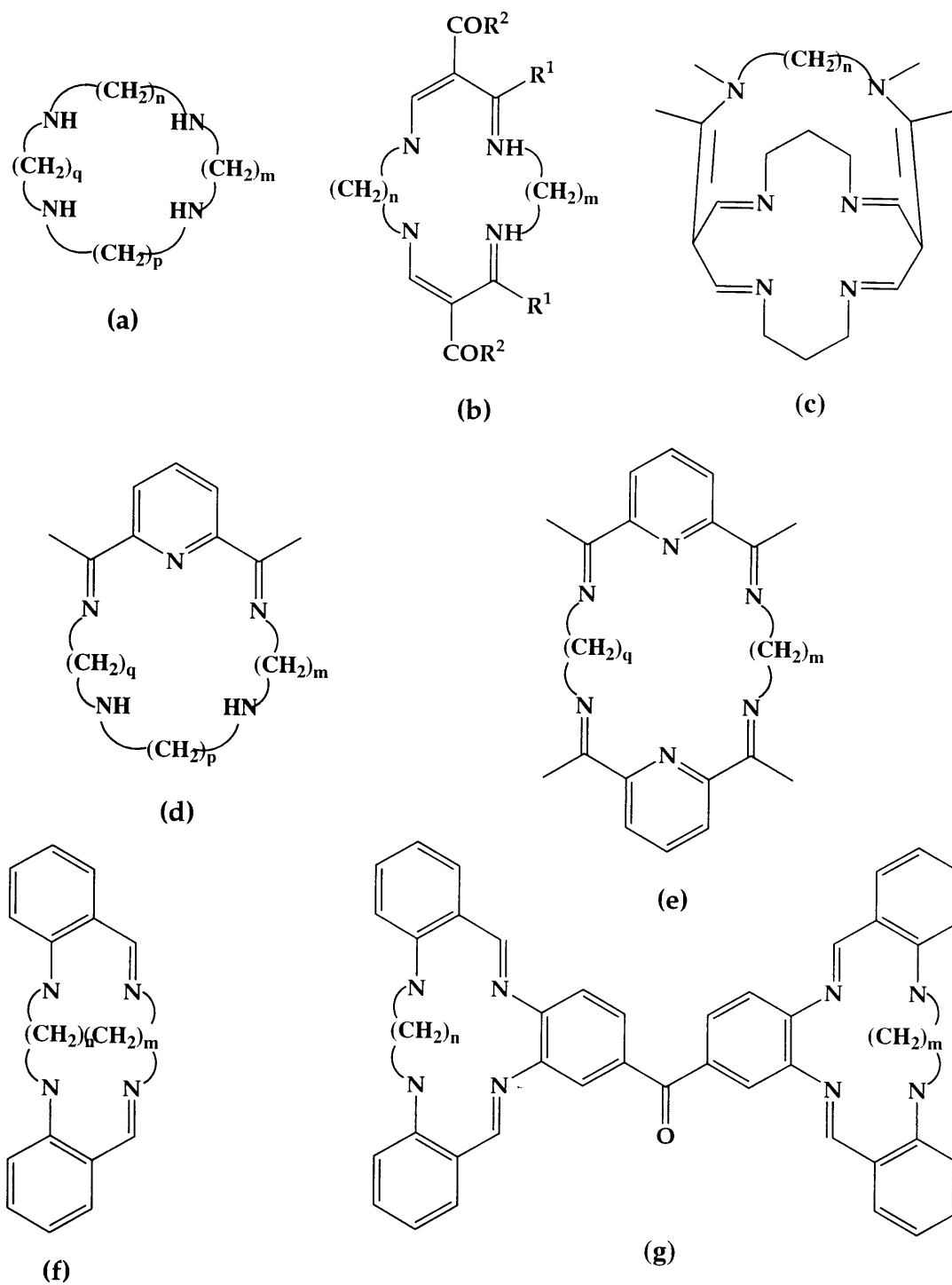
Figure 1.3. Examples of tetraazamacrocycles with methylene linker chains.
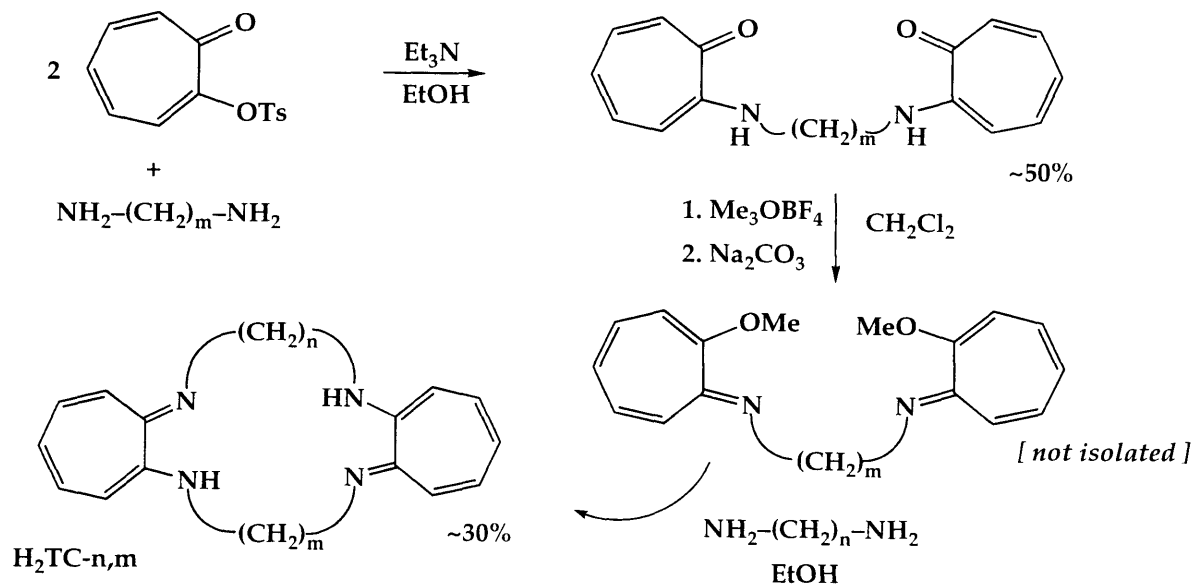
Figure 1.4. Synthesis of H₂TC-n,m, tropocoronand ligand.
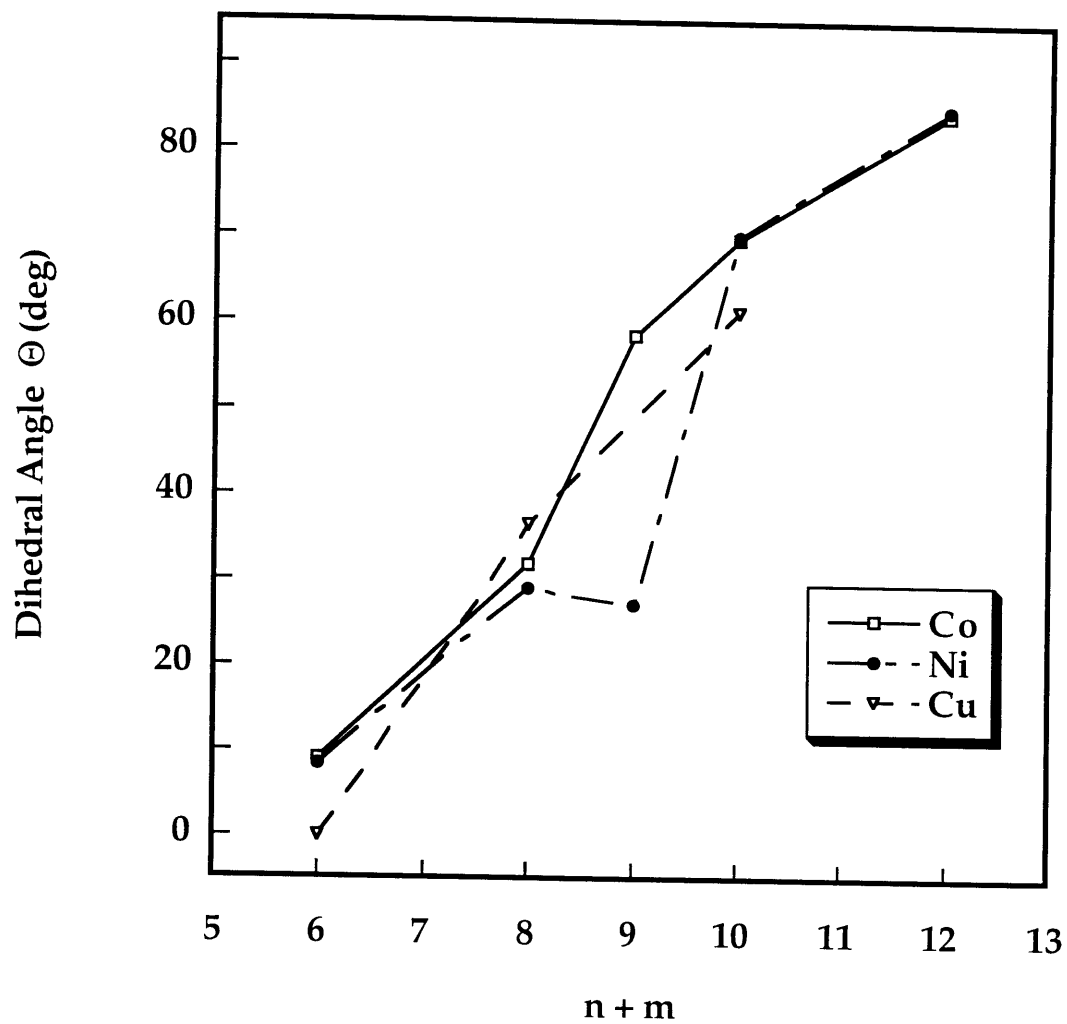
Figure 1.5. Plot of [M(TC-n,m)] dihedral angles Θ versus methylene linker chain lengths (n+m) for cobalt (squares) nickel (circles), and copper (triangles).

MONONUCLEAR

FOUR-COORDINATE

square planar ←——→ [structure] ←——→ tetrahedral

FIVE-COORDINATE

trigonal bipyramidal ←——→ square pyramidal

SIX-COORDINATE

octahedral ←——→ trigonal prism

DINUCLEAR
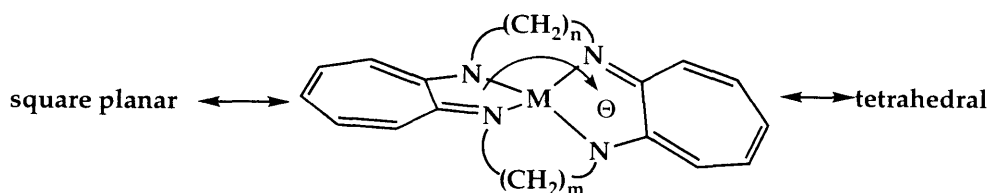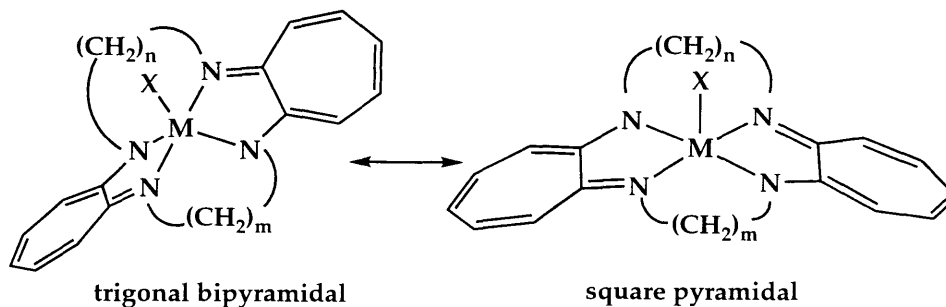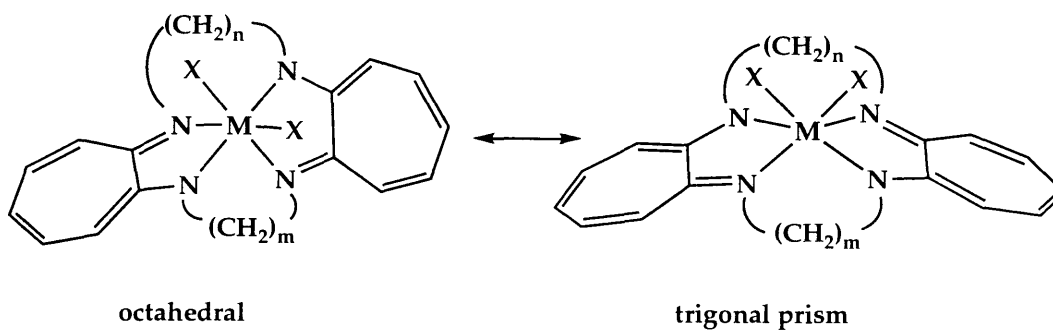
syn-dinuclear
bridged dinuclear ←——→ anti-dinuclear
open dinuclear
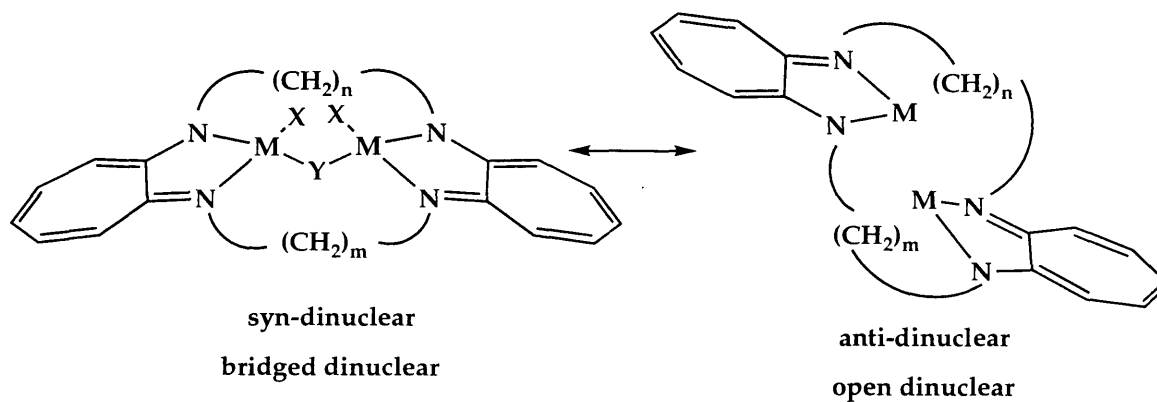
Figure 1.6. Examples of geometries and coordination number afforded with tropocoronand complexes.

Chapter 2

Zinc and Cadmium Tropocoronand Complexes

Introduction

The tropocoronand ligand, H_2TC-n,m, is a tetraazamacrocycle consisting of two aminotroponeiminate rings connected to each other through polymethylene linker chains of length m and n. Independent variation of n and m in the ligand synthesis has afforded tropocoronand macrocycles with ring sizes from 12 to 32.[1-3] Double deprotonation of the ligand provides a dianionic macrocycle capable of binding divalent transition metals to form the neutral complexes, [M(TC-n,m)]. Such complexes span the range of four-coordinate geometries from square-planar to tetrahedral.[4-6]
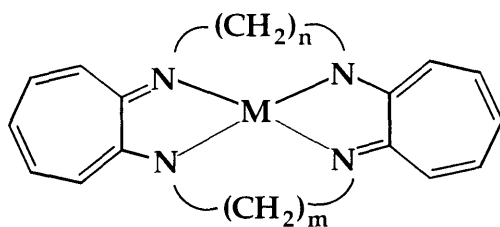
[M(TC-n,m)] tropocoronand

The larger the sum (n + m), the more a [M(TC-n,m)] complex is twisted from square-planar toward tetrahedral geometry. If no other structural perturbations occurred, as the number of methylene units increased, torsional strain within each linker chain would increase rapidly and destabilize the complex. To relieve the strain in the linker chains, the two seven-membered ring planes twist out of plane away from one another. The dihedral angle between the two five-membered chelate rings, Θ, measures the degree of twist from square-planar toward tetrahedral. When Θ is close to 0°, the two tropone rings and four macrocyclic nitrogen atoms are essentially coplanar forming a square-planar metal center. At the other extreme, when Θ approaches 90°, the two aromatic rings are mutually perpendicular and the metal is in a tetrahedral environment. Thus changing the tropocoronand linker chain lengths gives precise control of Θ and the resulting metal center coordination

environment. Previously we described in detail these geometric trends for the mononuclear Co(II),[6] Ni(II),[4] and Cu(II)[5] tropocoronand complexes, as summarized in Chapter 1 of this thesis.

Studies of the Co(II) and Ni(II) complexes further demonstrated that the electronic structure of the transition metal ion could affect the dihedral angle, in addition to the macrocycle ring size. For example, the TC-4,5 ligand adopts dihedral angles which differ by almost 30° for the Co(II) and Ni(II) complexes.[4,6] The d^7 Co(II) ion has a greater preference for tetrahedral than square-planar geometry compared to d^8 Ni(II), resulting in a larger Θ value for [Co(TC-4,5)]. Differences in ligand field stabilization energies therefore contribute to the larger tropocoronand ligand twist in [Co(TC-4,5)] versus [Ni(TC-4,5)].

In order to delineate more clearly electronic from geometric effects on Θ, we decided to examine closed shell systems, which permit the study of coordination geometries in the absence of ligand field effects arising from partially filled d-orbitals. The synthesis and structural characterization of the [Zn(TC-n,m)] series was therefore undertaken, the results of which are described in this chapter.

We were also interested to understand the extent to which differences in metal ion radii might affect the geometry of metal tropocoronands. Small differences in metal ion radii among the late transition metal ions lead only to relatively small structural changes[4-7], making it difficult to distinguish the effects of metal ion size from crystal packing forces, however. The [Cd(TC-n,m)] complexes were therefore prepared because of the large difference in ionic radii, 0.2 Å,[7] between Zn(II) and Cd(II), which affords an opportunity to measure accurately the effect of metal ion size on the ligand coordination properties.

In addition to these structural questions, the cyclic voltammetric studies of the [Co(TC-n,m)] complexes reported in Chapter 3 required knowledge about the

redox stability of the dianionic ligand. The [Zn(TC-n,m)] electrochemical properties were therefore investigated.

Experimental Section

General Information. All reactions were carried out in a nitrogen-filled glove box or by using standard Schlenk techniques. Pentane, toluene, and tetrahydrofuran were distilled from sodium benzophenone ketyl. Methylene chloride and pyridine were distilled from calcium hydride and acetonitrile was predried with P_2O_5 and then distilled from CaH_2. All solvents were distilled under dinitrogen. Tropocoronand ligands H_2TC-n,m were prepared as described.[2] [Zn(NCCH$_3$)$_4$](BF$_4$)$_2$ and [Cd(NCCH$_3$)$_6$](BF$_4$)$_2$ were prepared by substitution of $ZnCl_2$ or $CdCl_2$ for $CoCl_2$ in a literature synthesis for [Co(NCCH$_3$)$_4$](PF$_6$)$_2$.[8] All other reagents were obtained commercially and not purified further. UV-visible spectra were recorded on a Cary 1 E spectrophotometer. ^1H NMR spectra were measured on a Bruker AC 250 MHz spectrometer.

Synthetic Procedures. [Zn(py)(TC-3,3)]. A portion of H_2TC-3,3 (101.8 mg, 0.318 mmol) was dissolved in 12 mL of THF and two equiv of n-BuLi (0.794 mL, 0.635 mmol of 1.6 M solution in hexanes) were added with vigorous stirring. A deep orange solution was formed which lightened noticeably upon addition of one equiv of [Zn(NCCH$_3$)$_4$](BF$_4$)$_2$ (128 mg, 0.318 mmol). Several drops of pyridine then were added. After stirring for four h, the solvents were removed in vacuo and the yellow-orange solid was triturated twice with 2 mL of pentane. The crude product was extracted into 15 mL of CH_2Cl_2, which was filtered through Celite and concentrated to dryness. Dark gold needles (60 mg, 41% yield) suitable for X-ray crystallography were grown from cooling a supersaturated hot toluene solution of the compound to room temperature. ^1H-NMR (δ, ppm, C_6D_6) 1.72 (m, 4H, C-CH$_2$-C), 3.35 (m, 8H, N-CH$_2$-C), 6.31 (m, 4H, H$_c$/H$_b$-py), 6.41 (d, J = 11 Hz, 4H, H$_a$,), 7.06 (t,

1H, J = 10 Hz, H_c-py), 7.10 (t, 4H, J = 10 Hz, H_b), 8.04 (d, 2H, J = 6 Hz, H_a-py). UV-vis (THF) [λ_{max}, nm (ϵ_M, M^{-1} cm^{-1})] 294 (10,300), 389 (35,700), 435 (34,300), 456 (10,900). Anal. Calcd. for $ZnN_5C_{25}H_{27}$: C, 64.87; H, 5.88; N, 15.13. Found: C, 64.49; H, 5.84; N, 14.81.

[Zn(TC-3,4)]. A portion of H_2TC-3,4 (61.5 mg, 0.184 mmol) was dissolved in 8 mL of THF and doubly deprotonated with n-BuLi (0.230 mL, 0.368 mmol of 1.6 M solution in hexanes). One equiv of [$Zn(NCCH_3)_4$](BF_4)$_2$ (74.1 mg, 0.184 mmol) was added to the deep gold solution and allowed to stir for one h. The solvents were removed in vacuo, the crude product was triturated twice with 3 mL of pentane, and the dark orange product was extracted into CH_2Cl_2 and filtered through Celite. After removal of CH_2Cl_2 in vacuo, recrystallization from warm toluene gave dark orange needles suitable for X-ray crystallography in 20% yield (15.6 mg). ^{1}H-NMR (δ, ppm, C_6D_6) 1.63 (m, 6H, C-CH_2-C), 3.07 (m, 4H, N-CH_2-C), 3.38 (m, 4H, N-CH_2-C), 6.35 (t, J = 9 Hz, 2H, H_c), 6.50 (quart, 4H, H_a), 7.02 (t, J = 11 Hz, 4H, H_b). UV-vis (THF) [λ_{max}, nm (ϵ_M, M^{-1} cm^{-1})] 296 (11,100), 381 (42,000), 433 (24,800), 455 (14,900). Anal. Calcd. for $ZnN_4C_{21}H_{24}$: C, 63.40; H, 6.08; N, 14.08. Found: C, 62.97; H, 5.93; N, 13.92.

[Zn(TC-4,4)]. A portion of H_2TC-4,4 (129.0 mg, 0.370 mmol) was dissolved in 10 mL of THF and twice deprotonated with n-BuLi (0.48 mL, 0.768 mmol of 1.6 M solution in hexanes) at -30 °C. One equiv of $ZnCl_2$ (55.5 mg, 0.370 mmol) was added to the deep gold solution and allowed to stir for 4 h. The solvent was removed in vacuo and the yellow product extracted into CH_2Cl_2. Layering the concentrated solution with pentane produced 100.4 mg of yellow microcrystalline material (66% yield). Further recrystallization from hot toluene gave topaz needles suitable for X-ray crystallography. ^{1}H NMR (δ, ppm, C_6D_6) 1.66 (m, 8H, C-CH_2-C) 3.24 (m, 8H, N-CH_2-C) 6.32 (t, J = 9 Hz, 2H, H_c) 6.51 (d, J = 11 Hz, 4H, H_a) 6.96 (t, J = 11 Hz, 4H, H_b). UV-vis (THF) [λ_{max}, nm (ϵ_M, M^{-1} cm^{-1})] 293 (19,200), 381 (29,000), 433 (16,500), 457

(16,500). Anal. Calcd for $ZnN_4C_{22}H_{26}$: C, 64.16; H, 6.36; N, 13.60. Found: C, 64.23; H, 6.35; N, 13.51.

[Zn(TC-4,5)]. A portion of H_2TC-4,5 (200.0 mg, 0.551 mmol) was dissolved in 10 mL of THF and twice deprotonated with n-BuLi (0.69 mL, 1.103 mmol of 1.6 M solution in hexanes) at -30 °C. One equiv of $[Zn(NCCH_3)_4](BF_4)_2$ (222.4 mg, 0.551 mmol) was added to the deep gold solution and allowed to stir for 4 h. The solvents were removed in vacuo, the yellow/orange powder was triturated twice with 3 mL of pentane, and crude product extracted into CH_2Cl_2. After filtration through Celite, the solution was concentrated to dryness and recrystallization from a dilute hot toluene solution gave yellow/orange plates (42.1 mg, 18% yield) which were used for X-ray crystallography. ^1H NMR (δ, ppm, C_6D_6) 1.45 (m, 10 H, C-CH_2-C), 2.01 (m, 2 H, C-CH_2-C), 3.28 (m, 8H, N-CH_2-C) 6.32 (t, 2H, H_c) 6.49 (quart, 4H, H_a) 6.99 (m, 4H, H_b). UV-vis (THF) [λ_{max}, nm (ε_M, M^{-1} cm^{-1})] 296 (6,700), 381 (23,600), 434 (12,500), 460 (14,700). Anal. Calcd. for $ZnN_4C_{23}H_{28}$: C, 64.85; H, 6.63; N, 13.15. Found: C, 64.70; H, 6.55; N, 13.00.

[Zn(TC-5,5)]. A portion of H_2TC-5,5 (106.5 mg, 0.283 mmol) was dissolved in 10 mL of THF and twice deprotonated with n-BuLi (0.353 mL, 0.565 mmol of 1.6 M solution in hexanes) at -30 °C. One equiv of $ZnCl_2$ (42.4 mg, 0.283 mmol) was added to the yellow solution and allowed to stir for 4 h. Workup followed a similar procedure to that of [Zn(TC-4,4)]. After slow diffusion of pentane into a toluene solution, 57.3 mg of a yellow microcrystalline material (66% yield) were collected. Crystals suitable for X-ray crystallography were grown from hot toluene. ^1H NMR (δ, ppm, C_7D_8) 1.38 (m, 8H, C-CH_2-C) 1.93 (m, 4H, C-CH_2-C) 3.31 (m, 8H, N-CH_2-C) 6.22 (t, J = 9 Hz, 2H, H_c) 6.40 (d, J = 11 Hz, 4H, H_a) 6.95 (t, J = 11 Hz, 4H, H_b). UV-vis (THF) [λ_{max}, nm (ε_M, M^{-1} cm^{-1})] 293 (32,600), 380 (46,400), 436 (18,800), 463 (28,900). Anal. Calcd. for $ZnN_4C_{24}H_{30}$: C, 65.53; H, 6.87; N, 12.74. Found: C, 64.94; H, 6.72; N, 12.31.

[Zn(TC-6,6)]. A portion of H_2TC-6,6 (177.0 mg, 0.437 mmol) was dissolved in 10 mL of THF and doubly deprotonated with n-BuLi (590 μL, 0.944 mmol of 1.6 M in hexanes) at -30 °C. One equiv of $ZnCl_2$ (65.5 mg, 0.437 mmol) was added to the yellow solution and allowed to stir for 4 h. Workup followed a similar procedure to that for [Zn(TC-4,4)]. Recrystallization from boiling toluene gave deep yellow needles which were suitable for analysis and X-ray crystallography in 21% yield (43.1 mg). ^1H NMR (δ, ppm, CD_2Cl_2) 1.19 (m, 16H, C-CH_2-C) 2.05 (m, 8H, C-CH_2-C) 3.59 (m, 8H, N-CH_2-C) 6.08 (t, J = 9 Hz, 2H, H_c) 6.55 (d, J = 11 Hz, 4H, H_a) 6.84 (t, J = 11 Hz, 4H, H_b). UV-vis (THF) [λ_{max}, nm (ε_M, M^{-1} cm^{-1})] 287 (34,600), 383 (44,400), 432 (23,200), 457 (39,200). Anal. Calcd. for $ZnN_4C_{26}H_{34}$: C, 66.73; H, 7.32; N, 11.97. Found: C, 67.19; H, 7.54; N, 12.03.

[Cd(TC-4,4)]. A portion of H_2TC-4,4 (155.1 mg, 0.445 mmol) was dissolved in 10 mL of THF and doubly deprotonated with n-BuLi (556 μL, 0.890 mmol of 1.6 M in hexanes) at -30 °C. One equiv of [Cd(NCCH_3)_6](BF_4)_2 (237 mg, 0.445 mmol) was added to the yellow solution and allowed to stir for 4 h. Workup followed a similar procedure to that for [Zn(TC-4,4)]. Recrystallization from toluene gave dark orange rods in 26% yield (53.8 mg) which were suitable for analysis and X-ray crystallography. ^1H NMR (δ, ppm, C_6D_6) 1.61 (m, 8H, C-CH_2-C) 3.00 (m, 8H, N-CH_2-C) 6.34 (t, J = 9 Hz, 2H, H_c) 6.47 (d, J = 11 Hz, 4H, H_a) 7.03 (t, J = 11 Hz, 4H, H_b). UV-vis (CH_2Cl_2) [λ_{max}, nm (ε_M, M^{-1} cm^{-1})] 290 (3506), 386 (38,100), 435 (19,500), 461 (18,000). Anal. Calcd. for $CdN_4C_{22}H_{26}$: C, 57.58; H, 5.71; N, 12.21. Found: C, 57.17 ; H, 5.77 ; N, 11.97 .

[Cd(TC-4,5)]. A portion of H_2TC-4,5 (149.3 mg, 0.412 mmol) was dissolved in 10 mL of THF and doubly deprotonated with n-BuLi (515 μL, 0.823 mmol of 1.6 M in hexanes) at -30 °C. One equiv of [Cd(NCCH_3)_6](BF_4)_2 (219 mg, 0.412 mmol) was added to the yellow solution and allowed to stir for 4 h. Workup followed a similar procedure to that for [Zn(TC-4,4)]. Recrystallization from toluene gave dark orange

needles in 10.3% yield (20.0 mg) which were suitable for analysis and X-ray crystallography. ^{1}H NMR (δ, ppm, C_6D_6) 1.63 (m, 10H, C-CH$_2$-C) 3.05 (m, 4H, N-CH$_2$-C) 3.22 (m, 4H, N-CH$_2$-C) 6.33 (t, J = 9 Hz, 2H, H$_c$) 6.43 (quart, J = 11 Hz, 4H, H$_a$) 7.04 (t, J = 11 Hz, 4H, H$_b$). UV-vis (CH$_2$Cl$_2$) [λ_{max}, nm (ε_M, M^{-1} cm^{-1})] 286 (31,800), 361 (15,900), 381 (21,300), 437 (12,500), 464 (13,500). Anal. Calcd. for CdN$_4$C$_{23}$H$_{28}$: C, 58.42; H, 5.97; N, 11.85. Found: C, 58.42; H, 5.95; N, 11.57.

[Cd(TC-5,5)]. A portion of H$_2$TC-5,5 (74.6 mg, 0.198 mmol) was dissolved in 15 mL of THF and doubly deprotonated with n-BuLi (248 µL, 0.396 mmol of 1.6 M in hexanes) at -30 °C. One equiv of [Cd(NCCH$_3$)$_6$](BF$_4$)$_2$ (105 mg, 0.198 mmol) was added to the yellow solution and allowed to stir for 4 h. Workup followed a similar procedure to that for [Zn(TC-4,4)]. Recrystallization from toluene gave orange needles in 33% yield (31.8 mg) which were suitable for analysis and X-ray crystallography. ^{1}H NMR (δ, ppm, C_6D_6) 1.37 (m, 12H, C-CH$_2$-C) 3.24 (m, 8H, N-CH$_2$-C) 6.31 (t, J = 9 Hz, 2H, H$_c$) 6.40 (d, J = 11 Hz, 4H, H$_a$) 7.02 (t, J = 11 Hz, 4H, H$_b$). UV-vis (CH$_2$Cl$_2$) [λ_{max}, nm (ε_M, M^{-1} cm^{-1})] 291 (16,600), 385 (46,000), 440 (18,200), 466 (23,200). Anal. Calcd. for CdN$_4$C$_{24}$H$_{30}$: C, 59.20; H, 6.21; N, 11.51. Found: C, 59.02; H, 6.03; N, 11.63.

[Cd(TC-6,6)]. A portion of H$_2$TC-6,6 (96.6 mg, 0.239 mmol) was dissolved in 15 mL of THF and doubly deprotonated with n-BuLi (298 µL, 0.477 mmol of 1.6 M in hexanes) at -30 °C. One equiv of [Cd(NCCH$_3$)$_6$](BF$_4$)$_2$ (127 mg, 0.234 mmol) was added to the yellow solution and allowed to stir for 4 h. Workup followed a similar procedure to that for [Zn(TC-4,4)]. Recrystallization from boiling toluene gave deep yellow needles in 28% yield (27.6 mg) which were analytically pure and suitable for X-ray crystallography. ^{1}H NMR (δ, ppm, C_6D_6) 0.98 (m, 4H, C-CH$_2$-C) 1.17 (m, 4H, C-CH$_2$-C) 1.44 (m, 4H, C-CH$_2$-C) 1.91 (m, 4H, C-CH$_2$-C) 3.46 (m, 8H, N-CH$_2$-C) 6.26 (t, J = 9 Hz, 2H, H$_c$) 6.56 (d, J = 11 Hz, 4H, H$_a$) 6.94 (t, J = 11 Hz, 4H, H$_b$). UV-vis (CH$_2$Cl$_2$)

[λ_{max}, nm (ε_M, M^{-1} cm^{-1})] 290 (16,900), 387 (34,700), 437 (19,000), 463 (25,000). Anal. Calcd. for CdN$_4$C$_{26}$H$_{34}$: C, 60.64; H, 6.65; N, 10.88. Found: C, 60.50; H, 6.71; N, 10.85.

X-ray Crystallography. Single crystal diffraction data were collected on either an Enraf-Nonius CAD4 four-circle or a Siemens-CCD diffractometer. The general procedures for data collection and reduction with each machine are given below followed by information on structure solutions and refinement. Details of crystal growth are given in the experimental section above. Important crystallographic information for each complex including refinement residuals are reported in Table 2.1 for the zinc(II) tropocoronands and the same information is present in Table 2.2 for the cadmium(II) tropocoronands. Final positional and isotropic thermal parameters are listed in Tables 2.3 - 2.12.

Intensity data collected on an Enraf-Nonius CAD-4 diffractometer were obtained with graphite monochromated MoKα (λ = 0.71073 Å) radiation and techniques previously described.[9] Single crystals were mounted from Exxon Paratone-N on the ends of quartz fibers and cooled to the temperatures listed in Tables 2.1 and 2.2. A preliminary diffraction study of 25 reflections with 20 < 2Θ < 25° was used to determine each unit cell. Crystal quality was determined to be acceptable by four open-counter ω-scans and axial photographs, which also confirmed the choice of Laue class. After data collection, psi scans were obtained for an empirical absorption correction. Data were corrected for Lorentz and polarization effects.

The Siemens CCD X-ray diffraction system is controlled by a pentium-based PC running the SMART software package.[10] Crystals were mounted on the three-circle goniometer with χ fixed at +54.74°. Low temperatures, ~ -80 °C, were maintained with a Siemens LT-2A nitrogen cryostat, calibrated with a copper-constantin thermocouple. The diffracted graphite-monochromatized MoKα radiation (λ = 0.71073 Å) was detected on a phosphor screen with a charged coupled

device (CCD) operating at -54 °C held at a distance of 6.0 cm from the crystal. The detector has an array of 512 x 512 pixels, with a pixel size of approximately 120 microns. The detector centroid and crystal-to-detector distance were calibrated from a least-squares analysis of the unit cell parameters of a carefully centered ylid test crystal. After a crystal was centered optically within the X-ray beam, a series of 20 data frames varying by 0.3° increments in ω were collected and repeated at two additional different 2Θ and ϕ values to determine a preliminary unit cell. All data frames were collected as the sum of two five-second exposures and non-correlating events were eliminated to correct for high-energy background photons. A correction for the background detector current was also applied to the frames, and a small offset was added to all of the individual pixel values to prevent any statistical bias induced by truncating negative values to zero. Crystal quality was determined by plotting several reflections at 0.3° intervals of ω and crystals were chosen for data collection that had a majority of peaks with widths at half height of less then 1.5°. Reflections with $I > 20\sigma(I)$ from the 60 data frames were used to calculate a preliminary unit cell.

For the collection of the intensity data, the detector was positioned at a 2Θ value of -25° and the intensity images were measured at 0.3° intervals of ω for ten seconds each. The data frames were collected in three distinct shells which together measured more than 1.3 hemispheres of intensity data with maximum 2Θ values as listed in Tables 2.1 and 2.2. For the first shell, the crystal was positioned at $\phi = 0°$ and $\omega = -28°$ and a set of 606 frames was collected. A series of 435 frames was collected in the second shell with a starting position of $\phi = 90°$ and $\omega = -28.0°$. The third shell of 230 frames was collected at $\phi = 180°$ and $\omega = -28.00°$. The initial 50 frames of the first data shell were recollected at the end of data collection to check for crystal decay.

Raw data were integrated during data collection with the SAINT[11] program package on a Silicon Graphics Indy workstation. The background frame

information was updated according to eq 1, where B' is the update pixel value, B is the start pixel value and C is the pixel value in the current frame. The orientation

$$B' = (7B + C)/8 \qquad\qquad (1)$$

shifts were computed over a span of 16 frames in order to reduce any large shifts induced by poor statistics. The integration was also corrected for spatial distortions induced by the detector and pixels that resided outside of the detector active area or behind the beam stop were masked during frame integration. Integrated intensities for the three data shells were merged to one reflection file. Reflection rejection was based on the disagreement between the intensity of the reflection and the average intensity of the symmetry equivalent reflections. In the case of strong reflections ($I > 99\ \sigma(I)$) which contained only two equivalent reflections, the larger of the two was retained.

Structure Solution and Refinement. Structures were solved with the direct methods package SIR-92, an updated version of SIR-88[12] and a part of the TEXSAN[13] package of programs, which typically afforded positions for the majority of the non-hydrogen atoms. The remaining atoms were found from the resulting difference Fourier maps and refined by Fourier and full matrix least-squares techniques. For acentric space groups, refinements were performed isotropically with both enantiomorphs and the one with the smallest residuals chosen. Non-hydrogen atoms were refined anisotropically except as noted. All hydrogen atoms were generated at calculated positions and allowed to ride on their corresponding carbon atoms ($d_{C-H} = 0.95$ Å, $B_H = 1.2\ B_C$). Problems with individual structures are reported in the Results section.

Electrochemistry. Cyclic voltammetric measurements were performed under a nitrogen atmosphere using an EG&G Model 263 Potentiostat. A reference electrode consisting of a silver wire in a 0.1 M $AgNO_3$ in acetonitrile solution was used[14] for which the ferricinium/ferrocene potential was +0.20 V in CH_2Cl_2 and

+0.10 V in THF. A platinum wire (0.02 in.) was used as an auxiliary electrode and a 1.75 mm^2 platinum disc as the working electrode. Solute samples were typically 2 mM in [Zn(TC-n,m)] and 0.5 M solutions of (n-Bu$_4$N)(PF$_6$) were used.

Results

Syntheses. In our initial work on metal tropocoronands, the [Ni(TC-n,m)][4] and [Cu(TC-n,m)][5] complexes were prepared from reactions of the neutral ligand with the appropriate metal acetate in air. This procedure was not successful with [Zn(OAc)$_2$]·2H$_2$O because, upon addition of the metal salt to the neutral ligand, dark brown solutions formed from which no complexes could be isolated. Addition of excess triethylamine to neutralize the acetic acid did not improve the results. Thus the zinc(II) and cadmium(II) complexes were prepared under an inert atmosphere, analogous to the oxidatively sensitive cobalt(II) tropocoronands.[6] The procedure reported above gives the dark orange/deep yellow zinc(II) and cadmium(II) compounds in moderate yields. The complexes [Zn(TC-n,m)], n + m = 7, 8, 9, 10, 12 and [Cd(TC-n,m)], n + m = 8, 9, 10, 12, were readily synthesized from MX$_2$ and Li$_2$TC-n,m followed by extraction of the product into CH$_2$Cl$_2$ to remove LiX and recrystallization from toluene. The smallest macrocycles in these series define the lower limit of tropocoronand macrocycle size that can accommodate a four-coordinate complex for each metal. This phenomenon is discussed in detail below.

A toluene-soluble species could not be extracted from the crude reaction mixture of Li$_2$TC-3,3 and ZnCl$_2$, however. From THF we obtained a poor quality structure of the five-coordinate [Zn(LiCl)(TC-3,3)]·3THF species[15] with chloride occupying the axial position of a square pyramid. These results suggested that the Zn(II) ion was too large to fit in the N$_4$ plane of TC-3,3 but could be stabilized out-of-plane by a fifth ligand. A solvated starting material with a non-coordinating anion,

[Zn(NCCH$_3$)$_4$](BF$_4$)$_2$, was employed in the presence of pyridine to provide the extra ligand. In this manner, toluene-soluble [Zn(py)(TC-3,3)] was obtained.

Structural Characterization. Zinc. The structure of [Zn(py)(TC-3,3)] is square-pyramidal, (Figure 2.1) consistent with the other structurally characterized [MX(TC-3,3)] species discussed in Chapter 1. Final positional and isotropic thermal parameters for [Zn(py)(TC-3,3)] are listed in Table 2.3. The zinc atom sits on a crystallographic two-fold symmetry axis which relates the two aminotroponeiminate rings. The zinc atom is displaced from the N$_4$ plane by 0.57 Å and the Zn-py distance is 2.097(3) Å. The five-membered chelate rings are bent together by 15° in a saddle-type conformation to enforce good overlap between the macrocyclic nitrogen donors and the displaced zinc atom. The average Zn-N$_{TC}$ distance of 2.048(1) Å is listed in Table 2.13 together with other selected bond distances and angles.

The structures of the [Zn(TC-n,m)] complexes for n + m = 7, 8, 9, 10, 12 are presented in Figures 2.2 - 2.6. A plot of the dihedral angles Θ versus the total methylene linker chain length n + m is given in Figure 2.7 and Θ values for all structurally characterized [M(TC-n,m)] complexes are listed in Table 2.14. Selected distances and angles for individual zinc(II) tropocoronands are collected in Table 2.13 and linker chain torsion angles and deviations from the expected values are listed in Table 2.15.

As the macrocycle ring size increases in the [Zn(TC-n,m)] structures where n + m ≥ 7, the dihedral angles increase monotonically with the increase in (n + m), as plotted in Figure 2.7. The dihedral angle in the [Zn(TC-4,4)] complex is 51.2°, that in [Zn(TC-4,5)] is 58.9°, and those in [Zn(TC-5,5)] and [Zn(TC-6,6)] are 65.0° and 84.4°, respectively. These values are generally similar to those in the previously characterized [M(TC-n,m)] species. The dihedral angle of the [Zn(TC-4,4)] complex is 15° larger than the corresponding angle in any of the analogous Co(II), Ni(II), or

Cu(II) complexes, but Θ values in the more tetrahedral Zn complexes show little deviation those in the from analogous Co, Ni, or Cu centers, as shown in Table 2.14. The TC-4,5 Θ values are virtually identical for Co and Zn and those for TC-5,5 and TC-6,6 complexes span narrow ranges of 8.8° and 0.8° respectively. The chief difference between Zn and Co/Ni is the discontinuous changes in Θ versus (n + m) for [Co(TC-n,m)] and [Ni(TC-n,m)], depicted in Figure 2.8, due to spin-state transitions from low to high spin and attendant increases in LFSE. The change in zinc dihedral angles is continuous with n + m due to the lack of spin-state change, similar to Cu as shown in Figure 2.9.

Accompanying the increase in dihedral angle in the [Zn(TC-n,m)] series is a decrease in the average Zn-N distance. These distances are 2.02(2) Å for [Zn(TC-3,4)], 1.99(2) Å for [Zn(TC-4,4)], 1.99(1) Å for [Zn(TC-4,5)], 1.984(7) Å for [Zn(TC-5,5)] and 1.982(3) Å for [Zn(TC-6,6)]. For comparison, the average Zn-N distance in the acyclic complex [Zn(Ph$_2$ati)$_2$] is 1.98(1) Å.[16,17]

Cadmium. The structures of [Cd(TC-n,m)], n + m = 8, 9, 10, 12, are shown in Figures 2.10 - 2.13, respectively. Final positional and isotropic thermal parameters are listed in Tables 2.9 - 2.12. Selected distances and angles for the [Cd(TC-n,m)] series are collected in Table 2.16 and the ligand torsion angles with deviations from expected values in Table 2.17.

The dihedral angles observed for the [Cd(TC-n,m)] complexes are shown in Figure 2.7 and compared with those of the first-row metals in Table 2.14. The dihedral angles for [Cd(TC-n,m)], n + m = 9, 10, 12, are uniformly smaller than those of their Zn congeners. The crystal structure of [Cd(TC-4,4)] revealed pseudo square-planar geometry about the metal center with the cadmium center 0.11 Å out of the best plane defined by the four nitrogen atoms. This displacement is accompanied by a folding of the tropocoronand ligand similar to that seen in [Zn(py)(TC-3,3)]. The fold suggests that the TC-4,4 ligand is the smallest that can accommodate four-

coordinate cadmium and that smaller ligands would lead to [Cd(base)$_x$(TC-n,m)] complexes, x = 1 or 2, analogous to [Zn(py)(TC-3,3)].

The average Cd-N bond length decreases with the increase in n + m, exhibiting a similar trend to the [Zn(TC-n,m)] complexes. The average Cd-N distances are 2.25(1) Å for [Cd(TC-4,4)], 2.20(1) Å for [Cd(TC-4,5)], 2.191(1) Å for [Cd(TC-5,5)] and 2.188(7) Å for [Cd(TC-6,6)].

Spectroscopic Properties. The ^{1}H-NMR spectra of the Zn and Cd tropocoronands are quite similar to those of the diamagnetic [Ni(TC-n,m)] complexes reported earlier.[4] The aminotroponeiminate resonances, atom labels for which are shown in Figure 2.14, are readily distinguished from one another by the integrated intensities and splitting patterns. The H$_a$ protons appear as a doublet integrating for four protons and the H$_b$ and H$_c$ protons are present as triplets integrating for four and two protons respectively. Our new results include the first asymmetric [M(TC-n,m)] complexes studied by ^{1}H-NMR spectroscopy. Here the two H$_a$ and H$_b$ protons on the same aminotroponeiminate ring are no longer equivalent, but appear as two overlapping signals. The ^{1}H-NMR spectrum of [Zn(py)(TC-3,3)] shows resonances for bound pyridine distinct from those of the free ligand. Addition of excess pyridine results in only one signal indicating rapid exchange on the NMR time scale at room temperature.

The UV-vis spectral data summarized in Table 2.18 show strong intraligand charge transfer bands similar to those reported for other tropocoronand complexes. The only significant change through the series is in relative intensities of the two lowest energy charge transfer bands as the complexes shift in geometry from pseudo square-planar to tetrahedral. In the [Zn(TC-n,m)] series, the extinction coefficients for the absorbance near 434 nm decrease from 34,300 to 23,200 M^{-1}cm^{-1} in [Zn(py)(TC-3,3)] and those corresponding to the absorbance near 456 nm increase from 10,900 to 39,200 M^{-1}cm^{-1} in [Zn(TC-6,6)]. A similar pattern is present in the

[Cd(TC-n,m)] complexes. The absorption intensity at 435 nm decreases from $\varepsilon =$ 19,500 $M^{-1}cm^{-1}$ in [Cd(TC-4,4)] to 19,000 $M^{-1}cm^{-1}$ in [Cd(TC-6,6)] and the extinction coefficient for the 461 nm absorbance increases from 18,000 $M^{-1}cm^{-1}$ in [Cd(TC-4,4)] to 25,000 $M^{-1}cm^{-1}$ in [Cd(TC-6,6)].

Electrochemistry. Cyclic voltammetric studies on [Zn(TC-n,m)] revealed no reversible redox behavior. For each ligand, no irreversible reductions were observed within the solvent window of THF (0.4 < E° < - 3.0 V). Under oxidizing potentials, an irreversible wave was observed at approximately 0.50 volts versus Cp_2Fe^+/Cp_2Fe. Representative cyclic voltammograms are shown for [Zn(TC-4,4)] in Figure 2.15. All other tropocoronand ligands behaved similarly.

Discussion

Synthesis. The procedures above produce the divalent zinc(II) and cadmium(II) complexes in low-to-moderate yields. The two series of compounds differ primarily in their solubility, the latter being notably less soluble in solvents such as toluene and fluorobenzene. The compounds are stable for short periods of time in the solid state in air, but the yellow-gold solutions of [M(TC-n,m)], M = Zn, Cd, and crystals in mother liquor decompose in air to dark brown heterogeneous mixtures in a few hours. One possible mechanism of decomposition for these complexes may be transfer of a proton from water by the Lewis acidic metal center to protonate the ligand with concomitant decomposition of the complex and formation of a metal hydroxide species.

Structural Properties. Most structurally characterized zinc(II) complexes have either square-planar or tetrahedral geometry. Since d^{10} Zn(II) ion has no geometric preferences based on its electronic structure the complex geometries are determined solely by the steric demands or conformational restrictions of the ligands.

The majority of structurally characterized square-planar ZnN_4 complexes are Zn(II) porphyrins,[18-22] although non-porphyrin square-planar Zn(II) porphycene complexes have also been prepared.[23] The other structurally characterized four-coordinate ZnN_4 complexes have essentially tetrahedral geometries.[24-29] A few macrocyclic tetrahedral complexes are known such as those with triazacyclononane,[30] but the majority of tetrahedral ZnN_4 complexes have acyclic ligands. A rare structurally characterized example of a ZnN_4 complex with a geometry intermediate between square-planar and tetrahedral is $[Zn(Ph_2ati)_2]$ in which the dihedral angle between the two chelate rings is 66.5°.[16,17] This structure seems to be determined by the geometry required for minimal interaction between the bulky phenyl substituents.

The $[Zn(TC-n,m)]$ complexes nicely demonstrate the tuning potential of the tropocoronand macrocycle by affording several members with geometries between square-planar and tetrahedral. A rigorously square-planar four-coordinate complex was not obtained, however. Extrapolation of the plot of Θ versus n + m for $[Zn(TC-n,m)]$ to the n + m = 6 point predicts a dihedral angle of approximately 25°. This value would require a remarkable distortion for the TC-3,3 ligand, which has never been observed with a twist angle greater than 9°. The synthesis and structural characterization of $[Zn(py)(TC-3,3)]$ in which zinc is displaced by 0.57 Å from the N_4 plane and the fold angle is 15° further underscores the reason why a four-coordinate $[Zn(TC-3,3)]$ complex cannot be made. The Zn(II) ion does not fit in the macrocycle hole and the rigid TC-3,3 ligand cannot twist; it can only fold, upon coordination of a fifth ligand to accommodate the metal ion. Addition of one more methylene unit to the TC-3,3 tropocoronand enlarges the macrocycle hole and sufficiently reduces the torsional strain to form a four-coordinate zinc complex, $[Zn(TC-3,4)]$. The Zn atom is still displaced from the N_4 plane, but only by 0.012 Å, and the two seven-membered rings are twisted relative to one another at a dihedral angle of 35.5°. The

torsion angles for the C16 - C17 and C19 - C20 deviate from their predicted values by 50° and 22.6°, showing that substantial strain exists in these linker chains. The strained [Zn(TC-3,4)] complex, and our inability to prepare [Zn(TC-3,3)], demonstrate that the TC-3,4 macrocycle is the smallest tropocoronand ligand which will accommodate four-coordinate zinc.

The [Zn(TC-4,4)] complex is four-coordinate, similar to the Zn porphyrins but is not square-planar because the torsional strain in the linker chains forces the ligand to twist. Although this molecule has a five-seven-five-seven chelate pattern, in contrast to the four six-membered chelate rings in metalloporphyrins, this difference is not responsible for the ligand twist. A square-planar Zn porphycene complex with a five-seven-five-seven chelate ring set has been characterized with the Zn atom displaced from the N_4 plane by only 0.05 Å.[23] The porphycene ligand
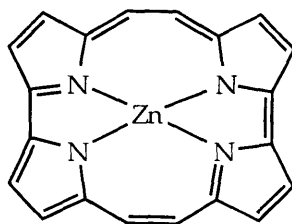
zinc porphycene

has all sp^2 hybridized carbon atoms which are completely conjugated and enforce planarity on the macrocycle. The saturated linker chains in [Zn(TC-4,4)] generate a larger macrocyclic hole and cause the ligand to twist. Such contraction of the "circumference" of a macrocyclic ring upon oxidation has been observed in other systems.[31]

The fact that the [Zn(TC-4,4)] dihedral angle is 20° larger than that of any other [M(TC-n,m)] complex is another manifestation of how the slightly larger Zn(II) ionic radius significantly affects the value of Θ. The remaining Θ values for [Zn(TC-4,5)], [Zn(TC-5,5)], and [Zn(TC-6,6)] are very similar to those for the other first-row [M(TC-n,m)] complexes listed in Table 2.14. These larger macrocycles bind much larger

metal ions, such as cadmium (r = 0.92 Å), without substantial strain and therefore show little effect of subtle changes in ionic radii. Large changes in metal ionic radii produce significant geometric changes as discussed below, however.

Cadmium(II), like zinc(II), has no electronically preferred geometries. Most of its complexes are six-coordinate, not four-coordinate, however. A recent search of the Cambridge Structural Database[32] found 184 complexes with cadmium and four nitrogen donors but only nine had just four ligands. The larger Cd(II) ion, 0.92 Å versus 0.74 Å in Zn(II),[7] readily accommodates two or more additional ligands. The only macrocyclic CdN_4 species reported to date are porphyrins investigated as clathrate hosts.[21] These complexes are rigorously square-planar, and no non-planar macrocyclic complexes of Cd have been reported, although a few acyclic tetrahedral CdN_4 species exist.[33-35] No macrocyclic complexes with geometries intermediate between square-planar and tetrahedral have been observed.

The ability of the tropocoronand ligand to tune the geometric properties and stabilize unusual metal coordination spheres is nicely manifest in the [Cd(TC-n,m)] complexes. The pseudo-tetrahedral [Cd(TC-n,m)] complexes all have smaller dihedral angles than the [Zn(TC-n,m)] homologues, however, as shown in Table 2.14 and Figure 2.7. The increased ionic radius of Cd(II) causes increases in the Cd-N over the Zn-N bond distance, and increases the α-to-ω separation, which is directly related to Θ. As the α–το–ω distance increases, torsional strain is relieved in the macrocycle and therefore less twist, as measured by Θ, is required to minimize the linker chain distortion for the same size macrocycle. Thus the [Cd(TC-n,m)] complexes have smaller twist angles than their zinc analogs. Thus, the average α–το–ω distance increases (Table 2.19) from 3.69 Å in [Zn(TC-4,5)] to 3.99 Å in [Cd(TC-4,5)] and Θ decreases by 10.3°. Between [Zn(TC-6,6)] and [Cd(TC-6,6)] the same distance increases from 4.49 Å to 4.76 Å and Θ is 4.4° smaller. For the TC-4,4 complexes, extension of the distance from 3.44 Å for Zn(II) to 3.76 Å with Cd(II)

reduces Θ, resulting in the small saddle-type fold of the macrocycle by 9.8° needed for [Cd(TC-4,4)].

The only [Cd(TC-n,m)] complex that is closer to square-planar than tetrahedral is [Cd(TC-4,4)]. Figure 2.7 shows a monotonic trend in Θ for n + m = 9, 10, 12 which if extrapolated to the n + m = 8 point, would suggest an angle of approximately 40° for the [Cd(TC-4,4)] complex. The ORTEP diagram for this complex in Figure 2.10 reveals that the ligand is twisted, but a detailed inspection of the structure reveals that it is also folded. The angle formed by Cd and the γ ring carbon atoms, C4-Cd-C11, is 9.8°, meaning that the dihedral angle between the two aminotroponeiminate rings is a consequence of both twisting and folding. Thus [Cd(TC-4,4)] was not included in the plot of Θ versus (n + m) in Figure 2.7 which describes only the twist angle.

The [Cd(TC-4,5)] complex shown in Figure 2.11 has a dihedral angle of 48.5°, almost exactly half-way between square-planar, Θ = 0°, and tetrahedral, Θ = 90°, geometries. Large thermal ellipsoids were observed for the central methylene linker carbon atoms C16, C21, and C22 which could not be modeled as disordered. Abnormal C-C distances among these atoms were also observed, Table 2.16, but the remaining structural parameters are unaffected. The [Cd(TC-5,5)] and [Cd(TC-6,6)] complexes have fold angles of 0.0° and 0.8°, respectively, consistent with less displacement of the cadmium center out of the N_4 plane (Table 2.20) and less folding.

The folding of the ligand in [Cd(TC-4,4)] also displaces the metal by 0.107 Å from the N_4 plane. This result, and the five-coordinate [Zn(py)(TC-3,3)] complex strongly suggests that [Cd(TC-3,3)] or [Cd(TC-3,4)] species could exist only if Cd were significantly displaced from the N_4 plane, which would occur upon binding of additional ligands, for example in the complexes analogous to the known [ZrX₂(TC-3,3)] species.[36] Pseudo-square-planar [Cd(TC-4,4)] is an important molecule because

it clearly demonstrates that the ligand twist is not the only mode of flexibility available to the tropocoronand macrocycle, and that twisting is not always required to relieve torsional strain.

The dihedral angle Θ between the aminotroponeiminate rings includes both tropocoronand twist and fold effects. These contributions can be discerned visually and distinguished quantitatively by changes in the α–to–ω distances as a function of increasing dihedral angle with reference to a perfectly planar ligand. In twisting the aminotroponeiminate rings rotate away from coplanarity, increasing the α–to–ω distance, and making the nitrogen atoms non-planar. When the ligand folds, the seven-membered rings bend toward each other, decreasing the α–to–ω distance and maintaining the N_4 square plane. These modes are shown schematically in Figure 2.16.

[Zn(py)(TC-3,3)] is unique among tropocoronand complexes because it is the first example of a divalent, first-row metal that does not form a square-planar complex with the TC-3,3 ligand. Several square-pyramidal $Zn(py)N_4$ complexes have been structurally characterized, however. Included are five-coordinate [Zn(py)porph] complexes, in which the average displacement of zinc out of the N_4 plane is 0.31 - 0.37 Å, less than the 0.54 Å value in [Zn(py)(TC-3,3)]. The Zn-pyridine distance in [Zn(py)porph] complexes ranges from 2.15 - 2.20 Å,[37] compared to 2.097(3) Å in [Zn(py)(TC-3,3)]. These differences are a consequence of the macrocycle hole size which is larger in the 16-membered porphyrins than in the 14-membered TC-3,3 ring. The larger macrocycle hole in porphyrin complexes affords weaker coordination of the axial base, less displacement of zinc out of the N_4 plane, and longer Zn-pyridine bond distances . The average $Zn-N_{TC}$ distance of 2.048(1) Å shows stronger electron donation from the TC ligand than from the porphyrin to zinc in [Zn(py)porph] complexes, where the average $Zn-N_{pyrrole}$ distance is 2.06 - 2.08 Å.[37]

Two other macrocyclic [Zn(base)N$_4$] complexes, [Zn(NR$_3$)(tmtaa)], R = Et, n-Pr, have been prepared[38] with the tmtaa ligand shown in Figure 1.2(i). These complexes were not structurally characterized but were assigned a square pyramidal geometry based on molecular modeling and ^{1}H-NMR spectroscopic studies. The four methyl groups of the tmtaa ligand would clash sterically with the phenyl ring ortho protons if the macrocycle were bent into a saddle conformation forcing the phenyl rings up and the methyl groups down.[39] Tmtaa is a 14-membered macrocycle with a five-six-five-six chelate ring pattern and nitrogens held coplanar like TC-3,3. It, too, is apparently too small to bind Zn(II) in the plane of the macrocycle. The fact that no [Zn(tmtaa)] complexes could be isolated parallels our results with the TC-3,3 tropocoronand.

The 0.54 Å displacement of Zn(II) from the N$_4$ plane in [Zn(py)(TC-3,3)] compared to much smaller values for the [M(TC-n,m)] complexes, M = Co, Ni, Cu, listed in Table 2.20, shows that the TC-3,3 ligand is sensitive to first-row metal ion radii. This effect explains the lack of [Zn(tmtaa)] complexes, vide supra, and lack of [Mn(tmtaa)] under conditions where [Fe(tmtaa)] and [Ni(tmtaa)] could be isolated. A similar effect of metal ion radius in complexes having the same ligand has been observed in tetraphenylporphyrin (TPP) systems. For first row [M(TPP)] species, the metal ions in [Cr(TPP)] and [Mn(TPP)] complexes were more displaced from the plane of the four pyrrolic nitrogens than analogous Fe, Co, Ni, Cu, or Zn complexes. Since Cr(II) and Mn(II) have larger ionic radii than the other first row metals,[7] the larger displacement of these ions from the porphyrin plane was attributed to their inability to fit in the macrocycle core.[18,40] Because the porphyrin is a 16-membered macrocycle like TC-4,4, both four coordinate Zn(porph) and five coordinate Zn(base)(porph) complexes can be prepared.

Table 2.20 shows the distance from the metal ion to the best N$_4$ plane for all the structurally characterized [M(TC-n,m)] complexes. This displacement is never

greater than 0.115 Å and larger displacements are observed only in the presence of a fifth ligand, e.g. [Zn(py)(TC-3,3)]. No displacements are observed for the [M(TC-5,5)] complexes because they all have a crystallographically imposed two-fold axis passing through the metal center. The Cu-N$_4$ distances are all quite small because this ion is the smallest of all those studied and fits well in the macrocycle hole. Notably in the [M(TC-3,3)] complexes, the Co(II) and Ni(II) species show larger displacements from the N$_4$ plane than Cu(II). As discussed above, the Zn(II) ion requires such a large displacement that the complex can only be isolated in the presence of a fifth ligand.

The Zn-N$_{avg}$ and Cd-N$_{avg}$ distances consistently decrease with increasing dihedral angle which is the opposite trend from that seen in the Co(II), Ni(II), and Cu(II) complexes. Insight into these trends is obtained from the related acyclic [M(R$_2$ati)$_2$] complexes, the M-N$_{avg}$ distances of which are taken as unconstrained for this type of metal-ligand bond. For example, in the [Cu(TC-n,m)] complexes, the Cu-N$_{avg}$ distance increases from 1.939(6) to 1.96(1) Å,[5] whereas the average Cu-N distance in [Cu(Ph$_2$ati)$_2$], is 1.937(5) Å.[16,17] This difference reflects the fact that the torsional demands of the larger macrocycles are incompatible with the small size of Cu(II). The smaller [Cu(TC-n,m)] complexes have Cu-N bond lengths closer to the unconstrained values.

The Zn-N$_{avg}$ distance in the acyclic complex [Zn(Ph$_2$ati)$_2$] is 1.98(1) Å,[16,17] which most closely matches the Zn-N$_{avg}$ distance of 1.982(3) Å in [Zn(TC-6,6)]. This result suggests that the Zn-N distances are closer to their ideal values in larger macrocycles rather than in smaller ones, as in the Cu series. Therefore a trend of M-N distances away from the ideal, unconstrained value is taken as an indicator of a poorer fit of the metal ion into the macrocycle. Cu(II) fits better into TC-3,3 and Zn(II) fits better into TC-6,6. No ati complexes with Cd(II) are available, but the trends in dihedral angles suggest that this metal ion would favor larger tropocoronand macrocycles.

In addition to the decrease in Θ and increase in M-N bond lengths in Cd(II) versus Zn(II) for the same ligand, the average value of angle α, (Tables 2.21 and 2.22 and Figure 2.14), increases from 115.6(8)° in the zinc(II) complexes to 117(1)° for those of cadmium(II) and the average β value decreases from 123(1)° to 121(1)° upon changing from Zn(II) to Cd(II). Both these trends are consistent with the larger Cd(II) ion forcing a wider angle within the five membered chelate ring at the expense of the angle adjacent to the linker chain. The remaining tropocoronand ligand parameters are quite consistent among the each of the metal complexes as well as between the members of the two series.

In the [M(TC-n,m)] complexes each linker chain forms a chelate ring involving an N-M-N unit afflicting a significant geometric constraint on the methylene carbon atoms. The chelate rings can potentially assume many different conformations, some more energetically favored than others. The restricted α–τo–ω distance in the aliphatic chelate rings is therefore the primary source of linker chain torsional strain, and these distances in the zinc(II) and cadmium(II) tropocoronands are reported in Table 2.19. The α–τo–ω distance in a particular [M(TC-n,m)] complex may restrict the chelate ring into a conformation that is more strained than in a complex with a different α–τo–ω distance. A recent study of Co(III) complexes with six-membered diamine chelate rings demonstrated that high energy conformations of the rings occurred when ligand steric restrictions prevented adoption of the energetically most-favored conformer.[41]

Increasing Θ in the [M(TC-n,m)] molecules, M = Co, Ni, Cu, increases the α–τo–ω distance and decreases the torsional strain in the linker chains. Therefore it might have been expected that, for a particular macrocycle with Zn and Cd, the complex with the longer α–τo–ω distance would show the least linker chain distortion. The structural data in Tables 2.15, 2.17, and 2.19 do not consistently support this hypothesis, however. The α–τo–ω distance in [Cd(TC-6,6)] is 0.18 Å

greater than in [Zn(TC-6,6)] and the average Cd torsion angles are smaller by 3°, as predicted. In contrast, the α–to–ω distance in [Zn(TC-5,5)] is 0.11 Å less than in [Cd(TC-5,5)], but the average distortion in the linker chains is 13.9° *less* in the C-C bonds and 5.4° *less* in the C-N bonds of [Zn(TC-5,5)] compared to [Cd(TC-5,5)]. Thus larger metal ions cause increased torsional strain at smaller α–to–ω distances because their size is better accommodated by greater distances and larger macrocyclic holes.

Cyclic voltammetric studies of the [Zn(TC-n,m)] complexes revealed ligand redox behavior in accord with their reactivity. The ligand is highly resistant to reduction, consistent with its stability in the 40% Na/Hg solutions used to generate Na[Co(TC-n,m)] species.[42] The irreversible oxidation waves observed in CH_2Cl_2 may reflect decomposition starting with the linker chains. Macrocycles with C-H bonds adjacent to nitrogen donors have been shown in some cases to be incompatible with highly oxidized metal centers.[43] Highly electrophilic Zr(IV) and Hf(IV) centers in tropocoronand complexes oxidize the linker chains[36] and it is reasonable to suppose that other oxidants would attack the linker chains. The tropocoronand macrocycles may thus not be isolable with transition metals in unusually high oxidation states, unless a mechanism for rapid reduction of the metal center is available apart from the ligand.

Conclusions

The existence and structures of mononuclear zinc(II) tropocoronands [Zn(TC-n,m)], n + m = 7, 8, 9, 10, 12, have afforded considerable insight into this class of coordination compound. The inability to obtain [Zn(TC-3,3)], the synthesis of [Zn(py)(TC-3,3)], and the structural analysis of [Zn(TC-3,4)], suggest that the Zn(II) radius, larger than that of Co(II), Ni(II), or Cu(II), prohibits formation of four-coordinate Zn(II) with a 14-membered tetraazamacrocycle in this class. Structures of

the larger zinc tropocoronands show significantly larger dihedral angles compared with copper analogs owing to the larger ionic radius of Zn(II) versus Cu(II). Monotonic changes of the twist angle Θ with increasing n + m in the [Zn(TC-n,m)] complexes contrast with the related Co(II) and Ni(II) complexes, consistent with the absence of LFSE or spin-state changes in Zn(II).

The [Cd(TC-n,m)] complexes, n + m = 8, 9, 10, 12, have dihedral angles Θ smaller than those of the Zn congeners. This result demonstrates that the increase in M-N distance with a larger metal diminishes Θ because of the increased α–to–ω distances. Displacement of Cd out of the N_4 plane in [Cd(TC-4,4)] revealed a saddle-type fold which had not been seen previously in [M(TC-n,m)] complexes. Fold and twist angles for [M(TC-n,m)] complexes both contribute to the dihedral angle between the aminotroponeiminate rings, but differ in their effect on the α–to–ω distance in the linker chains.

Cyclic voltammetric studies of [Zn(TC-n,m)] complexes demonstrated stability of the ligand to strongly reducing potentials, consistent with their observed chemical stability. An irreversible oxidation at only moderate oxidizing potentials demonstrated sensitivity to oxidizing media, consistent with the reactivity observed in some electrophilic Zr(IV) and Hf(IV) tropocoronand complexes.

References.

(1)   Imajo, S.; Nakanishi, K.; Roberts, M.; Lippard, S. J.; Nozoe, T. *J. Am. Chem. Soc.* **1983**, *105*, 2071-2073.

(2)   Zask, A.; Gonnella, N.; Nakanishi, K.; Turner, C. J.; Imajo, S.; Nozoe, T. *Inorg. Chem.* **1986**, *25*, 3400-3406.

(3)   Shindo, K.; Wakabayashi, H.; Ishikawa, S.; Nozoe, T. *Bull. Chem. Soc. Jpn.* **1993**, *66*, 2941-2948.

(4)   Davis, W. M.; Roberts, M. M.; Zask, A.; Nakanishi, K.; Lippard, S. J. *J. Am. Chem. Soc.* **1985**, *107*, 3864-3870.

(5)   Davis, W. M.; Zask, A.; Nakanishi, K.; Lippard, S. J. *Inorg. Chem.* **1985**, *24*, 3737-3743.

(6)   Jaynes, B. S.; Doerrer, L. H.; Liu, S.; Lippard, S. J. *Inorg. Chem.* **1995**, *34*, 5735-5744.

(7)   Shannon, R. D. *Acta Cryst.* **1976**, *A32*, 751-767.

(8)   Goldstein, A. S.; Drago, R. S. *Inorg. Chem.* **1991**, *30*, 4506-4510.

(9)   Carnahan, E. M.; Rardin, R. L.; Bott, S. G.; Lippard, S. J. *Inorg. Chem.* **1992**, *31*, 5193.

(10)   *SMART*; 4.0 ed.; Siemens Industrial Automation, Inc.: Madison, WI, 1995.

(11)   *SAINT*; 4.0 ed.; Siemens Industrial Automation, Inc.: Madison, WI, 1995.

(12)   Burla, M. C.; Camalli, M.; Cascarano, G.; Giacovazzo, C.; Polidori, G.; Spagna, R.; Viterbo, D. *J. Appl. Cryst.* **1989**, *22*, 389.

(13)   *TEXSAN: Single Crystal Analysis Software*; 2.0 ed.; Molecular Structure Corporation: Woodlands, TX, 1993.

(14)   Mann, C. K. In *Electroanalytical Chemistry*; Bard, A. J., Ed.; Marcel Dekker: New York, 1969; Vol. 3, pp 61.

(15)   [Zn(LiCl)(TC-3,3)]·3THF; $a = 12.288$ Å, $b = 14.482$ Å, $c = 18.152$ Å, $\alpha = 89.987°$, $\beta = 89.978°$, $\gamma = 90.045°$, $R = 0.20$, $R_w = 0.25$.

(16)   Laing, M., personal communication.

(17)   Laing, M. *A.C.A. (Summer)* **1976**, *76*.

(18)   Scheidt, W. R.; Kastner, M. E.; Hatano, K. *Inorg. Chem.* **1978**, *17*, 706-710.

(19)   Senge, M. O.; Eigenbrot, C. W.; Brennan, T. D.; Shusta, J.; Scheidt, W. R.; Smith, K. M. *Inorg. Chem.* **1993**, *32*, 3134-3142.

(20)   Byrn, M. P.; Curtis, C. J.; Khan, S. I.; Sawin, P. A.; Tsurumi, R.; Strouse, C. E. *J. Am. Chem. Soc.* **1990**, *112*, 1865-1874.

(21)   Byrn, M. P.; Curtis, C. J.; Goldberg, I.; Hsiou, Y.; Khan, S. I.; Sawin, P. A.; Tendick, S. K.; Strouse, C. E. *J. Am. Chem. Soc.* **1991**, *113*, 6549-6557.

(22)   Byrn, M. P.; Curtis, C. J.; Hsiou, Y.; Khna, S. I.; Sawin, P. A.; Tendick, S. K.; Terzis, A.; Strouse, C. E. *J. Am. Chem. Soc.* **1993**, *115*, 9480-9497.

(23)   Vogel, E.; Koch, P.; Hou, X.-L.; Lex, J.; Lausmann, M.; Kisters, M.; Aukaloo, M. A.; Richard, P.; Guilard, R. *Angew. Chem., Int. Ed. Engl.* **1993**, *32*, 1600-1604.

(24)   Abbotto, A.; Alanzo, V.; Bradamante, S.; Pagani, G. A.; Rizzoli, C.; Calestani, G. *Gazz. Chim. Ital.* **1991**, *121*, 365-368.

(25)   Alsfasser, R.; Vahrenkamp, H. *Chem. Ber.* **1993**, *126*, 695-701.

(26)   Bremer, J.; Uhlenbrock, S.; Pinkerton, A. A.; Krebs, B. *Z. anorg. allg. Chem.* **1993**, *619*, 1183-1195.

(27)   Hartmann, F.; Klaui, W.; Kremer-Aach, A.; Mootz, D.; Strerath, A.; Wunderlich, H. *Z. anorg. allg. Chem.* **1993**, *619*, 2071-2076.

(28)   Lipkowski, J. *J. Coord. Chem.* **1990**, *22*, 153-158.

(29)   Pickardt, J.; Gong, G.-T.; Wischnack, S.; Steinkopff, C. *Z. Naturforsch.* **1994**, *49b*.

(30)   Alcock, N. W.; Benniston, A. C.; Moore, P.; Pike, G. A.; Simon, C. R. *J. Chem. Soc., Chem. Commun.* **1991**, 706-708.

(31)   Hancock, R. D.; Martell, A. E. *Chem. Rev.* **1989**, *89*, 1875-1914.

(32)   Allen, F. H.; Davies, J. E.; Galloy, J. J.; Johnson, O.; Kennard, O.; Macrae, C. F.; Mitchell, E. M.; Mitchell, G. F.; Smith, J. M.; Watson, D. G. *J. Chem. Info. Comp. Sci.* **1991**, *31*, 187-204.

(33)   Barr, D.; Edwards, A. J.; Raithby, P. R.; Rennie, M.-A.; Verhorevoort, K.; Wright, D. S. *J. Chem. Soc., Chem. Commun.* **1994**, 1627-1628.

(34)   Menabue, L.; Saladini, M. *J. Inorg. Biochem.* **1993**, *49*, 201-207.

(35)   Wirringa, U.; Roesky, H. W.; Noltemeyer, M.; Schmidt, H.-G. *Angew. Chem., Int. Ed. Engl.* **1993**, *32*, 1628-1630.

(36)   Scott, M. J.; Lippard, S. J., unpublished results.

(37)   Anderson, H. L.; Bashall, A.; Henrick, K.; McPartlin, M.; Sanders, J. K. M. *Angew. Chem., Int. Ed. Engl.* **1994**, *33*, 429-431.

(38)   Neves, D. R.; Dabrowiak, J. C. *Inorg. Chem.* **1976**, *15*, 129-134.

(39)   Cotton, F. A.; Czuchajowska, J. *Polyhedron* **1990**, *9*, 2553-2566.

(40)   Scheidt, W. R.; Reed, C. A. *Inorg. Chem.* **1978**, *17*, 710-714.

(41)   DaCruz, M. F.; Zimmer, M. *Inorg. Chem.* **1996**, *35*, 2872-2877.

(42)   Jaynes, B. S.; Ren, T.; Masschelein, A.; Lippard, S. J. *J. Am. Chem. Soc.* **1993**, *115*, 5589-5599.

(43)   Collins, T. J. *Acc. Chem. Res.* **1994**, *27*, 279-285.

Table 2.1. Experimental Details of the X-ray Diffraction Studies of Zinc Tropocoronand Complexes.

	[Zn(py)(TC-3,3)]	[Zn(TC-3,4)]	[Zn(TC-4,4)]
formula	$ZnN_5C_{25}H_{27}$	$ZnN_4C_{21}H_{24}$	$ZnN_4C_{22}H_{26}$
fw	462.89	397.83	411.85
cryst. syst.	monoclinic	monoclinic	orthorhombic
space group	C2/c	P2$_1$/c	$Fdd2$
a, Å	19.637(2)	10.552(2)	8.517(2)
b, Å	8.6418(7)	8.522(2)	19.012(2)
c, Å	13.551(1)	20.130(4)	46.316(2)
β, deg	108.598(1)	93.59(3)	
V, Å^3	2179.6(4)	1806.7(1)	7450(1)
Z	4	4	16
ρ_{calcd}, g/cm^3	1.41	1.46	1.46
T, K	188	193	213
μ(Mo Kα), cm^{-1}	11.50	13.72	13.25
transmission coeff	0.889 - 0.978	0.932 - 0.968	0.941 - 1.000
2θ limits, deg	3 - 56.6	3-46.5	3 - 50
data limits	+h±k±l	+h±k±l	+h+k+l
total no. of data	12024	7277	2642
no. of unique data[a]	5122	2746	2085
no. of parameters	142	260	243
R[b]	0.059	0.043	0.042
R_w[c]	0.057	0.065	0.046
largest final shift	0.0007	0.001	0.000
largest peak, e/Å^3	0.701	0.411	0.393

[a]Observation criterion: $I > 3\sigma(I)$. [b]$R = \Sigma | |F_o| - |Fc| | / \Sigma |F_o|$. [c]$R_w = [\Sigma w(|F_o| - |F_c|)^2/\Sigma w |F_o|^2]^{1/2}$, where $w = 1/\sigma^2(F)$ and $\sigma^2(F)$ is defined in Carnahan, E. M.; Rardin, R. L.; Bott, S. G.; Lippard, S. J. *Inorg. Chem.* **1992**, *31*, 5193.

Table 2.1. (con't.) Experimental Details of the X-ray Diffraction Studies of Zinc(II) Tropocoronand Complexes.

	[Zn(TC-4,5)]	[Zn(TC-5,5)]	[Zn(TC-6,6)]
formula	$ZnN_4C_{23}H_{28}$	$ZnN_4C_{24}H_{30}$	$ZnN_4C_{26}H_{34}$
fw	425.88	439.90	467.96
cryst. syst.	monoclinic	hexagonal	orthorhombic
space group	$P2/c$	$P6_122$	$P2_12_12_1$
a, Å	19.9053(2)	10.955(1)	10.647(2)
b, Å	9.3733(2)	10.956(1)	11.4173(9)
c, Å	22.0993(3)	30.622(4)	19.027(1)
β, deg	106.552(1)		
V, Å^3	3952.2(7)	3183 (1)	2312.8 (6)
Z	8	6	4
ρ_{calcd}, g/cm^3	1.41	1.38	1.34
T, K	188	177.1	197.6
μ(Mo Kα), cm^{-1}	12.60	11.76	10.83
transmission coeff	0.911 - 0.967	0.678 - 1.000	0.941 - 1.000
2θ limits, deg	3 - 56.6	3 - 50	3 - 55
data limits	+h±k±l	+h+k+l	+h+k+l
total no. of data	24762	1425	3346
no. of unique data^a	5705	1229	3019
no. of parameters	505	130	275
R^b	0.092	0.063	0.048
$R_w{}^c$	0.097	0.046	0.052
max shift/esd, final	0.003	0.003	0.000
largest peak, e/Å^3	0.277	0.541	0.385

^{a}Observation criterion: $I > 3\sigma(I)$. $^bR = \Sigma||F_o| - |Fc||/\Sigma|F_o|$. $^cR_w = [\Sigma w(|F_o| - |F_c|)^2/\Sigma w|F_o|^2]^{1/2}$, where $w = 1/\sigma^2(F)$ and $\sigma^2(F)$ is defined in Carnahan, E. M.; Rardin, R. L.; Bott, S. G.; Lippard, S. J. *Inorg. Chem.* **1992**, *31*, 5193.

Table 2.2. Experimental Details of the X-ray Diffraction Studies of Cadmium Tropocoronand Complexes.

	[Cd(TC-4,4)]	[Cd(TC-4,5)]	[Cd(TC-5,5)]	[Cd(TC-6,6)]
formula	$CdN_4C_{22}H_{26}$	$CdN_4C_{23}H_{28}$	$CdN_4C_{24}H_{30}$	$CdN_4C_{26}H_{34}$
fw	458.87	472.91	486.92	514.97
cryst. syst.	monoclinic	monoclinic	monoclinic	orthorhombic
space group	$P2_1/c$	$P2_1/n$	$C2/c$	$P2_12_12_1$
a, Å	10.2448 (9)	9.6688(5)	12.9224 (4)	11.1429 (10)
b, Å	19.4349 (18)	22.991(1)	17.0359 (5)	11.5325 (2)
c, Å	9.9038 (9)	10.3002(5)	9.5653 (3)	18.3954 (3)
β, deg	101.107 (10)	117.268(1)	97.562 (10)	
V, Å^3	1934.9(5)	2033.7(6)	2087.4(4)	2363.9(3)
Z	4	4	4	4
ρ_{calcd}, g/cm^3	1.575	1.54	1.553	1.447
T, K	188	188	188	188
μ(Mo Kα), cm^{-1}	11.44	10.91	10.69	9.40
transmission coeff	0.921 - 0.976	0.881 - 0.943	0.945 - 0.990	0.907 - 0.962
2θ limits, deg	3 - 46.5	3 - 56.6	3 - 46.5	3 - 46.5
data limits	+h ±k ±l	+h ±k ±l	+h ±k ±l	+h ±k ±l
total no. of data	7665	12509	7105	9700
no. of unique data[a]	2022	3173	1730	1843
no. of parameters	239	253	133	280
R^b	.070	0.082	.027	.029
$R_w{}^c$	.077	0.076	.040	.036
largest final shift	0.0001	0.004	0.0002	0.0004
largest peak, e/Å^3	0.736	1.25	0.564	0.567

[a]Observation criterion: $I > 3\sigma(I)$. [b]$R = \Sigma||F_o| - |F_c||/\Sigma|F_o|$. [c]$R_w = [\Sigma w(|F_o| - |F_c|)^2/\Sigma w|F_o|^2]^{1/2}$, where $w = 1/\sigma^2(F)$ and $\sigma^2(F)$ is defined in Carnahan, E. M.; Rardin, R. L.; Bott, S. G.; Lippard, S. J. *Inorg. Chem.* **1992**, *31*, 5193.

Table 2.3. Final Positional and Isotropic Thermal Parameters for [Zn(py)(TC-3,3)].[a]

atom	x	y	z	B(eq) Å^2 [b]
Zn(1)	0.5000	0.15717(5)	0.7500	1.903(10)
N(1)	0.3958(1)	0.2283(2)	0.6839(2)	2.18(5)
N(2)	0.4715(1)	0.2176(2)	0.8776(2)	2.16(5)
N(3)	0.5000	-0.0854(3)	0.7500	2.01(7)
C(1)	0.3638(1)	0.2883(3)	0.7478(2)	2.21(6)
C(2)	0.2987(1)	0.3739(3)	0.7103(2)	3.01(7)
C(3)	0.2543(1)	0.4351(3)	0.7615(3)	3.92(9)
C(4)	0.2577(2)	0.4284(4)	0.8642(3)	4.83(10)
C(5)	0.3130(2)	0.3653(4)	0.9441(3)	3.97(8)
C(6)	0.3776(1)	0.3024(3)	0.9427(2)	3.04(7)
C(7)	0.4059(1)	0.2699(3)	0.8607(2)	2.24(6)
C(8)	0.3643(1)	0.2450(3)	0.5720(2)	2.73(7)
C(9)	0.4046(1)	0.1501(3)	0.5137(2)	2.87(6)
C(10)	0.4781(1)	0.2119(3)	0.5167(2)	2.79(7)
C(11)	0.4408(1)	-0.1654(3)	0.7453(2)	2.77(6)
C(12)	0.4390(2)	-0.3237(4)	0.7456(3)	4.65(9)
C(13)	0.5000	-0.4024(6)	0.7500	5.8(2)

[a]Numbers in parentheses are estimated standard deviations of the last significant figure. See Figure 2.1 for atom labeling scheme. [b]$B_{eq} = 4/3\ [a^2\beta_{11} + b^2\beta_{22} + c^2\beta_{33} + 2ab\cos(\gamma)\beta_{12} + 2ac\cos(\beta)\beta_{13} + 2bc\cos(\alpha)\beta_{23}]$.

Table 2.4. Final Positional and Isotropic Thermal Parameters for [Zn(TC-3,4)].[a]

atom	x	y	z	B(eq) Å^2 [b]
Zn(1)	0.54282(5)	0.18898(6)	0.88816(3)	2.07(1)
N(1)	0.7117(4)	0.2779(5)	0.8636(2)	2.08(9)
N(2)	0.5651(4)	0.0784(5)	0.8021(2)	2.60(10)
N(3)	0.3493(4)	0.1745(5)	0.8816(2)	2.08(9)
N(4)	0.5079(4)	0.2030(4)	0.9844(2)	1.99(9)
C(1)	0.7564(4)	0.2241(6)	0.8081(2)	2.1(1)
C(2)	0.8733(5)	0.2728(7)	0.7853(2)	3.1(1)
C(3)	0.9407(5)	0.2333(8)	0.7303(3)	3.8(1)
C(4)	0.9087(6)	0.1327(7)	0.6783(3)	3.8(1)
C(5)	0.7966(6)	0.0518(7)	0.6700(3)	4.0(2)
C(6)	0.6942(6)	0.0445(6)	0.7088(2)	3.3(1)
C(7)	0.6685(5)	0.1091(5)	0.7710(2)	2.1(1)
C(8)	0.2947(4)	0.1778(5)	0.9392(2)	2.0(1)
C(9)	0.1619(5)	0.1725(6)	0.9434(3)	2.7(1)
C(10)	0.0847(5)	0.1634(6)	0.9960(3)	3.0(1)
C(11)	0.1152(5)	0.1553(6)	1.0633(3)	3.3(1)
C(12)	0.2364(5)	0.1608(6)	1.0934(3)	2.7(1)
C(13)	0.3515(5)	0.1784(6)	1.0652(2)	2.4(1)
C(14)	0.3880(4)	0.1891(5)	0.9988(2)	2.1(1)
C(15)	0.7909(5)	0.3866(6)	0.9053(2)	2.5(1)
C(16)	0.7374(5)	0.4069(6)	0.9726(2)	2.6(1)
C(17)	0.7332(5)	0.2527(6)	1.0117(2)	2.3(1)
C(18)	0.6058(5)	0.2214(6)	1.0387(2)	2.2(1)
C(19)	0.4549(5)	-0.0053(6)	0.7709(3)	3.2(1)
C(20)	0.3431(5)	0.1104(7)	0.7603(2)	2.9(1)
C(21)	0.2690(5)	0.1353(6)	0.8210(3)	2.7(1)

[a]Numbers in parentheses are estimated standard deviations of the last significant figure. See Figure 2.2 for atom labeling scheme. [b]$B_{eq} = 4/3\ [a^2\beta_{11} + b^2\beta_{22} + c^2\beta_{33} + 2ab\cos(\gamma)\beta_{12} + 2ac\cos(\beta)\beta_{13} + 2bc\cos(\alpha)\beta_{23}]$.

Table 2.5. Final Positional and Isotropic Thermal Parameters for [Zn(TC-4,4)][a]

atom	x	y	z	B(eq) Å^2 [b]
Zn(1)	-0.912207(4)	-0.315561(16)	-0.433	2.05(3)
N(1)	-0.90723(3)	-0.34497(10)	-0.60597(6)	1.5(2)
N(2)	-0.80943(3)	-0.31520(11)	-0.46609(6)	1.7(3)
N(3)	-0.94695(3)	-0.30291(11)	-0.22101(6)	1.7(2)
N(4)	-0.99922(3)	-0.29505(11)	-0.49456(7)	1.8(2)
C(1)	-0.84410(3)	-0.34794(11)	-0.66544(9)	1.5(3)
C(2)	-0.82835(3)	-0.36925(13)	-0.78004(8)	1.8(3)
C(3)	-0.76979(4)	-0.37557(13)	-0.86778(8)	2.1(3)
C(4)	-0.70559(4)	-0.36123(15)	-0.87546(9)	2.5(3)
C(5)	-0.68606(3)	-0.33826(15)	-0.7851(10)	2.7(3)
C(6)	-0.72093(3)	-0.32506(13)	-0.65853(9)	2.1(3)
C(7)	-0.78812(3)	-0.32870(12)	-0.59426(8)	1.5(3)
C(8)	-1.00664(4)	-0.28850(14)	-0.22054(8)	1.7(3)
C(9)	-1.03751(4)	-0.27899(14)	-0.07945(9)	2.3(3)
C(10)	-1.09547(5)	-0.26173(16)	-0.05252(9)	3.1(4)
C(11)	-1.14418(4)	-0.25001(15)	-0.1533(10)	3.1(4)
C(12)	-1.14610(4)	-0.25439(15)	-0.31157(9)	2.4(3)
C(13)	-1.10226(4)	-0.26960(14)	-0.40698(9)	2.2(3)
C(14)	-1.03805(4)	-0.28421(12)	-0.38307(8)	1.6(3)
C(15)	-0.96534(3)	-0.36165(12)	-0.66762(8)	1.9(3)
C(16)	-1.03618(4)	-0.35209(13)	-0.61012(8)	2.1(3)
C(17)	-1.06654(3)	-0.32445(15)	-0.67996(9)	2.6(3)
C(18)	-1.02173(4)	-0.29740(14)	-0.65584(8)	2.1(3)
C(19)	-0.75950(4)	-0.30000(13)	-0.36796(9)	2.5(3)
C(20)	-0.79279(4)	-0.29026(14)	-0.21626(8)	2.3(3)
C(21)	-0.82826(4)	-0.31417(14)	-0.11964(8)	2.4(3)
C(22)	-0.90484(4)	-0.30710(14)	-0.07808(8)	2.6(3)

[a]Numbers in parentheses are estimated standard deviations of the last significant figure. See Figure 2.3 for atom labeling scheme. [b]$B_{eq} = 4/3 \ [a^2\beta_{11} + b^2\beta_{22} + c^2\beta_{33} + 2ab \cos(\gamma)\beta_{12} + 2ac \cos(\gamma)\beta_{13} + 2bc \cos(\gamma)\beta_{23}]$

Table 2.6. Final Positional and Isotropic Thermal Parameters for [Zn(TC-4,5)]^a

atom	x	y	z	B(eq) Å$^{2\,b}$
Zn(1)	0.36867(4)	-0.1357(1)	0.74237(5)	1.71(2)
Zn(2)	0.12996(4)	-0.3795(1)	0.24667(4)	1.61(2)
N(101)	0.4291(3)	-0.2586(8)	0.8101(3)	1.9(2)
N(102)	0.3074(3)	-0.2701(7)	0.7643(4)	1.9(2)
N(103)	0.3532(3)	-0.0571(8)	0.6472(4)	1.9(2)
N(104)	0.4061(3)	0.0570(7)	0.7692(3)	1.7(1)
N(201)	0.1019(3)	-0.2572(8)	0.3129(3)	1.8(2)
N(202)	0.2008(3)	-0.2396(7)	0.2681(3)	1.9(2)
N(203)	0.0973(3)	-0.4620(7)	0.1513(3)	1.6(1)
N(204)	0.1048(3)	-0.5731(8)	0.2728(3)	1.8(2)
C(101)	0.4030(4)	-0.3576(10)	0.8413(4)	2.1(2)
C(102)	0.4403(4)	-0.4514(10)	0.8932(4)	2.2(2)
C(103)	0.4249(5)	-0.561(1)	0.9316(4)	2.6(2)
C(104)	0.3678(4)	-0.6088(10)	0.9345(4)	2.4(2)
C(105)	0.3102(4)	-0.555(1)	0.8967(4)	2.5(2)
C(106)	0.2958(4)	-0.446(1)	0.8470(5)	2.4(2)
C(107)	0.3324(4)	-0.3622(9)	0.8166(4)	1.8(2)
C(108)	0.3725(4)	0.078(1)	0.6441(4)	2.2(2)
C(109)	0.3678(4)	0.146(1)	0.5792(4)	2.3(2)
C(110)	0.3800(4)	0.287(1)	0.5639(5)	3.1(2)
C(111)	0.3995(4)	0.401(1)	0.6065(5)	3.0(2)
C(112)	0.4175(4)	0.4003(10)	0.6786(5)	2.9(2)
C(113)	0.4185(4)	0.2924(10)	0.7238(5)	2.5(2)
C(114)	0.4003(3)	0.1476(10)	0.7154(4)	1.7(2)
C(115)	0.4926(4)	-0.2032(10)	0.8413(4)	2.1(2)
C(116)	0.4952(4)	-0.1144(10)	0.9061(4)	2.4(2)
C(117)	0.4428(4)	-0.005(1)	0.8959(4)	2.5(2)
C(118)	0.4359(4)	0.110(1)	0.8400(5)	2.7(2)
C(119)	0.2383(4)	-0.2613(9)	0.7344(5)	2.1(2)
C(120)	0.2185(4)	-0.1766(10)	0.6670(5)	2.4(2)
C(121)	0.2252(5)	-0.252(1)	0.6024(5)	3.2(2)
C(122)	0.2908(4)	-0.2741(9)	0.5943(5)	2.4(2)

Table 2.6. (con't.) Final Positional and Isotropic Thermal Parameters for [Zn(TC-4,5)]^a

atom	x	y	z	B(eq) Å^2 ^{b}
C(123)	0.3247(4)	-0.132(1)	0.5824(4)	2.5(2)
C(201)	0.1434(4)	-0.1567(10)	0.3448(4)	2.1(2)
C(202)	0.1330(4)	-0.069(1)	0.3995(4)	2.4(2)
C(203)	0.1656(4)	0.042(1)	0.4356(5)	2.5(2)
C(204)	0.2222(5)	0.1006(10)	0.4349(4)	2.6(2)
C(205)	0.2604(4)	0.0569(9)	0.3947(4)	2.3(2)
C(206)	0.2511(4)	-0.0522(10)	0.3451(4)	2.3(2)
C(207)	0.2004(4)	-0.1473(9)	0.3180(4)	1.8(2)
C(208)	0.0773(4)	-0.5961(9)	0.1493(4)	1.6(2)
C(209)	0.0519(4)	-0.669(1)	0.0849(4)	2.5(2)
C(210)	0.0317(4)	-0.808(1)	0.0693(5)	2.5(2)
C(211)	0.0315(4)	-0.922(1)	0.1113(5)	3.1(2)
C(212)	0.0503(4)	-0.9195(10)	0.1834(5)	2.7(2)
C(213)	0.0712(4)	-0.808(1)	0.2294(5)	2.5(2)
C(214)	0.0849(4)	-0.6616(9)	0.2210(4)	1.7(2)
C(215)	0.0529(4)	-0.312(1)	0.3426(4)	2.3(2)
C(216)	0.0817(4)	-0.403(1)	0.4072(4)	2.4(2)
C(217)	0.1316(4)	-0.507(1)	0.3992(4)	2.6(2)
C(218)	0.1110(4)	-0.623(1)	0.3443(4)	2.6(2)
C(219)	0.2544(4)	-0.2396(9)	0.2375(4)	1.9(2)
C(220)	0.2414(4)	-0.3298(9)	0.1702(4)	2.0(2)
C(221)	0.2000(5)	-0.259(1)	0.1048(4)	2.8(2)
C(222)	0.1292(4)	-0.2437(10)	0.0980(4)	2.4(2)
C(223)	0.0942(4)	-0.3875(10)	0.0866(4)	2.2(2)

^{a}Numbers in parentheses are estimated standard deviations of the last significant figure. See Figure 2.4 for atom labeling scheme. ^{b}B$_{eq}$ = 4/3 [a$^2\beta_{11}$ + b$^2\beta_{22}$ + c$^2\beta_{33}$ + 2ab cos(γ)β_{12} + 2ac cos(γ)β_{13} + 2bc cos (γ)β_{23}]

Table 2.7. Final Positional and Isotropic Thermal Parameters for [Zn(TC-5,5)].[a]

atom	x	y	z	$B(eq)$ $\mathring{A}^{2b}$
Zn(1)	-0.4158(1)	-0.832	-0.250	3.07(6)
N(1)	-0.42891)	-0.989(1)	-0.2858(1)	2.8(4)
N(2)	-0.223(1)	-0.673(1)	-0.2398(3)	3.1(5)
C(1)	-0.720(1)	-1.439	-0.250	4.9(8)
C(2)	-0.651(1)	-1.376(1)	-0.2896(4)	4.0(7)
C(3)	-0.564(1)	-1.237(1)	-0.2979(4)	3.1(6)
C(4)	-0.524(1)	-1.115(1)	-0.2717(3)	3.3(6)
C(5)	-0.347(1)	-0.974(1)	-0.3256(4)	3.9(6)
C(6)	-0.206(1)	-0.842(1)	-0.3239(4)	3.8(6)
C(7)	-0.099(1)	-0.839(1)	-0.2928(5)	4.1(7)
C(8)	-0.118(1)	-0.829(1)	-0.2441(5)	4.1(7)
C(9)	-0.101(1)	-0.690(2)	-0.2294(4)	3.9(6)
C(10)	-0.205(1)	-0.544(1)	-0.2420(4)	2.4(5)
C(11)	-0.083(1)	-0.425(1)	-0.2286(4)	3.3(5)
C(12)	-0.043(1)	-0.283(1)	-0.2305(4)	3.6(6)
C(13)	-0.108(1)	-0.217	-0.250	3.4(7)

[a]Numbers in parentheses are estimated standard deviations of the last significant figure. See Figure 2.5 for atom labeling scheme. [b]$B_{eq} = 4/3$ $[a^2\beta_{11} + b^2\beta_{22} + c^2\beta_{33} + 2ab \cos(\gamma)\beta_{12} + 2ac \cos(\beta)\beta_{13} + 2bc \cos(\alpha)\beta_{23}]$.

Table 2.8. Final Positional and Isotropic Thermal Parameters for [Zn(TC-6,6)].[a]

atom	x	y	z	B(eq) Å^{2b}
Zn(1)	-0.84328(8)	-0.09752(7)	-0.63099(5)	1.47(3)
N(1)	-0.9923(5)	-0.0544(5)	-0.6877(3)	1.3(3)
N(2)	-0.8672(5)	0.0642(5)	-0.5956(3)	1.3(3)
N(3)	-0.677795)	-0.1601(5)	-0.6595(3)	1.3(3)
N(4)	-0.8414(7)	-0.2411(5)	-0.5721(3)	1.5(3)
C(1)	-1.0440(7)	0.0491(6)	-0.6718(4)	1.1(1)
C(2)	-1.1550(7)	0.0908(7)	-0.7035(4)	1.6(3)
C(3)	-1.2272(7)	0.1861(7)	-0.6922(5)	2.1(4)
C(4)	-1.2140(8)	0.2790(7)	-0.6478(4)	2.1(4)
C(5)	-1.11108)	0.2980(7)	-0.6048(4)	2.0(4)
C(6)	-1.0056(7)	0.2311(7)	-0.5933(4)	1.6(4)
C(7)	-0.9692(7)	0.1174(6)	-0.6178(4)	1.4(3)
C(8)	-0.6462(7)	-0.2621(6)	-0.6308(4)	1.6(3)
C(9)	-0.5332(8)	-0.3237(7)	-0.6489(4)	2.1(4)
C(10)	-0.4838(7)	-0.4269(7)	-0.6258(5)	2.8(4)
C(11)	-0.524(1)	-0.5046(8)	-0.5765(5)	2.8(4)
C(12)	-0.633(1)	-0.4964(7)	-0.5370(5)	2.6(4)
C(13)	-0.7264(7)	-0.4126(7)	-0.5388(4)	2.2(3)
C(14)	-0.7424(7)	-0.3074(6)	-0.5783(4)	1.4(3)
C(15)	-1.0483(7)	-0.1312(6)	-0.7404(4)	1.7(3)
C(16)	-1.169(1)	-0.1949(7)	-0.7160(4)	2.3(4)
C(17)	-1.160(1)	-0.2454(6)	-0.6421(4)	2.3(3)
C(18)	-1.0716(8)	-0.3470(6)	-0.6344(5)	2.3(4)
C(19)	-1.0285(8)	-0.3721(7)	-0.5590(5)	2.4(4)
C(20)	-0.947(1)	-0.2760(7)	-0.5277(4)	2.2(4)
C(21)	-0.5966(7)	-0.1017(8)	-0.7096(4)	1.9(3)
C(22)	-0.4854(8)	-0.0340(7)	-0.6752(5)	2.2(4)
C(23)	-0.5258(7)	0.0502(7)	-0.6165(5)	2.2(4)
C(24)	-0.6110(8)	0.1461(7)	-0.6422(4)	2.3(4)
C(25)	-0.6893(8)	0.2047(7)	-0.5836(4)	1.9(4)
C(26)	-0.7826(7)	0.1215(7)	-0.5466(4)	1.8(4)

Table 2.8. (con't.) Final Positional and Isotropic Thermal Parameters for [Zn(TC-6,6)].[a]

[a]Numbers in parentheses are estimated standard deviations of the last significant figure. See Figure 2.6 for atom labeling scheme. [b]B_{eq} = 4/3 [$a^2\beta_{11}$ + $b^2\beta_{22}$ + $c^2\beta_{33}$ +2ab cos(γ)β_{12} + 2ac cos (β)β_{13} + 2bc cos(α)β_{23}].

Table 2.9. Final Positional and Isotropic Thermal Parameters for $[Cd(TC\text{-}4,4)]^a$

atom	x	y	z	B(eq) Å^2 [b]
Cd(1)	0.5831(1)	-0.07946(5)	0.2455(1)	2.96(2)
N(1)	0.4984(9)	0.0170(4)	0.3131(9)	1.5(2)
N(2)	0.3761(9)	-0.1020(5)	0.2799(10)	1.7(2)
N(3)	0.6992(10)	-0.1769(4)	0.2310(10)	1.8(2)
N(4)	0.732(1)	-0.0582(5)	0.1095(10)	2.1(2)
C(1)	0.380(1)	0.0156(5)	0.342(1)	1.3(2)
C(2)	0.327(1)	0.0723(6)	0.403(1)	2.2(3)
C(3)	0.202(1)	0.0872(6)	0.429(1)	2.2(3)
C(4)	0.087(1)	0.0511(7)	0.394(1)	3.0(3)
C(5)	0.074(1)	-0.0123(6)	0.337(1)	2.4(3)
C(6)	0.168(1)	-0.0569(6)	0.305(1)	2.2(3)
C(7)	0.305(1)	-0.0503(6)	0.310(1)	1.8(3)
C(8)	0.795(1)	-0.1752(6)	0.160(1)	1.9(3)
C(9)	0.887(1)	-0.2303(6)	0.163(1)	2.5(3)
C(10)	0.986(1)	-0.2450(6)	0.095(1)	2.7(3)
C(11)	1.029(1)	-0.2101(7)	-0.006(1)	2.8(3)
C(12)	0.982(1)	-0.1466(7)	-0.056(1)	2.8(3)
C(13)	0.890(1)	-0.1040(6)	-0.015(1)	2.6(3)
C(14)	0.808(1)	-0.1091(6)	0.084(1)	2.1(3)
C(15)	0.577(1)	0.0804(6)	0.328(1)	2.2(3)
C(16)	0.696(1)	0.0719(6)	0.259(1)	2.2(3)
C(17)	0.659(1)	0.0608(6)	0.104(1)	2.6(3)
C(18)	0.741(1)	0.0095(6)	0.048(1)	2.3(3)
C(19)	0.320(1)	-0.1719(6)	0.255(1)	2.8(3)
C(20)	0.422(1)	-0.2225(6)	0.224(1)	2.6(3)
C(21)	0.538(1)	-0.2347(6)	0.345(1)	2.4(3)
C(22)	0.669(1)	-0.2392(6)	0.298(1)	2.4(3)

[a]Numbers in parentheses are estimated standard deviations of the last significant figure. See Figure 2.10 for atom labeling scheme. [b]$B_{eq} = 4/3\ [a^2\beta_{11} + b^2\beta_{22} + c^2\beta_{33} + 2ab\cos(\gamma)\beta_{12} + 2ac\cos(\gamma)\beta_{13} + 2bc\cos(\gamma)\beta_{23}]$

Table 2.10. Final Positional and Isotropic Thermal Parameters for [Cd(TC-4,5)][a]

atom	x	y	z	B(eq) Å^2 [b]
Cd(1)	0.41807(5)	0.12659(2)	0.36100(5)	2.761(9)
N(1)	0.5747(6)	0.1889(2)	0.3345(5)	2.7(1)
N(2)	0.3414(6)	0.1338(2)	0.1238(5)	2.95(10)
N(3)	0.2310(6)	0.1063(2)	0.4185(6)	2.9(1)
N(4)	0.5280(6)	0.0790(2)	0.5685(5)	2.8(1)
C(1)	0.5616(7)	0.1961(3)	0.2014(7)	2.7(1)
C(2)	0.6529(8)	0.2367(3)	0.1723(7)	3.3(1)
C(3)	0.6812(9)	0.2473(3)	0.0563(8)	4.2(2)
C(4)	0.6260(10)	0.2167(4)	-0.0753(8)	4.7(2)
C(5)	0.517(1)	0.1727(3)	-0.1192(8)	4.7(2)
C(6)	0.4348(9)	0.1498(3)	-0.0512(7)	4.1(2)
C(7)	0.4389(7)	0.1596(2)	0.0844(6)	2.5(1)
C(8)	0.2650(7)	0.0732(3)	0.5325(7)	2.8(1)
C(9)	0.1535(7)	0.0584(3)	0.5816(7)	3.4(2)
C(10)	0.1564(9)	0.0207(3)	0.6905(8)	3.8(2)
C(11)	0.2732(9)	-0.0129(3)	0.7885(8)	4.0(2)
C(12)	0.4216(9)	-0.0143(3)	0.8065(7)	3.7(2)
C(13)	0.4880(8)	0.0145(3)	0.7344(7)	3.3(2)
C(14)	0.4338(7)	0.0553(2)	0.6170(6)	2.4(1)
C(15)	0.7004(9)	0.2188(3)	0.4614(8)	4.8(2)
C(16)	0.750(1)	0.1826(4)	0.6130(9)	8.3(3)
C(17)	0.7840(8)	0.1159(4)	0.5991(9)	6.5(2)
C(18)	0.6967(8)	0.0696(3)	0.6499(7)	4.3(2)
C(19)	0.2066(8)	0.1008(3)	0.0161(7)	4.0(2)
C(20)	0.0976(9)	0.0805(3)	0.0702(8)	5.2(2)
C(21)	-0.014(1)	0.1275(5)	0.064(1)	10.2(4)
C(22)	0.053(1)	0.1589(5)	0.205(1)	9.8(3)
C(23)	0.0705(7)	0.1245(3)	0.3270(8)	4.5(2)

[a]Numbers in parentheses are estimated standard deviations of the last significant figure. See Figure 2.11 for atom labeling scheme. [b]$B_{eq} = 4/3 [a^2\beta_{11} + b^2\beta_{22} + c^2\beta_{33} + 2ab \cos(\gamma)\beta_{12} + 2ac \cos(\gamma)\beta_{13} + 2bc \cos(\gamma)\beta_{23}]$

Table 2.11. Final Positional and Isotropic Thermal Parameters for [Cd(TC-5,5)][a]

atom	x	y	z	B(eq) $\AA^2$ [b]
Cd(1)	0.5000	0.11916(2)	0.2500	1.753(9)
N(1)	0.3983(2)	0.2214(1)	0.2627(2)	1.62(5)
N(2)	0.4235(2)	0.0166(1)	0.1430(2)	1.46(5)
C(1)	0.5000	0.4747(3)	0.2500	5.1(2)
C(2)	0.4227(3)	0.4373(2)	0.3109(5)	3.85(10)
C(3)	0.3983(3)	0.3582(2)	0.3165(4)	2.34(7)
C(4)	0.4450(2)	0.2898(2)	0.2684(3)	1.74(6)
C(5)	0.4587(2)	-0.0537(2)	0.1853(3)	1.51(6)
C(6)	0.4263(3)	-0.1228(2)	0.1108(3)	1.82(7)
C(7)	0.4452(2)	-0.2017(2)	0.1353(3)	2.08(7)
C(8)	0.5000	-0.2386(2)	0.2500	2.21(10)
C(9)	0.2881(2)	0.2159(2)	0.2826(3)	1.86(6)
C(10)	0.2374(2)	0.1397(2)	0.2282(3)	1.99(6)
C(11)	0.2156(2)	0.1334(2)	0.0683(4)	2.20(7)
C(12)	0.3053(3)	0.1066(2)	-0.0097(3)	2.05(7)
C(13)	0.3435(2)	0.0228(2)	0.0197(3)	1.81(6)

[a]Numbers in parentheses are estimated standard deviations of the last significant figure. See Figure 2.12 for atom labeling scheme. [b]$B_{eq} = 4/3\ [a^2\beta_{11} + b^2\beta_{22} + c^2\beta_{33} + 2ab\cos(\gamma)\beta_{12} + 2ac\cos(\gamma)\beta_{13} + 2bc\cos(\gamma)\beta_{23}]$

Table 2.12. Final Positional and Isotropic Thermal Parameters for [Cd(TC-6,6)]^a

atom	x	y	z	B(eq) Å$^{2\,b}$
Cd(1)	0.33762(3)	0.08753(3)	0.37351(2)	2.755(9)
N(1)	0.5022(4)	0.0389(4)	0.3165(2)	2.34(10)
N(2)	0.3785(4)	-0.0898(5)	0.4076(2)	2.6(1)
N(3)	0.1559(4)	0.1400(4)	0.3401(2)	2.6(1)
N(4)	0.3017(4)	0.2494(4)	0.4308(2)	2.4(1)
C(1)	0.5503(5)	-0.0637(5)	0.3314(3)	2.2(1)
C(2)	0.6612(5)	-0.0996(5)	0.3009(3)	2.7(1)
C(3)	0.7273(5)	-0.2001(6)	0.3043(3)	3.2(1)
C(4)	0.7073(5)	-0.3012(5)	0.3431(3)	3.2(1)
C(5)	0.6112(6)	-0.3206(5)	0.3874(3)	3.1(1)
C(6)	0.5133(6)	-0.2517(5)	0.4037(3)	2.7(1)
C(7)	0.4775(5)	-0.1383(5)	0.3831(3)	2.2(1)
C(8)	0.1149(5)	0.2391(5)	0.3660(3)	2.2(1)
C(9)	0.0000(6)	0.2829(5)	0.3458(3)	2.9(1)
C(10)	-0.0644(5)	0.3789(5)	0.3646(3)	3.2(1)
C(11)	-0.0377(6)	0.4671(6)	0.4114(4)	3.7(2)
C(12)	0.0674(6)	0.4789(5)	0.4498(3)	3.6(2)
C(13)	0.1688(5)	0.4108(5)	0.4505(3)	2.9(1)
C(14)	0.1980(5)	0.3025(5)	0.4173(3)	2.1(1)
C(15)	0.5635(5)	0.1225(5)	0.2702(3)	2.7(1)
C(16)	0.6625(5)	0.1918(5)	0.3096(3)	3.1(1)
C(17)	0.6191(5)	0.2507(5)	0.3782(4)	3.0(1)
C(18)	0.5268(5)	0.3468(5)	0.3661(3)	2.9(1)
C(19)	0.4691(5)	0.3929(5)	0.4356(3)	3.3(1)
C(20)	0.3935(5)	0.3026(5)	0.4763(3)	2.8(1)
C(21)	0.2968(6)	-0.1528(5)	0.4559(3)	3.3(1)
C(22)	0.2116(6)	-0.2349(6)	0.4169(4)	3.8(2)
C(23)	0.1358(6)	-0.1761(6)	0.3582(4)	3.9(2)
C(24)	0.0473(6)	-0.0856(6)	0.3855(4)	4.0(2)
C(25)	-0.0046(6)	-0.0074(6)	0.3281(4)	3.9(2)
C(26)	0.0858(5)	0.0694(6)	0.2904(3)	3.4(1)

Table 2.12. (con't.) Final Positional and Isotropic Thermal Parameters for [Cd(TC-6,6)]^a

---

^{a}Numbers in parentheses are estimated standard deviations of the last significant figure. See Figure 2.13 for atom labeling scheme. ^{b}B$_{eq}$ = 4/3 [a$^2\beta_{11}$ + b$^2\beta_{22}$ + c$^2\beta_{33}$ + 2ab cos(γ)β_{12} + 2ac cos(γ)β_{13} + 2bc cos (γ)β_{23}]

Table 2.13. Selected Bond Distances and Angles for Zinc Tropocoronands.[a]

	Distances		Angles	
[Zn(py)(TC-3,3)]	Zn-N1	2.049 (2)	N1-Zn-N1*	145.1 (1)
	Zn-N2	2.047 (2)	N1-Zn-N2	77.83 (9)
	Zn-N3	2.097(3)	N1-Zn-N2*	93.31 (8)
	Zn-N$_{TCavg}$	2.048(1)	N2-Zn-N2*	150.4 (1)
			N1-Zn-N3	107.45 (6)
			N2-Zn-N3	104.78 (6)
[Zn(TC-3,4)]	Zn-N1	2.026 (4)	N1-Zn-N2	79.2 (2)
	Zn-N2	1.998 (4)	N1-Zn-N3	153.9 (2)
	Zn-N3	2.042 (4)	N1-Zn-N4	115.6 (2)
	Zn-N4	1.997 (4)	N2-Zn-N3	95.0 (2)
	Zn-N$_{avg}$	2.01(3)	N2-Zn-N4	155.1 (2)
			N3-Zn-N4	79.8 (2)
[Zn(TC-4,4)]	Zn-N1	2.013 (5)	N1-Zn-N2	81.5 (2)
	Zn-N2	1.975 (5)	N1-Zn-N3	150.7 (2)
	Zn-N3	2.008 (5)	N1-Zn-N4	100.0 (2)
	Zn-N4	1.975 (6)	N2-Zn-N3	117.0 (2)
	Zn-N$_{avg}$	1.99(2)	N2-Zn-N4	141.7 (2)
			N3-Zn-N4	79.7 (2)
[Zn(TC-4,5)]	Zn1-N101	1.976(7)	N101-Zn1-N102	81.4(3)
	Zn1-N102	1.988(7)	N101-Zn1-N103	140.6(3)
	Zn1-N103	1.969(7)	N101-Zn1-N104	101.4(3)
	Zn1-N104	1.995(7)	N201-Zn2-N202	81.5(3)
	Zn2-N201	1.976(7)	N201-Zn2-N203	140.0(3)
	Zn2-N202	1.993(7)	N201-Zn2-N204	100.8(3)
	Zn2-N203	1.985(6)	N102-Zn1-N103	120.4(3)
	Zn2-N204	2.010(7)	N102-Zn1-N104	140.5(3)
	Zn-N$_{avg}$	1.99(1)	N103-Zn1-N104	82.2(3)
			N202-Zn2-N203	120.7(3)

Table 2.13. (con't.) Selected Bond Distances and Angles for Zinc Tropocoronands. [a]

	Distances		Angles	
[Zn(TC-4,5)]			N202-Zn2-N204	142.9(3)
			N203-Zn2-N204	81.0(3)
[Zn(TC-5,5)]	Zn-N1	1.99 (1)	N1-Zn-N1*	82.6 (5)
	Zn-N2	1.977 (8)	N1-Zn-N2	115.5 (5)
	Zn-N$_{avg}$	1.948(7)	N1-Zn-N2*	135.6 (4)
			N2-Zn-N2*	80.8 (7)
Zn(TC-6,6)]	Zn-N1	1.981 (6)	N1-Zn-N2	81.4 (2)
	Zn-N2	1.982 (6)	N1-Zn-N3	130.9 (3)
	Zn-N3	1.978 (6)	N1-Zn-N4	121.4 (3)
	Zn-N4	1.985 (6)	N2-Zn-N3	123.0 (2)
	Zn-N$_{avg}$	1.982(3)	N2-Zn-N4	125.4 (2)
			N3-Zn-N4	81.2 (3)

[a]Numbers in parentheses are estimated standard deviations of the last significant figure. Atoms are labeled as indicated in Figures 2.1-2.6.

Table 2.14. Dihedral Angles for [M(TC-n,m)] Complexes.

n + m	Θ (deg) for [M(TC-n,m)]				
	Co[a] (0.72 Å)[b]	Ni[c] (0.69 Å)	Cu[d] (0.71 Å)	Zn (0.74 Å)	Cd (0.92 Å)
6	9.0	8.3	0.0	e	e
7	f	f	f	35.5	e
8	31.8	28.9	36.6	51.2	g
9	58.7	27.1	f	58.9	48.6
10	69.9	70.1	61.3	65.0	54.5
12	84.5	85.2	e	84.4	80.0

[a]Jaynes, B. S.; Doerrer, L. H.; Liu, S.; Lippard, S. J. *Inorg. Chem.* **1995**, *34*, 5735-5744. [b]Shannon, R. D. *Acta Cryst.* **1976**, *A32*, 751-767. [c]Davis, W. M.; Roberts, M. M.; Zask, A.; Nakanishi, K.; Lippard, S. J. *J. Am. Chem. Soc.* **1985**, *107*, 3864-3870. [d]Davis, W. M.; Zask, A.; Nakanishi, K.; Lippard, S. J. *Inorg. Chem.* **1985**, *24*, 3737-3743. [e]complex not accessible [f]structure not determined [g]see discussion for [Cd(TC-4,4)] in text

Table 2.15. Torsion angles, ω (deg), within the Linker Chains of the Zinc Tropocoronands.[a]

			ω	$\mid \Delta_{ideal} \mid$ [b]
[Zn(py)(TC-3,3)]	C-N	C1-N1-C8-C9	-172.6 (2)	22.6
		C7-N2-C10*-C9*	-179.1 (1)	29.1
		average		26(5)
	C-C	C8-C9	-73.3 (3)	13.3
		C10-C9	61.9 (3)	1.9
		average		8(8)
[Zn(TC-3,4)]	C-N	C1-N1-C15-C16	-167.7 (4)	17.7
		C7-N2-C19-C20	-110.5 (5)	20.5
		C8-N3-C21-C20	-171.1 (4)	21.1
		C14-N4-C18-C17	-173.9 (4)	23.9
		average		21(3)
	C-C	C15-C16	61.1(5)	1.1
		C16-C17	-130.0(4)	50.0
		C17-C18	-63.2(5)	3.2
		C19-C20	-82.6(5)	22.6
		C20-C21	-50.8(6)	9.2
		average		17(20)
[Zn(TC-4,4)]	C-N	C1-N1-C15-C16	-169.2(6)	19.2
		C7-N2-C19-C20	-170.7(6)	20.7
		C21-C22-N3-C8	158.9(6)	8.9
		C14-N4-C18-C17	-82.5(8)	7.5
		average		14(7)
	C-C	C15-C16	75.6(8)	15.6
		C16-C17	-59.4(9)	0.6
		C17-C18	48.0(9)	12.0
		C19-C20	54.5(8)	5.5
		C20-C21	-126.6(7)	53.4
		C21-C22	-60.4(8)	0.4
		average		14(20)

Table 2.15. (con't) Torsion angles, ω (deg), within the Linker Chains of the Zinc Tropocoronands.[a]

			ω	$|\Delta_{ideal}|$[b]
[Zn(TC-4,5)]	C-N	C101-N101-C115-C116	-69(1)	21
		C107-N102-C119-C120	-168.0(7)	18.0
		C108-N103-C123-C122	167.0(7)	17.0
		C114-N104-C118-C117	-177.0(7)	27.0
		C201-N201-C215-C216	-70(1)	20
		C207-N202-C219-C220	-167.8(7)	17.8
		C208-N203-C223-C222	-170.1(7)	20.1
		C214-N204-C218-C217	-177.3(7)	27.3
		average		21(2)
	C-C	C115-C116	-48(1)	12
		C116-C117	-59(1)	1
		C117-C118	-78(1)	18
		C119-C120	76.5(9)	16.5
		C120-C121	-73(1)	13
		C121-C122	-68(1)	8
		C122-C123	-81.2(9)	21.2
		C215-C216	-45(1)	15
		C216-C217	-63(1)	3
		C217-C218	-79(1)	19
		C219-C220	78.3(9)	18.3
		C220-C221	-73(1)	13
		C221-C222	-70(1)	10
		C222-C223	-85.4(9)	25.4
		average		13(7)
[Zn(TC-5,5)]	C-N	C4-N1-C5-C6	-152(1)	2
		C8-C9-N2-C10	-158(1)	8
		average		5(4)
	C-C	C5-C6	71(2)	11
		C6-C7	-71(2)	11
		C7-C8	-69(1)	9

Table 2.15. (con't) Torsion angles, ω (deg), within the Linker Chains of the Zinc Tropocoronands.[a]

			ω	$\mid \Delta_{ideal} \mid$ [b]
[Zn(TC-5,5)]	C-C	C8-C9	-76(1)	16
		average		11(3)
[Zn(TC-6,6)]	C-N	C1-N1-C15-C16	-74.3(9)	15.7
		C7-N2-C26-C25	-83.0(8)	7.0
		C22-C21N3-C8	79.5(9)	0.5
		C14-N4-C20-C19	-75(1)	15
		average		9(7)
	C-C	C15-C16	-43.9(9)	16.1
		C16-C17	-68.8(8)	8.8
		C17-C18	160.6(7)	19.4
		C18-C19	-66.7(9)	6.7
		C19-C20	51(1)	9
		C21-C22	-52(1)	8
		C22-C23	-62.4(9)	2.4
		C23-C24	159.7(6)	20.3
		C24-C25	-63.3(9)	3.3
		C25-C26	55.2(9)	4.8
		average		9(6)

[a]The sign of ω is positive if, when looking from atom 2 to atom 3, a clockwise motion of atom 1 would superimpose it on atom 4. Atoms 1 and 4 are omitted for C-C angles. [b]Δ_{ideal} = [$\mid$ ω $\mid$ - ideal angle] where ideal angles are 30°, 90°, or 150° for C-N and 60° or 180° for C-C.

Table 2.16. Selected Bond Distances and Angles for Cadmium Tropocoronands.[a]

		Distances		Angles
[Cd(TC-4,4)]	Cd-N1	2.233 (8)	N1-Cd-N2	71.6 (3)
	Cd-N2	2.256 (9)	N1-Cd-N3	165.6 (3)
	Cd-N3	2.255 (9)	N1-Cd-N4	111.9 (3)
	Cd-N4	2.26 (1)	N2-Cd-N3	111.7 (3)
	Cd-N$_{avg}$	2.25(1)	N2-Cd-N4	152.7 (3)
			N3-Cd-N4	71.9 (4)
[Cd(TC-4,5)]	Cd-N1	2.189(8)	N1-Cd-N2	73.4(3)
	Cd-N2	2.211(7)	N1-Cd-N3	151.0(3)
	Cd-N3	2.195(8)	N1-Cd-N4	113.2(3)
	Cd-N4	2.194(8)	N2-Cd-N3	114.4(3)
	Cd-N$_{avg}$	2.20(1)	N2-Cd-N4	151.9(3)
			N3-Cd-N4	73.9(3)
[Cd(TC-5,5)]	Cd-N1	2.190 (2)	N1-Cd-N1*	75.0 (1)
	Cd-N2	2.192 (2)	N1-Cd-N2	114.89 (9)
	Cd-N$_{avg}$	2.191(1)	N1-Cd-N2*	147.30 (8)
			N2-Cd-N2*	74.5 (1)
[Cd(TC-6,6)]	Cd-N1	2.185 (5)	N1-Cd-N2	73.9 (2)
	Cd-N2	2.187 (5)	N1-Cd-N3	135.1 (2)
	Cd-N3	2.200 (5)	N1-Cd-N4	127.3 (2)
	Cd-N4	2.181 (5)	N2-Cd-N3	121.9 (2)
	Cd-N$_{avg}$	2.188(7)	N2-Cd-N4	134.5 (2)
			N3-Cd-N4	74.4 (2)

[a]Numbers in parentheses are estimated standard deviations of the last significant figure. Atoms are labeled as indicated in Figures 2.10-2.13.

Table 2.17. Torsion angles, ω (deg), within the Linker Chains of the Cadmium Tropocoronands.[a]

			ω	$|\Delta_{ideal}|$ [b]
[Cd(TC-4,4)]	C-N	C1-N1-C15-C16	-168(1)	18
		C7-N2-C19-C20	-179(1)	29
		C21-C22-N3-C8	167(1)	17
		C14-N4-C18-C17	-173(1)	23
		average		22(6)
	C-C	C15-C16	64(1)	4
		C16-C17	-140(1)	40
		C17-C18	-59(1)	1
		C19-C20	65(1)	5
		C20-C21	-139(1)	41
		C21-C22	-60(1)	0
		average		15(20)
[Cd(TC-4,5)]	C-N	C1-N1-C15-C16	-152(1)	2
		C7-N2-C19-C20	-172.9(9)	22.9
		C8-N3-C23-C22	-178(1)	28
		C14-N4-C18-C17	-163.5(9)	13.5
		average		16(11)
	C-C	C15-C16	50(1)	10
		C16-C17	-128(1)	52
		C17-C18	-57(1)	3
		C19-C20	82(1)	22
		C20-C21	-92(2)	32
		C21-C22	-65(2)	5
		C22-C23	-103(1)	43
		average		24(20)
[Cd(TC-5,5)]	C-N	C4-N1-C9-C10	161.6(3)	11.6
		C5-C6-N2-C13	3.8(4)	26.2
		average		19(10)
	C-C	C9-C10	-73.3(3)	13.3

Table 2.17. (con't.) Torsion angles, ω (deg), within the Linker Chains of the Cadmium Tropocoronands.[a]

			ω	$\lvert \Delta_{ideal} \rvert$ [b]
[Cd(TC-5,5)]	C-C	C10-C11	83.4(3)	23.4
		C11-C12	65.3(4)	5.3
		C12-C13	86.9(3)	26.9
		average		17(15)
[Cd(TC-6,6)]	C-N	C1-N1-C15-C16	-80.1(6)	9.9
		C7-N2-C21-C22	-81.5(7)	8.5
		C25-C26-N3-C8	82.7(7)	7.3
		C14-N4-C20-C19	-80.5(6)	9.5
		average		9(1)
	C-C	C15-C16	-53.4(6)	6.6
		C16-C17	-65.9(6)	5.9
		C17-C18	171.0(5)	9.0
		C18-C19	-64.4(6)	4.4
		C19-C20	54.3(7)	5.7
		C21-C22	-55.7(7)	4.3
		C22-C23	-64.9(7)	5.1
		C23-C24	165.4(5)	4.6
		C24-C25	-63.9(7)	3.9
		C25-C26	54.9(7)	5.1
		average		6(1)

[a]The sign of ω is positive if, when looking from atom 2 to atom 3, a clockwise motion of atom 1 would superimpose it on atom 4. Atoms 1 and 4 are omitted for C-C angles. [b]Δ_{ideal} = [$\lvert \omega \rvert$ - ideal angle] where ideal angles are 30°, 90°, or 150° for C-N and 60° or 180° for C-C.

Table 2.18. Summary of UV-vis Data for Zinc and Cadmium Tropocoronands.

complex	λ_{max} (nm) (ε_M, M^{-1} cm^{-1})				
[Zn(py)(TC-3,3)]	294 (10,300)		389 (35,700)	435 (34,300)	456 (10,900)
[Zn(TC-3,4)]	296 (11,100)		381 (42,000)	433 (24,800)	455 (14,900)
[Zn(TC-4,4)	293 (19,200)		381 (29,000)	433 (16,500)	457 (16,500)
[Zn(TC-4,5)]	296 (6,700)		381 (23,600)	434 (12,500)	460 (14,700)
[Zn(TC-5,5)]	293 (32,600)		380 (46,400)	436 (18,800)	463 (28,900)
[Zn(TC-6,6)]	287 (34,600)		383 (44,400)	432 (23,200)	457 (39,200)
[Cd(TC-4,4)]	290 (3500)		386 (38,100)	435 (19,500)	461 (18,000)
[Cd(TC-4,5)]	286 (31,800)	361 (15,900)	381 (21,300)	438 (12,500)	464 (13,500)
[Cd(TC-5,5)]	292 (16,600)		385 (46,000)	440 (18,200)	466 (23,200)
[Cd(TC-6,6)]	290 (16,900)		387 (34,700)	437 (19,000)	463 (25,000)

Table 2.19. Zinc and Cadmium Tropocoronand α to ω Distances.

complex	α-ω (Å) chain #1	α-ω (Å) chain #2	complex	α-ω (Å) chain #1	α-ω (Å) chain #2
[Zn(TC-3,4)]	2.56	3.70			
[Zn(TC-4,4)]	3.16	3.72	[Cd(TC-4,4)]	3.76	3.77
[Zn(TC-4,5)][a]	3.19	4.18	[Cd(TC-4,5)]	3.95	4.02
[Zn(TC-5,5)]	4.15	4.15	[Cd(TC-5,5)]	4.26	4.26
[Zn(TC-6,6)]	4.47	4.51	[Cd(TC-6,6)]	4.62	4.72

[a]Average from two crystallographically independent molecules.

Table 2.20. Displacement (Å) of M(II) From Best N_4 Plane in [M(TC-n,m)] Complexes.

n + m	Co	Ni	Cu	Zn	Cd
6	0.09	0.101	0.0		
7				0.012	
8	0.017	0.012	0.021	0.054	0.107
9	0.115	0.049		0.007	0.007
10	0.0	0.0	0.0	0.0	0.0
12	0.038	0.063		0.044	0.001

Table 2.21. Summary of Intraligand Structural Information for Zinc Tropocoronand Complexes.[a]

	[Zn(py)(TC-3,3)]	[Zn(TC-3,4)]	[Zn(TC-4,4)]	[Zn(TC-4,5)]	[Zn(TC-5,5)]	[Zn(TC-6,6)]
a, C-C						
min-max	1.373(5)-1.498(4)	1.370(9)-1.514(7)	1.36(1)-1.52(1)	1.35(1)-1.52(1)	1.36(2)-1.52(2)	1.35(1)-1.52(1)
mean	1.41(4)	1.41(5)	1.41(5)	1.41(5)	1.41(5)	1.41(6)
b, N-C						
min-max	1.315(3)-1.328(3)	1.318(6)-1.328(6)	1.296(8)-1.322(9)	1.30(1)-1.34(1)	1.32(2)-1.32(2)	1.304(9)-1.339(9)
mean	1.322(9)	1.323(4)	1.31(1)	1.33(1)	1.32(0)	1.33(2)
c, C-C						
min-max	1.523(4)-1.528(3)	1.505(7)-1.542(8)	1.497(9)-1.53(1)	1.51(1)-1.58(1)	1.49(2)-1.52(2)	1.50(1)-1.56(1)
mean	1.526(4)	1.52(2)	1.52(1)	1.53(2)	1.51(1)	1.53(2)
d, N-C						
min-max	1.450(3)-1.459(3)	1.465(6)-1.479(6)	1.448(9)-1.470(9)	1.44(1)-1.48(1)	1.47(2)-1.48(2)	1.449(9)-1.46(1)
mean	1.455(6)	1.472(6)	1.45(1)	1.46(1)	1.475(7)	1.455(6)
α, Zn-N-C						
min-max	116.5(2)-117.2(2)	115.4(3)-117.7(3)	113.3(5)-118.2(5)	114.8(6)-115.3(6)	113.7(9)-116.9(9)	115.2(5)-115.9(5)
mean	116.9(2)	116.4(9)	115(2)	115.0(2)	115(2)	115.5(3)
β, Zn-N-C						
min-max	121.4(2)-122.6(2)	117.8(3)-125.9(3)	117.4(5)-126.1(4)	117.6(5)-125.8(6)	123.9(8)-125.7(7)	123.0(5)-123.9(5)
mean	122.0(8)	123(4)	122(4)	123(4)	125(1)	123.4(4)
γ, ring						
min-max	123.5(2)-132.6(3)	123.0(4)-133.8(5)	121.8(7)-134.6(7)	122.0(8)-134.0(9)	124(1)-131(1)	123.0(7)-133.0(7)
mean	128(4)	129(4)	128(4)	128(4)	128(3)	129(4)
δ, N-C-C						
min-max	113.8(2)-113.9(2)	113.2(4)-114.7(4)	112.7(6)-115.8(6)	113.1(7)-114.6(8)	112.3(7)-114.6(7)	113.1(6)-114.5(6)
mean	113.85(7)	113.7(6)	113(1)	114.0(6)	113(2)	113.8(6)

Table 2.21. (con't.) Summary of Intraligand Structural Information for Zinc Tropocoronand Complexes.[a]

	[Zn(py)(TC-3,3)]	[Zn(TC-3,4)]	[Zn(TC-4,4)]	[Zn(TC-4,5)]	[Zn(TC-5,5)]	[Zn(TC-6,6)]
ε, N-C-C						
min-max	121.9(3)-122.6(3)	122.3(4)-123.8(4)	121.2(7)-125.6(7)	121.5(8)-123.8(8)	120(1)-123(1)	122.5(7)-123.1(7)
mean	122.3(5)	122.9(7)	123(2)	122.4(9)	122(2)	122.8(3)

[a]See Figure 2.14 for bond and angle labeling scheme. Bond lengths are in Å and angles in degrees.

Table 2.22. Summary of Intraligand Structural Information for Cadmium Tropocoronand Complexes.[a]

	[Cd(TC-4,4)]	[Cd(TC-4,5)]	[Cd(TC-5,5)]	[Cd(TC-6,6)]
a, C-C				
min-max	1.35(2)-1.51(2)	1.35(1)-1.51(1)	1.377(5)-1.525(6)	1.364(8)-1.518(7)
mean	1.40(5)	1.41(5)	1.42(6)	1.41(5)
b, N-C				
min-max	1.31(1)-1.32(1)	1.31(1)-1.34(1)	1.307(4)-1.323(4)	1.316(7)-1.331(7)
mean	1.313(5)	1.33(1)	1.32(1)	1.324(7)
c, C-C				
min-max	1.48(2)-1.50(2)	1.43(2)-1.63(2)	1.512(4)-1.527(5)	1.50(1)-1.543(8)
mean	1.51(2)	1.53(7)	1.521(7)	1.52(1)
d, N-C				
min-max	1.44(1)-1.48(1)	1.46(1)-1.48(1)	1.462(4)-1.467(4)	1.452(7)-1.466(7)
mean	1.46(2)	1.473(9)	1.464(4)	1.458(6)
α, Cd-N-C				
min-max	117.7(7)-119.0(9)	116.5(6)-117.8(6)	115.5(2)-117.4(2)	117.1(4)-118.3(4)
mean	118.3(5)	117.3(6)	116(1)	117.8(5)
β, Cd-N-C				
min-max	120.1(7)-121(1)	120.3(8)-123.1(7)	123.1(2)-123.8(2)	120.3(4)-121.1(4)
mean	120.8(4)	122(1)	123.5(5)	120.6(3)
χ, ring				
min-max	122(1)-135(1)	121.6(9)-135(1)	122.1(2)-133.8(3)	122.6(5)-134.0(6)
mean	128(4)	128(5)	128(4)	129(4)
δ, N-C-C				
min-max	115(1)-116(1)	114.5(8)-115.9(9)	115.1(2)-115.7(2)	114.7(5)-115.6(5)
mean	115.5(6)	115.0(6)	115.4(4)	115.1(4)
ε, N-C-C				
min-max	121(1)-123(1)	122.0(9)-122.4(9)	122.0(3)-122.1(3)	121.4(5)-122.4(5)
mean	122.0(8)	122.3(2)	122.05(7)	121.9(5)

[a]See Figure 2.14 for bond and angle labeling scheme. Bond lengths are in Å and angles in degrees.
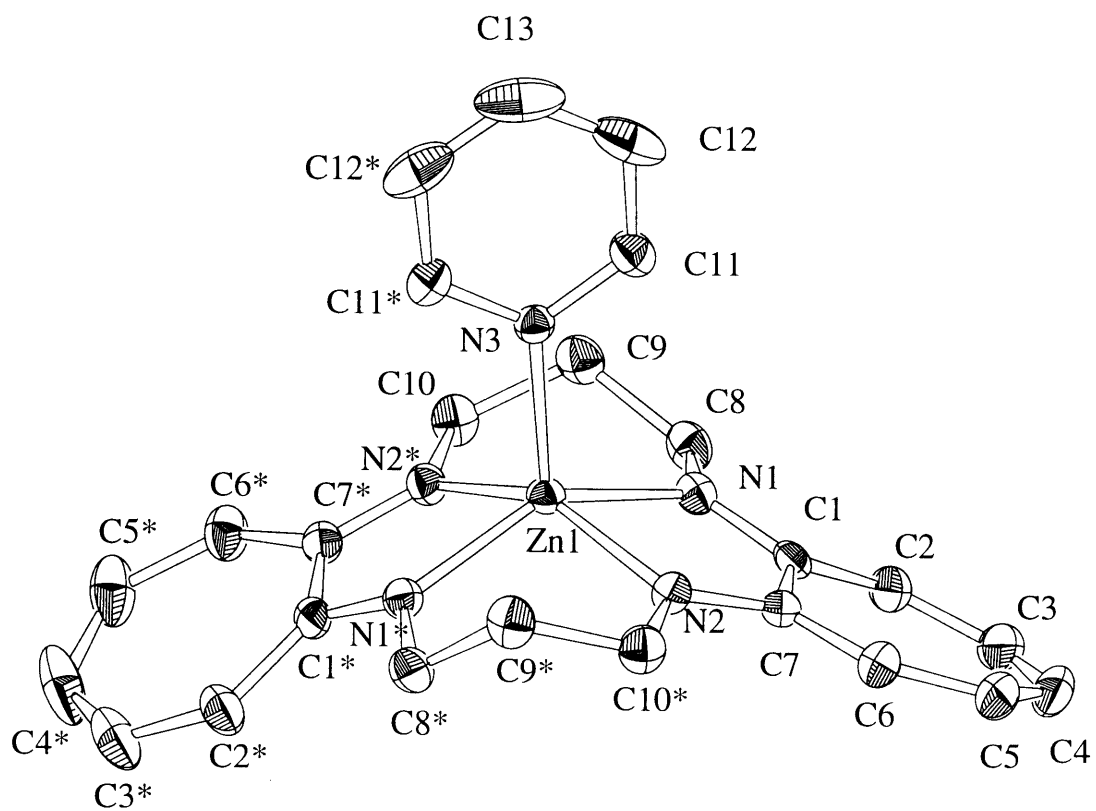
Figure 2.1. ORTEP drawing for [Zn(py)(TC-3,3)] showing 40% probability ellipsoids for all non-hydrogen atoms.
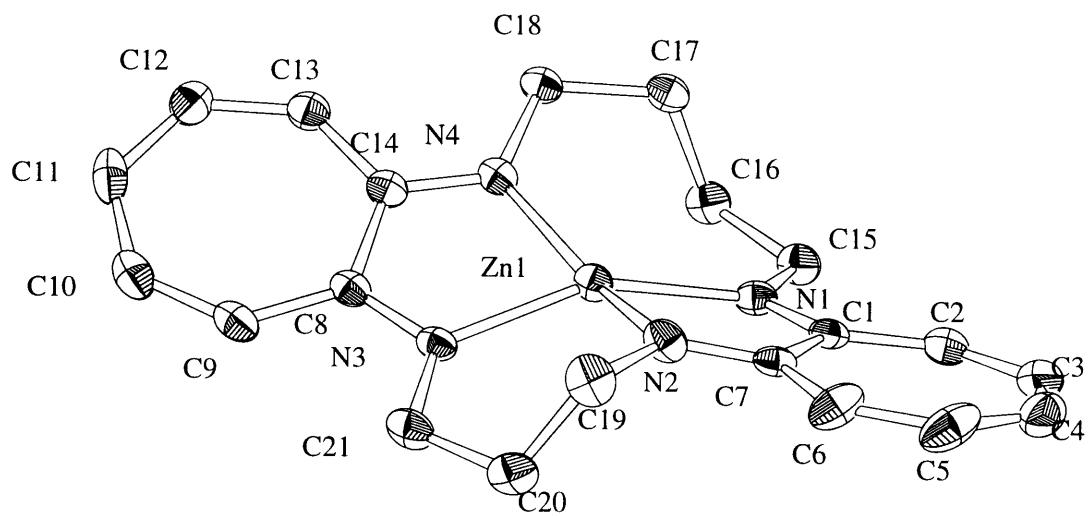
Figure 2.2. ORTEP drawing for [Zn(TC-3,4)] showing 40% probability ellipsoids for all non-hydrogen atoms.
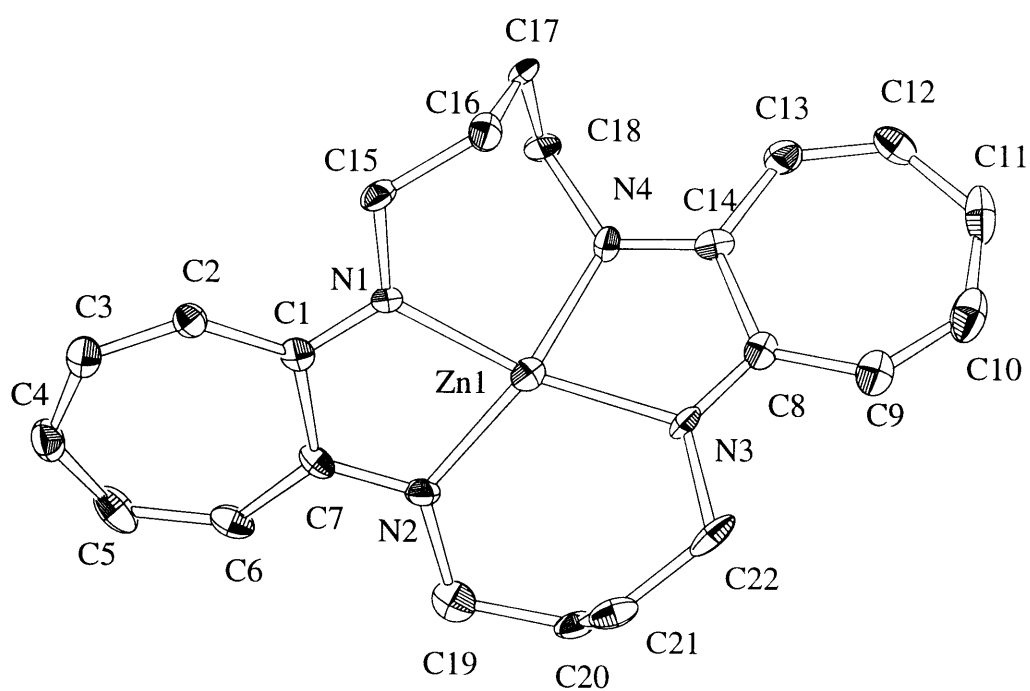
Figure 2.3. ORTEP drawing for [Zn(TC-4,4)] showing 40% probability ellipsoids for all non-hydrogen atoms.
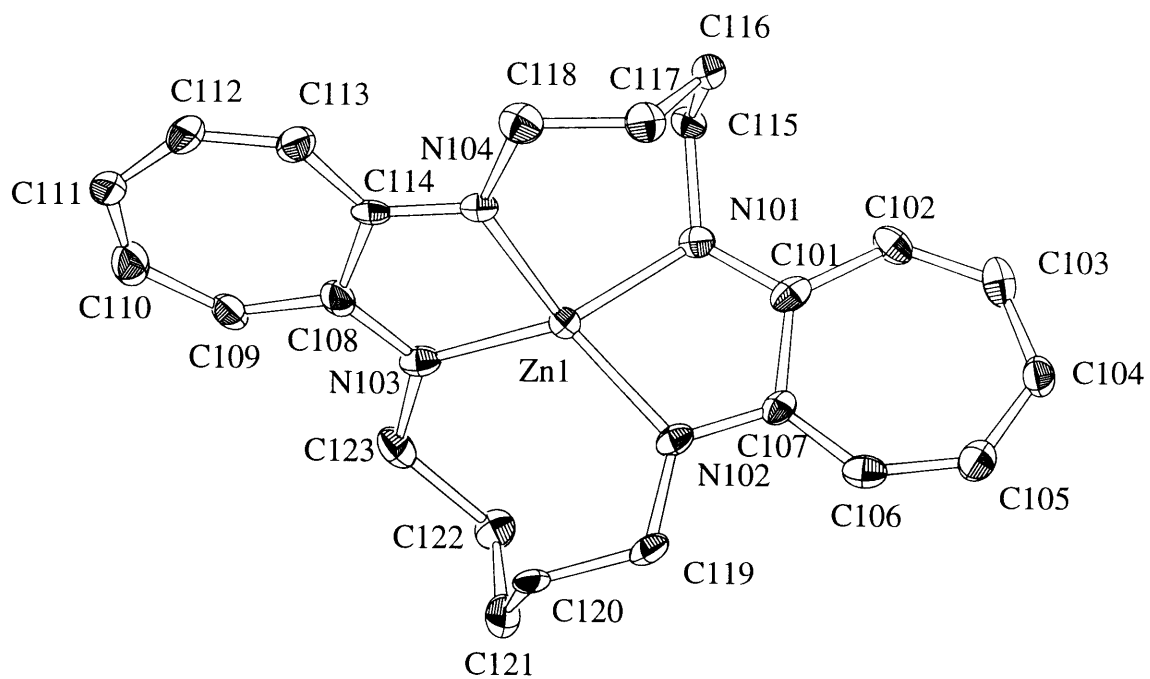
Figure 2.4. ORTEP drawing for one molecule of [Zn(TC-4,5)] from the asymmetric unit showing 40% probability ellipsoids for all non-hydrogen atoms.

113
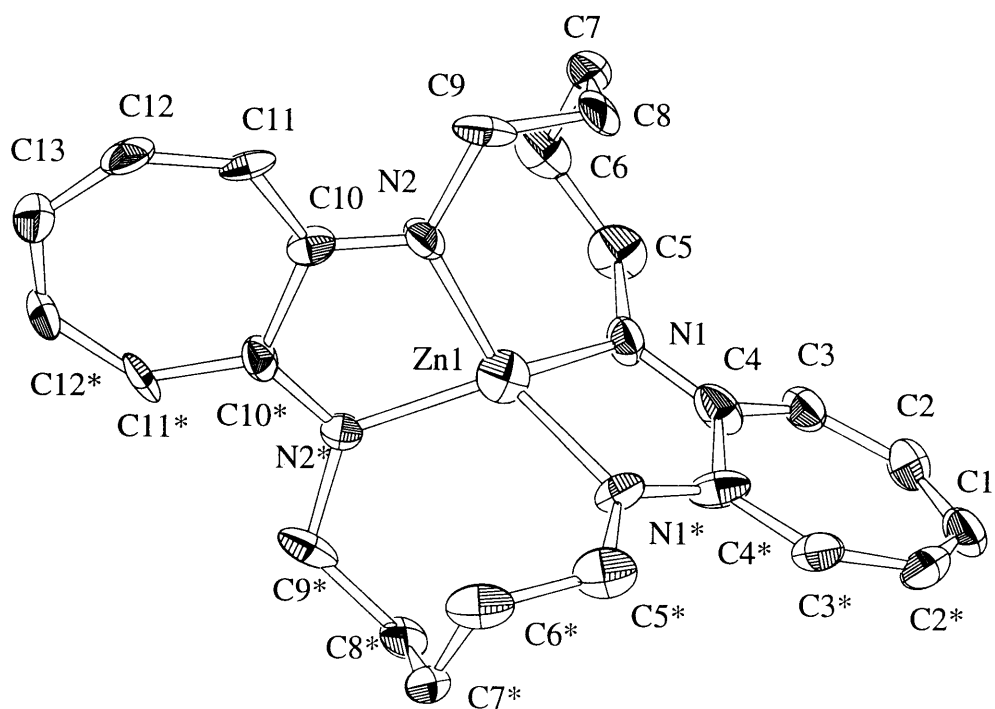
Figure 2.5. ORTEP drawing for [Zn(TC-5,5)] showing 40% probability ellipsoids for all non-hydrogen atoms.
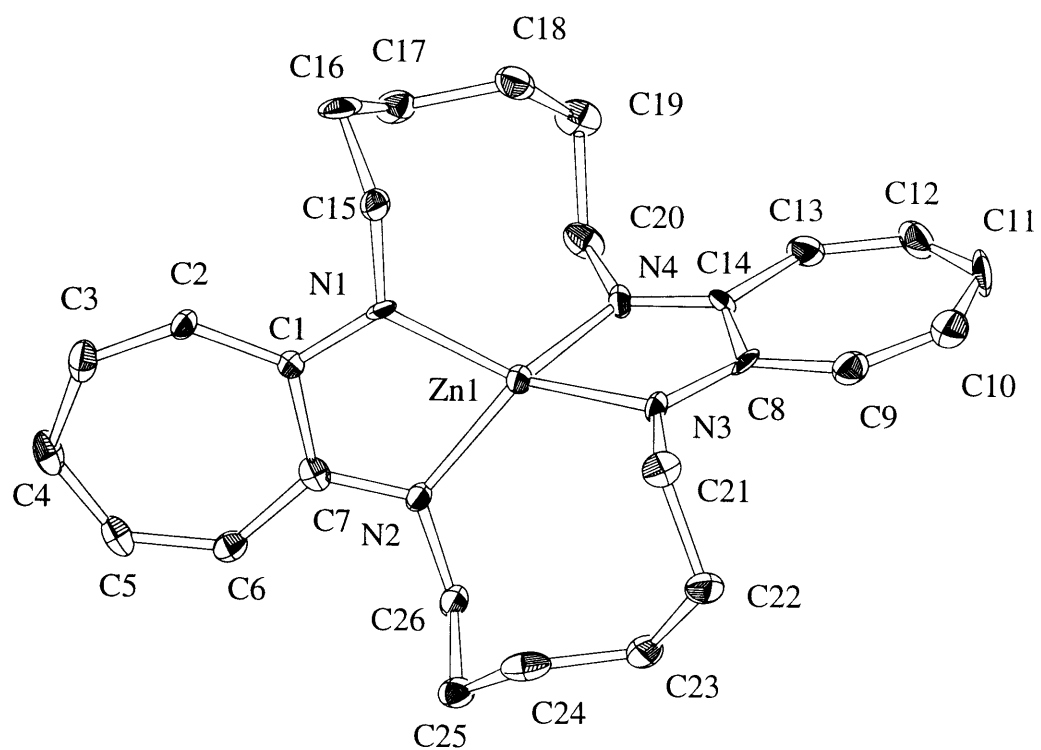
Figure 2.6. ORTEP drawing for [Zn(TC-6,6)] showing 40% probability ellipsoids for all non-hydrogen atoms.
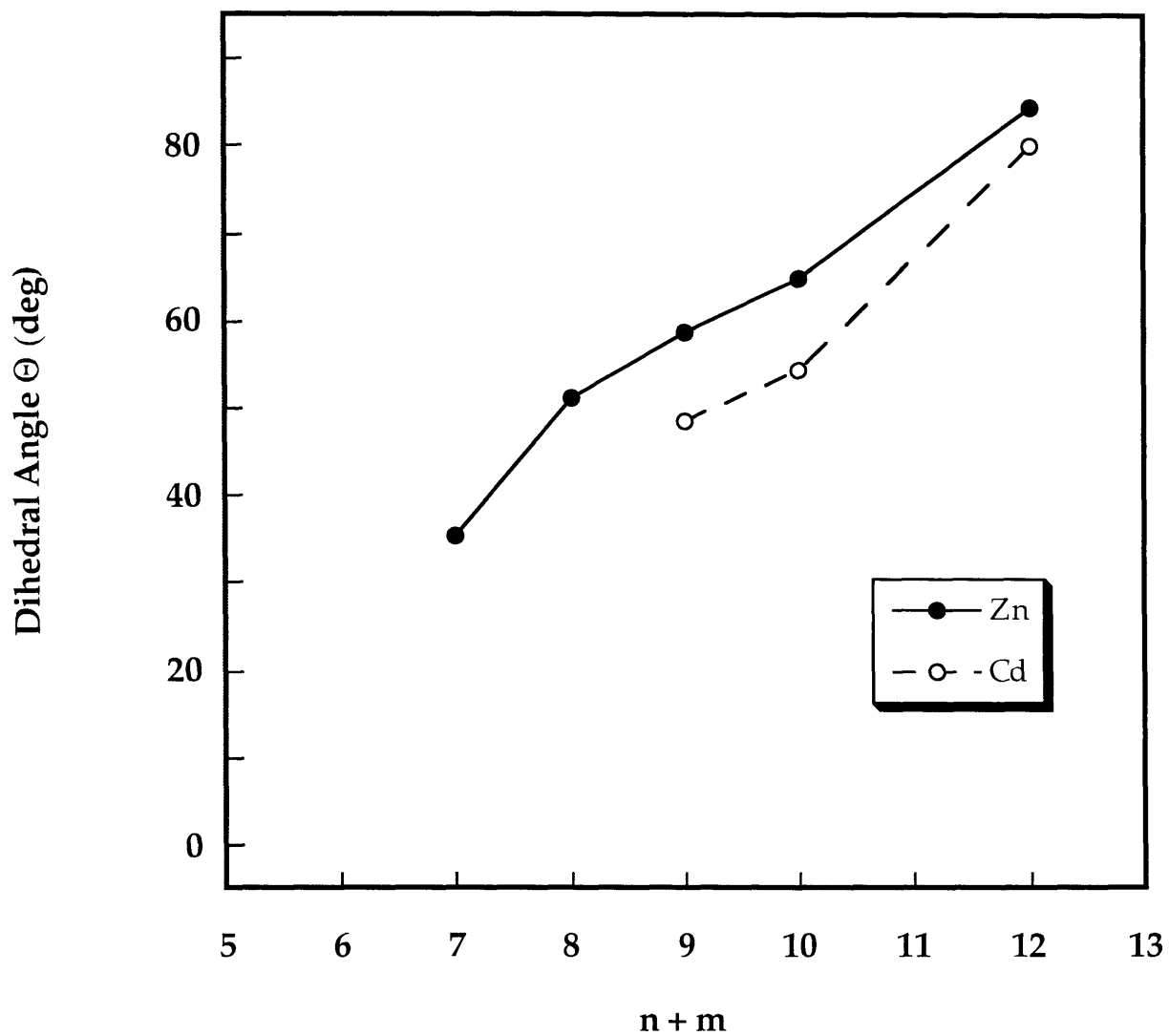
Figure 2.7. Comparison of [Zn(TC-n,m)] and [Cd(TC-n,m)] dihedral angles, Θ, as a function of linker chain length, (n+m).
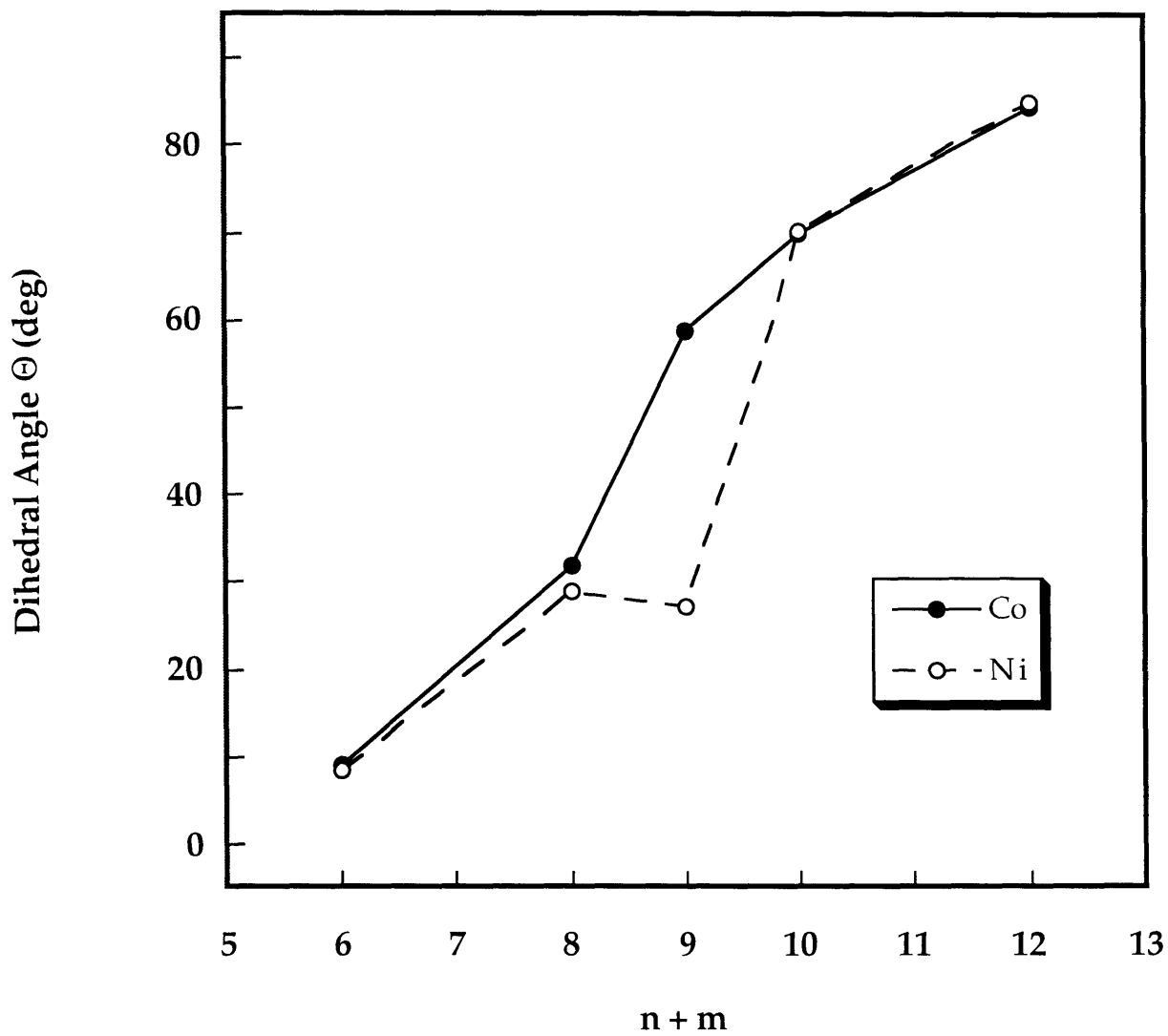
Figure 2.8. Comparison of [Co(TC-n,m)] and [Ni(TC-n,m)] dihedral angles as a function of linker chain length, (n + m).
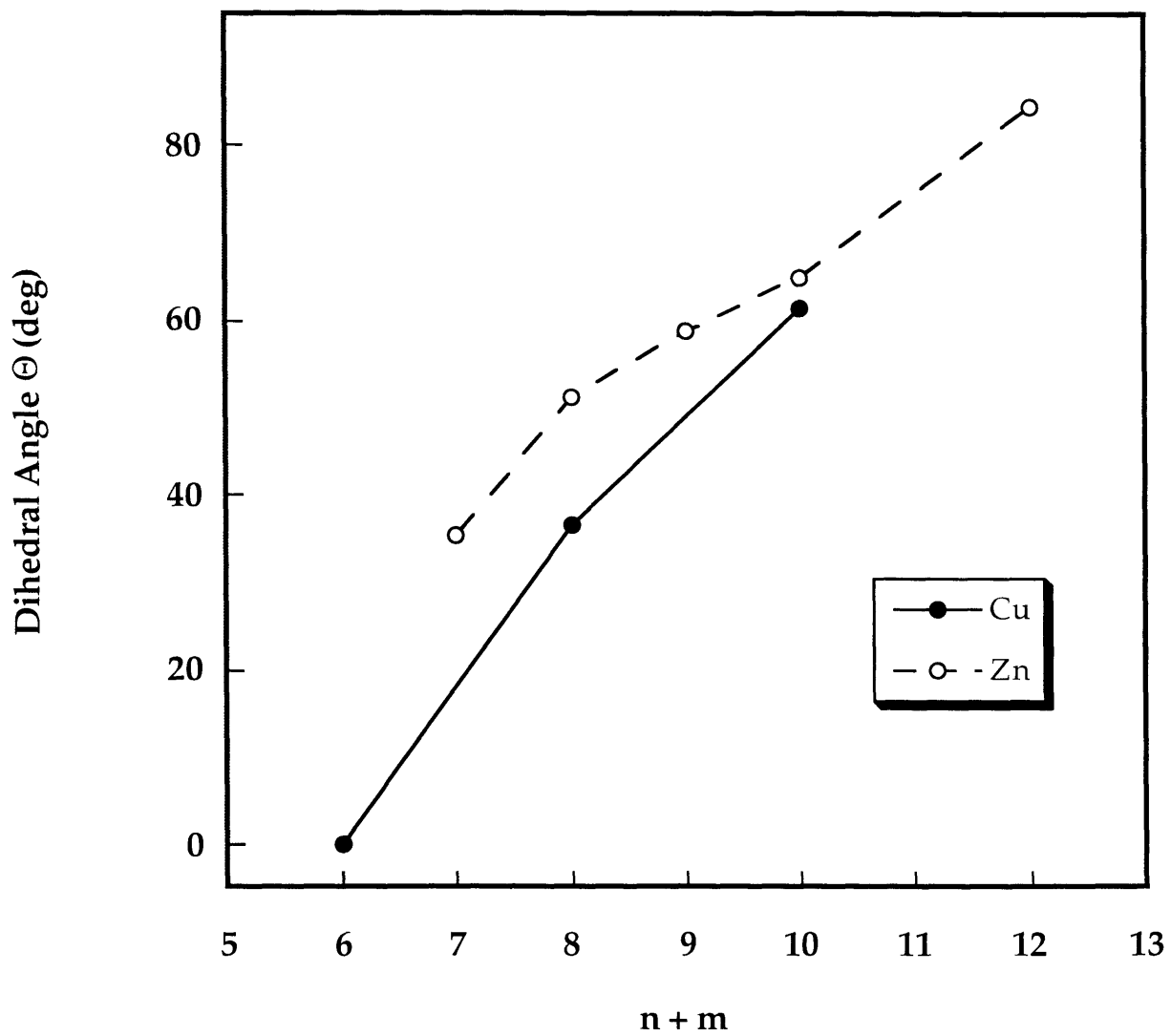
Figure 2.9. Comparison of [Cu(TC-nm)] and [Zn(TC-n,m)] dihedral angles as a function of linker chain length, (n + m).
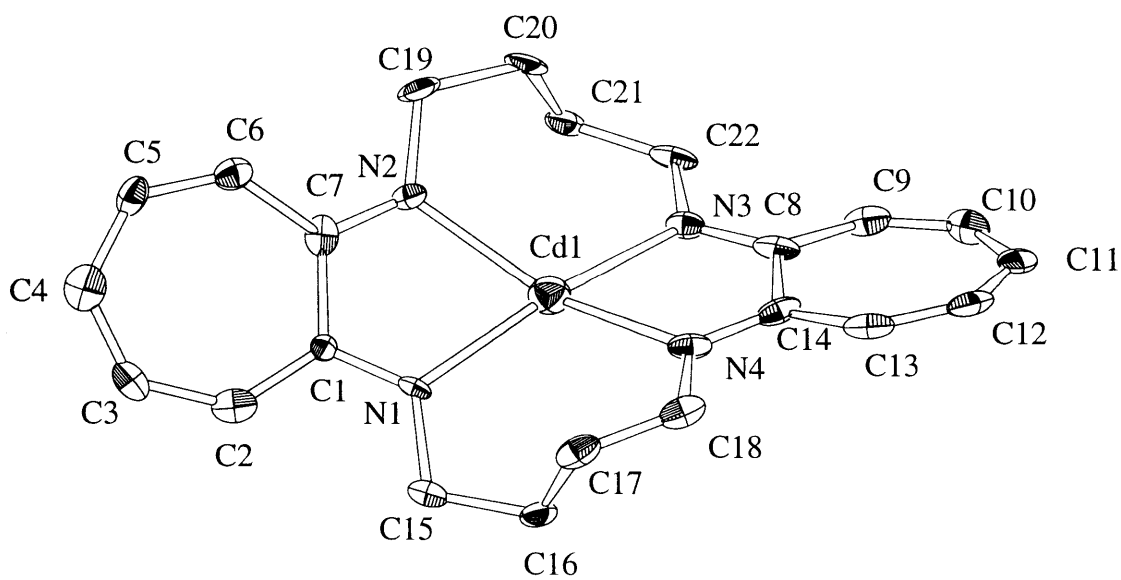
Figure 2.10. ORTEP drawing for [Cd(TC-4,4)] showing 40% probability ellipsoids for all non-hydrogen atoms.
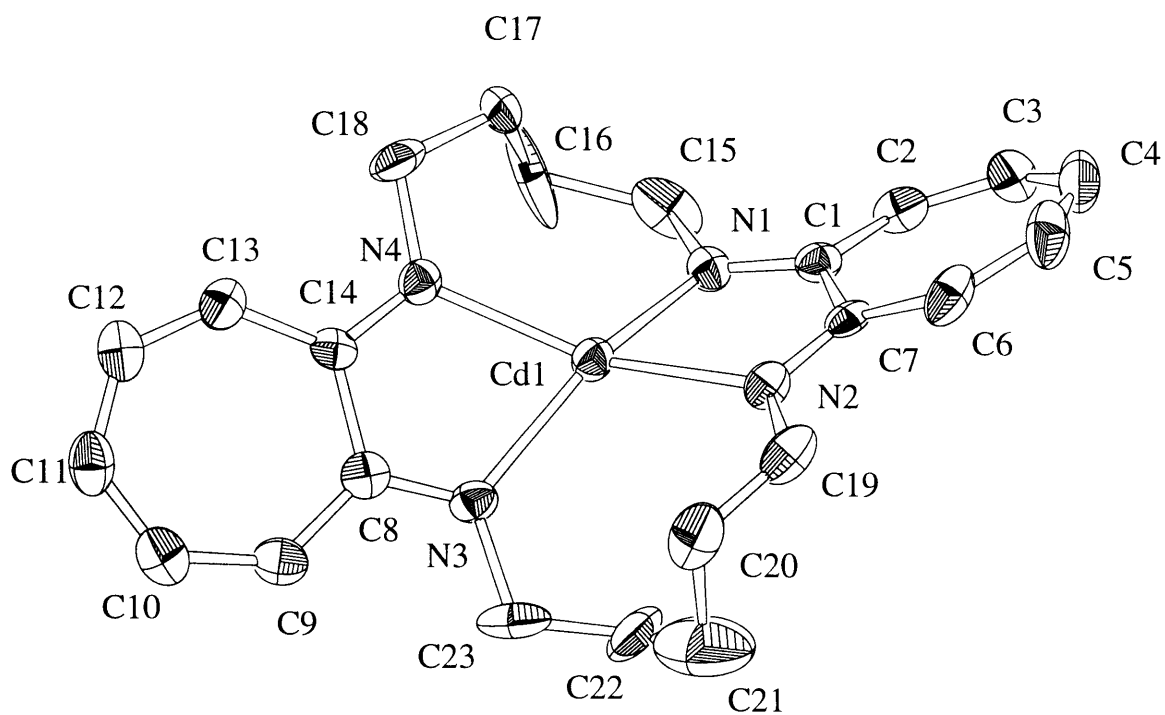
Figure 2.11. ORTEP drawing for one molecule of [Cd(TC-4,5)] from the asymmetric unit showing 40% probability ellipsoids for all non-hydrogen atoms.
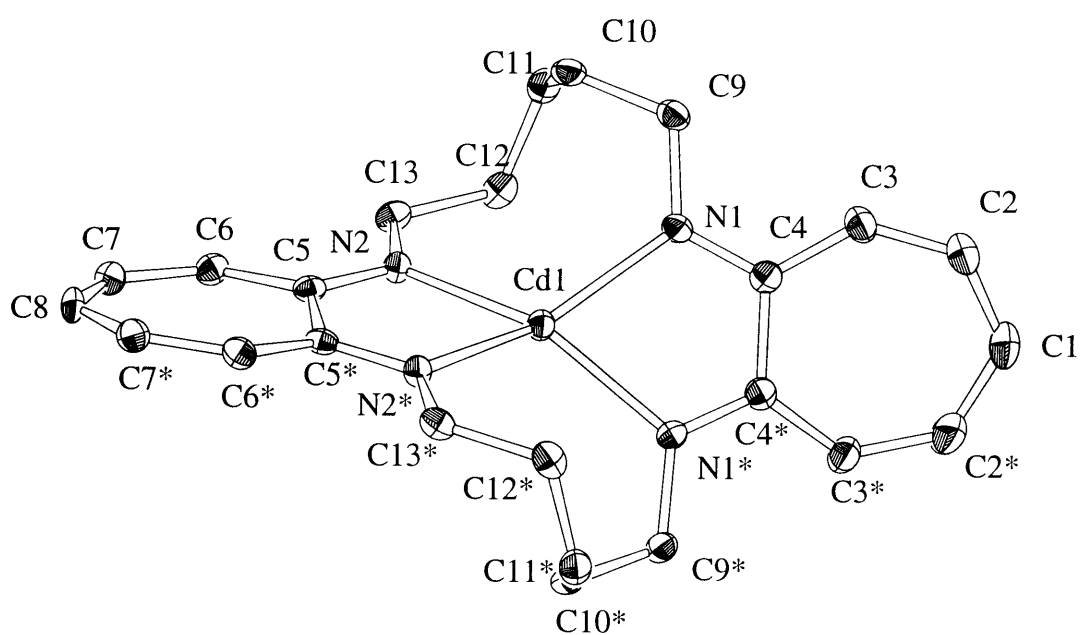
Figure 2.12. ORTEP drawing for [Cd(TC-5,5)] showing 40% probability ellipsoids for all non-hydrogen atoms.
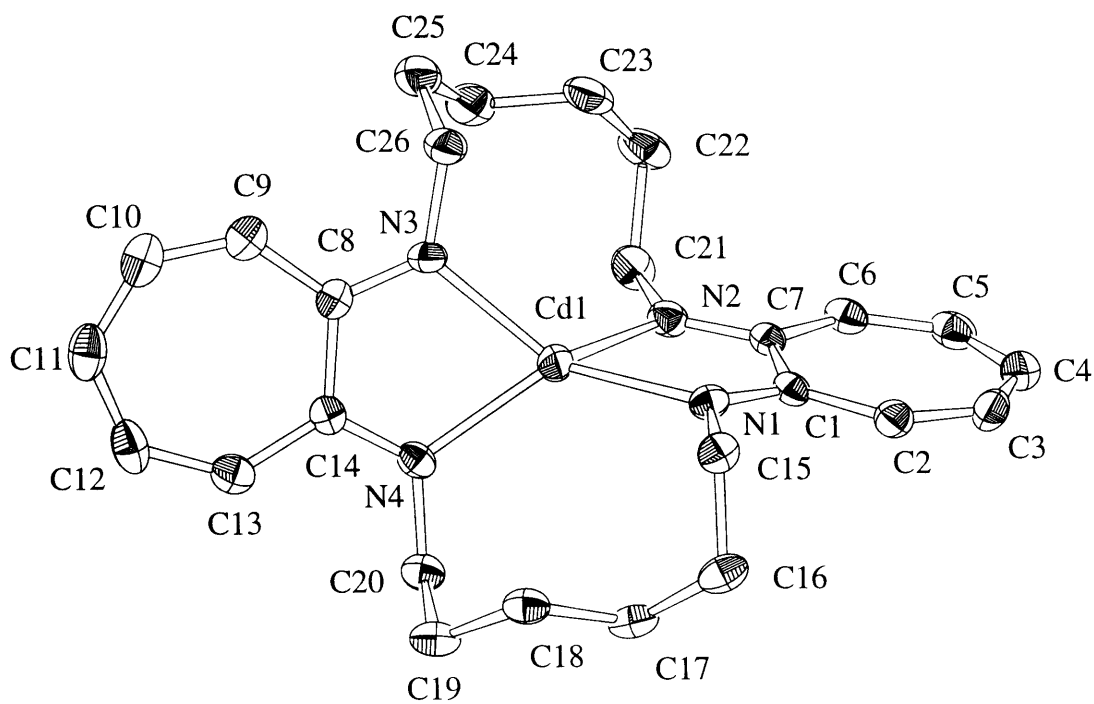
Figure 2.13. ORTEP drawing for [Cd(TC-6,6)] showing 40% probability ellipsoids for all non-hydrogen atoms.
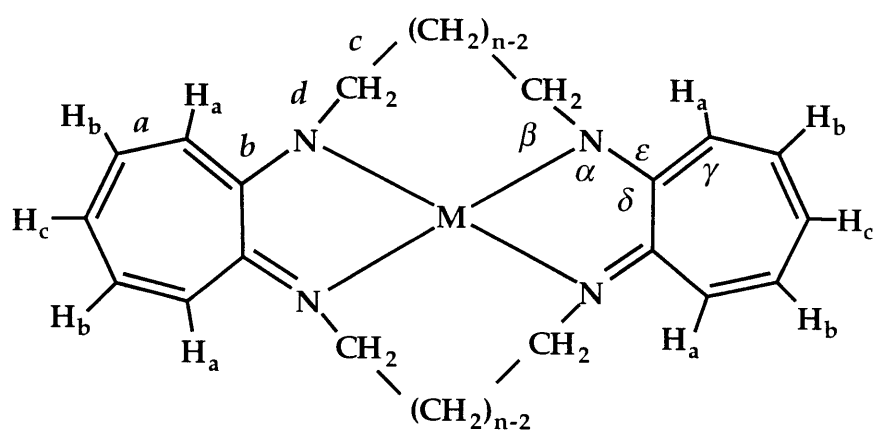
Figure 2.14. Labeling Scheme for ^{1}H-NMR Resonances, Bonds, and Angles in [M(TC-n,m)] Complexes.
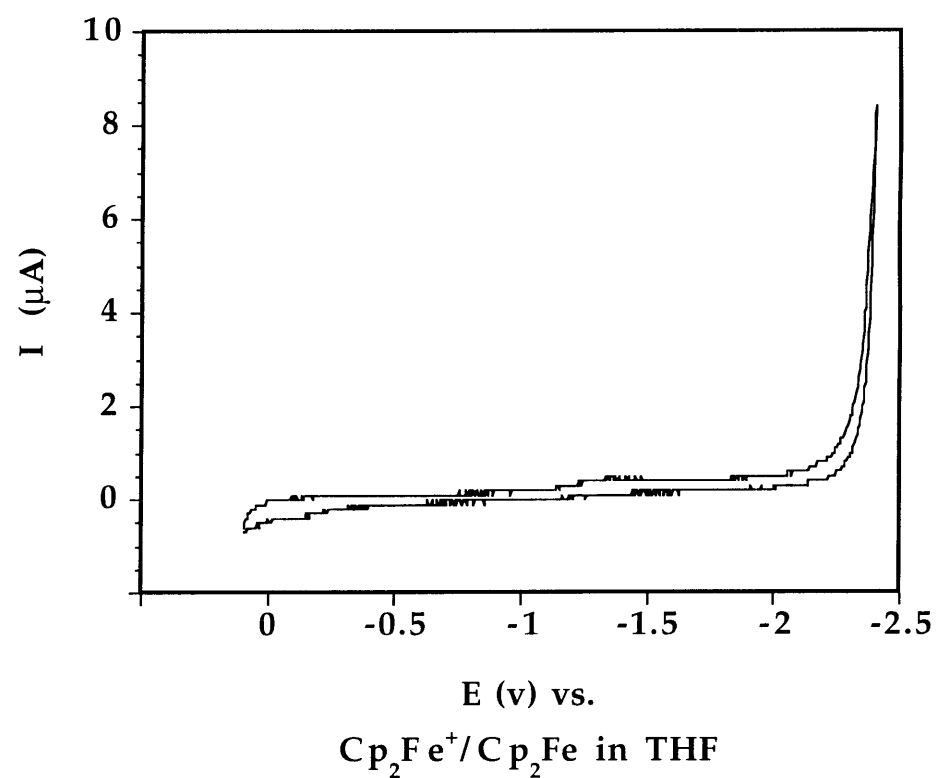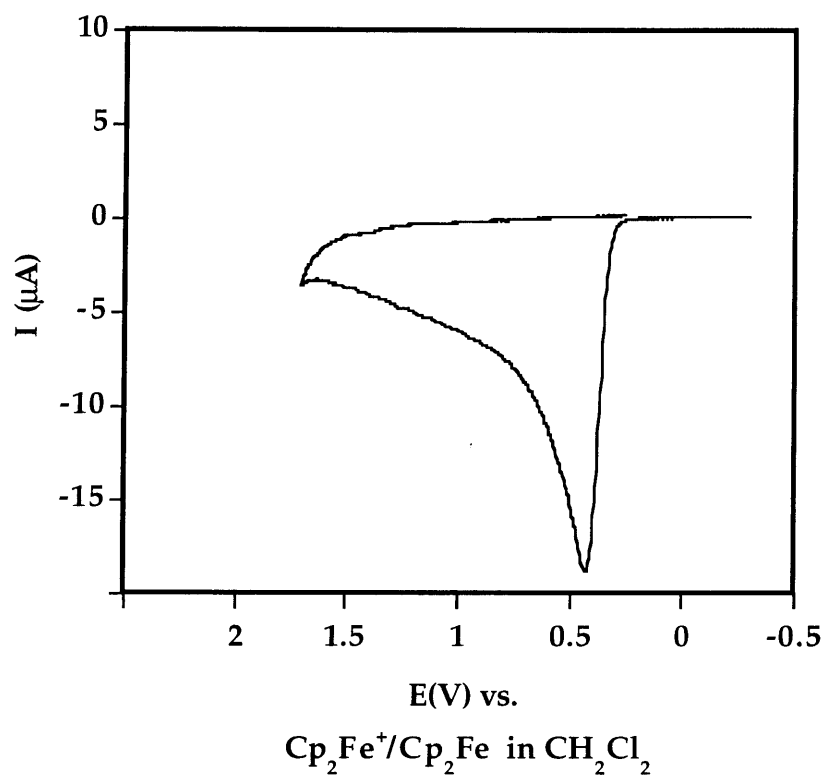
Figure 2.15. Cyclic voltammetry of [Zn(TC-4,4)] in CH_2Cl_2 (right) and THF (left).
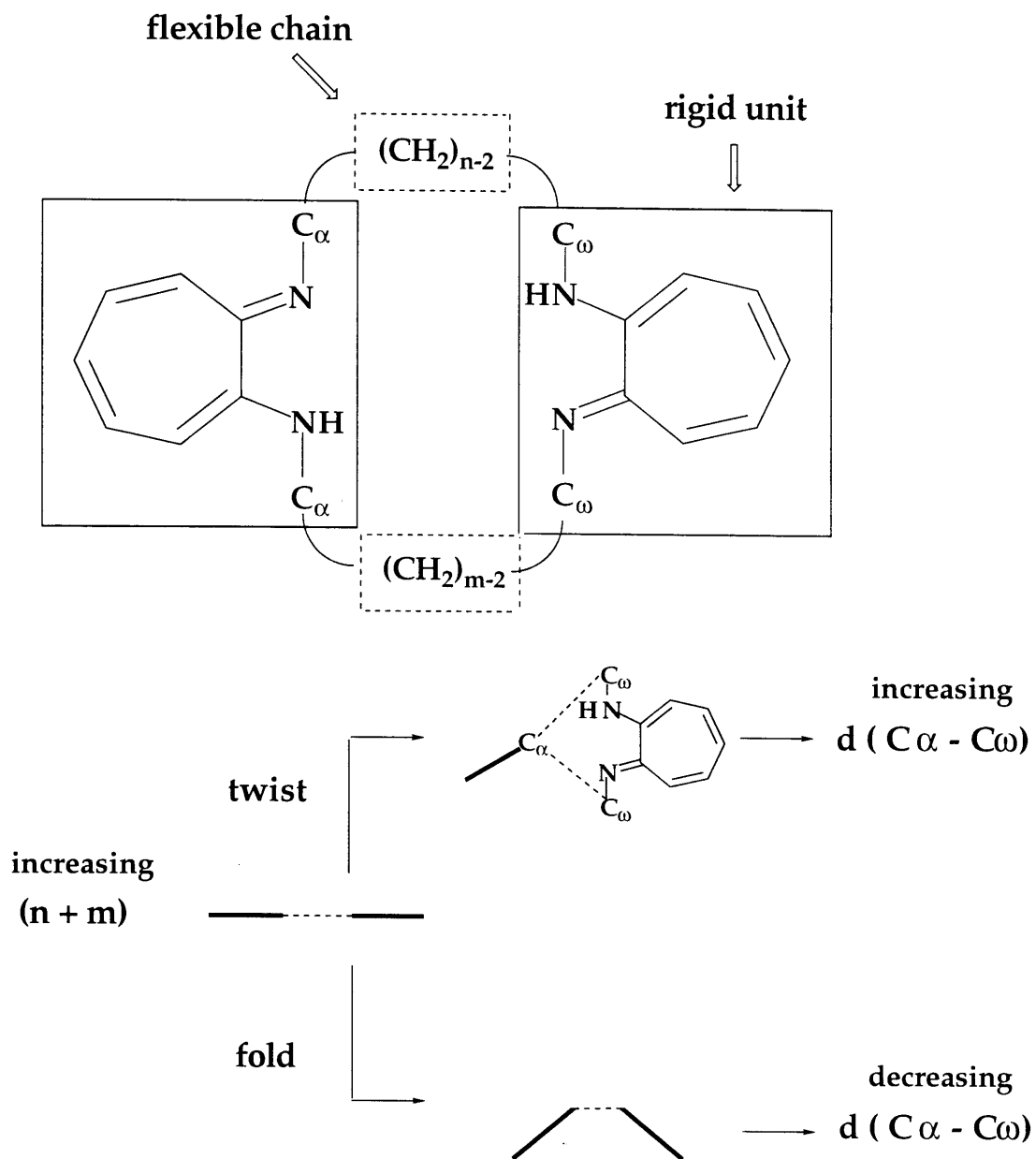
Figure 2.16. Tropocoronand twisting and folding modes.

Chapter 3

Ligand Field Tuning in

Cobalt Tropocoronand Complexes

Introduction

The physical and chemical properties of transition metal compounds derive from their partially-filled frontier d-orbitals. Interactions between these d-orbitals and the ligand donor set reflect the coordination geometries as explained by ligand field theory.[1] The concept of a ligand field was first developed by physicist Hans Bethe in 1929[2] to describe the electronic effects on a central atom by the atoms surrounding it in a crystal. Although this theory was first applied to the study of main group elements in crystals, leading to the name crystal field theory, it has been extensively developed since Bethe's original work. Ligand field theory can now successfully explain many of the electronic, magnetic, and structural properties of transition metal complexes. Most recently molecular orbital (MO) theory has been used to enhance ligand field theory by including the effects of orbital mixing and describing quantitatively changes in orbital energies.

A basic principle of ligand field theory is that the bonding of ligands to a metal ion removes the degeneracy of the five d-orbitals. The new splitting pattern depends primarily on the metal coordination geometry but also on the strength and type (σ and/or π) of ligand donor atoms and the number of d-electrons which give rise to different ligand field stabilization energies (LFSE). Qualitative drawings of the ligand fields for the two most common four-coordinate geometries, square-planar and tetrahedral, are shown in Figure 3.1.

Uncommon geometries can be obtained when the arrangement of donor atoms about the metal center is controlled by ligand design. A macrocyclic ligand ties several donor atoms together and restricts their relative motions in the coordination sphere The tetraazamacrocyclic ligand tropocoronand, H_2TC-n,m, in particular affords a wide variety of coordination geometries as reviewed in Chapter 1. Four-, five-, and six-coordinate transition metal complexes have been synthesized which show that tuning the ligand size also tunes the tropocoronand complex

geometry. By increasing the number of methylene linker units, n and/or m in the macrocycle, the hole size is increased, forcing the ligand into different

$$\text{structure: } -(CH_2)_n^- \text{ and } -(CH_2)_m^- \text{ bridging N atoms around M}$$
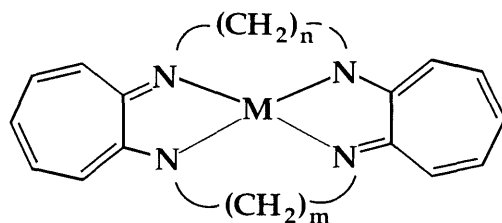
[M(TC-n,m)] tropocoronand

conformations around the metal center. This ligand tuning of metal geometry has been studied in detail for the divalent [M(TC-n,m)] complexes where M = Co,[3] Ni,[4] Cu,[5] Zn,[6] and Cd.[6] The tropocoronand ligand simultaneously tunes the electronic character about the metal center, as described by the ligand field, while tuning the steric properties described by the coordination geometry. Our previous investigations of tropocoronand chemistry have emphasized this ligand steric tuning, but we now focus in this chapter on the concomitant electronic tuning of the [Co(TC-n,m)] ligand fields.

The previously reported[3] stuctural and physical properties of the [Co(TC-n,m)] complexes lay the foundations for investigating the cobalt tropocoronand ligand field and are summarized in Table 3.1. Crystallographic studies of five [Co(TC-n,m)] complexes revealed four-coordinate geometries ranging from almost square-planar in [Co(TC-3,3)] to essentially tetrahedral in [Co(TC-6,6)], as defined by the dihedral angle Θ. The sharp increase in the dihedral angle Θ from 32° to 59° between [Co(TC-4,4)] and [Co(TC-4,5)] divides the complexes into pseudo square-planar and pseudo tetrahedral coordination environments. This discontinuity in ligand twist corresponds to a spin state change from $S = 1/2$ to $S = 3/2$.[3] The complexes would thus seem to be divided into two classes based on their structures and ground state magnetic properties.

The [Co(TC-n,m)] electronic spectra,[3] summarized in Table 3.1, also indicate a division between pseudo square-planar and pseudo tetrahedral complexes. Moreover, differences among the members of two types are revealed which provide direct evidence of quantitative ligand field differences, and therefore electronic tuning, throughout the series of five complexes. The d-d band above 700 nm in the low-spin, pseudo square-planar complexes [Co(TC-3,3)] and [Co(TC-4,4)] decreases in energy with increasing Θ. The high-spin, pseudo-tetrahedral complexes show minimal differences in the energies of their d-d bands. The electronic spectra for all five complexes contain intense charge transfer bands, however, which overlap the d-d transitions in some cases and make assignments difficult.

Qualitative ligand field splitting patterns for square-planar and tetrahedral geometries, corresponding to [Co(TC-3,3)] and [Co(TC-6,6)], respectively, are well-known (Figure 3.1).[7,8] The three inner members of the series, [Co(TC-4,4)], [Co(TC-4,5)], and [Co(TC-5,5)], have intermediate geometries in which the relative ordering of d-orbital energies is less easy to predict. The simple ligand field diagrams in Figure 3.1 assume dihedral angles of 0° and 90° with only σ-donation from the ligands. The numerous structural studies of tropocoronands[9] have shown a range of dihedral angles and four sp^2-hybridized nitrogen atoms which have significant π-donating capability. Therefore, in order to determine the d-orbital splittings in the intermediate four-coordinate geometries of [Co(TC-n,m)], and the effect of π donation from the ligand nitrogen atoms, MO calculations were carried out. The [Co(TC-n,m)] EPR spectra were also recorded to study the ligand field changes as a function of the dihedral angle Θ.

Changes in the magnitude of ligand field splitting energies might also be affected by oxidation to Co(III) or reduction to Co(I). The Co(I) and Co(III) oxidation states are known to be chemically accessible[10,11] for the pseudo-square-planar complexes and we were interested in the effect of ligand twist on the Co(III)/(II) and

Co(II)/(I) redox potentials. Electrochemical studies reported here address this question and the results are interpreted in terms of the new MO calculations.

Together the MO calculations, EPR investigations, and electrochemical studies of the [Co(TC-n,m)] series improve our understanding of the electronic tuning by tropocoronand ligands. Exploitation of changes in ligand field splitting energies with variations in geometry and oxidation state should facilitate our search for tunable reactivity in metal tropocoronand complexes.

Experimental

Reagents. The [Co(TC-n,m)] complexes were synthesized as previously reported.[3] The electrolyte (n-Bu₄N)(PF₆) was purchased from Aldrich Chemical Co. and recrystallized three times from hot acetone. Toluene and THF were distilled from sodium benzophenone ketyl and CH_2Cl_2 from CaH_2 under dinitrogen.

Molecular Orbital Calculations. General. The hypothetical complex $[Co(NH_2)_4]^{p-}$ was used to model $[Co(TC-n,m)]^{q+}$ for Co(I), Co(II), and Co(III), with the local and master coordinate systems chosen as depicted in Figure 3.2. A series of ten calculations was performed, the first on a square-planar complex in which $\Theta = 0°$ and last on a tetrahedral one where $\Theta = 90°$. Eight intermediate steps were taken at $10°$ increments of Θ. The $(NH_2)^-$ groups were chosen to preserve sp^2 hybridization at nitrogen. The ligands were situated between the x and y axes so that rotation of the planes defined by N1-Co-N2 and N3-Co-N4 away from each other would simulate the tropocoronand ligand twist angle Θ and retain the two-fold symmetry of the [Co(TC-n,m)] complexes. This arrangement of the x and y axes relative to the ligands has been used previously in the study of low spin cobalt(II) complexes including porphyrins and phthalocyanines[12] and salen derivatives.[13] Atomic orbital are designated as d_{xz} and molecular orbitals are designated as Ψ_{xz}.

Fenske-Hall. Version 5.1 of the non-empirical Fenske-Hall program[14] was used on a VAX 4000-90 workstation with basis functions generated according to Herman and Skillman's numerical $X\alpha$ atomic orbital program[15] and published $X\alpha$ to STO modifications.[16,17] Calculations were carried out on the crystallographically characterized complexes [Co(TC-3,3)], [Co(TC-4,4)], [Co(TC-4,5)], [Co(TC-5,5)], and [Co(TC-6,6)] and $[Co(NH_2)_4]^{2-}$ to justify the use of $[Co(NH_2)_4]^{2-}$ models in studies of $[Co(NH_2)_4]^{p-}$ with p = 1, 2, 3. In the [Co(TC-n,m)] calculations the x-axis was oriented toward the γ-carbon atom of the aminotroponeiminate ring and the y-axis toward the linker chain, as shown in Figure 3.2.

Extended Hückel. The extended Hückel calculations were carried out on a Gateway 2000 Pentium personal computer with the CACAO program[18] which was also used to generate a Walsh diagram and molecular orbitals for $[Co(NH_2)_4]^{2-}$. The model complex was studied at the same dihedral angles as in the Fenske-Hall calculations except that the end members were 0.1° and 89.9° to maintain the same symmetry throughout the calculation. A complex with dihedral angle of 0.0° has D_{4h} symmetry and a complex with a dihedral angle of 90° has D_{2d} symmetry whereas all the intermediate geometries have D_2 symmetry. When the calculation results showed some mixing of ligand and metal orbitals, the labels were chosen after the atomic orbital with the greatest fractional contribution. Metal orbitals were typically 80-85% pure.

Electrochemistry. Cyclic voltammetric measurements were performed under a nitrogen atmosphere by using an EG&G Model 263 potentiostat. A reference electrode consisting of a silver wire in a 0.1 M AgNO$_3$ in acetonitrile solution[19] was used, for which the ferricinium/ferrocene potential was +0.40 V in CH$_2$Cl$_2$ and +0.10 V in THF. A platinum wire (0.02 in.) was used as an auxiliary electrode and a 1.75 mm^2 platinum disc as the working electrode. Solute samples were typically 2

mM in [Co(TC-n,m)] and 0.5 M solutions of (n-Bu$_4$N)(PF$_6$) were used as the supporting electrolyte.

EPR. Data were collected on a Bruker Model 300 ESP X-band spectrometer at 9.42 GHz fitted with an Oxford Instruments EPR 900 helium cryostat under non-saturating conditions. Solutions were prepared in 3:1 toluene-THF which glasses well at 77 K. Only extremely broad signals were observed for powdered samples diluted in KBr under the same conditions. Data were fit using the EPR-SIM program.[20]

Results and Discussion

MO Calculations. If the tropocoronand ligand in an [M(TC-n,m)] complex were to generate a ligand field of four nitrogen σ-donors in a purely square-planar or tetrahedral geometry, the splittings shown in Figure 3.1 would obtain. Application of the angular overlap model (AOM) method[21,22] allows the contributions from two π-type orbitals to be predicted and an estimate to be made of the relative d-orbital energies in these geometries. The σ and π contributions to each orbital as determined by the AOM method are listed in Table 3.2 and the resultant ligand field splittings are presented in Figure 3.3. Since the coordinate system and relative ligand/axis orientations shown in Figure 3.2 were used in the AOM determination, the energies of the Ψ_{xy} and $\Psi_{x^2-y^2}$ orbitals are reversed in the left side of Figure 3.3 from those in Figure 3.1. Both the qualitative ligand field argument considering only σ donation and the AOM method produce the same relative ordering of the d-orbitals, but the AOM method also shows which orbitals are influenced by π-bonding, represented by the term e_π.

On the right side of Figure 3.3 are given the results of the Fenske-Hall calculations for [Co(TC-3,3)] and [Co(TC-6,6)]. The relationship of these orbitals with those predicted by the AOM model are shown by dashed lines. For [Co(TC-3,3)], the

relative energies of the Ψ_{xz} and Ψ_{yz} orbitals lie above that of the Ψ_{z^2} orbital rather than below the $\Psi_{x^2-y^2}$ orbital energy as predicted by the AOM method. The actual e_π contributions therefore must be different from those predicted by the AOM. This discrepancy arises because the AOM estimation assumes that each ligand has two equally contributing, mutually perpendicular π bonding orbitals. The sp^2-hybridized nitrogen atoms in [Co(TC-3,3)] have only one orbital available for π bonding which lies along the z-axis. There are no π interactions in the xy plane of [Co(TC-3,3)], only in the xz and yz planes. The $4e_\pi$ component estimated for the $\Psi_{x^2-y^2}$ orbital is therefore not present, resulting in the relatively higher energies of Ψ_{xz} and Ψ_{yz} which have such a π-bonding component. The ordering of Ψ_{xz} and Ψ_{yz} relative to Ψ_{z^2} depends upon the magnitudes of e_σ and e_π and, from the Fenske-Hall results, we may conclude that $2\, e_\pi > e_\sigma$.

The effects of π-bonding are also manifest in the ligand field splitting diagram for [Co(TC-6,6)]. In the pseudo-tetrahedral geometry, π donation from the nitrogen atoms is not confined to the xy plane, but influences all the orbitals. The observed splitting of the e and t_2 sets predicted by the Fenske-Hall method is the result of the two-fold symmetry of the tropocoronand ligand, which removes the degeneracy of the Ψ_{xz} and Ψ_{yz} orbitals. There is a greater contribution along the x- than the y-axis because the former is aligned with the π electrons of the aminotroponeiminate rings, destabilizing the Ψ_{xz} and Ψ_{xy} orbitals compared to Ψ_{yz}. The Ψ_{z^2} orbital is less stable than $\Psi_{x^2-y^2}$ because none of the nitrogen donors is in the xy plane but all have a component along the z-axis. These calculated energies of the d-orbital manifold for the end members of the [Co(TC-n,m)] series demonstrate the important effects of π-donation from the nitrogen atoms.

The molecular orbital energies of all the structurally characterized [Co(TC-n,m)] complexes are shown in Figure 3.4. The complex [Co(TC-3,3)], with $\Theta = 9°$ and approximately square-planar geometry, has its Ψ_{xy} orbital most destabilized, as

expected from the choice of axes in Figure 3.2. The $\Psi_{x^2-y^2}$ orbital is most stable for related reasons, the Ψ_{xz} and Ψ_{yz} orbitals are similar in energy and the Ψ_{z^2} orbital is slightly less stabilized than the $\Psi_{x^2-y^2}$ orbital. As Θ increases, there is little change in the energy of the lower four orbitals in [Co(TC-4,4)], but the Ψ_{xy} orbital drops appreciably in energy. This trend continues for [Co(TC-4,5)], [Co(TC-5,5)], and [Co(TC-6,6)]. The d_{xy} orbital is significantly stabilized as the dihedral angle increases and the geometry twists from square-planar. In addition there are slight decreases in the energies of the $\Psi_{x^2-y^2}$ and Ψ_{z^2} orbitals with increasing ligand twist and the Ψ_{xz} and Ψ_{yz} orbitals become more separated in energy. The large difference in orbital energies between [Co(TC-4,4)] and [Co(TC-4,5)] corresponds to the sharp change in Θ between these compounds, demonstrating the direct connection between ligand field energies and metal coordination geometry.

The results of a similar series of calculations for the hypothetical $[Co(NH_2)_4]^{2-}$ complex are presented in Figure 3.5. Ten different geometries were studied at $10°$ increments between $0°$ and $90°$. The plot reproduces the main features of the [Co(TC-n,m)] calculations in Figure 3.4 and justifies using such a model in further work. The Ψ_{xy} orbital is substantially lowered in energy with increasing Θ and there is a slight decrease for the $\Psi_{x^2-y^2}$ orbital across the series. Because of the higher symmetry in the model complex, the Ψ_{xz}/Ψ_{yz} orbitals are degenerate when $\Theta = 0°$ and the Ψ_{xy} and Ψ_{xz} orbitals are degenerate for $\Theta = 90°$. In between these extremes, the Ψ_{xz} orbital is the HOMO when $S = 1/2$ and the Ψ_{xy} is the HOMO for the $S = 3/2$ spin state. The major difference between the [Co(TC-n,m)] and $[Co(NH_2)_4]^{2-}$ calculations is the crossing of the Ψ_{z^2} and Ψ_{yz} orbitals between 60 and $70°$ in the model, which is not present in the [Co(TC-n,m)] calculations.

In order to investigate this disparity, we examined the effect of changing the cobalt oxidation state. Figure 3.6 presents results for the one-electron oxidized Co(III) model, $[Co(NH_2)_4]^-$. The energy changes as a function of Θ generally

resemble those of the Co(II) model. Twisting the symmetry toward tetrahedral geometry gradually stabilizes the Ψ_{xy} orbital with little effect on the $\Psi_{x^2-y^2}$ orbital. Like the Co(II) case, the degeneracy of the Ψ_{xz}/Ψ_{yz} pair is lost with distortion toward tetrahedral symmetry, the Ψ_{xy} and Ψ_{xz} orbitals become degenerate, and the Ψ_{z^2} orbital crosses above the Ψ_{yz}. With Co(III), however, the crossover occurs between 50 and 60°, a smaller angle than for Co(II).

The calculated orbital energies for the Co(I) model, $[Co(NH_2)_4]^{3-}$, are shown in Figure 3.7. As for Co(II) and Co(III), the Ψ_{xy} orbital is gradually stabilized as Θ increases and the $\Psi_{x^2-y^2}$ orbital decreases slightly in energy. The degeneracy of the Ψ_{xz}/Ψ_{yz} pair is removed and the Ψ_{xz} orbital energy increases to that of the Ψ_{xy} orbital for $\Theta = 90°$. The absolute orbital energies calculated for the three oxidation states differ greatly from one another because of the different charges on the three model complexes. The Fenske-Hall method does not take into account the potential well caused by cations.[23] If the three sets of results were placed on the same relative energy scale the absolute values of the orbital energies would be very similar.

The major difference among the calculations for the three oxidation states is the relative energy of the Ψ_{z^2} orbital as a function of twist angle. The ligand field splitting varies in a similar manner for the other four orbitals in the Co(I), Co(II), and Co(III) cases. At low dihedral angles, the Ψ_{z^2} orbital decreases slightly in energy with Θ for Co(I) and increases slightly for Co(II) and Co(III) (Figures 3.5 - 3.7). In all oxidation states, the energy of the Ψ_{z^2} orbital at $\Theta = 0°$ lies between that of the $\Psi_{x^2-y^2}$ and the degenerate Ψ_{xz}/Ψ_{yz} pair. As Θ increases in the Co(II) and Co(III) cases, the Ψ_{z^2} orbital increases in energy and crosses above the energy of the Ψ_{yz} orbital. The crossover point occurs between 60 and 70° for Co(II) and between 50 and 60° for Co(III). In the Co(I) case, however, the Ψ_{z^2} orbital continuously decreases in energy, never crossing the Ψ_{xz} orbital energy. This behavior is /observed for the [Co(TC-n,m)] calculations (Figure 3.4).

Change in the Ψ_{z^2} orbital energy as a function of oxidation state and Θ can be understood by consulting Figure 3.8, where the atomic orbital components of this molecular orbital are depicted. The MO has predominantly d_{z^2} character, with mixing in of the $d_{x^2-y^2}$ and ligand π orbitals to which only the p_x and p_y orbitals from each nitrogen donor contribute significantly. Two trends are apparent in this graph. First, as Θ increases the d_{z^2} and $d_{x^2-y^2}$ orbitals mix to a greater extent, although the latter never becomes dominant. Second, the fractional contribution of the ligand (Np_x,p_y) becomes greater with increasing oxidation state. The net result is that the ligand interaction is increasingly antibonding with increasing Θ, resulting in the highest molecular orbital energy for Ψ_{z^2} at the highest angle (Figures 3.5 and 3.6). For Co(I), the $d_{x^2-y^2}$ contribution increases from zero to 23% and the total ligand contribution increases to 7% as Θ increases from 0° to 90°. When $\Theta = 90°$ for Co(II), the $d_{x^2-y^2}$ contribution is 18% and the ligand contribution has increased to 27%. For Co(III) at 90°, the $d_{x^2-y^2}$ contribution is 12% and that of the ligand 50%. The increased anti-bonding contribution from the ligand at the expense of d-orbital composition is responsible for higher Ψ_{z^2} orbital energies at higher oxidation states. In the Co(I) calculations, the destabilizing interaction of the four in-plane nitrogen donors is negligible and the energy of the Ψ_{z^2} orbital also decreases at higher dihedral angles. In the Fenske-Hall results for the [Co(TC-n,m)] series shown in Figure 3.4, the Ψ_{z^2} orbital decreases in energy with increasing Θ. Figures 3.4 and 3.7 suggest that, in cobalt tropocoronands, the π-antibonding interaction of the nitrogen atoms does not make a significant contribution the Ψ_{z^2} orbital, although π-bonding is important overall in the [Co(TC-n,m)] complexes.

To study the effects of the ligand twist on orbital symmetry and corroborate our Fenske-Hall work, we carried out extended Hückel MO (EHMO) calculations on $[Co(NH_2)_4]^{2-}$. The results are depicted as a Walsh diagram in Figure 3.9. This correlation diagram shows that complex has D_{2d} symmetry in between D_{4h}

symmetry at $\Theta = 0°$ and D_{2d} symmetry when $\Theta = 90°$. The relative orbital energies are in good agreement with those obtained by the Fenske-Hall method, Figure 3.5. Reproduced are the crossover of the Ψ_{yz} and the Ψ_{z^2} orbitals, removal of the degeneracy of Ψ_{xz} and Ψ_{yz}, and the final degeneracy of Ψ_{xy} and Ψ_{xz} orbitals. This consistency reinforces our confidence in the predicted effect of π-donation from the ligand in the [Co(TC-n,m)] and three hypothetical $[Co(NH_2)_4]P^-$ calculations, which destabilize the Ψ_{xz} relative to the Ψ_{z^2} orbital.

Changes in overlap of the ligand nitrogen atoms with the metal for the four highest energy molecular orbitals at three different Θ values are graphically presented in Figures 3.10 and 3.11. In each diagram the nitrogen contribution is shown as one orbital which is a combination of the s, p_x, p_y, and p_z components. The contribution from the metal is also drawn as one orbital, which is in some cases an unequal combination of two d-orbitals, and the MO label is taken from the dominant atomic orbital. Figure 3.10 shows the two highest MO's, the Ψ_{xy} and Ψ_{xz} orbitals in the xz plane at dihedral angles of 0°, 50°, and 90°. Figure 3.11 shows next highest orbitals, the Ψ_{z^2} and Ψ_{yz}, in the xy and yz planes respectively, at the same dihedral angle values.

The decrease in antibonding interaction and the development of an in-phase interaction of the metal d_{xy} orbital with the nitrogen atoms with increasing ligand twist is shown in Figures 3.10(a-c). This orbital is least stable at 0° because it has four anti-bonding sigma interactions with the ligand donor atoms. At higher Θ values, the overlap is reduced and the orbital energy decreases. Figures 3.10(d-f) illustrate the increase in anti-bonding pi interaction of the d_{xz} orbital with the nitrogen atoms as the ligand twist increases, which results in higher orbital energy at larger Θ values.

It was seen earlier in Figure 3.8 that the initial overlap between the d_{z^2} orbital and the nitrogen atoms is minimal. This small interaction is also evident in Figure

3.11(a). As Θ increases, the out-of-phase overlap of the nitrogen p_x and p_y components with the metal orbital increases. This greater anti-bonding contribution with increasing dihedral angle accounts for the gradual destabilization of the Ψ_{z^2} orbital seen in Figures 3.5, 3.6, and 3.9. The energy of the Ψ_{z^2} orbital does not decrease in Figure 3.7 because the fractional contribution of the ligand is insignificant. In Figures 3.11(d-f), the d_{yz} orbital antibonding interactions with the ligand nitrogen atoms are seen not to depend on Θ. These interactions vary in orientation but not phase or magnitude as a function of Θ, resulting in minimal energy changes as shown in Figures 3.4 - 3.7, 3.9.

These MO calculations reveal that the effect of strong π donation from the tropocoronand ligand nitrogen atoms to cobalt is to raise the Ψ_{xz} orbital energy above that of Ψ_{z^2}, in contrast to the situation with pure sigma donors. When the ligand twists from square-planar to tetrahedral geometry, the Ψ_{xz} orbital becomes even less stable because anti-bonding π-donation, localized along the x-axis, increases. There is no such interaction along the y-axis, so that the Ψ_{yz} energy changes little. The MO studies as a function of oxidation state and Θ indicate a very electron rich metal center. The [Co(TC-n,m)] results agree best with the model Co(I) results in which the Ψ_{z^2} is well below the Ψ_{xz} orbital in energy.

EPR Spectroscopy. The frozen solution EPR spectra of [Co(TC-n,m)] complexes, n + m = 6, 8, 9, 10, 12, are presented in Figures 3.12 - 3.16, respectively. These spectra, like those for other d^7 complexes, are visible only at low temperatures, ~ 40 K for $S = 1/2$ cases and ~ 5 K for $S = 3/2$ ground states. The lack of ^{14}N resolved superhyperfine coupling with the unpaired electrons for every [Co(TC-n,m)] complex examined demonstrates that the orbitals occupied by the unpaired electrons are predominantly metal in character, with little ligand contribution. This result is consistent with the MO calculations, which revealed that π-donation to

cobalt is strong, making the metal center relatively electron rich; MO calculations also revealed that ligand contributions to the frontier molecular orbitals are small.

The g-values derived from the [Co(TC-n,m)] frozen solution EPR spectra reflect differences in the ground state energies of the complexes caused by the ligand twist. Since unambiguous determination of the molecular axes relative to the laboratory axes is possible only with single crystal EPR data, we arbitrarily designate the observed signals as g_1, g_2 and g_3. The results are interpreted by comparison to similar complexes in the literature for which single crystal data are available and by use of the ligand field picture discussed above.

Four-coordinate porphyrin and salen low-spin Co(II) complexes have been extensively investigated by EPR spectroscopy. Co(II) porphyrins, which have N_4 coordination like the tropocoronands, display axial spectra owing to the D_{4h} symmetry of the ligand and the $^2A_{1g}$ ground state.[24] Co(II) salen complexes with N_2O_2 ligands have lower, C_{2v}, symmetry and rhombic spectra. Mixing of excited doublet and quartet states also has a substantial effect on the $g_\perp$ and $g_{||}$ values in low-spin Co(II) complexes.[12]

The [Co(TC-3,3)] and [Co(TC-4,4)] EPR data are consistent with previously reported spectra of low-spin Co(II) complexes having ligands with two-fold symmetry.[25] Both [Co(TC-3,3)] and [Co(TC-4,4)] are rhombic with $g_1 >> g_2$ or g_3. In the [Co(TC-3,3)] spectrum, Figure 3.12(a), $g_1 = 2.665$ and there is no hyperfine splitting, in contrast to the g_2 and g_3 signals at 2.077 and 1.955, respectively. The latter appear as two overlapping eight line patterns owing to hyperfine coupling with the ^{59}Co ($I = 7/2$) nucleus. The hyperfine splitting is sufficiently large to be resolved for both components and was fitted as $A_{22} \sim 70 \times 10^{-4}$ cm^{-1} and $A_{33} \sim 30 \times 10^{-4}$ cm^{-1}. The calculated spectrum shown in Figure 3.12(b) was obtained by using the parameters are listed in Table 3.3. The A_{11} component of hyperfine splitting, fit as 10×10^{-4} cm^{-1}, was not resolved in the experiment. The very broad feature

between the g_1 and g_2, g_3 components is believed to be a trace of the Co(III) product from inadvertent oxidation. The air-sensitive [Co(TC-3,3)] complex is the most easily oxidized member of this family of compounds, as indicated by the cyclic voltammetric studies discussed below and previous synthetic work.[26] The [Co(TC-3,3)]+ cation has a ground sate of $S = 1$.[27] The [Co(TC-4,4)] EPR spectrum is shown in Figure 3.13(a), and a fit is included as Figure 3.13(b). As for [Co(TC-3,3)], $g_1 > g_2 \sim g_3$ and the hyperfine splitting from cobalt is not resolved for the g_1 component. The g_2 and g_3 signals at 2.098 and 1.982 are fit to hyperfine splittings of 44 and 29 X 10^{-4} cm^{-1} respectively.

Both fits of the EPR spectra for the low spin complexes are noisy between the g_1 and g_2, g_3, a feature which could only be removed by increasing the linewidths to the point of losing the resolved hyperfine structure. The fits do not take into account mixing of low energy excited doublet or quadruplet states, which have been shown to alter significantly Co(II) EPR spectra.[12] It is possible that the noise might be eliminated by including the appropriate matrices for zero-field splitting, conventionally D and E for rhombic spectra, but this option is not possible with frozen solution EPR data. The g_2 and g_3 components are less similar in square-planar [Co(TC-3,3)] than in [Co(TC-4,4)]; the latter is more twisted toward tetrahedral geometry. Purely tetrahedral complexes have axial spectra in which $g_2 = g_3$. Thus, as the ligand twists toward $\Theta = 90°$, it can be expected that g_2 would approach g_3.

The remaining two pseudo-tetrahedral complexes have EPR spectra that are more axial in character, (Figures 3.15, 3.16). For [Co(TC-5,5)] a single eight line pattern appears near $g_1 = 8$ (800 Gauss) with a very weak feature near $g_{2,3} = 2$ (3100 Gauss). Similar signals are observed in [Co(TC-6,6)] but with different intensities and splitting patterns. Only a broad resonance appears near 1000 Gauss and the hyperfine splitting is not resolved. The g = 2 resonance near 3100 G in the [Co(TC-6,6)] spectrum is split into an eight-line pattern. No reasonable fit could be obtained

for either of these spectra. Conditions could not be found under which the [Co(TC-5,5)] and [Co(TC-6,6)] spectra were more similar to one another and in neither case could the high and low field signals both be well resolved.

In the [Co(TC-5,5)] and [Co(TC-6,6)] spectra, g_2 approaches g_3 as Θ approaches 90°. Only two features are distinguishable in Figures 3.15 and 3.16, indicating that $g_2 \cong g_3$, as expected for essentially tetrahedral ligand fields. These results qualitatively resemble others reported in the literature for high spin Co(II) tetrahedral complexes.[28-32] There is typically a resonance at very low field in which hyperfine splitting is sometimes resolved, similar to the eight line pattern seen in Figure 3.18, and another resonance near $g = 2$, also evident in Figures 3.15 and 3.16.

The [Co(TC-4,5)] complex is pseudo-tetrahedral (Table 3.1) and high-spin ($S = 3/2$) as previously demonstrated by its properties This result led us to anticipate a spectrum similar to those in Figures 3.15 and 3.16 for the other high-spin complexes. As shown in Figure 3.14(a), however, a rhombic signal appears. This spectrum is more consistent with those for low-spin tropocoronand complexes, although the fit (Figure 3.14(b)) is poorer than those for the TC-3,3 or TC-4,4 complexes. The g_1 component still shows no hyperfine coupling and is significantly greater than g_2 or g_3. The latter two signals appear as two overlapping eight-line patterns and were fit with A_{22} and A_{33} as 44 and 30 X 10^{-4} cm^{-1} respectively.

EPR spectra of high-spin Co(II) complexes vary widely, and the observed g' values can mislead the assignment of coordination number and/or geometry.[33] Depending on the degree of distortion from tetrahedral symmetry, the spectra may be axial (little or no distortion) or rhombic. Greater variations from the pattern described for purely tetrahedral symmetry are correlated with more distortion from tetrahedral such that rhombic, not axial, spectra are observed. This effect has been described in detail for the [Co(SPh)$_4$]$^{2-}$ anion. When crystallized with the (Ph$_4$P)$^+$ counterion, this anion has D_{2d} site symmetry,[34] but with (Me$_4$N)$^+$, S_4 symmetry is

observed.[35] The single crystal spectrum of (Ph$_4$P)$_2$[Co(SPh)$_4$] is axial[36] and reveals significant distortion from tetrahedral symmetry in its large zero-field splitting component. The anion in (Me$_4$N)$_2$[Co(SPh)$_4$] has such extreme distortion from tetrahedral symmetry that spectrum is rhombic.[35]

Another factor complicating high-spin Co(II) EPR spectra is the relative energies of the two Kramer's doublets, $\pm$ 1/2 and $\pm$ 3/2, generated in the magnetic field. In the presence of large zero-field splitting, the $\pm$ 1/2 doublet may be *lower* than the $\pm$ 3/2 doublet.[33] If the $\pm$ 1/2 doublet is significantly lower, the spin Hamiltonian can be described with an S' = 1/2 model. The correct energy ordering can be determined from the sign of D in single crystal EPR studies, positive D corresponding to the $\pm$ 1/2 doublet being lowest and negative D to the $\pm$ 3/2 doublet being lowest.

The larger magnetic moment for [Co(TC-4,5)], μ = 4.93 μ_B, versus μ = 4.71 μ_B, for [Co(TC-5,5)],[3] suggests a large zero-field splitting in the less tetrahedral complex. This difference could provide enough asymmetry to produce a rhombic, rather than an axial, pattern, similar to that of (Me$_4$N)$_2$[Co(SPh)$_4$]. The smaller dihedral angle for [Co(TC-4,5)] than [Co(TC-5,5)] or [Co(TC-6,6)] means greater distortion from tetrahedral symmetry. Such a distortion and the large zero-field splitting could lower the $\pm$ 1/2 doublet and produce an S' = 1/2 effective spin Hamiltonian. Thus, although the anomalous g' values for [Co(TC-4,5)] cannot be fully explained with the data in hand, the rhombic pattern is consistent with the other observed structural and magnetic properties, which show large zero-field splitting and a substantial distortion away from tetrahedral symmetry. This series of EPR spectra is further proof that the ligand twist is electronically tuning the metal center, thereby changing the ground and excited state energies as reflected in the observed g values.

Electrochemistry. Cyclic voltammograms were obtained for [Co(TC-n,m)], n + m = 6, 8, 9, 10, 12 dissolved in THF and CH$_2$Cl$_2$. Representative traces for [Co(TC-

3,3)] in THF and [Co(TC-4,4)] in CH_2Cl_2 are presented in Figures 3.17 and 3.18, respectively. Reversible waves for the Co(III)/(II) potentials were obtained. The half-wave potentials and ratios of peak cathodic to peak anodic current are summarized in Table 3.4. Reversible behavior at the electrode during the redox process was established from linear plots of the cathodic and anodic peak currents versus the square root of the scan speed, $v^{1/2}$. A representative plot is given for [Co(TC-4,5)] in CH_2Cl_2 in Figure 3.19. In THF, a quasi-reversible wave attributed to the Co(II)/(I) redox couple was observed (Figure 3.17) which did not display fully reversible behavior over several scans. An irreversible wave, Ep_a, appeared at approximately 0.5 V in CH_2Cl_2 for each complex (Figure 3.18). This feature is attributed to ligand decomposition, based on control experiments with [Zn(TC-n,m)].[6] The Co(II)/(I) half-wave potentials and the Ep_a values for the irreversible oxidations are also indicated in Table 3.4. A plot of the Co(III)/(II) and Co(II)/(I) potentials as a function of dihedral angle Θ is given in Figure 3.20.

The value of $E_{1/2}$ depends in part upon the HOMO and LUMO energies in the reactant and product complexes. The MO calculations above describe variations in d-orbital energies as a function of Θ. These calculations also indicate that the only orbital affected in a major way by a change in oxidation state is the $\Psi_z{}^2$ orbital which is neither the HOMO nor the LUMO. Thus we may assume that the HOMO and LUMO energies of the Co(II) complexes and the oxidized Co(III) and reduced Co(I) products are approximately the same. By using the known electronic configurations and spin states of previously characterized Co(II) and Co(III) tropocoronand complexes, the product HOMOs and LUMOs will be postulated, as described below.

For the sake of simplicity, we first consider the limiting four-coordinate square-planar and tetrahedral geometries first to analyze the low-spin and high-spin Co(II) complexes. Figure 3.21 shows two possible electronic configurations arising from reduction in a square-planar Co(II) complex and two configurations for

oxidation. The related possibilities for reduction and oxidation of a high-spin tetrahedral complex are given in Figure 3.22. The orbital energies are based on the MO calculations shown in Figure 3.3.

Some of the possible product electronic configurations can be initially eliminated as unlikely on the basis of LFSEs. For example, as shown in Figure 3.21, reduction of low-spin Co(II) is expected to yield low spin Co(I) because the difference in energy between the d_{xy} orbital and the d_{xz} is much larger than the pairing energy. Figure 3.22 indicates that reduction of high-spin Co(II) will yield an $S = 0$ system if $\Delta E(d_{xy}\text{-}d_{xz})$ > pairing energy. Filling in electrons reveals that reduction of either low-spin or high-spin Co(II) to $S = 0$ electron configurations requires an electron to be placed in the d_{xz} orbital. The newly occupied orbital, therefore, has higher energy at larger dihedral angles and it is expected that reduction would become more difficult with larger Θ values. This conclusion is consistent with the known preference of d^8 ions for square-planar over tetrahedral geometry based on the large LFSE of the former.[37]

Oxidation of low-spin Co(II) to Co(III), Figure 3.21, is more likely to form an $S = 1$ than $S = 2$ species. This prediction is confirmed by the observed magnetic properties of four-coordinate [Co(TC-n,m)]X complexes.[27] Oxidation of high-spin Co(II) could lead to an $S = 0$ or $S = 1$ system. The latter two possibilities are indistinguishable in this analysis because the tetrahedral orbital splitting energy is much smaller than in the low-spin, square-planar case and could be comparable to the pairing energy. No Co(III) tropocoronands with n + m $\geq$ 9 have yet been prepared. For oxidation in low-spin Co(II) removal of one electron from the Ψ_{yz} orbital should become more difficult with increasing Θ because Ψ_{yz} increases in energy. On the other hand, removal of one electron from the HOMO, the Ψ_{xy} orbital, in high-spin Co(II) would be more facile with increasing Θ because the orbital from which the electron is removed lies higher in energy. Because the

HOMO energy changes non-linearly as a function of Θ, non-linear changes in the Co(III)/(II) potential might also be expected. This analysis indicates that a trend uniformly favoring or opposing oxidation as a function of Θ cannot be predicted on the basis of the HOMO or LFSE's because the d^6 electronic configuration has no strong preference for square-planar versus tetrahedral geometry.

It is also important to consider the changes in ion size upon electron transfer. As demonstrated in Chapter 2, a larger metal ion prefers a smaller Θ value in a [M(TC-n,m)] complex. Since the ionic radius of cobalt decreases with increasing oxidation state, Co(III) < Co(II) < Co(I), we would expect oxidation to be favored at large Θ and reduction at small Θ values.

The $E_{1/2}$ values measured for the Co(II)/(I) potential in THF decrease linearly with increasing Θ as plotted in Figure 3.20. This trend is consistent with the higher d_{xz} energy at larger twist angles, which requires more energy to populate at higher Θ values. The more square-planar macrocycles are also better suited to a d^8 ion, rather than the pseudo-tetrahedral species, at high twist angles because of the large square-planar LFSE. Furthermore, the Co(I) oxidation state is most favored at small Θ values because the increase in size from Co(II) to Co(I) is better accommodated by the smaller macrocycles. The general trend is that, as the ligand twists the metal to more tetrahedral geometries, it is more difficult to reduce Co(II) to Co(I). Our picture of the tropocoronand electronic tuning fully supports this behavior.

The Co(III)/(II) potentials in both THF and CH_2Cl_2 generally increase at larger Θ values, although the correlations are non-linear. The potentials in CH_2Cl_2, in particular, vary widely. This result was not unexpected owing to the known sensitivity of [Co(TC-n,m)] complexes to oxidation in CH_2Cl_2.[26] The solubility of the complexes and the solvent potential windows required use of CH_2Cl_2 to see the ligand decomposition feature near 0.5 V, however. The HOMO changes between low-spin and high-spin Co(II) complexes. If the Co(III)/(II) potential depended

directly on the energy of this orbital, it would therefore not vary linearly as a function of Θ. The preference of smaller ions for larger Θ values suggests that oxidation should be favored by the larger macrocycles because Co(III) is smaller than Co(II), but this trend is the opposite that shown in Figure 3.20. Oxidation is generally more difficult in the tropocoronand complexes with larger dihedral angles and greater ligand twist. This analysis indicates that multiple factors may affect the redox energy in opposing directions, giving rise to a non-linear change in $E_{1/2}$ as a function of Θ.

The shift of redox potentials to favor the best fit of a transition metal ion in a particular macrocycle has been observed for other polyazamacrocyclic ligands.[38] In more flexible aliphatic macrocycles, larger ions are better accommodated by larger ligands, in contrast to the behavior of the more rigid tropocoronand macrocycles. Detailed cyclic voltammetric and EPR studies of macrocyclic Ni(II) complexes with different size ligands showed that larger ligands favored reduction to Ni(I) and rendered oxidation to Ni(III) more difficult.[39] Comparison of substituted 1,4,7-triazacyclononane complexes with analogous 1,5,9-triazacyclododecane species demonstrated that the smaller macrocycle favored smaller ions such as Fe(III) or Co(III) and that the larger macrocycle favored larger ions such as Co(II) or Ni(II).[40] Tetraazamacrocyclic complexes showed a preference for Cu(III) in 15-membered macrocycles but a preference for Ni(III) in 13-membered macrocycles, as determined by cyclic voltammetry.[41] The optimum Ni^{II}-N distance in these systems is 1.85 Å and that of Cu^{II}-N is 1.93 Å, consistent with the larger macrocycle favoring the larger ion.

The change in redox potentials in the series of [Co(TC-n,m)] complexes demonstrates how increasing distortion from square-planar to tetrahedral in four-coordinate systems can moderate $E_{1/2}$. The variation of Co(III)/(II) potentials as a function of macrocycle structure has been studied in other systems as well. Rather

than changing the coordination geometry, Busch and coworkers have studied the effect of altering the macrocycle size while maintaining the geometry by examining octahedral trans-$[Co(MAC)X_2]$ systems where (MAC) is a 13 - 16 membered tetraazamacrocycle.[42] These complexes are all octahedral, but the size of the macrocycle affects the degree of configurational strain energy present. The large LFSE for octahedral Co(III) forces the macrocycles to remain planar at the expense of increased intraligand strain. Upon reduction to Co(II), the LFSE drops significantly such that a rigorous octahedral geometry is no longer maintained and less strained configurations are achieved. Therefore, reduction was more favored in complexes with greater ligand strain energy because the absence of a larger LFSE in d^7 Co(II) permitted the release of strain. Similarly, the 14-membered macrocyclic complex had the least strain energy and was most difficult to reduce to Co(II).

The variation of the Co(III)/(II) potential in macrocyclic systems of varying size without substantial ligand conformational strain has also been investigated. Lacunar cobalt cyclidene systems (cf. Figure 1.3(c)) are 15- or 16-membered tetraazamacrocycles with four imino nitrogen donors bridged by a polymethylene chain.[43] In these systems, the tetraazamacrocycle imposes square-planar geometry at the metal center. Oxidation of d^7 Co(II) to d^6 Co(III) strongly favors octahedral coordination and, in the absence of a chain or with a long chain, solvent molecules complete the coordination sphere. Smaller chains restrict access to the metal center, keeping solvent molecules out of the lacuna, and disfavoring Co(III) relative to Co(II). Therefore, little variation in Co(III)/(II) potentials occurs for the 15- versus 16-membered macrocycles, but decreasing the polymethylene chain length led to more difficult oxidations.

From the data reported here and from previously published work, it can be seen that the redox potentials of transition metals in macrocyclic complexes are affected in several ways. First, the metal oxidation state which best accommodates

the size of the macrocycle is favored. Second, release of conformational strain upon electron transfer can favor electron configurations with smaller LFSEs. Third, geometric restrictions of the macrocycle favor d-electron counts for which the LFSEs match the preferred ligand configuration. The result in cobalt tropocoronands is that the $E_{1/2}$ values are finely tuned over approximately 0.25 V to stabilize increasingly Co(II) relative to both oxidation and reduction at increasingly large Θ values.

The tropocoronand ligand twist effects on cobalt $E_{1/2}$ values demonstrate fine tuning of transition metal redox potentials. Coarse tuning of redox potentials was demonstrated previously in our laboratory for Fe(III)/(II) potentials in FeX_6 systems.[44] In these studies the ligand donor atoms were varied from O_6 to N_2O_4, N_3O_3 and N_6 resulting in a 0.87 V increase in $E_{1/2}$. In the [Co(TC-n,m)] complexes, the N_4 donor set composition is held constant, but its geometry is varied resulting in a 340 mV increase in the Co(II)/(I) potential and a 230 mV decrease in the Co(III)/(II) potential over the series, as plotted in Figure 3.20.

Conclusions

The present investigation of [Co(TC-n,m)] complexes has demonstrated that electronic tuning of the metal center accompanies the steric tuning described previously. A qualitative picture of the ligand-field splitting for [Co(TC-n,m)] complexes has been developed by MO calculations on structurally characterized Co(II) complexes and on model complexes in the Co(I), Co(II), and Co(III) oxidation states. Nitrogen π-donation to cobalt and the tropocoronand ligand twist produce substantial changes in the ligand field splitting energies from those predicted for σ-donors with strictly square-planar or tetrahedral symmetries. Variation of the dihedral angle Θ therefore affects the ground state energies of [Co(TC-n,m)] complexes. The rhombic EPR spectra of the $S = 1/2$ [Co(TC-n,m)] complexes are

consistent with other square-planar Co(II) compounds having C_2 symmetry. The more tetrahedral $S = 3/2$ complexes have axial spectra similar to previously characterized tetrahedral Co(II) complexes, but the spectrum of [Co(TC-4,5)] corresponds to neither extreme. Here the tropocoronand twist has produced a high spin complex in which the large zero-field splitting and pseudo-tetrahedral geometry give rise to a rhombic EPR spectrum, similar to the low-spin tropocoronand complexes.

The changes in the frontier d-orbital energies afford changes in the $E_{1/2}$ potentials for oxidation to Co(III) and reduction to Co(I). The ligand twist fine tunes the Co(III)/(II) and Co(II)/(I) redox potentials owing to changes as a function of Θ in (1) the relative energies of the frontier orbitals, (2) the LFSE for reactant and product oxidation states, and (3) the size of the metal ion relative to the macrocycle hole as a function of dihedral angle. The results are consistent with the proposed ligand field model based on MO calculations.

References

(1)   Figgis, B. N. *Introduction to Ligand Fields*; Interscience Publishers: New York, 1966.

(2)   Bethe, H. *Ann. Physik* **1929**, *3*, 133-206.

(3)   Jaynes, B. S.; Doerrer, L. H.; Liu, S.; Lippard, S. J. *Inorg. Chem.* **1995**, *34*, 5735-5744.

(4)   Davis, W. M.; Roberts, M. M.; Zask, A.; Nakanishi, K.; Lippard, S. J. *J. Am. Chem. Soc.* **1985**, *107*, 3864-3870.

(5)   Davis, W. M.; Zask, A.; Nakanishi, K.; Lippard, S. J. *Inorg. Chem.* **1985**, *24*, 3737-3743.

(6)   Doerrer, L. H., Chapter 2.

(7)   Douglas, B. E.; McDaniel, D. H.; Alexander, J. J. *Concepts and Models of Inorganic Chemistry*; John Wiley & Sons, Inc.: New York, 1983.

(8)   Cotton, F. A. *Chemical Applications of Group Theory*; John Wiley & Sons, Inc.: New York, 1990.

(9)   Doerrer, L. H., Chapter 1.

(10)   Jaynes, B. S.; Ren, T.; Liu, S.; Lippard, S. J. *J. Am. Chem. Soc.* **1992**, *114*, 9670-9671.

(11)   Jaynes, B. S.; Ren, T.; Masschelein, A.; Lippard, S. J. *J. Am. Chem. Soc.* **1993**, *115*, 5589-5599.

(12)   McGarvey, B. R. *Can. J. Chem.* **1975**, *53*, 2498-2511.

(13)   Urbach, F. L.; Bereman, R. D.; Topich, J. A.; Hariharan, M.; Kalbacher, B. J. *J. Am. Chem. Soc.* **1974**, *96*, 5063-5069.

(14)   Hall, M. B.; Fenske, R. F. *Inorg. Chem.* **1972**, *11*, 768.

(15)   Herman, F.; Skillman, S. *Atomic Structure Calculations*; Prentice-Hall: Englewood Cliffs, NJ, 1963.

(16)   Bursten, B. E.; Fenske, R. F. *J. Chem. Phys.* **1977**, *67*, 3138.

(17)   Bursten, B. E.; Jensen, R. J.; Fenske, R. F. *J. Chem. Phys.* **1978**, *68*, 3320.

(18)   Mealli, C. M.; Proserpio, D. M. *J. Chem. Ed.* **1990**, *67*, 399-402.

(19)   Mann, C. K. In *Electroanalytical Chemistry*; Bard, A. J., Ed.; Marcel Dekker: New York, 1969; Vol. 3, pp 61.

(20)   Wilson, J. M., *EPR-SIM*, 1990, Cambridge, MA

(21)   Purcell, K. F.; Kotz, J. C. *An Introduction to Inorganic Chemistry*; Saunders College: Philadelphia, 1980.

(22)   Larsen, E.; La Mar, G. N. *J. Chem. Ed.* **1974**, *51*, 633-640.

(23)   Fenske, R. F.; Radtke, D. D. *Inorg. Chem.* **1968**, *7*, 479-487.

(24)   Walker, F. A. *J. Magn. Reson.* **1974**, *15*, 201-218.

(25)   Malatesta, V.; McGarvey, B. R. *Can. J. Chem.* **1975**, *53*, 3791-3800.

(26)   Jaynes, B. S., PhD thesis, Massachusetts Institute of Technology, 1992

(27)   Doerrer, L. H., Chapter 4.

(28)   Symons, M. C. R.; Taiwo, T.; Sargeson, A. M.; Ali, M. M.; Tabl, A. S. *Inorg. Chim. Acta* **1996**, *241*, 5-8.

(29)   Drulis, H.; Dyrek, K.; Hoffman, K. P.; Hoffman, S. K.; Weselucha-Birczynska, A. *Inorg. Chem.* **1985**, *24*, 4009-4012.

(30)   Werth, M. T.; Tang, S.-F.; Formicka, G.; Zeppezauer, M.; Johnson, M. K. *Inorg. Chem.* **1995**, *34*, 218-228.

(31)   Makinen, M. W.; Kuo, L. C.; Yim, M. B.; Wells, G. B.; Fukuyama, J. M.; Kim, J. E. *J. Am. Chem. Soc.* **1985**, *107*, 5245-5255.

(32)   Louati, A.; Kuncaka, A.; Gross, M.; Haubtmann, C.; Bernard, M.; Andre, J.-J.; Brunette, J.-P. *J. Organmet. Chem.* **1995**, *486*, 95-104.

(33)   Banci, L.; Bencini, A.; Benelli, C.; Gatteschi, D.; Zanchini, C. *Structure and Bonding* **1982**, *52*, 37-86.

(34)   Swenson, D.; Baenziger, N. C.; Coucouvanis, D. *J. Am. Chem. Soc.* **1978**, *100*, 1932-1934.

(35)   Fukui, K.; Masuda, H.; Ohya-Nishiguchi, H.; Kamada, H. *Inorg. Chim. Acta* **1995**, *238*, 73-81.

(36)   Fukui, K.; Kojima, N.; Ohya-Nishiguchi, H.; Hirota, N. *Inorg. Chem.* **1992**, *31*, 1338-1344.

(37)   Cotton, F. A.; Wilkinson, G. *Advanced Inorganic Chemistry*; 5th ed.; John Wiley & Sons, Inc.: New York, 1988.

(38)   Busch, D. H. *Acc. Chem. Res.* **1978**, *11*, 392-400.

(39)   Lovecchio, F. V.; Gore, E. S.; Busch, D. H. *J. Am. Chem. Soc.* **1974**, *96*, 3109-3117.

(40)   Zhang, D.; Busch, D. H. *Inorg. Chem.* **1994**, *33*, 5138-5143.

(41)   Kimura, E.; Koike, T.; Machida, R.; Nagai, R.; Kodama, M. *Inorg. Chem.* **1984**, *23*, 4181-4188.

(42)   Hung, Y.; Martin, L. Y.; Jackels, S. C.; Tait, A. M.; Busch, D. H. *J. Am. Chem. Soc.* **1977**, *99*, 4029-4039.

(43)   Chavan, M. Y.; Meade, T. J.; Busch, D. H.; Kuwana, T. *Inorg. Chem.* **1986**, *25*, 314-321.

(44)   Rosenzweig, A. C.; Feng, X.; Lippard, S. J. In *Applications of Enzyme Biotechnology*; Kelly, J. W., Ed.; Plenum Press: New York, 1991.

Table 3.1 Physical Properties of [Co(TC-n,m)] Complexes

	Θ (deg)	spin state (S)	approximate geometry	d-d transition bands (nm {e_M, $M^{-1}cm^{-1}$})
[Co(TC-3,3)]	9.0	1/2	square-planar	614 (2490), 738 (870)
[Co(TC-4,4)]	31.8	1/2	square-planar	592 (44000, 801 (1270)
[Co(TC-4,5)]	59.0	3/2	tetrahedral	598 (1180)
[Co(TC-5,5)]	69.9	3/2	tetrahedral	596 (820)
[Co(TC-6,6)]	84.5	3/2	tetrahedral	565 (1170), 599 (950), 670 (100)

153

Table 3.2. AOM Orbital Energies for ML_4 complexes with Square-planar and Tetrahedral Geometries.

d-orbital	square-planar σ only	square-planar σ and π	tetrahedral σ only	tetrahedral σ and π
z^2	e_σ	e_σ	- -	$8/3\,e_\pi$
$x^2\text{-}y^2$	$3\,e_\sigma$	$3\,e_\sigma$	- -	$8/3\,e_\pi$
xz	- -	$2\,e_\pi$	$4/3\,e_\sigma$	$4/3\,e_\sigma + 8/9\,e_\pi$
yz	- -	$2\,e_\pi$	$4/3\,e_\sigma$	$4/3\,e_\sigma + 8/9\,e_\pi$
xy	- -	$4\,e_\pi$	$4/3\,e_\sigma$	$4/3\,e_\sigma + 8/9\,e_\pi$
total	$4\,e_\sigma$	$4\,e_\sigma + 8\,e_\pi$	$4\,e_\sigma$	$4\,e_\sigma + 8\,e_\pi$

Table 3.3. Fitting Values for Simulated [Co(TC-n,m)] EPR Spectra.

complex	g_1	g_2	g_3	A_{11}	A_{22}	A_{33}	line width
				$\times 10^{-4}$ cm^{-1}			(G)
[Co(TC-3,3)]	2.665	2.077	1.955	10	69	26	13
[Co(TC-4,4)]	2.610	2.098	1.982	8	44	29	10
[Co(TC-4,5)]	2.610	2.035	2.025	10	44	30	15

Table 3.4. Cyclic Voltammetric Data for [Co(TC-n,m)] Complexes.[a]

complex	THF			CH_2Cl_2		
	Co(II)/Co(I)	Co(III)/Co(II)	I_{p_c}/I_{p_a}	Co(III)/Co(II)	I_{p_c}/I_{p_a}	E_{p_a}
[Co(TC-3,3)]	-2.12	-0.49	0.87	-0.43	0.95	0.49
[Co(TC-4,4)]	-2.22	-0.41	0.97	-0.56	0.84	0.54
[Co(TC-4,5)]	-2.35	-0.38	0.91	-0.30	1.00	0.52
[Co(TC-5,5)]	-2.40	-0.24	1.00	-0.34	0.95	0.49
[Co(TC-6,6)]	-2.46	-0.26	0.98	-0.37	0.96	0.55

[a]All potentials are given in volts and referenced to Cp_2Fe^+/Cp_2Fe at 0.0 V in the appropriate solvent.

L

L ———————————— L   +y

L

+x

square-planar complex, ML$_4$

$\overline{}$ b_{1g}
d$_{x2-y2}$

$\overline{}$ a_{1g}
d$_{z2}$

$\overline{}$ b_{2g}
d$_{xy}$

$\overline{}$ $\overline{}$ e_g
d$_{xz}$ d$_{yz}$

D$_{4h}$

$\overline{}$ $\overline{}$ $\overline{}$ $\overline{}$ $\overline{}$

d$_{z2}$ d$_{yz}$ d$_{xz}$ d$_{xy}$ d$_{x2-y2}$

+z

L

L

L   +y

+x

L

T$_d$ $\overline{}$ $\overline{}$ $\overline{}$ t_2
d$_{xz}$ d$_{yz}$ d$_{xy}$

$\overline{}$ $\overline{}$ e
d$_{x2-y2}$ d$_{z2}$

tetrahedral complex, ML$_4$
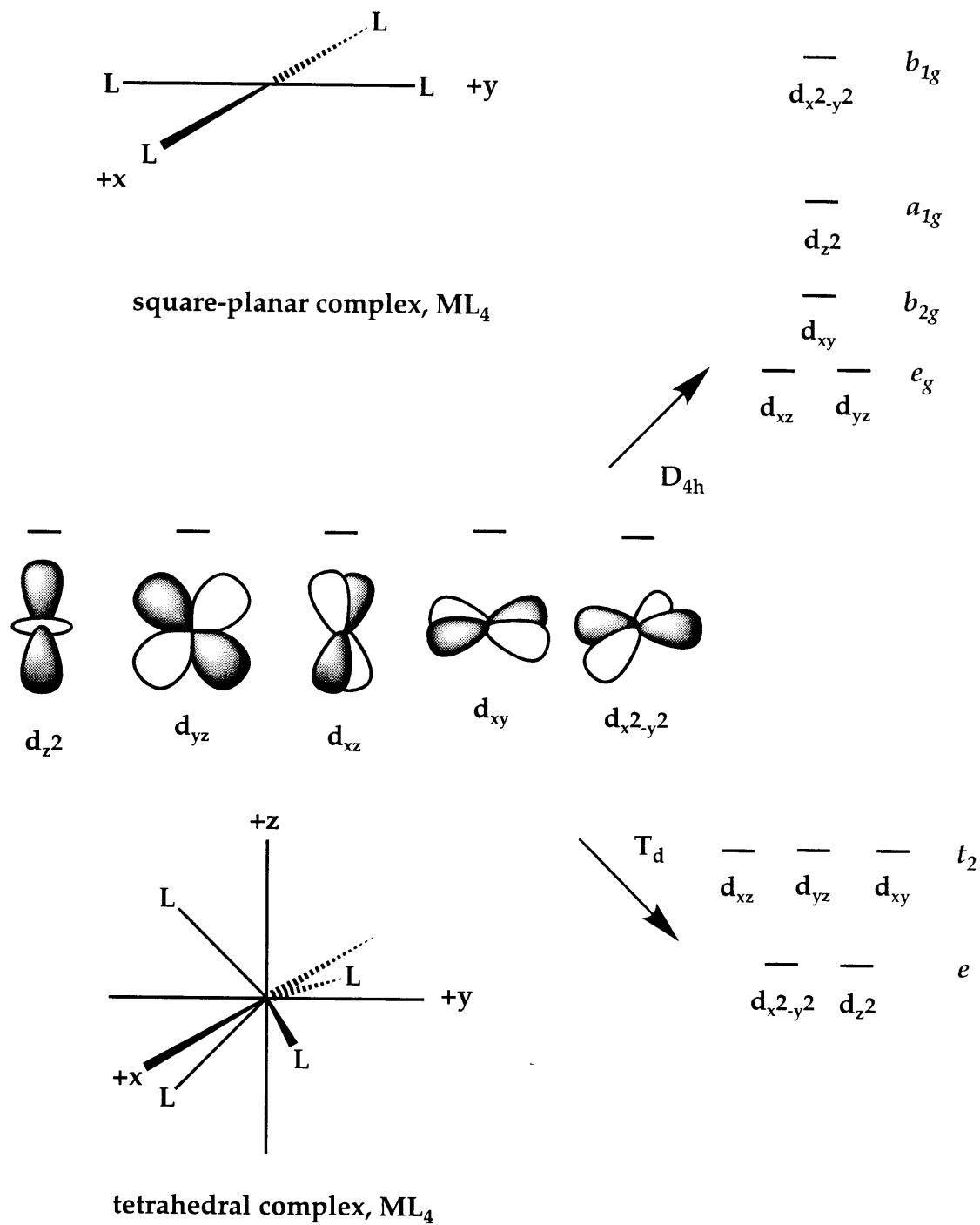
Figure 3.1. Ligand field splitting diagrams for square-planar and tetrahedral complexes.
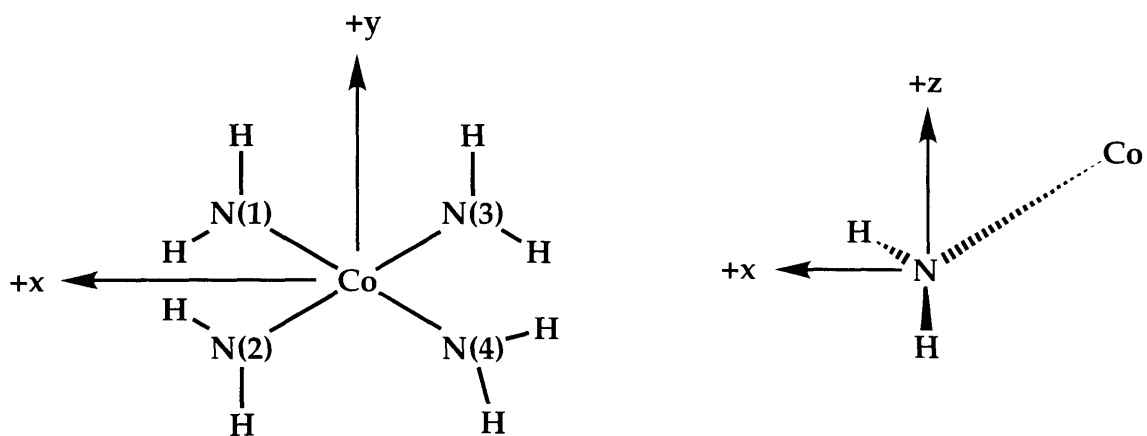
Master Coordinate System   Local Coordinate System
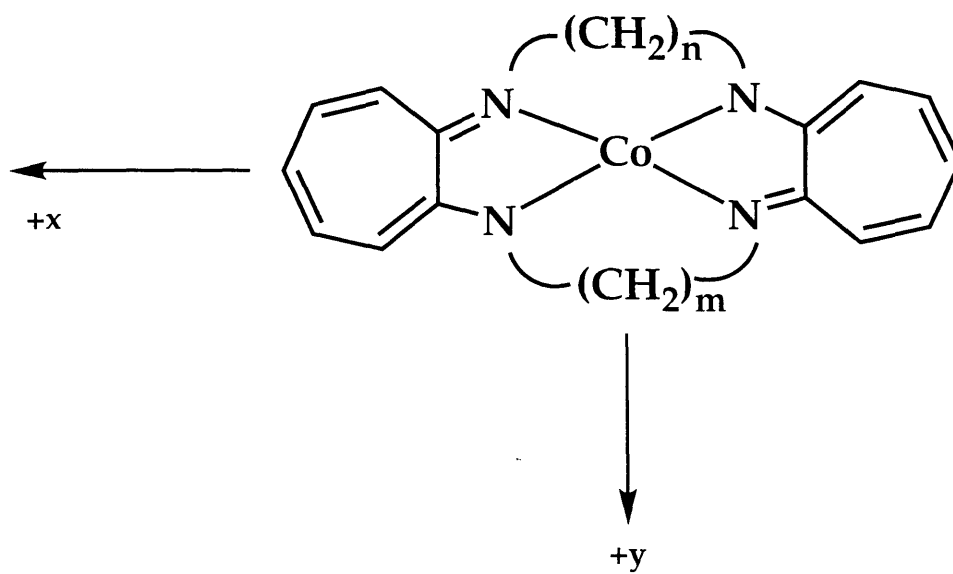
Cobalt Tropocoronand Coordinate System

Figure 3.2. Coordinate systems used for Fenske-Hall and Extended Hückel Calculations.

predicted by AOM

from Fenske-Hall calculations on
tropocoronand complexes

square-planar

$3\,e_\sigma$ — — — — — — — — — — — — — — Ψ_{xy}

d_{xy}

e_σ —

d_{z^2}

$4\,e_\pi$ —

$d_{x^2-y^2}$

$2\,e_\pi$ — —

$d_{xz}\quad d_{yz}$

Ψ_{xz}
Ψ_{yz}

Ψ_{z^2}

$\Psi_{x^2-y^2}$

[Co(TC-3,3)]

$4/3\,e_\sigma + 8/9\,e_\pi$ — — —

$d_{xz}\quad d_{yz}\quad d_{xy}$

Ψ_{xy}
Ψ_{xz}

tetrahedral

$8/3\,e_\pi$ — —

$d_{x^2-y^2}\quad d_{z^2}$

Ψ_{yz}

Ψ_{z^2}

$\Psi_{x^2-y^2}$
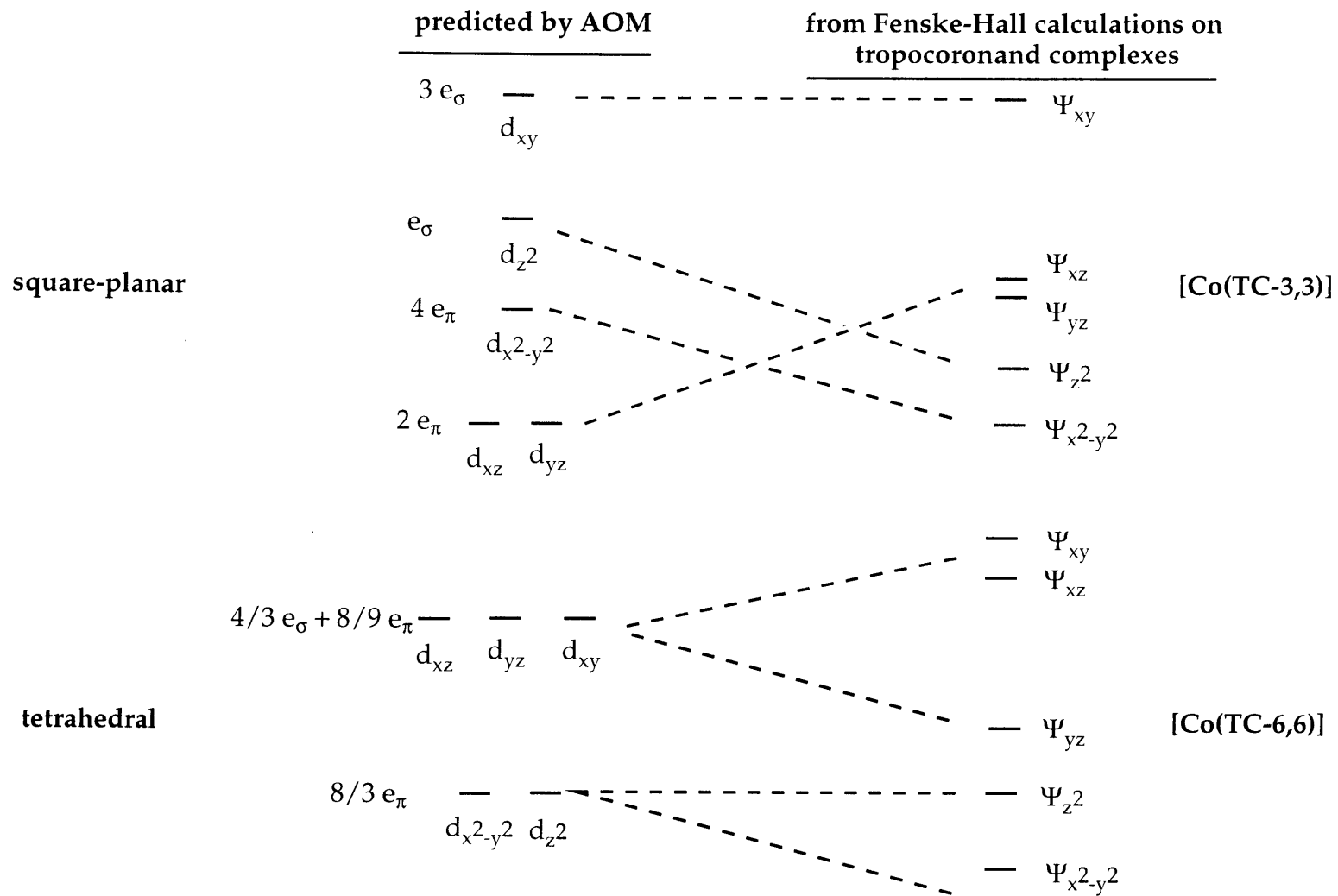
[Co(TC-6,6)]

Figure 3.3. AOM predicted splitting patterns for square-planar and tetrahedral geometries and Fenske-Hall calculated energy levels for [Co(TC-3,3)] and [Co(TC-6,6)].
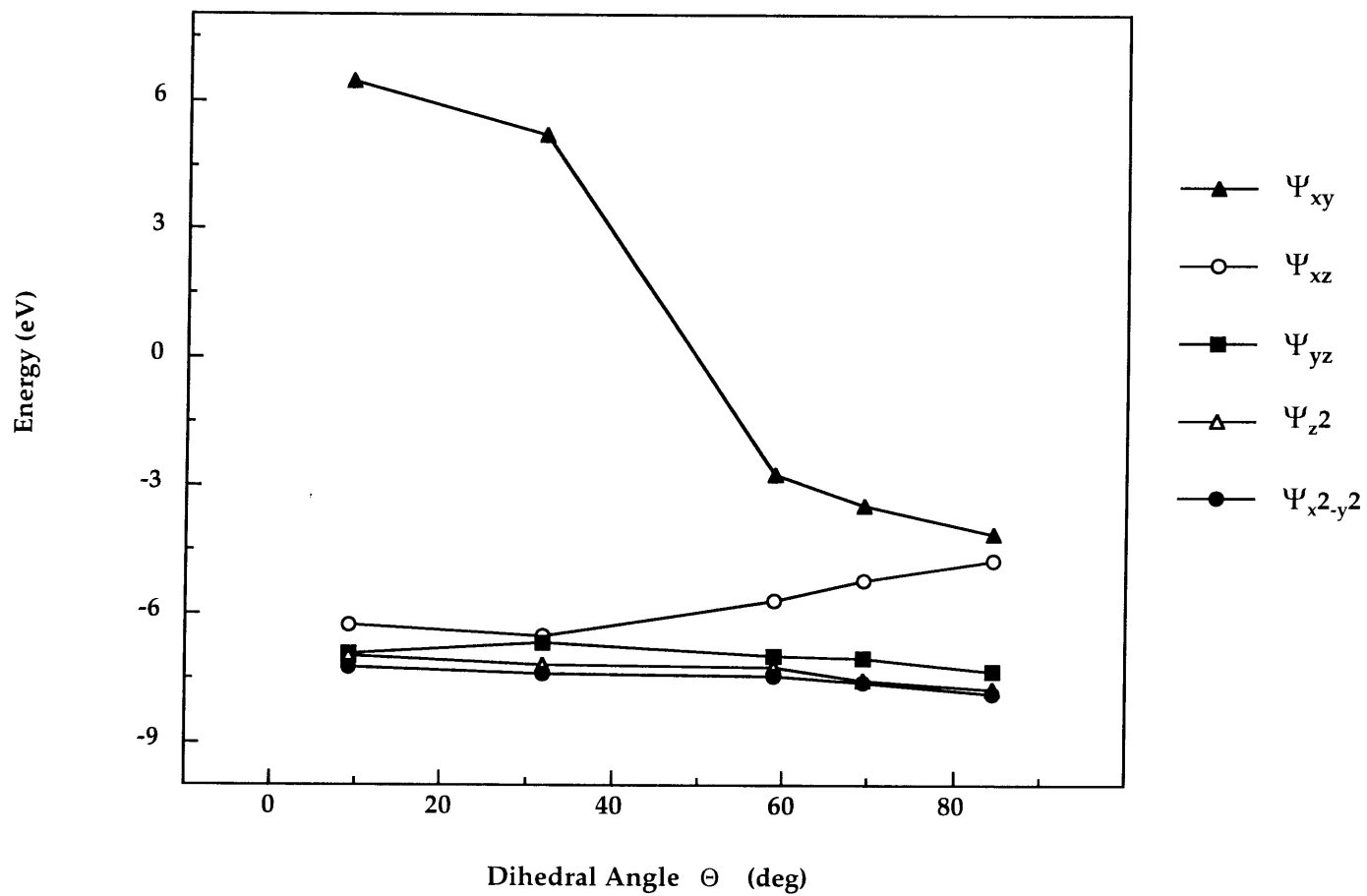
Figure 3.4. Energies of frontier molecular orbitals from Fenske-Hall calculations on [Co(TC-n,m)].
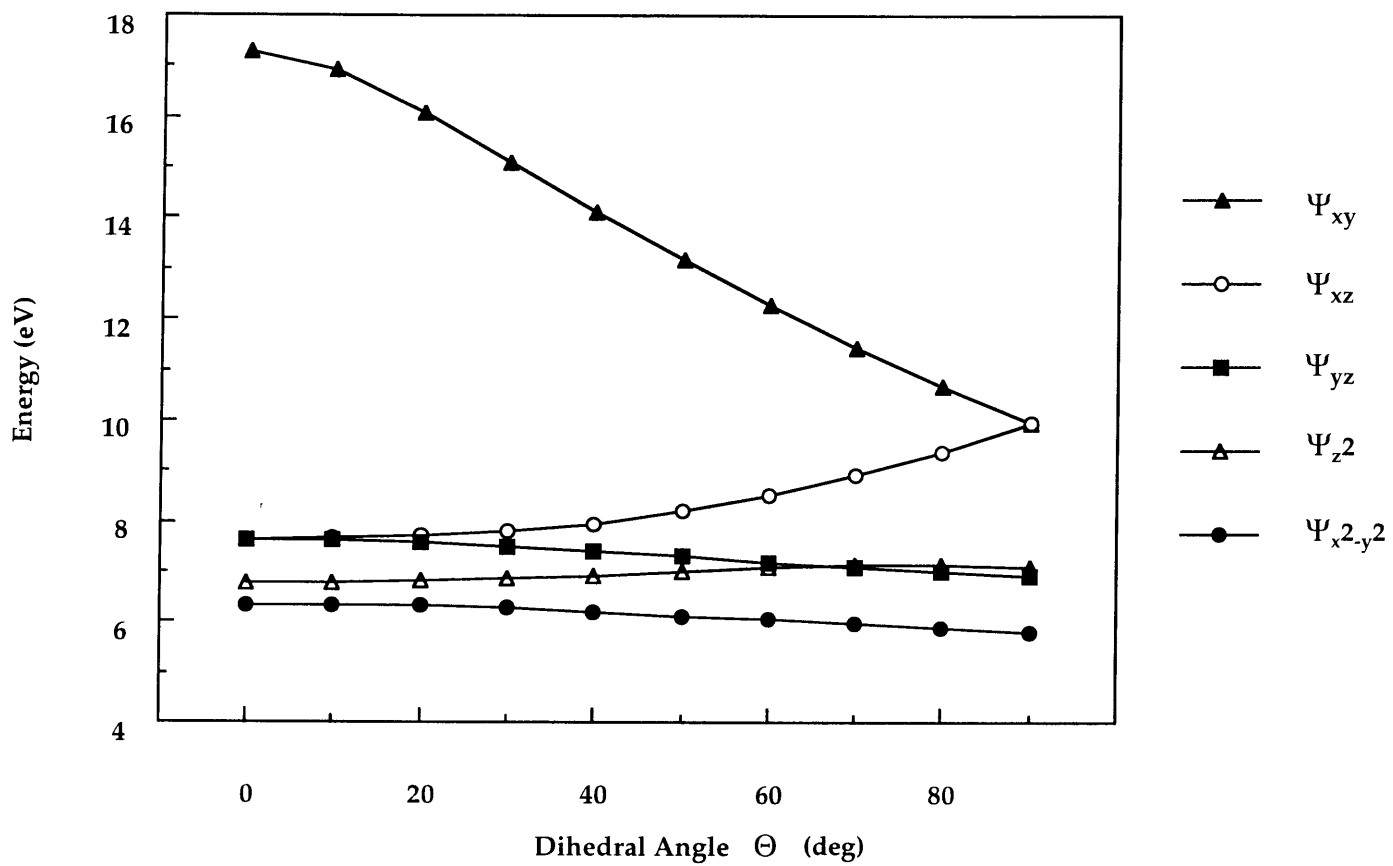
Figure 3.5. Energies of frontier molecular orbitals from Fenske-Hall calculations on $[Co(NH_2)_4]^{2-}$.
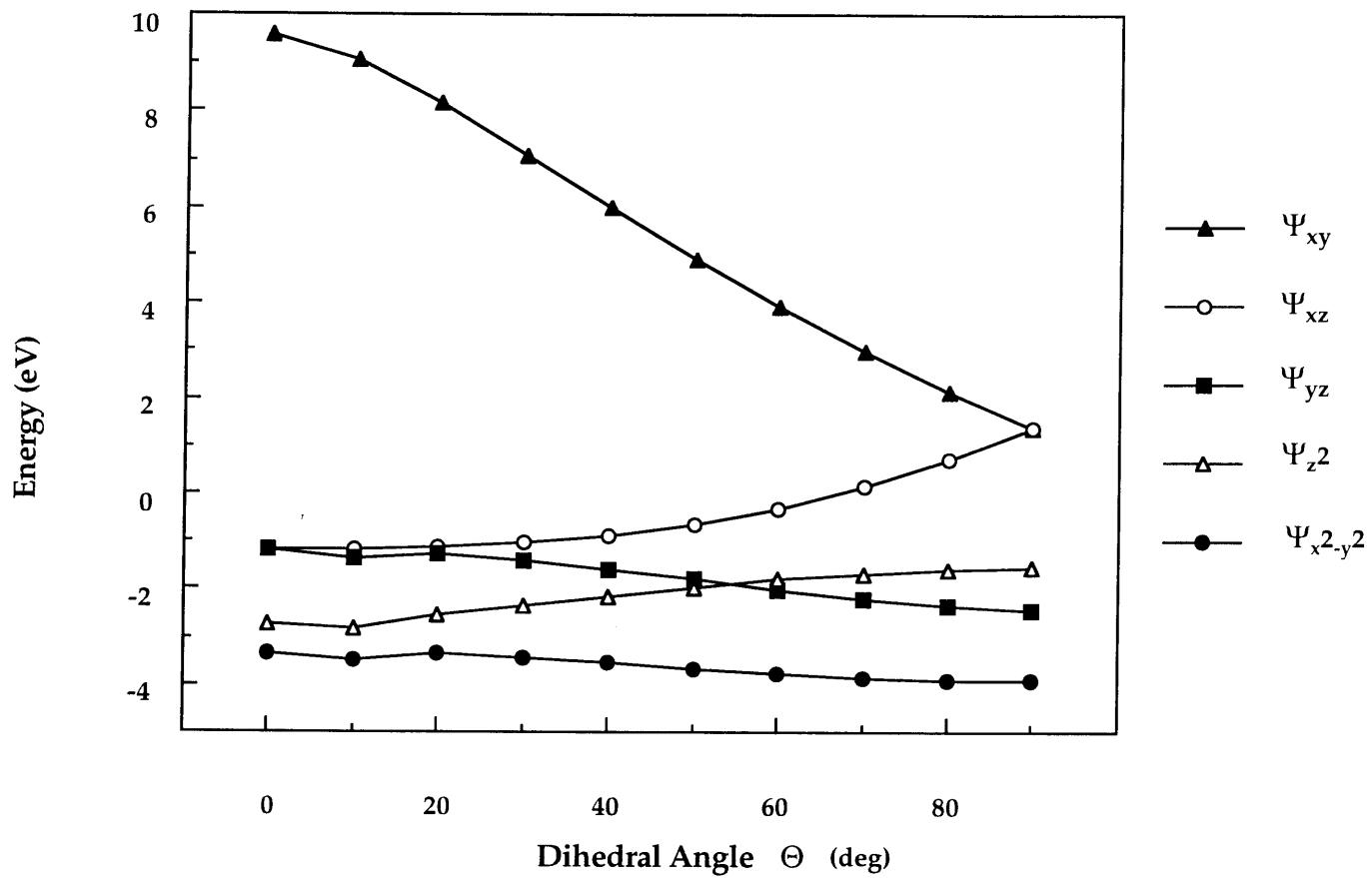
Figure 3.6. Energies of frontier molecular orbitals from Fenske-Hall calculations on $[Co(NH_2)_4]^-$.
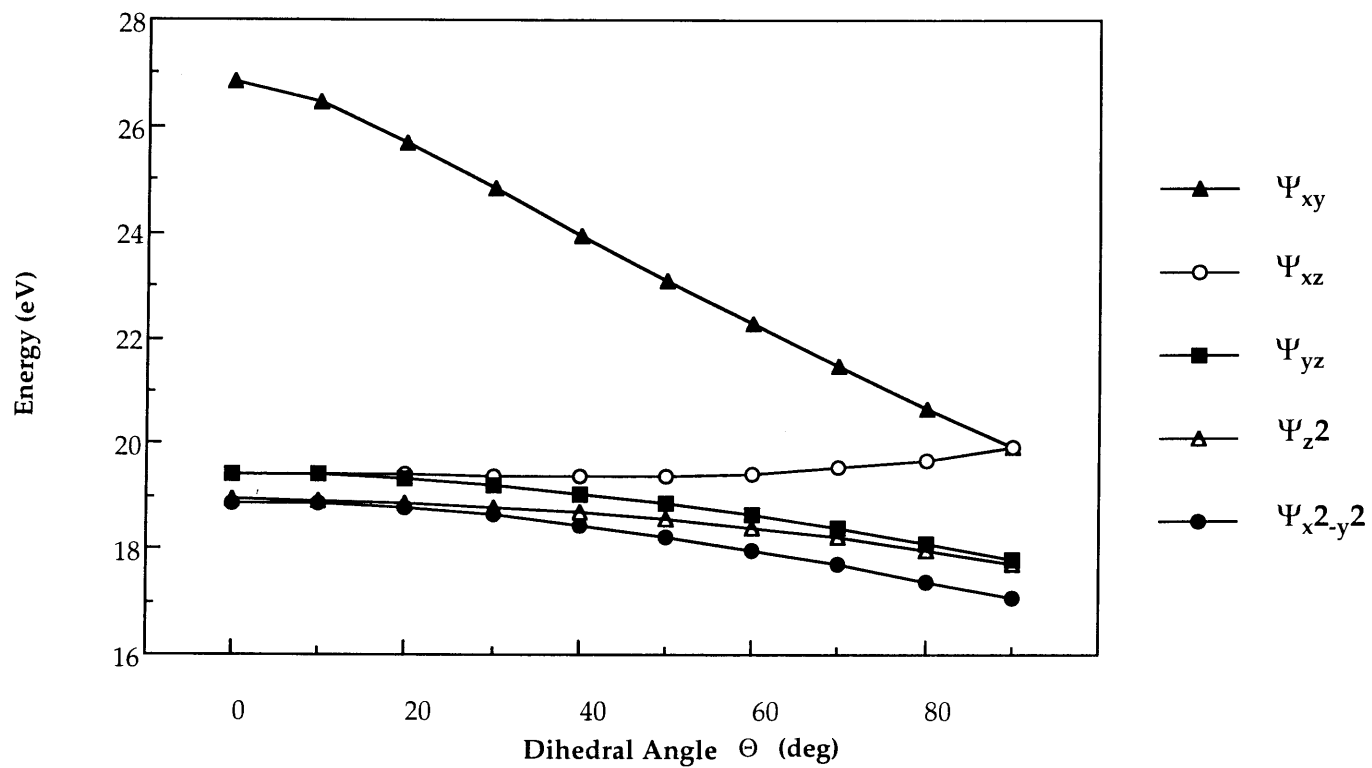
Figure 3.7. Energies of frontier molecular orbitals from Fenske-Hall calculations on $[Co(NH_2)_4]^{3-}$.
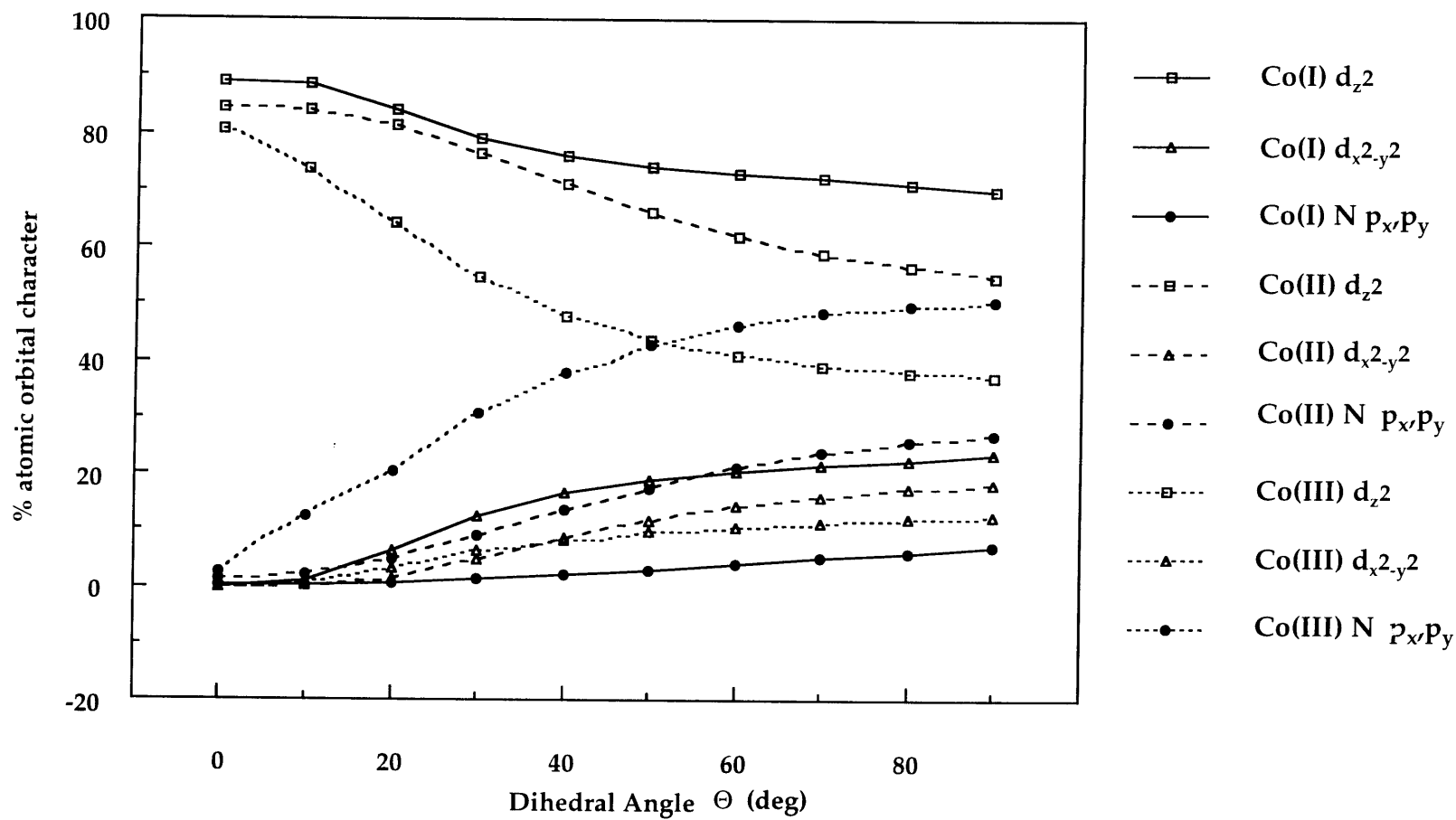
Figure 3.8. Atomic orbital contributions to molecular orbital having mainly d_z2 character as a function of dihedral angle and oxidation state.
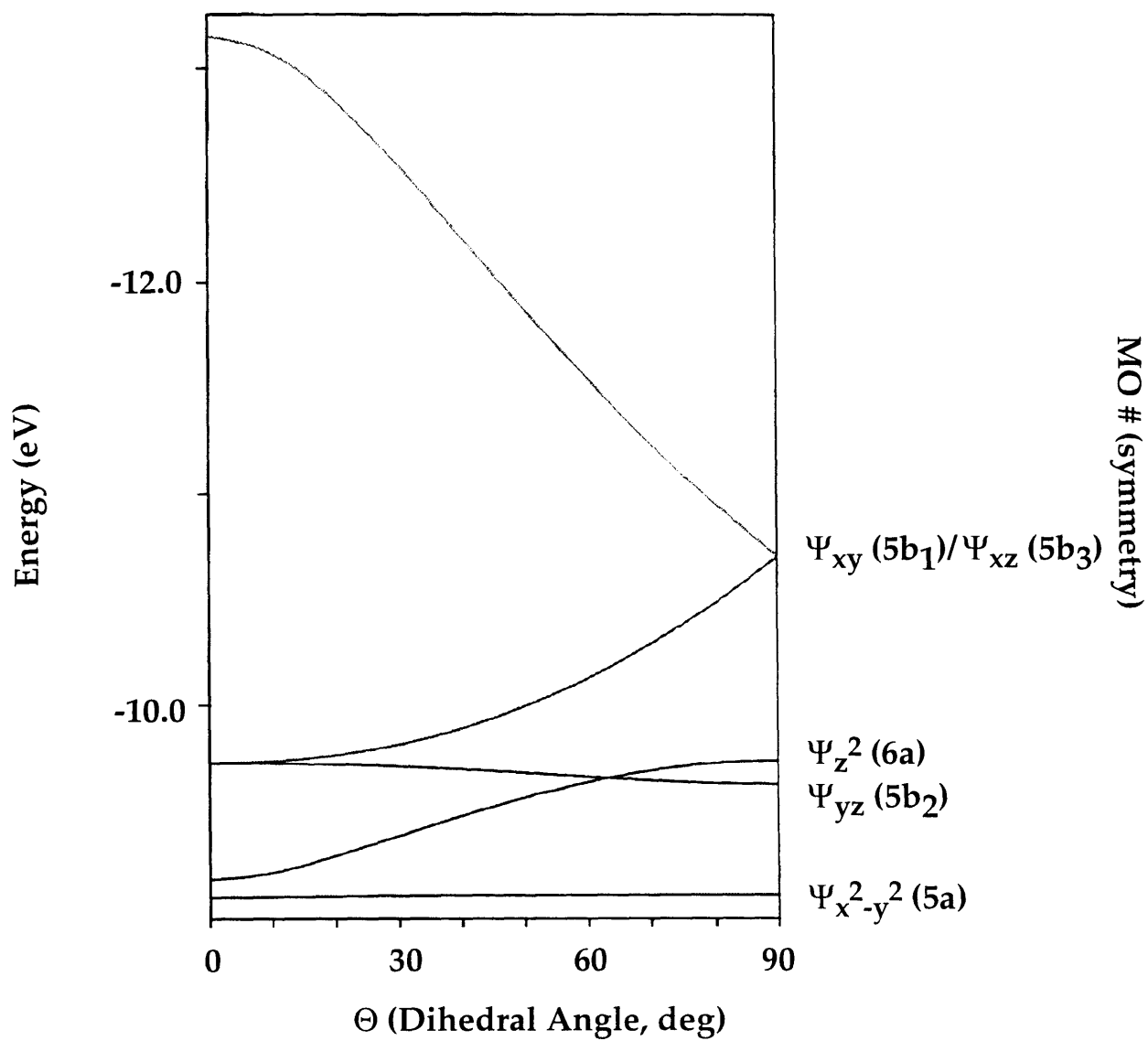
Figure 3.9. Walsh diagram for $[Co(NH_2)_4]^{2-}$ with D_2 symmetry.
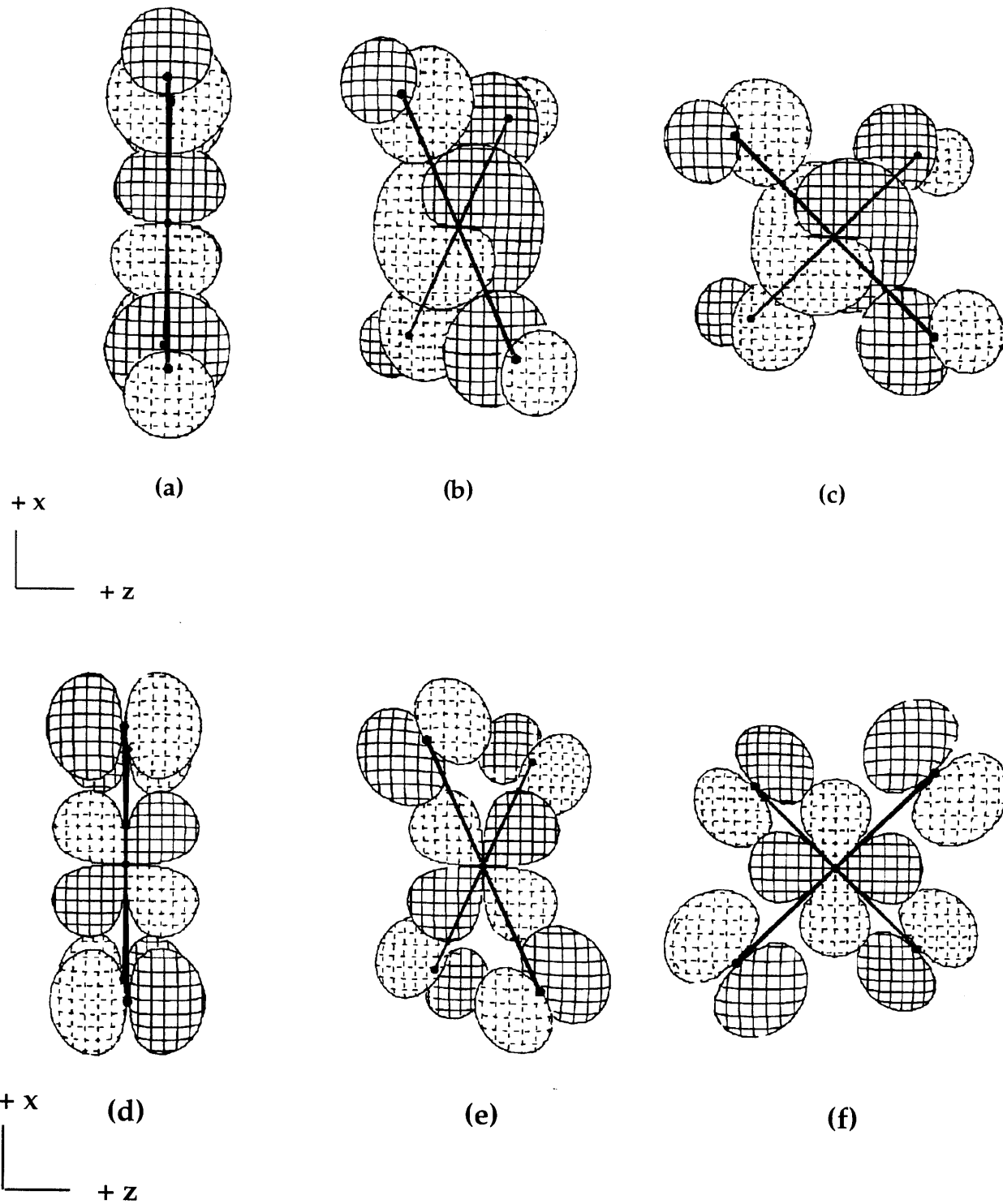
Figure 3.10. MO diagrams for d_{xy} (a) $\Theta = 0°$ (b) $\Theta = 50°$ (c) $\Theta = 90°$ and d_{xz} (d) $\Theta = 0°$ (e) $\Theta = 50°$ (f) $\Theta = 90°$.

(a)

+ y

+ x

(b)

(c)

(d)

+ z

+ y

(e)

(f)
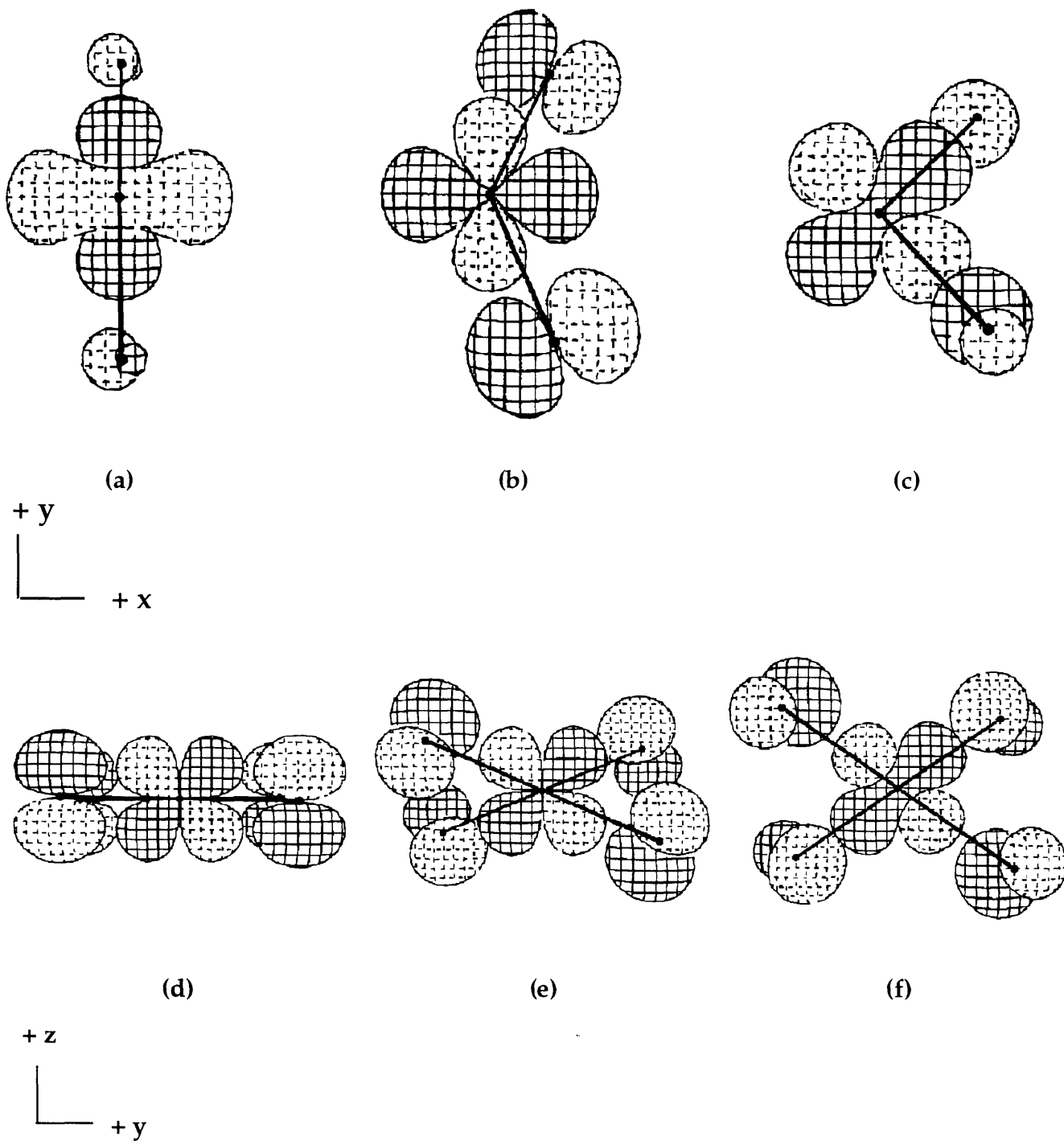
Figure 3.11. MO diagrams for $d_z{}^2$ (a) $\Theta = 0°$ (b) $\Theta = 50°$ (c) $\Theta = 90°$ and d_{yz} (d) $\Theta = 0°$ (e) $\Theta = 50°$ (f) $\Theta = 90°$. Only two nitrogen atoms are shown in (a) - (c) for clarity.
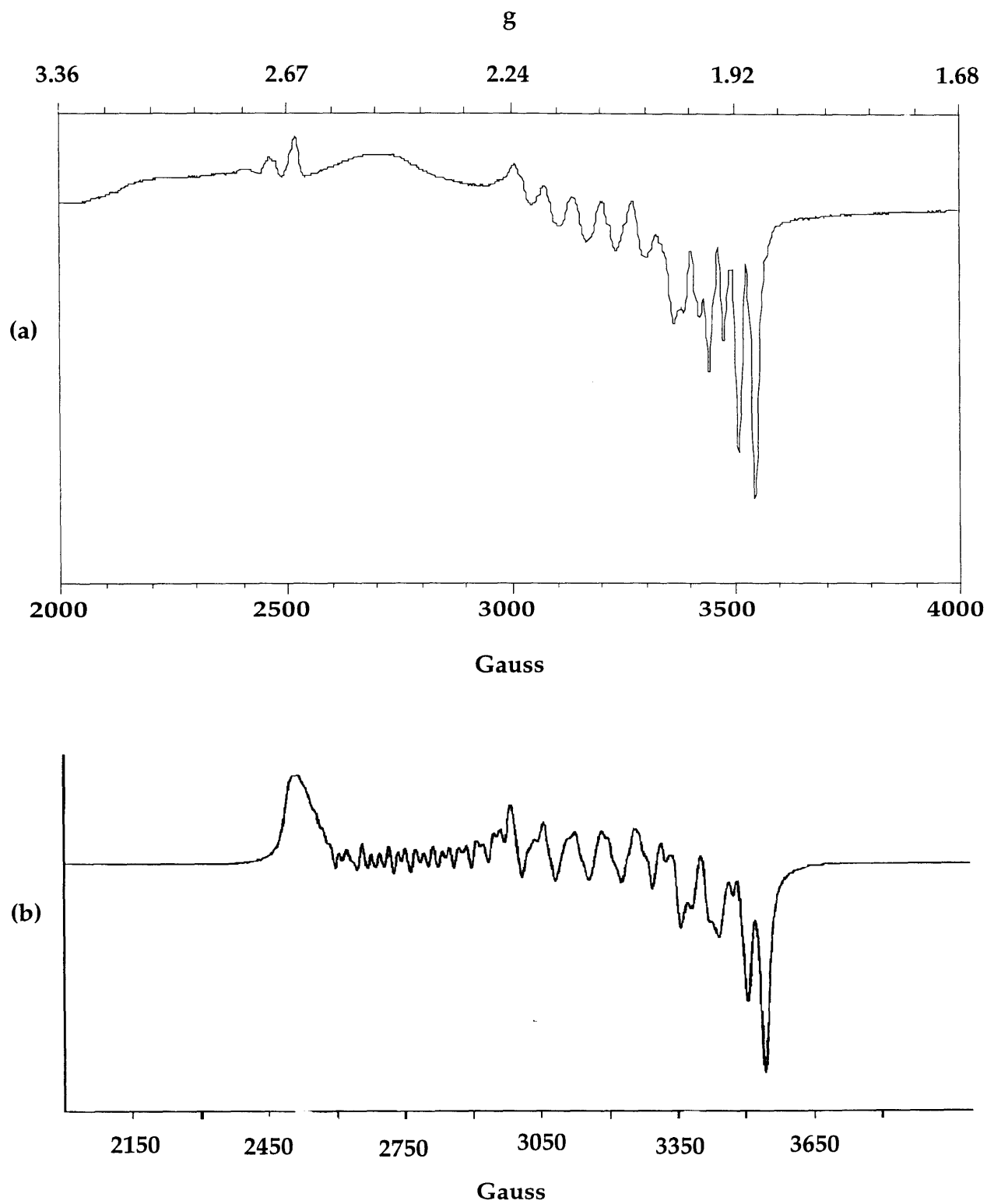
Figure 3.12. (a) Experimental EPR spectrum of 24.9 mM [Co(TC-3,3)] collected at 50.0 K, 50.0 mW, modulation amplitude 1.0 and (b) fitted spectrum of [Co(TC-3,3)].
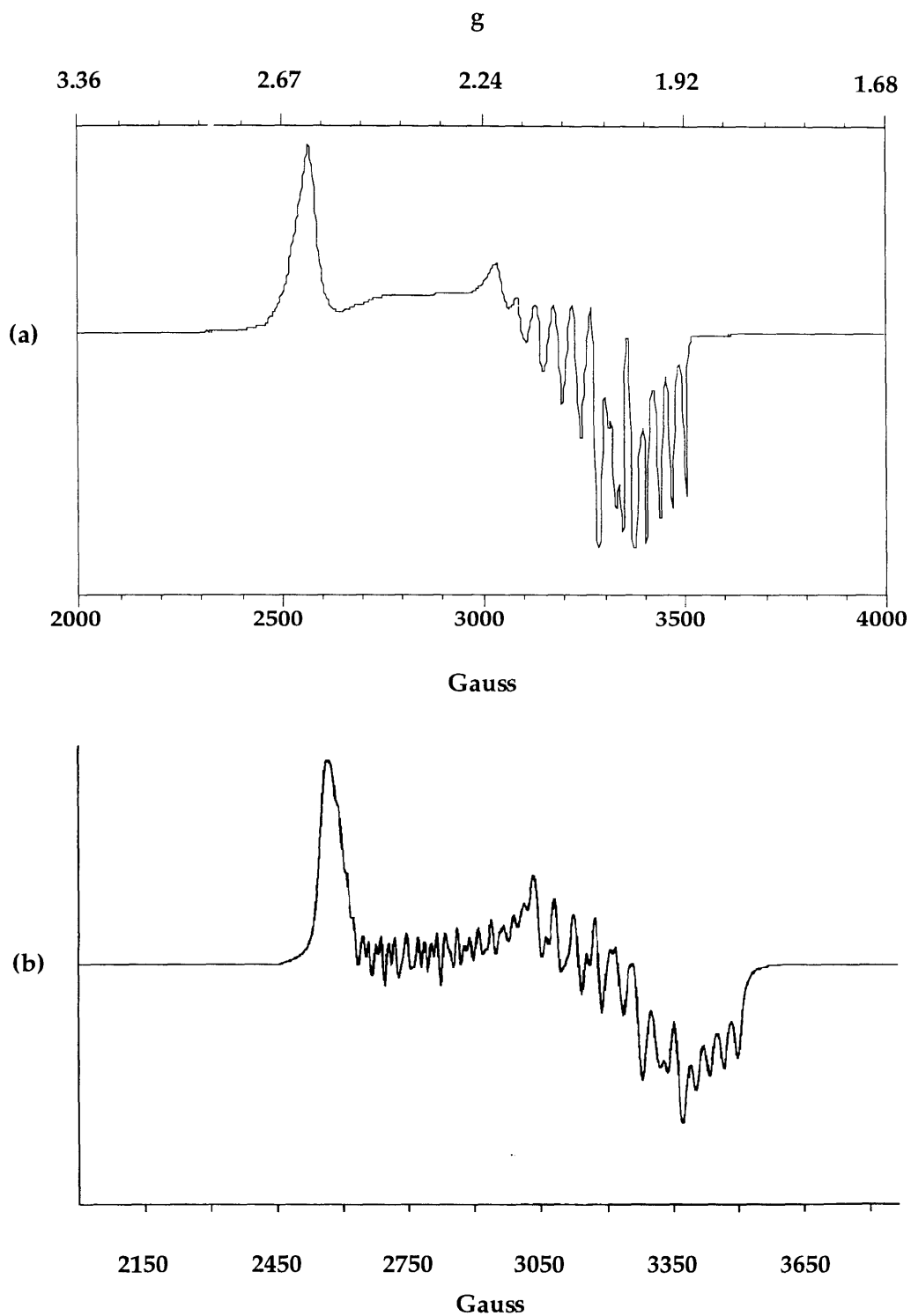
Figure 3.13. (a) Experimental EPR spectrum of 7.6 mM [Co(TC-4,4)] collected at 30.0 K, 50.0 mW, modulation amplitude 1.0 and (b) fitted spectrum of [Co(TC-4,4)].
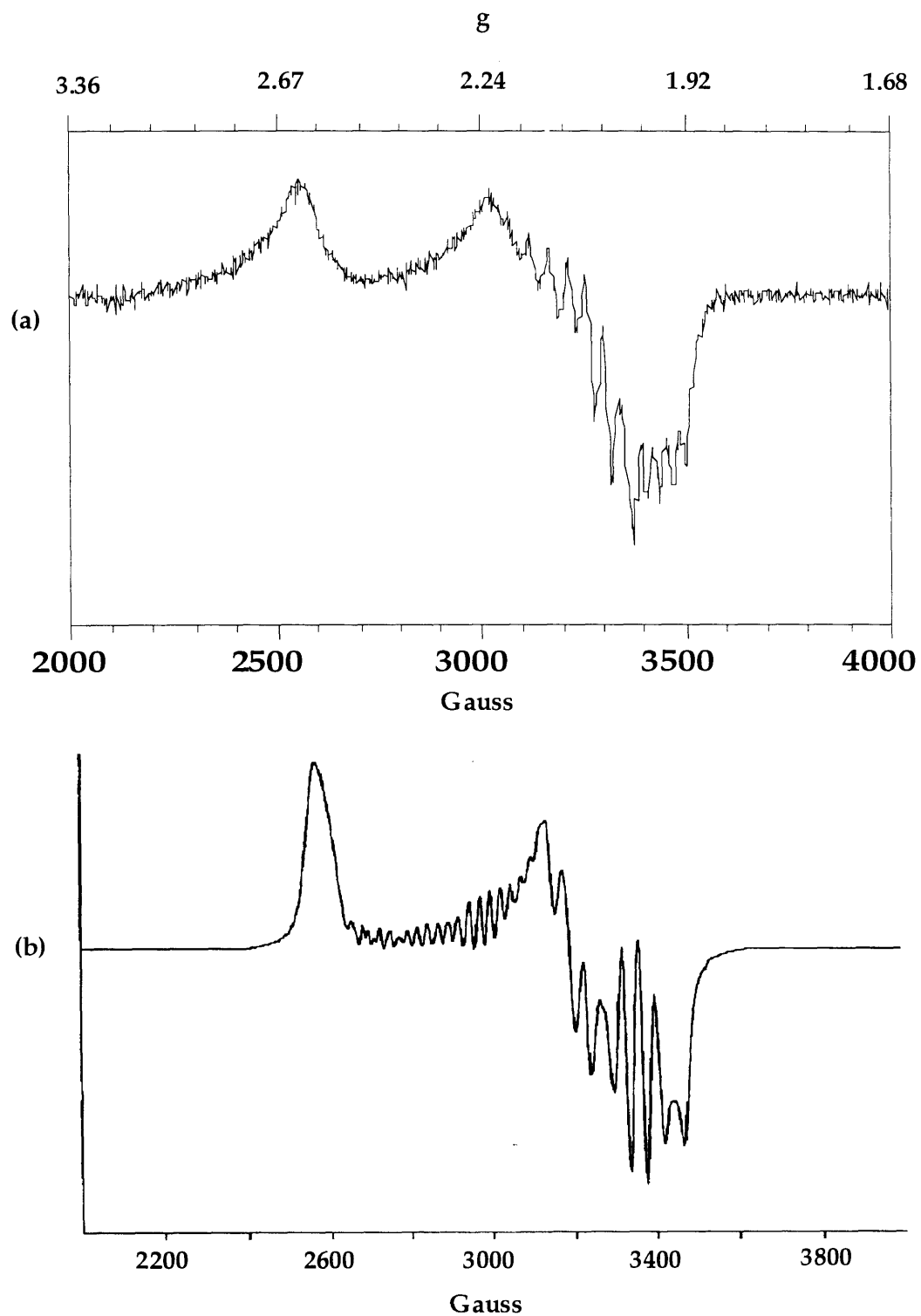
Figure 3.14. (a) Experimental EPR spectrum of 20.5 mM [Co(TC-4,5)] collected at 40.0 K, 50 mW, modulation amplitude 1.0 and (b) fitted spectrum of [Co(TC-4,5)].

g

6.71   3.53   2.24   1.68   1.34   1.12

0   1000   2000   3000   4000   5000   6000

Gauss
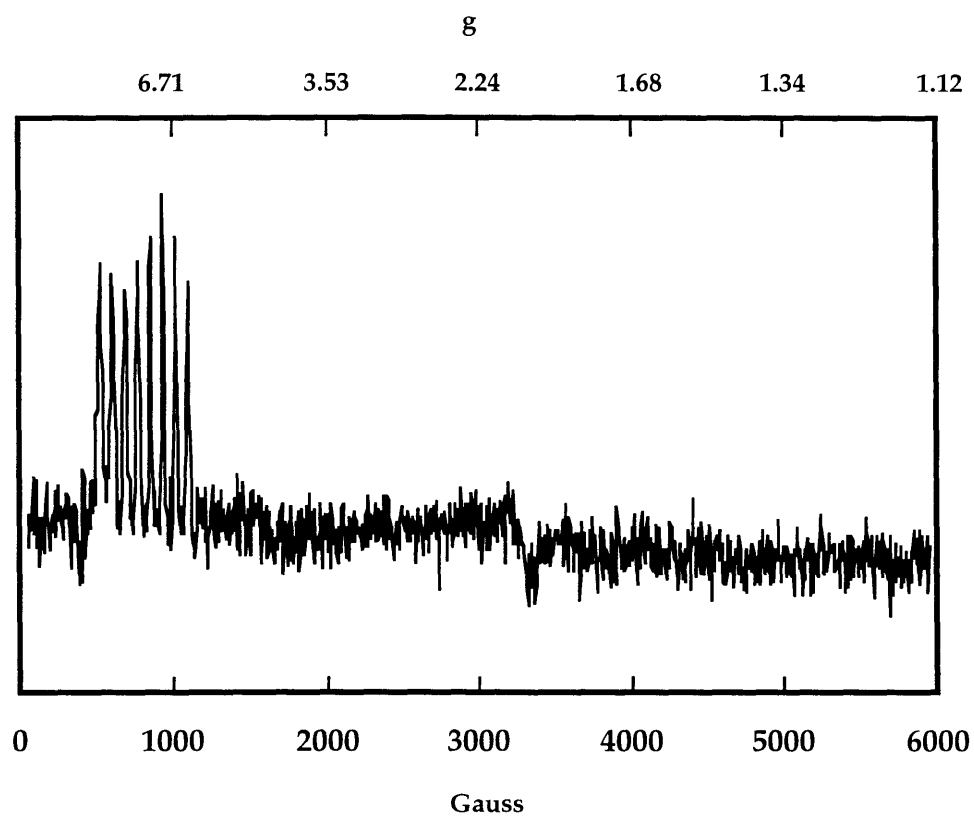
Figure 3.15. Experimental EPR spectrum of 19.6 mM [Co(TC-5,5)] collected at 5.0 K, 5.0 mW and modulation amplitude 1.0.
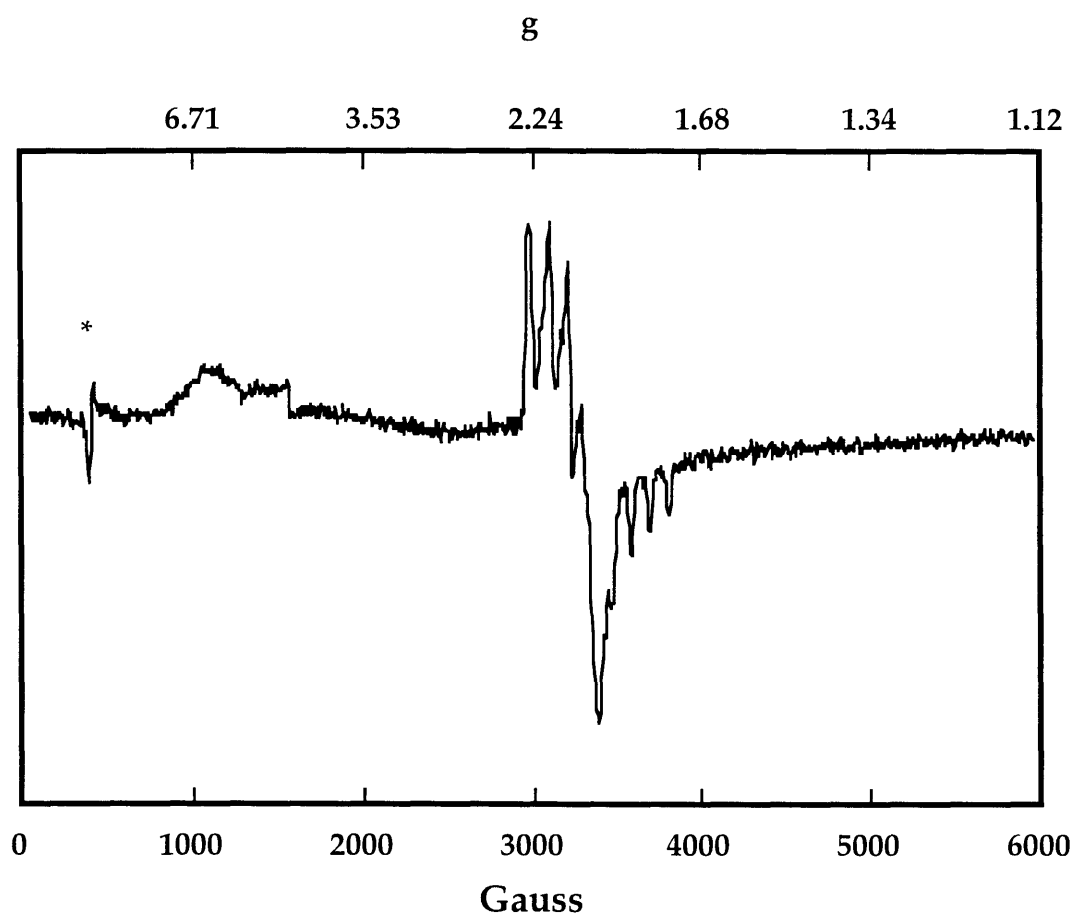
Figure 3.16. Experimental spectrum of 6.0 mM [Co(TC-6,6)] collected at 10.0 K, 5.0 mW, modulation amplitude 10.0. Asterisk indicates paramagnetic impurity in spectrometer cavity.
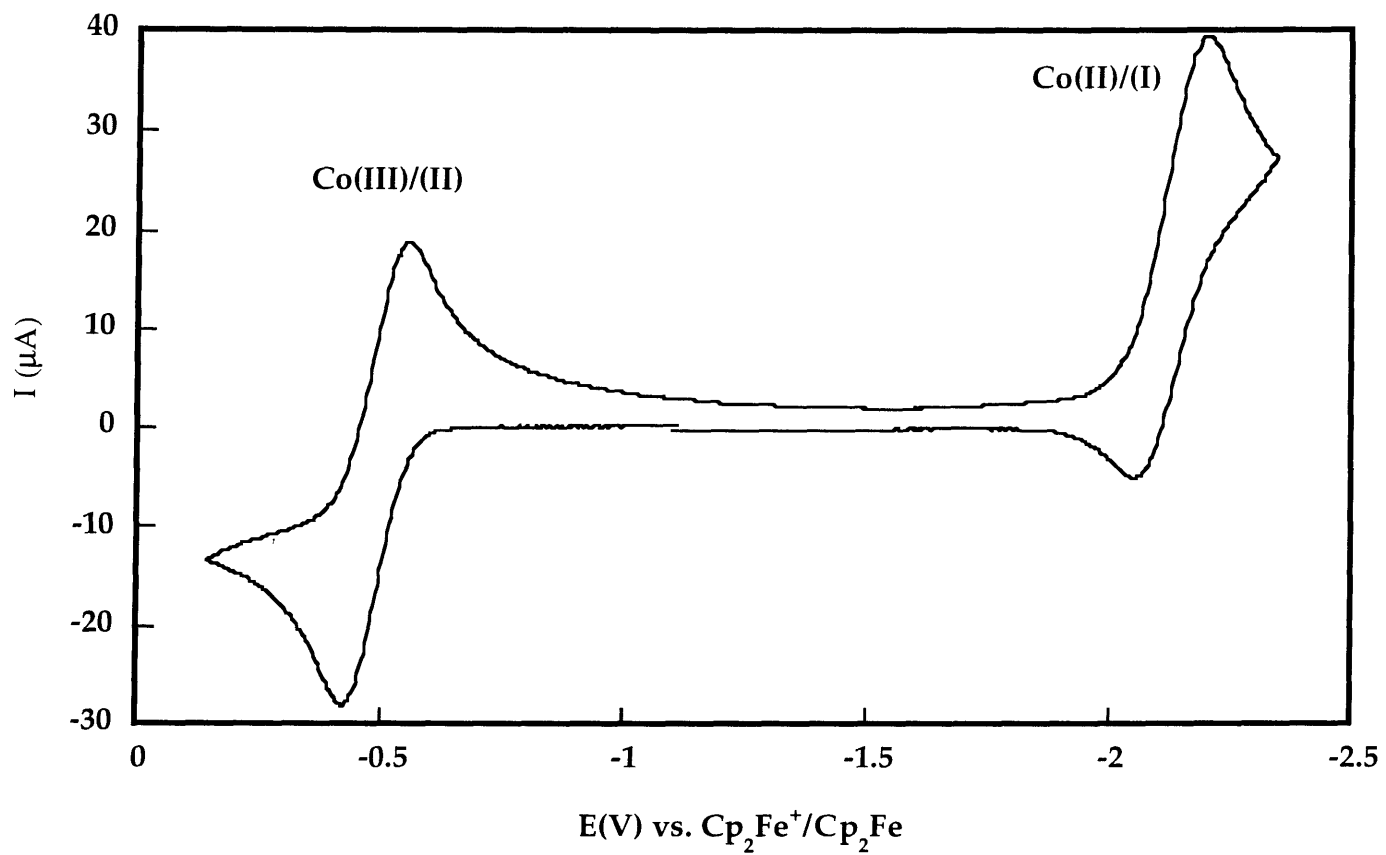
Figure 3.17. Cyclic voltammogram of [Co(TC-3,3)] in THF with 0.5 M (n-Bu$_4$N)(PF$_6$) and 100 mV/s anodic scan speed.
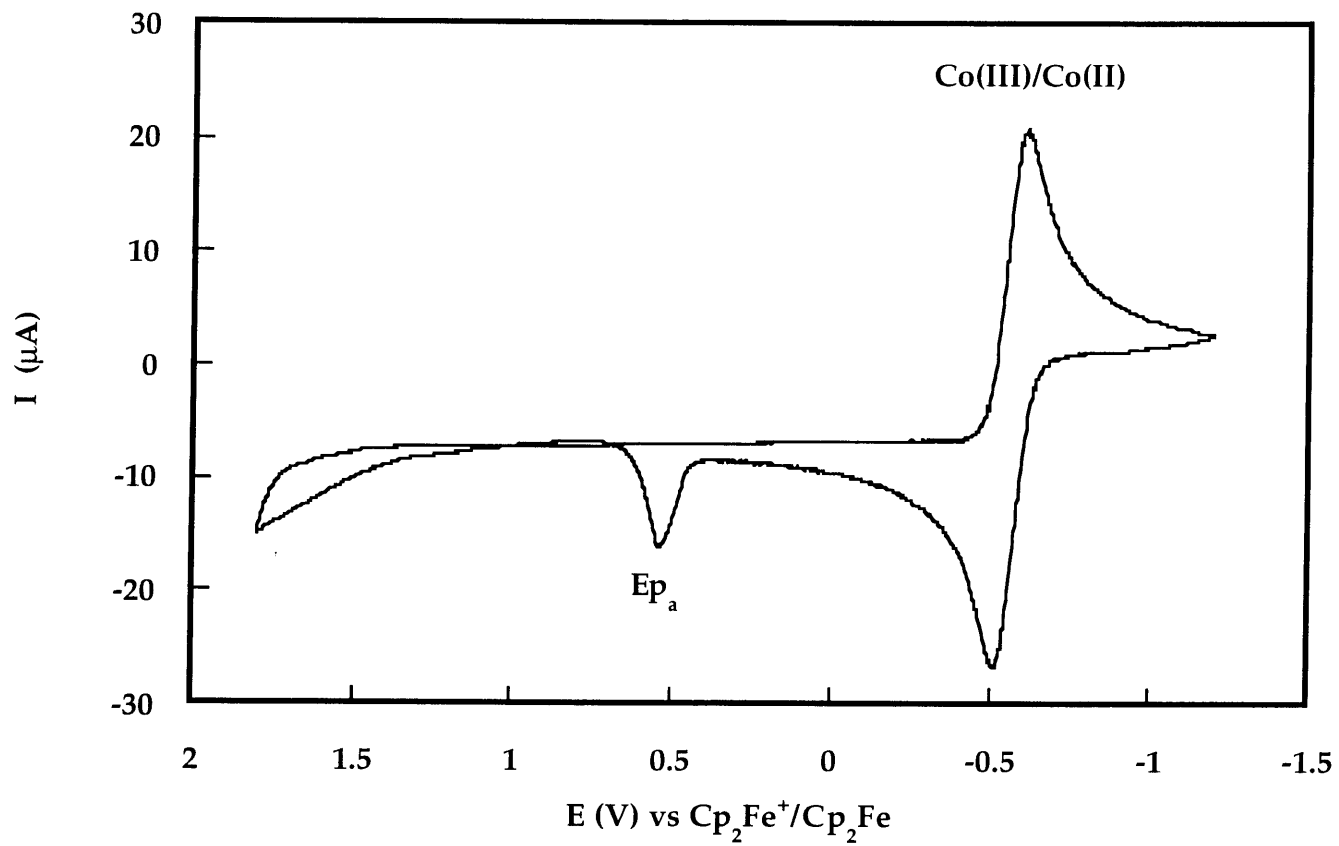
Figure 3.18. Cyclic voltammogram of [Co(TC-4,4)] in CH_2Cl_2 with 0.5 M $(n\text{-}Bu_4N)(PF_6)$ and 100 mV/s anodic scan speed.
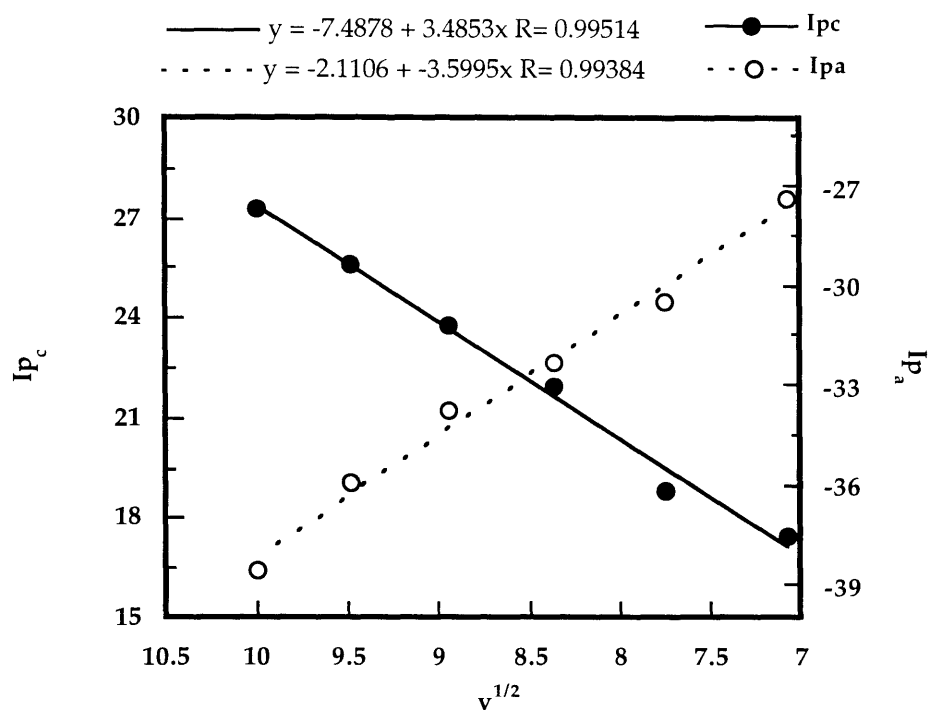
Figure 3.19. Plot of anodic and cathodic currents versus (scan speed)$^{1/2}$ for [Co(TC-4,5)] in CH$_2$Cl$_2$.
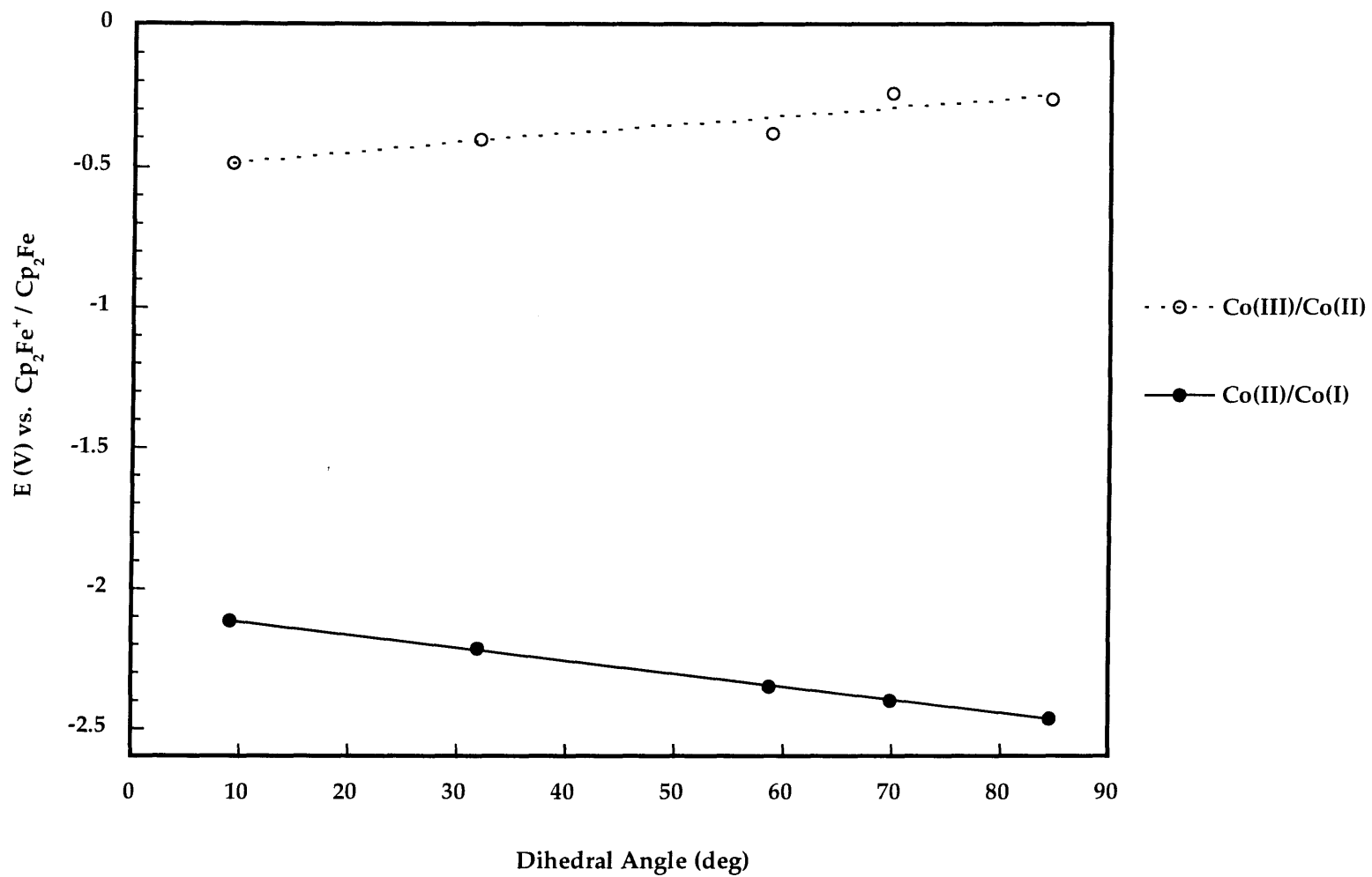
Figure 3.20. Co(III)/(II) and Co(II)/(I) redox potentials for [Co(TC-n,m)] complexes.

— Ψ_{xy} — Ψ_{xy}

Co(I) d^8 l.s.

$\#$ Ψ_{xz}

$\#$ Ψ_{yz}

$\#$ Ψ_{z^2}

$\#$ $\Psi_{x^2-y^2}$

Co(III) d^6 l.s.

$+$ Ψ_{xz}

$+$ Ψ_{yz}

$\#$ Ψ_{z^2}

$\#$ $\Psi_{x^2-y^2}$

— Ψ_{xy}

$+ e^-$

$- e^-$

$+$ Ψ_{xy}

$+$ Ψ_{xz}

$\#$ Ψ_{yz}

$\#$ Ψ_{z^2}

$\#$ $\Psi_{x^2-y^2}$

Co(II) d^7 l.s.

$+$ Ψ_{xy}

$+ e^-$

$- e^-$

$+$ Ψ_{xz}

$\#$ Ψ_{yz}

$\#$ Ψ_{z^2} **Co(I) d^8 h.s.**

$\#$ $\Psi_{x^2-y^2}$

Co(III) d^6 h.s.

$+$ Ψ_{xz}

$+$ Ψ_{yz}

$+$ Ψ_{z^2}

$\#$ $\Psi_{x^2-y^2}$
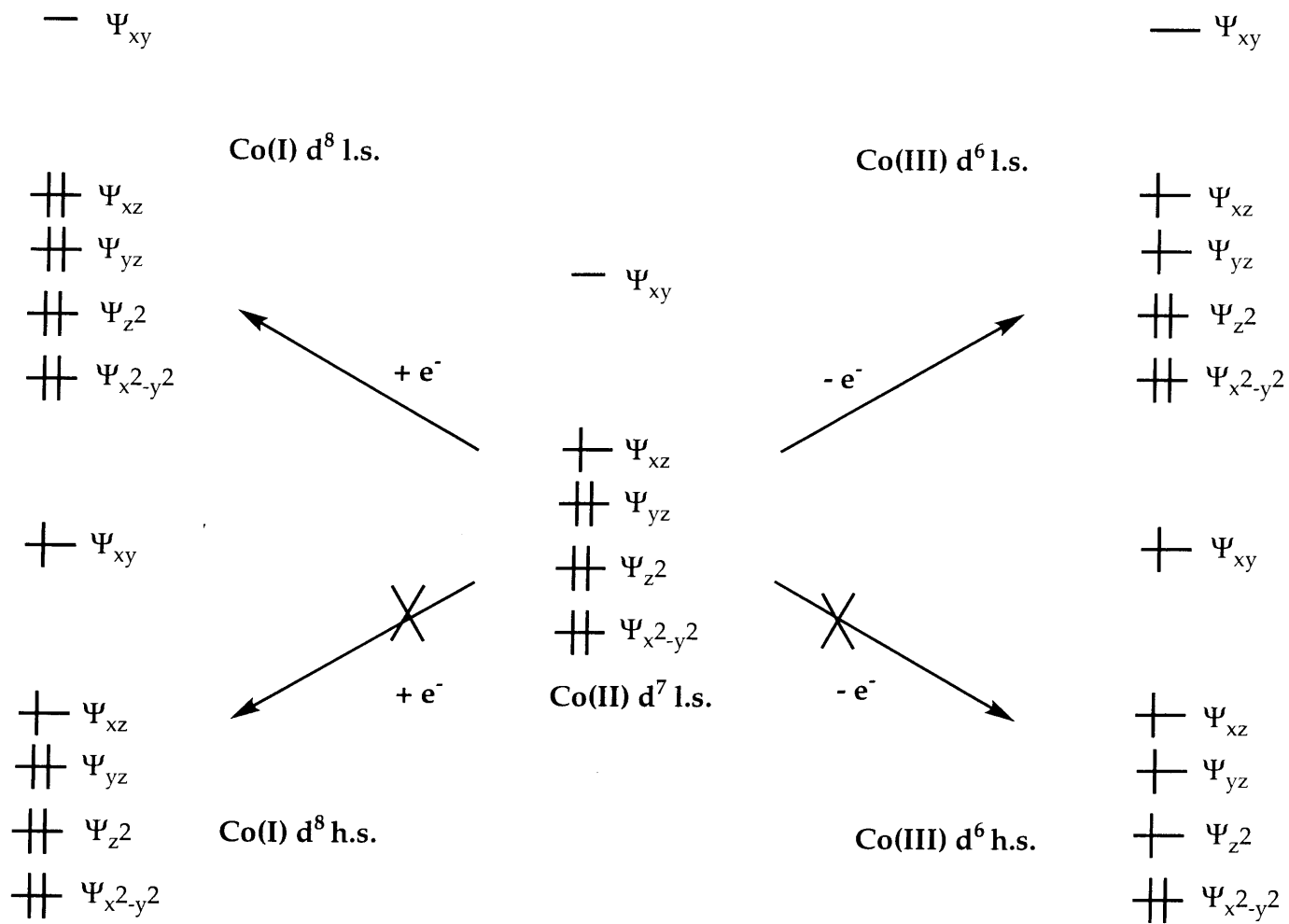
Figure 3.21. Oxidation and reduction of low-spin Co(II) complexes.
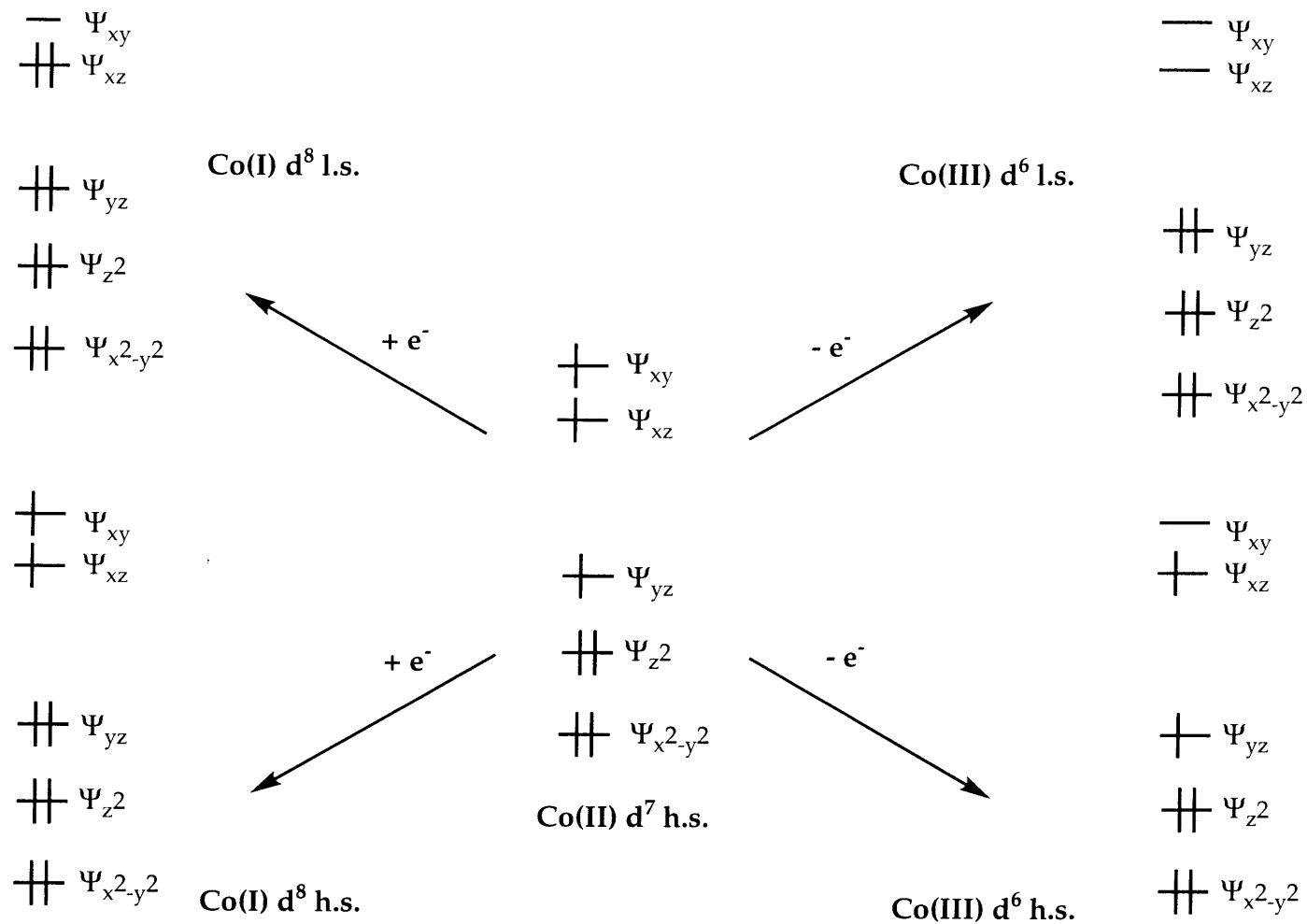
Figure 3.22. Oxidation and reduction of high-spin cobalt(II) complexes.

Chapter 4

Tuning of the Reactivity of Four Coordinate Cobalt(III)

Tropocoronand Complexes by the Macrocycle Size

Introduction

Cobalt(III) complexes occupy an important place in the history of coordination chemistry, having greatly aided Alfred Werner's understanding transition metal stereochemistry. Since that time, Co(III) complexes have been used extensively to further our understanding of coordination compounds. The high LFSE and relative kinetic inertness of octahedral Co(III) compounds have made them the subjects of many experimental studies. Much less common are four- or five-coordinate Co(III) complexes which have the potential for new reactivity behavior.

The coordination number and geometry at a metal center are readily controlled through the use of macrocyclic ligands, which can enforce a particular environment based on ligand structure. Tropocoronand macrocycles have been used to prepare a series of four-coordinate Co(II) complexes, [Co(TC-n,m)], n + m = 6, 7, 8, 9, 10, 12 with a range of geometries from square-planar to tetrahedral.[1] These complexes have been previously used as starting materials for preparing five-coordinate Co(III) halo and alkyl tropocoronands. By appropriate choice of n and m, the geometry of the complex [CoX(TC-n,m)] X = halide,[2] could be tuned from square-pyramidal, in [CoCl(TC-3,3)] to a rare example of trigonal-bipyramidal geometry in [CoCl(TC-4,4)]. The [CoR(TC-n,m)] alkyls homolyze to Co(II) and R· under mild conditions, the rate of which depends on the macrocycle size. One goal of the work described here was to investigate other five-coordinate Co(III) tropocoronand compounds with different fifth ligands to determine the generality of tropocoronand tuning of structure and reactivity.

Reduced coordination numbers can also be achieved with macrocyclic ligands which can provide structural rigidity and electronic stabilization to a complex with fewer donor atoms than the acyclic analog. Thus, another goal of these studies was to explore whether the tropocoronand ligands could support the rare coordination number of four for Co(III). With two open coordination sites, reactivity unavailable

to six- or five-coordinate Co(III) complexes might be observed that could also be tuned with the tropocoronand ligand system. To date, four-coordinate Co(III) complexes have only been observed in geometries very close to square-planar and with a limited set of ligands.[3-8]

Experimental

General Information. All reactions were carried out in a dinitrogen-filled glove box or on a Schlenk line unless otherwise noted. The complexes [Co(TC-3,3)], **1a**, and [Co(TC-4,4)], **1b**, were synthesized according to the literature.[1] Pentane, toluene, diethyl ether, and tetrahydrofuran were distilled from sodium benzophenone ketyl. Methylene chloride, fluorobenzene, and chlorobenzene were distilled from CaH_2. Acetonitrile was predried with P_2O_5 and distilled from CaH_2 and all solvents were distilled under dinitrogen. $[Cp_2Fe]PF_6$ was obtained commercially and purified by subliming out $[Cp_2Fe]$. NO was purchased from Matheson (99+ %) and dried according to a literature procedure.[9] Other reagents were prepared as described below.

UV-vis data were recorded with a Hewlett Packard 8452A diode array or Cary 1E spectrophotometer. Magnetic moments were determined by the Evans method[10,11] on a 250 MHz Bruker instrument using $(TMS)_2O$ as an internal standard in CD_2Cl_2. ^1H-NMR data were also collected on a 250 MHz Bruker instrument.

Synthetic Procedures. AgBPh$_4$. A portion of $AgNO_3$ (1.15 g, 6.77 mmol) was dissolved in 65 mL of deionized water in a 200 mL round-bottom flask and one equiv of $NaBPh_4$ (2.32 g, 6.77 mmol) was added with vigorous stirring. The reaction flask was wrapped in aluminum foil to protect the light-sensitive starting materials and products. Immediately upon mixing a fine white powder precipitated. After 30 min, 2.26 g (78%) of this powder were collected by filtration on a glass frit, pumped

dry under vacuum and used without further purification. The reagents and product are stable to air but the BPh$_4$⁻ group is sensitive to heat and light. Decomposition is indicated by gradual discoloration to orange-brown.

[(Et$_2$O)Ag](BAr'$_4$).[12] In 5.0 mL of distilled H$_2$O was dissolved a portion of AgNO$_3$ (2.0 g, 11.8 mmol). One-tenth of an equiv of NaBAr'$_4$ (1.04 g, 1.2 mmol) (Ar' = 3,5-bis(trifluoromethyl)phenyl), prepared according to a literature procedure,[13] was dissolved in 3 mL of Et$_2$O. The solutions were stirred in a 25 mL Erlenmeyer flask and transferred to a separatory funnel. The aqueous layer was discarded and a second aliquot of AgNO$_3$ (2.0 g, 11.8 mmol) in 5.0 mL of H$_2$O was added to the ether solution. After shaking again, the aqueous layer was discarded, the ether layer was transferred to a 25 mL Erlenmeyer wrapped in aluminum foil and the solution was dried over Ag$_2$CO$_3$ for 15 min. The solids were removed by filtration and the ether solution concentrated to dryness in vacuo. The crude white powder was recrystallized from Et$_2$O at -30 °C in 83% yield (1.02 g), based on the formulation [(Et$_2$O)Ag][BAr'$_4$], and identified by its NMR spectrum. ^{1}H-NMR (CD$_2$Cl$_2$, δ, ppm) 1.16 (t, J = 7 Hz, 6H, CH$_3$) 3.52 (quart, J = 7 Hz, 4H, CH$_2$) 7.66 (br, 4H, p-H) 7.98 (8H, o-H).

(Me$_4$N)(SC$_6$F$_5$). A 50 mL round-bottom flask was charged with Me$_4$NOH·5H$_2$O (4.53 g, 25.0 mmol) in 15 mL ethanol and purged with N$_2$ for five min. One equiv of C$_6$F$_5$SH (5.0g, 25.0 mmol) was added via syringe and the solution was allowed to stir for another five min. The solvents were removed in vacuo and triturated with 5 mL MeOH to remove residual water. The crude product was washed with 10 mL of DME and 5 mL of pentane and dried in vacuo. A white powder was obtained (6.09 g, 89% yield) which showed a single resonance in the ^{1}H-NMR spectrum. ^{1}H-NMR (d$_6$-DMSO) 3.22 ppm.

[Co(TC-3,3)](BPh$_4$) (2a). A portion of [Co(TC-3,3)] (46.4 mg, 0.123 mmol) was dissolved in 10 mL of CH$_2$Cl$_2$ and one equiv of AgBPh$_4$ (52.5 mg, 0.123 mmol) was

added. The solution color changed from green-black to deep pink-purple and was allowed to stir 6 h. The insoluble materials were removed by filtration, the filtrate was concentrated in vacuo and the product recrystallized from CH_2Cl_2 layered with pentane. ^{1}H-NMR (CD_2Cl_2) μ_{eff} = 3.1 μ_B. UV-vis (CH_2Cl_2) [λ_{max}, nm (ε_M, M^{-1} cm^{-1})] 338 (16,600), 388 (13,600), 454 (9500), 497 (9800), 544 (25,300), 574 (9300). Anal. Calcd. for $CoN_4C_{44}H_{42}B$: C, 75.87; H, 6.08; N, 8.04. Found: C, 75.49; H, 6.19; N, 7.93.

[Co(TC-3,3)]BAr'$_4$ (2a'). A portion of [Co(TC-3,3)] (12.3 mg, 33 μmol) was dissolved in 4 mL of toluene and one equiv of Et$_2$O·AgBAr'$_4$ (31.6 mg, 33 μmol) was added as a solid. A deep pink-purple color was immediately observed. After stirring for 1 h, the solution was filtered through Celite to remove Ag^0 and the filtrate volume was reduced to 2 mL in vacuo. Small purple blocks were obtained from vapor diffusion of pentane into the toluene solution in 23 % yield (9.1 mg). ^{1}H-NMR (CD_2Cl_2) μ_{eff} = 3.2 μ_B. UV-vis (CH_2Cl_2) [λ_{max}, nm (ε_M, M^{-1} cm^{-1})] 342 (16,200), 389 (12,100), 496 (10,500), 545 (28,300). Anal. Calcd. for $CoN_4C_{54.5}H_{40}BF_{24}$ (2a'·1/2 C$_5$H$_{12}$): C, 51.47; H, 3.17; N, 4.41. Found: C, 50.96; H, 3.38; N, 4.41.

[Co(TC-4,4)]BPh$_4$ (2b). A portion of [Co(TC-4,4)] (139.6 mg, 0.344 mmol) was dissolved in 10 mL of CH_2Cl_2 and one equiv of AgBPh$_4$ was added. The solution color changed from deep green to wine-red/maroon and was allowed to stir for 4 h. Ag^0 was removed by filtration, the filtrate was concentrated in vacuo, and the product was recrystallized from CH_2Cl_2 and pentane to give analytically pure material in 40% yield (107 mg). Evans method: (CD_2Cl_2) μ_{eff} = 3.60 μ_B. UV-vis (CH_2Cl_2) [λ_{max}, nm (ε_M, M^{-1} cm^{-1})] 372 (25,400), 532 (10,000), 804 (7800). Anal. Calcd for $CoN_4C_{46}H_{46}B$: C, 76.25; H, 6.40; N, 7.73. Found: C, 75.74; H, 6.24; N, 8.08.

[Co(THF)(TC-3,3)]BPh$_4$ (3). A concentrated solution of 2a in 10 mL of CH_2Cl_2 was prepared, 5 mL of THF were layered on top, and mixture was allowed to cool to -40 °C. Dark orange crystalline blocks of 3 were obtained in 55% yield (130 mg). ^{1}H-NMR (δ, ppm, 1:1 CD$_2$Cl$_2$:THF-d$_8$) 0.83, 1.21, 1.74, 2.92, 3.57, 6.18, 6.49, 6.82. UV-vis

(CH_2Cl_2) [λ_{max}, nm (ε_M, M^{-1} cm^{-1})] 274 (29,200), 338 (8700), 400 (10,400), 450 (12,000), 545 (5,900). Anal. Calcd. for $CoN_4C_{48}H_{50}BO$: C, 75.00; H, 6.56; N, 7.29. Found: C, 74.84; H, 6.76; N, 7.20.

[Co(NO)(TC-3,3)] (**4a**). A portion of **1a** (38.3 mg, 0.101 mmol) was dissolved in 10 mL of THF in a Schlenk flask under N_2. The flask was sealed to the atmosphere and purged with NO while stirring. Immediately upon addition of NO the dark green solution turned brown. After 15 min the solvent was removed in vacuo to give a brown powder which was recrystallized from hot fluorobenzene in 22 % yield (9 mg). Evans method moment (CD_2Cl_2), μ_{eff} = 3.1 μ_B. IR (ν_{NO} ,KBr) 1656 cm^{-1}. UV-vis (CH_2Cl_2) [λmax, nm (ε_M, M^{-1} cm^{-1})] 342 (14,300), 417 (12,000), 547 (4350), 677 (2300). Anal. Calcd. for $CoN_5C_{20}H_{22}O$: C, 58.97; H, 5.44; N, 17.19. Found: C, 57.71; H, 5.37; N, 15.54.

[Co(NO)(TC-4,4)] (**4b**). A portion of **1b** (161 mg, 0.397 mmol) was dissolved in 15 mL of THF in a 25 mL Schlenk flask. The initially dark green solution turned brown upon exposure to NO and, after 20 min of purging the solution with NO, the solvent was removed in vacuo to give a brown powder which was recrystallized from hot fluorobenzene in 65% yield (110 mg). ^{1}H-NMR (δ, ppm, CD_2Cl_2) 1.59 (m, 4H, C-CH_2-C) 1.76 (m, 4H, C-CH_2-C) 3.52 (m, 4H, N-CH_2-C) 3.76 (m, 4H, N-CH_2-C) 6.12 (2H, t, J = 9 Hz, H_c) 6.62 (4H, d, J = 11 Hz, H_a) 6.85 (4H, t, J = 11 Hz, H_b). IR (ν_{NO}, KBr) 1584 cm^{-1}. UV-vis (CH_2Cl_2) [λ_{max}, nm (ε_M, M^{-1} cm^{-1})] 409 (20,300), 486 (9200), 796 (2400). Anal. Calcd. for $CoN_5C_{22}H_{26}O$: C, 60.69; H, 6.02; N, 16.09. Found: C, 60.68; H, 6.25; N, 15.55.

[Co(SC_6F_5)(TC-3,3)] (**5a**). A portion of **1a** (205.7 mg, 0.545 mmol) was dissolved in 15 mL of CH_2Cl_2 and one equiv of $[Cp_2Fe]PF_6$ (180.4 mg, 0.545 mmol) was added with stirring. The dark-green color changed to the deep pink-purple of $[Co(TC-3,3)]^+$ observed in **2a** above. After 4 h, the solvents were removed in vacuo and triturated twice with 5 mL of pentane. The dark purple powder was washed three times with

10 mL of pentane until the golden color of [Cp$_2$Fe] was no longer observed in the pentane wash. The remaining solid was taken up in 15 mL of CH$_2$Cl$_2$ and filtered through Celite. To the filtrate was added one equiv of (Me$_4$N)(SC$_6$F$_5$) (149.1 mg, 0.545 mmol) which had been dissolved in 5 mL of THF. The purple solution began to turn orange brown and was stirred for 3 h until the solution was dark orange-brown, after which time the solvents were removed in vacuo. The resultant brown powder was dissolved in CH$_2$Cl$_2$, filtered through Celite to remove (Me$_4$N)(PF$_6$) and concentrated in vacuo. The product was recrystallized from hot fluorobenzene in 29 % yield (92.1 mg). Evans method (CD$_2$Cl$_2$) μ_{eff} = 3.1 μ_B. UV-vis (CH$_2$Cl$_2$) [λ_{max}, nm (ε_M, M^{-1} cm^{-1})] 391 (12,900), 477 (15,300), 573 (7700). Anal. Calcd. for CoN$_4$C$_{26}$H$_{22}$SF$_5$: C, 54.17; H, 3.85; N, 9.72. Found: C, 54.15; H, 4.18; N, 9.53.

[Co(SC$_6$F$_5$)(TC-4,4)] (5b). A portion of 1b (101.2 mg, 0.249 mmol) was dissolved in CH$_2$Cl$_2$ and oxidized with one equiv of [Cp$_2$Fe]PF$_6$ (82.4 mg, 0.249 mmol) to form the dark maroon cation [Co(TC-4,4)]$^+$ in situ which was allowed to react with one equiv of (Me$_4$N)(SC$_6$F$_5$) (68.1 mg, 0.249 mmol). Procedures and workup followed those reported for 5a. A dark orange-brown solution in CH$_2$Cl$_2$ was obtained which was concentrated to dryness and the product was recrystallized from hot fluorobenzene in 43 % yield (64.8 mg). Evans method (CD$_2$Cl$_2$) μ_{eff} = 3.2 μ_B. UV-vis (CH$_2$Cl$_2$) [λ_{max}, nm (εM, M-1 cm-1)] 371 (21,300), 456 (22,600), 561 (7100), 669 (3000), 742 (3600). Anal. Calcd. for CoN$_4$C$_{28}$H$_{26}$SF$_5$: C, 55.63; H, 4.34; N, 9.27. Found: C, 55.85; H, 4.57; N, 9.13.

X-ray Crystallography. General Procedures. Single crystal diffraction data were collected on either an Enraf-Nonius CAD4 four-circle or a Siemens-CCD diffractometer. The general procedures for data collection and reduction with each instrument follow those given in Chapter 2. Structures were solved with the direct methods package SIR-92, an updated version of SIR-88[14] and incorporated into the TEXSAN[15] package of programs, which typically afforded positions for the majority

of the non-hydrogen atoms. The remaining atoms were found from the resulting difference Fourier maps and refined by full matrix least-squares and Fourier techniques. For acentric space groups, refinements were performed isotropically with both enantiomorphs and the one with the smaller residuals chosen. Non-hydrogen atoms were refined anisotropically except as noted. All hydrogen atoms were generated at calculated positions and allowed to ride on their corresponding carbon atoms ($d_{C-H} = 0.95$ Å, $B_H = 1.2 B_C$).

Important crystallographic information for each complex including refinement residuals are given in Table 4.1 for the cationic Co(III) complexes **2a'**, **2b**, and **3**. The same information is present in Table 4.2 for the neutral Co(III) complexes **4a**, **4b**, **5a**, and **5b**. Final positional and isotropic thermal parameters are listed in Tables 4.3 - 4.9. Anisotropic thermal parameters are provided as supporting information.

[Co(TC-3,3)]BAr'4·1/2 C5H12 (2a'). Single crystal X-ray diffraction data were collected on a dark purple block with approximate dimensions of 0.25 x 0.25 x 0.30 mm. Peak profiles were slightly broad. One molecule of pentane per unit cell was found which was translationally disordered across the inversion center. The trifluoromethyl groups showed three-fold rotational disorder. To obtain a better model, the data were filtered to remove reflections having $|\Delta I|/\sigma \geq 10$ and RSYM = $[|I-<I>/|<I>|] > 0.07$, which accounted for 5.48 % of the total data. Reflections with negative intensity, $\Theta > 45°$, and seven severely outlying reflections were also removed. The pentane disorder was modeled by setting the terminal carbon C3S to half occupancy and the CF_3 group disorders were solved for and the site occupancies were refined at each position.

[Co(TC-4,4)]BPh4·1.5C6H5Cl (2b). Small dark maroon blocks suitable for X-ray crystallography were grown by slow diffusion of toluene into a saturated chlorobenzene solution at -40 °C. A single crystal X-ray diffraction study of a

specimen with dimensions 0.20 x 0.20 x 0.16 mm showed 1.5 molecules of chlorobenzene in the asymmetric unit. The chlorobenzene fully occupied was refined anisotropically. The half-occupied molecule was located on an inversion center with chlorine atom Cl2 disordered over four positions. Hydrogen atoms H56 and H58 were each disordered over two of these four sites between the two asymmetric units. The carbon atoms C54, C55, and C57 were refined isotropically.

[Co(THF)(TC-3,3)]BPh4 (3). A thin plate of dimensions 0.06 mm x 0.2 mm x 0.4 mm bound by {100}, {010}, and {001} was mounted in silicone grease on a quartz fiber for the single-crystal X-ray diffraction experiment. Initial study on the diffractometer indicated a triclinic cell. Three open-counter ω-scans of low-angle reflections ($\Delta\bar{\omega}_{1/2} = 0.270$, no fine structure) and axial photographs confirmed the crystal quality. Data were collected with ω-2Θ scans and an analytical absorption correction was applied. The phenyl rings of the tetraphenylborate anion were refined as rigid groups.

[Co(NO)(TC-3,3)] (4a). Crystals for X-ray crystallography were grown from slow vapor diffusion of pentane into THF at room temperature. A thin brown plate of dimensions 0.1 x 0.4 x 0.4 mm was mounted in silicone grease at room temperature on the Siemens CCD system. Initial data collected indicated an orthorhombic crystal system which was confirmed by ultimate structure solution. The correct enantiomorph of the $Cmc2_1$ space group was chosen by isotropic refinement of the structure in both enantiomorphs and that with the lower residual was chosen (0.061 versus 0.056).

[Co(NO)(TC-4,4)] (4b). Small, dark brown plates were grown by cooling a fluorobenzene solution of **4b** layered with pentane. One with dimensions 0.2 x 0.1 x 0.05 mm was mounted in silicone grease on the end of a quartz fiber at room temperature and used for data collection. Structure solution in $P2_1/c$ revealed a

disorder of the nitrosyl oxygen atoms over two positions which were refined to a 60:40 site occupancy ratio for O1 and O1*, respectively.

[Co(SC$_6$F$_5$)(TC-3,3)] (5a). Fine brown needles used for X-ray crystallography were grown from fluorobenzene solutions layered with pentane. A needle of approximate dimensions 0.1 x 0.2 x 0.3 mm was mounted on the end of a quartz fiber in silicone grease at room temperature.

[Co(SC$_6$F$_5$)(TC-4,4)]·C$_7$H$_8$ (5b·C$_7$H$_8$). Dark brown plates used for X-ray crystallography were grown from toluene layered with pentane. A specimen with dimensions 0.1 x 0.18 x 0.45 mm was mounted on the end of a quartz fiber in silicone grease and a preliminary study on the diffractometer indicated a triclinic cell. Four open-counter ω-scans of low-angle reflections ($\Delta\bar{\omega}_{1/2} = 0.276$, no fine structure) and axial photographs revealed the crystal quality to be acceptable. Data were collected with ω-2Θ scans and an empirical absorption correction was applied. One molecule of toluene was found in the lattice and was refined isotropically.

UV-Visible studies. Reaction of 2a with THF to form 3. A 2 mL aliquot of an 80 μM solution of **2a** in CH$_2$Cl$_2$ was prepared and its UV-vis spectrum recorded. Aliquots of 1, 10, 20, 30, 50, 100, 150, 200, 300, 500, and 1000 μL of THF were added sequentially. At each addition the cuvette was shaken to ensure complete mixing and the spectrum was recorded after each addition. The resultant spectra showed gradual formation of **3** from **2a** (Figure 4.1). Data were fit at 338 and 398 nm to eq 1

$$K_{eq}[THF] = \frac{(\varepsilon_1 bc_0 - A)}{(A - \varepsilon_2 bc_0)} \tag{1}$$

in which ε_1 is the extinction coefficient for **2a**, ε_2 the extinction coefficient for **3**, A is the absorbance at variable concentrations of THF, b is the cell path length, c_0 is the initial concentration of **2a**, and K$_{eq}$ is the formation constant.

Reaction of [Co(TC-3,3)]$^+$ with Benzene Thiolate A 2.56 mL aliquot of a 12.6 μM [Co(TC-3,3)]PF$_6$ solution in CH$_2$Cl$_2$ was placed in a UV-vis cell with a teflon

septum and cooled to -78 °C. One equivalent of a 5.87 mM solution (5.5 μL) of (Me₄N)(SC₆F₅) in THF was added. Spectra were recorded at approximately 20 s intervals and are presented in Figure 4.2, demonstrating the rapid formation of [Co(TC-3,3)].

Molecular Orbital Calculations. Extended Hückel calculations were carried out on a Gateway 2000 Pentium PC with the CACAO program[16] for [CoCl(NH₂)₄]⁻, [CoSPh(NH₂)₄]⁻, and [Co(NO)(NH₂)₄]⁻ in idealized trigonal bipyramidal geometries. The arrangement of ligands relative to a right-handed axis system is shown in Figure 4.3. All angles at cobalt were taken as 90° or 120°. The following distances and angles were taken from the crystallographically determined parameters in [CoCl(TC-4,4)], **4b**, and **5b**: Co-N$_{TC}$ = 1.92 Å, Co-Cl = 1.80 Å, Co-NO = 1.80 Å, Co-N-O = 130°, Co-S = 2.29 Å, Co-S-C = 121°. In the models [CoSPh(NH₂)₄]⁻ and [Co(NO)(NH₂)₄]⁻, the NO and SPh groups were bent along the principal axis of the trigonal bipyramid, consistent with the structures of **4b** and **5b**.

Results

Cationic Co(III) Tropocoronands. Oxidation of [Co(TC-3,3)], **1a**, to four-coordinate [Co(TC-3,3)]X was readily achieved in CH₂Cl₂ with either AgX or Cp₂FeX in the presence of the non-coordinating anions X = BPh₄⁻, BAr'₄⁻, PF₆⁻, BF₄⁻, or OTf⁻ (Figure 4.4). Immediately upon addition of the oxidizing agent to a green solution of **1a**, the color turned deep pink-purple. Purification of the product was achieved by filtering the solution to remove Ag⁰ or washing the dried product powder with pentane to remove [Cp₂Fe]. The ferricinium reagents reacted more completely than the silver salts because of the insolubility of the latter, but the instability of [Cp₂Fe]BPh₄ in CH₂Cl₂ required the silver reagent to obtain the BPh₄⁻ derivative. The electronic spectra of the products were identical, indicating the absence of any weak interaction between the cation and anion in non-coordinating solvent.

Structural characterization of the four-coordinate cations was facilitated by using the bulky BPh_4^- and BAr'_4^- anions, which pack well with the tropocoronand ligand in [Co(TC-3,3)]BPh_4, **2a**, and [Co(TC-3,3)]BAr'_4, **2a'**. Methylene chloride was usually employed for the oxidation because the products are insoluble in other solvents such as toluene, THF, or CH_3CN. An exception is the BAr'_4^- analog; **2a'** is soluble in toluene. Crystals suitable for X-ray analysis could not be grown for [Co(TC-3,3)]X except with X = BAr'_4^- because of the limited solubility of the other salts in CH_2Cl_2.

Oxidation of [Co(TC-4,4)], **1b**, proceeded similarly under the same conditions (Figure 4.5). Deep green solutions of **1b** in CH_2Cl_2 immediately turned to a dark maroon upon oxidation with AgX or Cp_2FeX. The [Co(TC-4,4)]X products were slightly more soluble than the TC-3,3 analogs, being sparingly soluble in fluoro- or chlorobenzene, but are still significantly soluble only in CH_2Cl_2. Structural characterization was achieved with the BPh_4^- salt, **2b**.

The four-coordinate nature of the cations in **2a** and **2b** led us to study binding of Lewis bases to the metal centers. Upon reaction of **2a** with an excess of THF, CH_3CN, or Et_2O, a five-coordinate complex readily formed. Changes in the electronic spectra upon addition of THF are shown in Figure 4.1. After correcting for the effects of dilution a formation constant of 3.4(3) M^{-1} was estimated at 25 °C. The adduct [Co(THF)(TC-3,3)]BPh_4, **3**, was structurally characterized. Solvent binding was reversible and **2a** could be regenerated from **3** in vacuo. Under the same conditions **2b** did not react. Crystallographic characterization of **2b** showed that the metal center is not sterically prohibited from binding. An electronic barrier is therefore believed to be responsible.

Attempts to synthesize [Co(TC-n,m)]X for n + m > 8 were unsuccessful. With either Ag^+ or Cp_2Fe^+, Ag^0 or Cp_2Fe was obtained but only Co(II) tropocoronands could be isolated following workup.

As suggested by their distinctive colors, the electronic spectra of **2a**, **2b**, and **3**, are noticeably different from one another and from previously characterized [CoX(TC-n,m)] complexes. Spectroscopic data collected in Table 4.10 comprise the known cobalt(III) tropocoronand complexes. The five-coordinate Co(III) tropocoronand halide[2] and alkyl[17] complexes are brown in solution whereas **2a** and **2a'** are deep pink-purple and turn dark pink-orange upon binding a Lewis base such as THF to form **3**. Compounds **2a** and **2a'** show no absorptions in the visible range above 600 nm. Strong charge-transfer bands at 545 nm are reduced in intensity in **3**. The dark wine-red color of **2b** arises from a charge-transfer band of moderate intensity at 532 nm and a d-d band at 804 nm. Compound **2a** does not have the latter feature, suggesting substantially different ligand fields, and hence metal center geometries, for the two four-coordinate Co(III) cations. This expectation was confirmed by the structural analyses, as discussed below.

The four-coordinate cations **2a**, **2a'**, and **2b** are paramagnetic in solution at room temperature, with μ_{eff} = 3.1, 3.2, and 3.6 μ_B respectively. The expected spin-only magnetic moment for an $S = 1$ system is 2.83 μ_B, indicating significant spin-orbit coupling. The ^{1}H-NMR spectrum of **3** has three broad resonances in the aromatic region, where the aminotroponeiminate and tetraphenylborate ring proton shifts are expected, and four broad resonances in the aliphatic region where the methylene linker chain and THF are anticipated.

The structure of four-coordinate cobalt(III) in **2a'** is four-coordinate as revealed by the ORTEP diagram in Figure 4.6. The geometry is quite similar to that of the neutral precursor **1a**. Selected distances and angles are listed in Table 4.11. There are no close contacts between the cation and anion, and a disordered pentane molecule is also present in the crystal lattice. The average Co-N bond length of 1.861(5) Å in **2a'** is the same as that in **1a**, 1.864(9) Å.[1] The cobalt center in **2a'** is

essentially square planar with a dihedral angle Θ of 7.8° and the cobalt is displaced from the best N_4 plane by only 0.09 Å.

The structure of **3** (Figure 4.7) shows THF bound to cobalt, forming a five-coordinate square pyramidal unit. The metal atom is displaced by 0.26 Å out of the best plane through the four N donor atoms. The average Co-N bond length is 1.886(5) Å, comparable to the Co-N_{avg} distances of 1.891(2) Å in [CoCl(TC-3,3)][2] and 1.891(3) Å in [CoEt(TC-3,3)].[17] The Co-O bond length is 2.128(6) Å, typical of Co-THF bond lengths. A search of the Cambridge Structural Database[18] revealed twenty Co-THF distances with a mean value of 2.1(1) Å and a range of 2.021 - 2.450 Å. No other solvent is present in the lattice and no close contacts occur between the cation and anion.

In contrast to the structural similarities between the **2a'** cation and **1a**, the structure of cation **2b** is significantly different from that of **1b**. As shown in Figure 4.8, the tropocoronand ligand is twisted with a dihedral angle Θ of 41° and has an average Co-N distance of 1.86(2) Å. The dihedral angle in **1b** is only 32°, with Co-N_{avg} of 1.88(2) Å. Additional details are given in Table 4.11.

Co(III) Tropocoronand Nitrosyl Complexes. Immediately upon exposure to NO, dark green solutions of [Co(TC-n,m)] turn brown. This color change suggests oxidation of Co(II) to Co(III), since all known five-coordinate Co(III) tropocoronands are brown in solution, with the exception of [Co({O=C}CH_3)(TC-4,4)],[17] which is blue-green. The reaction of **1a** and **1b** with NO is irreversible under vacuum; NO is not lost from the solid or solutions and the compounds are stable to boiling fluorobenzene (84 °C).

The electronic spectra of **4a** and **4b** are included with those of the other Co(III) TC-3,3 and TC-4,4 tropocoronand complexes in Table 4.10. Although the solution colors appear similar to the eye, the electronic spectrum of **4a** is distinct from those of **5a**, [CoCl(TC-3,3)],[2] and [CoEt(TC-3,3)][17] and radically different from the spectra of

the cationic Co(III) species **2a, 2b**, and **3**. In the infrared spectra, the ν(N=O) bands at 1656 cm^{-1} and 1584 cm^{-1} for **4a** and **4b**, respectively, are consistent with data for other bent Co nitrosyls, although these vary widely and do not correspond with any other property of Co nitrosyls.[19]

Compound **4a** is paramagnetic at room temperature with a μ$_{eff}$ of 3.1 μ$_B$, in solution, but **4b** is diamagnetic. The latter is the first example of a diamagnetic trigonal bipyramidal Co(III) complex. All ligand protons are clearly resolved in the ^{1}H-NMR spectrum and show the same characteristic shifts and multiplicities observed in the diamagnetic [Zn(TC-n,m)],[20] [Cd(TC-n,m)],[20] and [Ni(TC-nm)], n + m = 6, 8, 9, complexes.[21] Extended Hückel calculations explain this novel feature as discussed below.

The structure of **4a** is given as an ORTEP diagram in Figure 4.9, and selected bond lengths and angles are reported in Table 4.12. The cobalt atom sits on a mirror plane that relates the two halves of the molecule. The two central methylene linker carbon atoms, C9 and C11 and the nitrosyl group lie on this mirror plane. The linker chains adopt different conformations, the six-membered chelate ring containing C10 and C11 being in a boat conformation whereas the ring with C8 and C9 has a chair conformation. As in compound **3**, the structure of **4a** is square-pyramidal with cobalt displaced out of the best N$_4$ plane by 0.54 Å and an average N$_{TC}$-Co-N$_{NO}$ angle of 100(2)°. The average Co-N$_{TC}$ distance of 1.907(2) Å is similar to other Co(III)-N$_{avg}$ distances in [CoEt(TC-3,3)][17] and [CoCl(TC-3,3)]^2 cited above. The N-O distance of 1.18(1) Å and Co-N-O angle of 125(1)° are consistent with a Co^{III}(NO$^-$) valence-bond description.[22] Repeated attempts to obtain satisfactory elemental analyses were unsuccessful due to consistently low yields of the crude material and difficulty in purifying small quantities by recrystallization.

The structure of **4b** is given in Figure 4.10 and selected distances and angles are given in Table 4.12. Cobalt has a trigonal-bipyramidal geometry, the equatorial

plane contains the nitrosyl group and atoms N1 and N3, which form angles of 129.7(5)°, 115.6(6)°, and 114.7(6)°. The N2-Co-N4 angle is 176.6(6)° and the bent nitrosyl group lies in the plane of these axial ligands. The oxygen atom of the nitrosyl group is disordered over two positions in the N2-Co-N4 plane which refined to a 60:40 site occupancy ratio for O1 and O1*, respectively. The average Co-N_{TC} distance of 1.92(1) Å is essentially the same as that in **4a**. The average N-O distance of 1.19(4) Å and Co-N-O angle of 132(3)° are also consistent with a Co^{III} (NO^-) valence-bond description analogous to **4a**. Both nitrosyl complexes have the {CoNO}^{8} configuration.[23]

Cobalt(III) Tropocoronand Thiolate Complexes. From [Co(TC-n,m)]PF$_6$, generated in situ, neutral five-coordinate [Co(SR)(TC-n,m)] complexes could be obtained. Reaction of the four-coordinate Co(III) cations in CH$_2$Cl$_2$ with (Me$_4$N)(SR) was accelerated by dissolving the thiolate in THF. Compound **3** did not form under these conditions, consistent with the greater affinity of RS$^-$ versus THF for cobalt(III). The choice of thiolate is critical because in reactions with more electron-releasing thiolates RSH where R = Me, Et, i-Pr, t-Bu, or Ph, the initially formed [Co(SR)(TC-n,m)] species decomposed by internal electron transfer to form [Co(TC-n,m)] and the corresponding disulfide. At room temperature the pink or purple color of [Co(TC-n,m)]$^+$ changed during the time of mixing with (Me$_4$N)(SR) to dark green characteristic of [Co(TC-n,m)]. At -78 °C a brown color was observed briefly upon addition of (Me$_4$N)(SR), which changed to dark-green in less than three minutes. Increased absorbance at 452 nm which indicates the presence of [Co(TC-3,3)] and accompanies the reaction of [Co(TC-3,3)]$^+$ with SPh$^-$ at -78 °C is shown in Figure 4.2. Diphenylsulfide was detected in the reaction mixture by GC/MS spectroscopy. With R = C$_6$F$_5$ the product is quite stable even in boiling fluorobenzene (84 °C). Electronic spectra consistent with [Co(TC-n,m)]$^+$ are observed

upon addition of one equivalent of MeOTf or Me_3OBF_4 to **5a** or **5b,** the thiolate presumably being removed as $MeSC_6F_5$.

Single crystal X-ray crystallographic characterization of **5a** produced the structure presented in Figure 4.11, with selected bond lengths and angles given in Table 4.13. The geometry at cobalt is square pyramidal with cobalt displaced by 0.29 Å from the best N_4 plane. The average S-Co-N angle is 98(5)° and the average trans N-Co-N angle is 163(6)°, indicating a slightly distorted square pyramid. The Co-N_{avg} distance of 1.893(6) Å is consistent with previously reported Co-N_{avg} values in five-coordinate Co(III) complexes,[2,17] and the bend angle at sulfur of 105.6° is consistent with sp^3 hybridization of sulfur and little donation of lone pair electron density to cobalt. The Co-S bond length of 2.262(3) Å is the next to shortest such distance observed among the six other crystallographically characterized $Co-SC_6F_4X$ moieties, where X = H, F, according to a recent search of the Cambridge Stuctural Database,[18] which showed a range of 2.259 - 2.497 Å and a mean of 2.36(3) Å. The related S-C distances have a mean of 1.748(8) Å and a range of 1.731 - 1.786 Å compared to the S-C distance in **5a** of 1.77(1) Å. The pentafluorobenzenethiolate ring is oriented above the C8 - C14 aminotroponeiminate ring with a ring centroid-to-centroid distance of 3.65 Å.

The structure of **5b**, given in Figure 4.12, is trigonal bipyramidal with the thiolate ligand in an equatorial position. The principal axis of the pyramid is defined by N1 and N3 with a N-Co-N angle of 178.2(3)° and the angles in the equatorial plane defined by S, N2, and N4 are 123.0(2)°, 116.6(2)°, and 120.1(3)°. The pentafluorobenzenethiolate ring is bent along the principal pyramid axis toward N1 with a Co-S-C angle of 107.3(3)°. As in **5a**, the sulfur is sp^3 hybridized and its lone pairs do not interact with the metal center. The Co-S and S-C distances of 2.292(3) and 1.75(1) Å are similar to those in **5a** also.

Discussion

Four-coordinate benzene dithiolate Co(III) compounds were first described 30 years ago.[4] The requirement of strongly donating ligands to stabilize Co(III) with only four donor ligands was noted[4,24] and further demonstrated in studies of square-planar Co(III)ethane-1,2-dithiolate[8,25] and tetrakis(benzenethiolate) complexes.[26] Square-planar Co(III) was also achieved with the strongly donating biuretato ligands[5,27,28] and diamide-dialkoxide ligands.[29-31] All of these complexes comprise a family of formally Co(III) ions with a tetraanionic ligand set. The first macrocyclic square-planar cobalt(III) complex was synthesized with a tetraamido tetraanionic ligand.[6,7] Neutral Co(III) square-planar complexes have been prepared with a trianionic alkylated derivative of the diamide-dialkoxide[32] mentioned above. A neutral $Co^{III}N_4$ complex of octaethylbilindione, a non-macrocyclic tetrapyrrole unit, has been structurally characterized;[3] it has a dihedral angle of 25.4° about the metal center. Co(III) has also been generated in an N_2O_2 environment in a binucleating macrocycle and characterized by UV-Vis spectroscopy.[33] Prior to the synthesis of **2a'** in this work, however, no mononuclear cationic square-planar Co(III) complex had ever been reported.

In addition to the requirement for strongly donating ligands, the features required to stabilize high oxidation state transition metal complexes have been investigated in detail,[34] with particular attention on tetraamido donor ligands. These "rules" include absence of C-H bonds β to, and heteroatoms with available lone pairs α or γ to an oxidizing metal center, because such moieties can provide electron density to the metal leading to ligand decomposition. Tropocoronand ligands do not have any heteroatoms with available lone pairs because the nitrogen atoms are already involved in stable π-bonding interactions with the seven-membered ring. There are C-H bonds β to metal center which are stable in the presence of four-coordinate Co(III), however, because the aminotroponeiminate

nitrogen atoms cannot support the requisite increase in bond order following C-H bond activation.

Although evidence for oxidation states higher than Co(III) has been obtained for the tetraamido systems,[6] similar behavior is not likely to obtain with the $Co^{III}N_4$ tropocoronand complexes. The Co(III)/(II) potentials occur at -1.48 V versus Cp_2Fe^+/Cp_2Fe in the tetraamido complexes,[29] in contrast to the value of approximately -0.4 V in analogous tropocoronands.[35] Oxidation of Co(III) in the tetraamido systems is near + 0.55 V[6] versus Cp_2Fe^+/Cp_2Fe, whereas the cobalt tropocoronand complexes display an irreversible oxidation attributed to ligand degradation near this potential.[35] Thus the dianionic tropocoronand ligand is strongly donating enough to stabilize $Co^{III}N_4$ but is not as strong a donor as a tetraanionic tetraamido system. The cobalt(III) tropocoronands are therefore not expected to exhibit higher oxidation states. Identification of the mode of oxidative decomposition of the ligand, and modification to prevent such degradation, might allow access to higher oxidation states. The tetraamido ligands evolved through just such an iterative design process.[34]

A comparison of the structures of **1a** with **2a'** and of **1b** with **2b** provides another opportunity to observe the effects of metal ion size and increased charge on the [M(TC-n,m)] dihedral angle. The Zn and Cd studies demonstrated that smaller dihedral angles are expected for larger metal ions and, similarly, larger dihedral angles are expected for smaller metal ions. For example, the [Cd(TC-5,5)] dihedral angle Θ of 54.5° is 10.5° smaller than that of 65° in [Zn(TC-5,5)][20]and the ionic radius of Cd(II) (0.92 Å)[36] is 0.18 Å larger than that of Zn(II) (0.74 Å).[36] Therefore the smaller size of Co(III) relative to Co(II) contracts the Co-N bond distances and an increase in Θ is required to compensate for a shorter α-to-ω methylene linker chain distance. These effects are observed with the TC-4,4 but not with TC-3,3 the ligand. A lower limit has apparently been reached for contraction of the Co-N distance in

2a', which is the smallest such distance observed in cobalt tropocoronands. The rigidity of the TC-3,3 ligand prevents it from twisting and there is no change in the Co-to-N_4 plane distance between **1a** and **2a'**.

Binding of THF to **2a** but not **2b** is consistent with the unavailability of the Ψ_z^2 orbital as the LUMO for compounds having the larger dihedral angles, as predicted by the MO calculations in Chapter 3. Figure 3.4 shows that, for dihedral angles less than 10°, as in the case of **2a'**, the Ψ_z^2 orbital is just below the HOMO (Ψ_{xz}/Ψ_{yz} orbitals). The dihedral angle Θ in **2a'** increases by 33° in **2b**, a change which is accompanied by a decrease in the energy of the Ψ_z^2 orbital and an increase in the energy of the HOMO, Ψ_{xz}. It is conceivable that binding of THF to **2a** to form **3** is thermodynamically favorable enough to compensate for the rearrangement that must occur to make an empty Ψ_z^2 orbital available to the THF oxygen lone pair. With **2b** however, the reaction is unfavorable under the conditions studied. The strong π-donor character of the tropocoronand ligand causes the Ψ_{xz} orbital to be the HOMO for all $[Co(TC\text{-}n,m)]^+$ species, rather than the Ψ_z^2, as would be expected in a complex with only σ-type donors. The ligand twist that occurs as the sum $n + m$ increases causes a widening in the energy gap between the Ψ_z^2 and frontier orbitals, making it unreactive.

The solution magnetic moments of **2a, 2a'**, and **2b** are similar to those reported for other $Co^{III}X_4$, $S = 1$, complexes reported in the literature.[4,5,25-27,29,37] Consistent with the magnetic moments of the $S = 3/2$ systems discussed in Chapter 3, the less symmetric species, **2b**, shows more spin orbit coupling than **2a** and **2a'**, implying two closely spaced orbitals for which ΔE is less than the pairing energy.

Compounds **4a** and **4b** exemplify the two types of pentacoordinate geometries known for $\{CoNO\}^8$ systems, square pyramidal and trigonal bipyramidal The limited flexibility of the TC-3,3 ligand imposes the square-pyramidal symmetry on **4a**. No other geometry has been observed for any [MX(TC-3,3)] complex. Many

other square-pyramidal cobalt complexes with bent nitrosyl groups have been structurally characterized, including [Co(NO)TPP],[38] [Co(dmgH)$_2$(NO)],[39] and a substituted tmtaa complex [Co(NO)(Me$_2$(COOEt)$_2$taa)].[40] The bond distances and angles in **4a** are unexceptional compared to these other cobalt nitrosyl complexes.

The trigonal bipyramidal geometry in **4b** is much less common for Co(III), but has been observed previously in the tropocoronand complex [CoCl(TC-4,4)].[2] Aside from this compound, only a few [CoX$_3$(PR$_3$)$_2$][41-44] complexes occur with this geometry. The torsional angles in the linker chains of [CoCl(TC-4,4)] and [CoMe(TC-4,4)][17] revealed that the trigonal bipyramidal geometry was less strained than square-planar geometry for the TC-4,4 ligand. Because the methyl group can only bind as a σ-donor, and not as a π-donor or acceptor, it cannot interact in the equatorial plane with the d$_{x^2-y^2}$ orbital, which is shared with two other ligands. In the axial position, binding to the d$_{z^2}$ orbital is not similarly shared. Nitrosyl is a σ-donor and π-acceptor and can bind in the equatorial position like chloride, which is a σ- and π-donor.

Among the structurally characterized five-coordinate {CoNO}^{8} complexes, bent nitrosyl groups occur almost exclusively in the axial positions of square pyramidal structures, like **4a**, and linear nitrosyl groups in the equatorial positions of trigonal bipyramids.[45,46] Compound **4b** is only the second structurally characterized example of a {CoNO}^{8} system with a bent nitrosyl in an equatorial position of a trigonal bipyramid. The other example is [Co(NO)Cl$_2$(PMe$_3$)$_2$],[47] in which the nitrosyl is clearly bent, but disorder of the NO group and a chlorine atom over two sites prevented accurate determination of the nitrosyl bond distances and angles. The disorder in **4b** has been successfully modeled, revealing distances and angles similar to those in **4a**. The compounds [Co(NO)I$_2$(PMe$_3$)$_2$][47] and [Co(NO)Cl$_2$(PMePh$_2$)$_2$][48] also have trigonal bipyramidal geometry like [Co(NO)Cl$_2$(PMe$_3$)$_2$], but the nitrosyl groups are linear and the symmetry is C$_{2v}$.

Nitrosyl bending in [Co(NO)Cl$_2$(PMe$_3$)$_2$] facilitates electron donation from the d$_z^2$ to the NO π* orbitals.[47,49] The complex [Co(NO)Cl$_2$(PMe$_3$)$_2$] has a bent nitrosyl group and stronger phosphine donors than [Co(NO)Cl$_2$(PMePh$_2$)$_2$] bearing a linear nitrosyl. These results are completely consistent with this argument. Finally, MO calculations in Chapter 3 revealed that the tropocoronand ligand is a strong π-donor; this result is consistent with the bent NO groups in **4a** and **4b**.

Compound **4b** is distinct from all other trigonal bipyramidal cobalt nitrosyls and all other trigonal bipyramidal Co(III) tropocoronand complexes because it is diamagnetic. This property can be explained by the extended Hückel MO calculations presented in Figure 4.13, which plots the relative d-based molecular orbital energies of three trigonal bipyramidal models, [CoCl(NH$_2$)$_4$]$^-$, [Co(NO)(NH$_2$)$_4$]$^-$, and [Co(SPh)(NH$_2$)$_4$]$^-$, based on the compounds [CoCl(TC-4,4)], **4b** and **5b**. The energy of the d$_{xy}$ orbital greatly increases when NO is the fifth ligand compared to the thiolate and chloride cases owing to interaction with the NO π* orbitals. Neither chloride nor sulfur has π* acceptor orbitals to interact with the d$_{xy}$ orbital. This difference in ligand field splitting also explains the observed diamagnetism of **4b** compared to [CoCl(TC-4,4)] and **5b** which are both paramagnetic. The d$_{xy}$ orbital in **4b** is sufficiently raised in energy that the gap between the d$_{xy}$ orbital and the d$_{x^2-y^2}$ orbital is greater than the pairing energy, resulting in an S = 0 complex.

Cobalt complexes in which a thiolate is monodentate and not a part of a chelate ring are rare owing to the proclivity for RS$^-$ to reduce or to bridge metal atoms.[50] Structurally characterized examples have either strongly electron withdrawing R groups, RS$^-$ = SC$_6$F$_4$H$^-$[51,52] or SC$_6$F$_5^-$,[53] or low oxidation states Co(II)[54-56] or Co(I)[57,58] which are unlikely to be reduced further. The requirement of a strongly electron-withdrawing thiolate in [Co(SR)(TC-n,m)] complexes in order to avoid electron transfer from sulfur to Co(III) is therefore not surprising. The

geometries of **5a** and **5b** are very similar to those of [CoCl(TC-3,3)], [CoCl(TC-4,4)], **4a** and **4b**. The formerly rare trigonal-bipyramidal geometry for Co(III) is now routinely accessible because of the tuning properties of the TC-4,4 macrocycle which stabilize this geometry over square-pyramidal.

Conclusions

Four cationic Co(III) tropocoronand complexes, **2a, 2a', 2b**, and **3**, have been prepared by oxidation of [Co(TC-n,m)] in the presence of non-coordinating anions. These species are the first mononuclear cationic $Co^{III}X_4$ species. Structural characterization of **2a'** and **2b** revealed an increase in the dihedral angle Θ as a function of macrocycle size, as observed for the [Co(TC-n,m)] series. The added twist in **2b** arises from the smaller size of Co(III) versus Co(II). The resulting dihedral angle of 41° is the largest distortion from planarity yet observed in any $Co^{III}X_4$ complex. Addition of THF to **2a'** and **2b** produces a five-coordinate solvento species **3** only in the case of **2a'**. The failure of **2b** to react is ascribed to the unavailability of the d_z^2 orbital for binding the oxygen lone pair and constitutes proof of ligand tuning of reactivity by electronic effects.

Reaction of NO with [Co(TC-3,3)] and [Co(TC-4,4)] afforded the five-coordinate bent nitrosyls **4a** and **4b**. Compound **4b** is highly unusual, having the bent nitrosyl group in the equatorial position of a trigonal bipyramid and an $S = 0$ ground state. The strong donor character of the tropocoronand ligand and the ability of TC-4,4 to stabilize the trigonal bipyramidal over square-pyramidal geometry are responsible for these features. Reaction of the electron-poor thiolate $SC_6F_5^-$ with the cationic Co(III) complexes produced the five-coordinate thiolates **5a** and **5b**, the geometries of which match those of the corresponding [CoX(TC-n,m)] halides and **4a** and **4b**. With more electron-donating thiolates, oxidation of RS^- to RSSR with reduction of Co(III) to Co(II) occurs.

References

(1)   Jaynes, B. S.; Doerrer, L. H.; Liu, S.; Lippard, S. J. *Inorg. Chem.* **1995**, *34*, 5735-5744.

(2)   Jaynes, B. S.; Ren, T.; Liu, S.; Lippard, S. J. *J. Am. Chem. Soc.* **1992**, *114*, 9670-9671.

(3)   Balch, A. L.; Mazzanti, M.; Noll, B. C.; Olmstead, M. M. *J. Am. Chem. Soc.* **1994**, *116*.

(4)   Baker-Hawkes, M. J.; Billig, E.; Gray, H. B. *J. Am. Chem. Soc.* **1966**, *88*, 4870-4875.

(5)   Birker, P. J. M. W. L.; Bour, J. J.; Steggerda, J. J. *Inorg. Chem.* **1973**, *12*, 1254-1259.

(6)   Collins, T. J.; Powell, R. D.; Slebodnick, C.; Uffelman, E. S. *J. Am. Chem. Soc.* **1991**, *113*, 8419-8425.

(7)   Collins, T. J.; Uffelman, E. S. *Ang. Chem.* **1989**, *101*, 1509-1511.

(8)   Rao, C. P.; Dorfman, J. R.; Holm, R. H. *Inorg. Chem.* **1986**, *25*, 428-439.

(9)   Ruggiero, C. E.; Carrier, S. M.; Antholine, W. E.; Whittaker, J. W.; Cramer, C. J.; Tolman, W. B. *J. Am. Chem. Soc.* **1993**, *115*, 11285-11298.

(10)   Evans, D. F. *J. Chem. Soc.* **1959**, 2003-2005.

(11)   Sur, S. N. *J. Magn. Reson.* **1989**, *82*, 169-173.

(12)   Brookhart, M., personal communication.

(13)   Brookhart, M.; Grant, B.; Volpe Jr., A. F. *Organometallics* **1992**, *11*, 3920-3922.

(14)   Burla, M. C.; Camalli, M.; Cascarano, G.; Giacovazzo, C.; Polidori, G.; Spagna, R.; Viterbo, D. *J. Appl. Cryst.* **1989**, *22*, 389.

(15)   *TEXSAN: Single Crystal Analysis Software*, 1993, Woodlands, TX

(16)   Mealli, C. M.; Proserpio, D. M. *J. Chem. Ed.* **1990**, *67*, 399-402.

(17)   Jaynes, B. S.; Ren, T.; Masschelein, A.; Lippard, S. J. *J. Am. Chem. Soc.* **1993**, *115*, 5589-5599.

(18)   Allen, F. H.; Davies, J. E.; Galloy, J. J.; Johnson, O.; Kennard, O.; Macrae, C. F.; Mitchell, E. M.; Mitchell, G. F.; Smith, J. M.; Watson, D. G. *J. Chem. Info. Comp. Sci.* **1991**, *31*, 187-204.

(19)   Feltham, R. D.; Enemark, J. H. *Topics in Stereochemistry* **1982**, *12*, 155-215.

(20)   Doerrer, L. H., Chapter 2.

(21)   Davis, W. M.; Roberts, M. M.; Zask, A.; Nakanishi, K.; Lippard, S. J. *J. Am. Chem. Soc.* **1985**, *107*, 3864-3870.

(22)   Eisenberg, R.; Meyer, C. D. *Acc. Chem. Res.* **1975**, *8*, 26-34.

(23)   Enemark, J. H.; Feltham, R. D. *Coord. Chem. Rev.* **1974**, *13*, 339-406.

(24)   Eisenberg, R.; Dori, Z.; Gray, H. B.; Ibers, J. A. *Inorg. Chem.* **1968**, *7*, 741-748.

(25)   Dorfman, J. R.; Rao, C. P.; Holm, R. H. *Inorg. Chem.* **1985**, *24*, 453-454.

(26)   Fikar, R.; Koch, A. S.; Millar, M. M. *Inorg. Chem.* **1985**, *24*.

(27)   Bour, J. J.; Beurskens, P. T.; Steggerda, J. J. *J. Chem. Soc., Chem. Commun.* **1972**, 221-222.

(28)   Birker, P. J. M. W. L.; Beurskens, P. T. *J. R. Neth. Chem. Soc.* **1974**, *93*, 218-220.

(29)   Collins, T. J.; Richmond, T. G.; Santarsiero, B. D.; Treco, B. G. R. T. *J. Am. Chem. Soc.* **1986**, *108*, 2088-2090.

(30)   Collins, T. J.; Ozaki, S.; Richmond, T. G. *J. Chem. Soc., Chem. Commun.* **1987**, 803-804.

(31)   Ozaki, S.; Mimura, H.; Yasuhara, N.; Masui, M.; Yamagata, Y.; Tomita, K.; Collins, T. J. *J. Chem. Soc., Perkin Trans. 2* **1990**, 353-360.

(32)   Brewer, J. C.; Collins, T. J.; Smith, M. R.; Santarsiero, B. D. *J. Am. Chem. Soc.* **1988**, *110*, 423-428.

(33)   McCollum, D. G.; Yap, G. P. A.; Rheingold, A. L.; Bosnich, B. *J. Am. Chem. Soc.* **1996**, *118*, 1365-1379.

(34)   Collins, T. J. *Acc. Chem. Res.* **1994**, *27*, 279-285.

(35)   Doerrer, L. H., Chapter 3.

(36)   Shannon, R. D. *Acta Cryst.* **1976**, *A32*, 751-767.

(37)   Van der Put, P. J.; Schilperoord, A. A. *Inorg. Chem.* **1974**, *13*, 2476-2481.

(38)   Scheidt, W. R.; Hoard, J. L. *J. Am. Chem. Soc.* **1973**, *95*, 8281-8288.

(39)   Englert, U.; Strähle, J. *Gazz. Chim. Ital.* **1988**, *118*, 845-855.

(40)   Görls, H.; Reck, G.; Jäger, E.-G.; Müller, K.; Seidel, D. *Cryst. Res. Technol.* **1990**, *25*, 1277-1286.

(41)   McAuliffe, C. A.; Godfrey, S. M.; Mackie, A. G.; Pritchard, R. G. *Angew. Chem.* **1992**, *104*, 932.

(42)   Levason, W.; Ogden, J. S.; Spicer, M. D. *Inorg. Chem.* **1989**, *28*.

(43)   Von Enckevort, W. J. P.; Hendriks, H. M.; Beurskens, P. T. *Cryst. Struct. Commun.* **1977**, *6*, 531.

(44)   Jensen, K. A.; Nygaard, B.; Pedersen, C. T. *Acta Chem. Scand.* **1963**, *17*, 1126.

(45)   Johnson, P. L.; Enemark, J. H.; Feltham, R. D.; Swedo, K. B. *Inorg. Chem.* **1976**, *15*, 2989-2993.

(46)   Enemark, J. H.; Feltham, R. D.; Riker-Nappier, J.; Bizot, K. F. *Inorg. Chem.* **1975**, *14*, 624-632.

(47)   Alnaji, O.; Peres, Y.; Dartiguenave, M.; Dahan, F.; Dartiguenave, Y. *Inorg. Chim. Acta* **1986**, *114*, 151-158.

(48)   Brock, C. P.; Collman, J. P.; Dolcetti, G.; Farnham, P. H.; Ibers, J. A.; Lester, J. E.; Reed, C. A. *Inorg. Chem.* **1973**, *12*, 1304-1313.

(49)   Hoffman, R.; Chen, M. M. L.; Elian, M.; Rossi, A. R.; Mingos, D. M. P. *Inorg. Chem.* **1974**, *13*, 2666-2675.

(50)   Dance, I. G. *Polyhedron* **1986**, *5*, 1037-1104.

(51)   Doppelt, P.; Fischer, J.; Ricard, L.; Weiss, R. *New J. Chem.* **1987**, *11*, 357-364.

(52)   Doppelt, P.; Fisher, J.; Weiss, R. *J. Am. Chem. Soc.* **1984**, *106*, 5188-5193.

(53)   Thompson, J. S.; Sorrell, T.; Marks, T. J.; Ibers, J. A. *J. Am. Chem. Soc.* **1979**, *101*, 4193-4200.

(54)   Corwin Jr., D. T.; Fikar, R.; Koch, S. A. *Inorg. Chem.* **1987**, *26*, 3079-3080.

(55)   Jiang, F.; Wei, G.; Huang, Z.; Lei, X.; Hong, M.; Kang, B.; Liu, H. *J. Coord. Chem.* **1992**, *25*, 183-191.

(56)   Wei, G.; Hong, M.; Huang, Z.; Liu, H. *J. Chem. Soc., Dalton Trans.* **1991**, 3145-3148.

(57)   Vastag, S.; Marko, L.; Rheingold, A. L. *J. Organomet. Chem.* **1990**, *397*, 231-238.

(58)   Wei, G.; Huang, Z.; Lei, X.; Cao, R.; Jiang, F.; Hong, M.; Liu, H. *Acta Cryst., C.* **1992**, *48*, 2130-2132.

Table 4.1. X-ray Diffraction Studies of Cationic Cobalt(III) Complexes **2a'**, **2b**, and **3**.

	2a'·1/2 C$_5$H$_{12}$	**2b·1.5 C$_6$H$_5$Cl**	**3**
formula	CoF$_{24}$N$_4$C$_{54.5}$BH$_{40}$	CoCl$_{1.5}$N$_4$C$_{55}$H$_{53.5}$	CoON$_4$C$_{48}$BH$_{50}$
fw	1271.60	882.67	768.69
cryst. syst.	triclinic	triclinic	triclinic
space group	P$\bar{1}$	P$\bar{1}$	P$\bar{1}$
a, Å	12.9312(3)	11.0221	11.538(4)
b, Å	15.2457(3)	14.8430	13.560(3)
c, Å	16.5766(3)	15.3981	14.432(3)
α	112.627(1)	69.9444	91.38(2)
β, deg	102.464(1)	71.5358	111.45(2)
γ	105.888(1)	87.7914	109.17(2)
V, Å^3	2704.74(9)	2237.626	1958(1)
Z	2	2	2
radiation	MoK$_\alpha$, λ = 0.71609 Å	MoK$_\alpha$, λ = 0.71609 Å	MoK$_\alpha$, λ = 0.71609 Å
ρ_{calcd}, g/cm^3	1.574	1.326	1.304
T, K	183	193	163
μ (cm^{-1})	4.43	5.16	4.81
transmission coeff	0.847 - 1.000	0.907 - 0.964	0.940 - 0.981
2θ limits, deg	3 - 45	3 - 47	3 -44
data limits	+h±k±l	+h±k±l	+h±k±l
total no. of data	10519	7023	5494
no. of unique data	6400[a]	3883[b]	3095[b]
no. of parameters	779	548	308
R^c	0.080	0.069	0.066
$R_w{}^d$	---	0.059	0.074
$wR^2{}^e$	0.191	---	---
largest shift/esd, final	0.000	0.000	0.002
largest peak, e/Å^3	0.628	1.5266	0.645

[a]Observation criterion: I > 2σ(I). [b]Observation criterion: I > 3σ(I). $^cR = \Sigma ||F_o| - |Fc||/\Sigma|F_o|$. ^dR_w = $[\Sigma w(|F_o| - |F_c|)^2/\Sigma w|F_o|^2]^{1/2}$, where w = 1/σ^2(F) and σ^2(F) is defined in Carnahan, E. M.; Rardin, R. L.; Bott, S. G.; Lippard, S. J. *Inorg. Chem.* **1992**, *31*, 5193. $^ewR^2 = \{[\Sigma(wF_o2-F_c^2)^2]/\Sigma w(F_o)]\}^{1/2}$ where w = 1/[σ^2(F$_o^2$)+(0.0816(P))^2 + 11.23(P)] and P = [max(F$_o^2$, 0) + x(F$_c^2$)]/3.

Table 4.2. X-ray Diffraction Studies of Neutral Cobalt(III) Tropocoronand Complexes.

	4a	4b	5a	5b·C_7H_8
formula	$CoON_5C_{20}H_{22}$	$CoON_5C_{22}H_{26}$	$CoSF_5N_4C_{26}H_{22}$	$CoSF_5N_4C_{35}H_{34}$
fw	407.36	435.41	576.47	696.63
cryst. syst.	orthorhombic	monoclinic	orthorhombic	triclinic
space group	$Cmc2_1$	$P2_1/c$	$Pbca$	$P\bar{1}$
a, Å	16.1983(8)	12.7912(12)	12.2478(2)	9.546(2)
b, Å	12.2557(7)	16.1375(16)	9.0636(2)	13.309(4)
c, Å	8.8952(5)	9.8617(10)	41.9264(2)	13.470(6)
α, deg				71.04(3)
β, deg		104.077(2)		89.43(2)
γ, deg				77.91(2)
V, Å^3	1765.88	1972.66	4654.21	1579.5(9)
Z	4	4	8	2
radiation	MoK$_\alpha$,λ=0.71609 Å	MoK$_\alpha$,λ=0.71609 Å	MoK$_\alpha$,λ=0.71609 Å	MoK$_\alpha$,λ=0.71609 Å
ρ_{calcd}, g/cm^3	1.529	1.466	1.645	1.471
T, K	188	183	188	193
μ(Mo Kα), cm^{-1}	9.91	8.95	8.92	6.74
transmission coeff	0.970 - 0.846	0.913 - 0.822	0.819 - 1.000	0.953 - 0.928
2θ limits, deg	3 - 46.5	3 - 56.6	3 - 46.5	3 - 53
data limits	+h, +k, +l	+h, +k, ±l	+h, +k, +l	+h, ±k, ±l
total no. of data	6205	12079	17074	7291
no. of unique data^a	732	1540	2022	4117
no. of parameters	115	261	334	363
R^b	0.056	0.089	0.079	0.089
R_w^c	0.056	0.094	0.075	0.083
max shift/esd, final	0.004	0.000	0.000	0.011
largest peak, e/Å^3	0.585	0.744	.075	0.203

^{a}Observation criterion: $I > 3\sigma(I)$. $^bR = \Sigma||F_o| - |Fc||/\Sigma|F_o|$. $^cR_w = [\Sigma w(|F_o| - |F_c|)^2/\Sigma w|F_o|^2]^{1/2}$, where $w = 1/\sigma^2(F)$ and $\sigma^2(F)$ is defined in Carnahan, E. M.; Rardin, R. L.; Bott, S. G.; Lippard, S. J. *Inorg. Chem.* **1992**, *31*, 5193.

Table 4.3. Final Positional and Isotropic Thermal Parameters for [Co(TC-3,3)]BAr′$_4$, **2a′**.[a]

atom	x	y	z	B(eq) Å^{2b}
Co	0.3460(1)	0.4698(1)	0.1399(1)	1.3(2)
N(1)	0.4488(4)	0.4090(3)	0.1128(3)	1.4(2)
N(2)	0.2915(4)	0.4217(4)	0.107(3)	1.5(2)
N(3)	0.2498(4)	0.5389(4)	0.1670(3)	1.5(2)
N(4)	0.4124(4)	0.5329(4)	0.2702(3)	1.4(2)
C(1)	0.4501(5)	0.3773(4)	0.0254(4)	1.5(2)
C(2)	0.5339(5)	0.3432(5)	-0.0012(5)	1.9(3)
C(3)	0.5482(6)	0.3088(5)	-0.0871(5)	2.3(3)
C(4)	0.4861(7)	0.2991(5)	-0.1704(5)	2.5(3)
C(5)	0.3921(7)	0.3238(5)	-0.1878(5)	2.4(3)
C(6)	0.3367(6)	0.3614(5)	-0.1298(4)	2.1(3)
C(7)	0.3568(5)	0.3855(4)	-0.0348(4)	1.4(2)
C(8)	0.2847(5)	0.6129(4)	0.2575(4)	1.5(2)
C(9)	0.2321(5)	0.6829(5)	0.2860(5)	1.8(3)
C(10)	0.2526(6)	0.7602(5)	0.3728(5)	2.0(3)
C(11)	0.3339(6)	0.7930(5)	0.4583(5)	2.1(3)
C(12)	0.4164(6)	0.7552(5)	0.4754(5)	2.2(3)
C(13)	0.4381(6)	0.6756(5)	0.4144(4)	1.9(3)
C(14)	0.3814(5)	0.6082(4)	0.3177(4)	1.4(2)
C(15)	0.5327(5)	0.3988(5)	0.1810(4)	1.7(3)
C(16)	0.4976(5)	0.4058(5)	0.2631(4)	1.8(3)
C(17)	0.4992(5)	0.5102(5)	0.3219(4)	1.8(3)
C(18)	0.1882(5)	0.4267(5)	-0.0414(4)	1.8(3)
C(19)	0.1047(5)	0.4283(5)	0.0096(4)	1.9(3)
C(20)	0.1456(5)	0.5256(5)	0.0990(4)	1.8(3)
C(21)	0.8380(5)	0.2163(4)	0.2003(4)	1.3(2)
C(22)	0.8056(5)	0.2129(4)	0.1132(4)	1.4(2)
C(23)	0.7341(5)	0.1200(5)	0.0337(4)	1.7(3)
C(24)	0.6961(5)	0.0311(5)	0.0431(4)	1.6(3)
C(25)	0.7292(5)	0.0369(4)	0.01309(4)	1.4(2)
C(26)	0.8009(4)	0.1289(4)	0.2125(4)	1.1(2)

Table 4.3. (con't) Final Positional and Isotropic Thermal Parameters for [Co(TC-3,3)]BAr′₄, **2a′**.[a]

atom	x	y	z	B(eq) Å^{2b}
C(27)	0.8479(6)	0.3101(6)	0.1070(4)	2.1(3)
C(28)	0.6203(7)	-0.0702(7)	-0.0403(5)	2.8(3)
C(31)	0.6400(4)	0.0249(4)	0.2948(4)	1.1(2)
C(32)	0.5619(5)	-0.0313(4)	0.3199(4)	1.3(2)
C(33)	0.5977(5)	-0.0723(4)	0.3771(4)	1.3(2)
C(34)	0.7135(5)	-0.0561(4)	0.4077(4)	1.3(2)
C(35)	0.7907(5)	0.0001(4)	0.3812(4)	1.2(2)
C(36)	0.7573(4)	0.0435(4)	0.3252(3)	1.1(2)
C(37)	0.4380(5)	-0.0480(5)	0.2852(5)	1.7(3)
C(38)	0.7538(6)	-0.0974(5)	0.4697(4)	1.9(3)
C(41)	0.9627(5)	0.0032(4)	0.2591(4)	1.3(2)
C(42)	1.0583(5)	-0.0152(4)	0.2438(4)	1.3(2)
C(43)	1.1620(5)	0.0659(5)	0.2742(4)	1.5(2)
C(44)	1.1691(4)	0.1658(4)	0.3203(4)	1.3(2)
C(45)	1.0722(5)	0.1832(4)	0.3338(4)	1.3(2)
C(46)	0.9664(4)	0.1034(4)	0.3048(4)	1.1(2)
C(47)	1.0478(6)	-0.1230(6)	0.1964(5)	2.3(3)
C(48)	1.2793(5)	0.2574(5)	0.3565(5)	1.9(3)
C(51)	0.9671(4)	0.2578(4)	0.4916(4)	1.3(2)
C(52)	0.9913(5)	0.3409(4)	0.5759(4)	1.5(2)
C(53)	0.9380(5)	0.4094(4)	0.5808(4)	1.7(3)
C(54)	0.8592(5)	0.3911(4)	0.4995(4)	1.4(2)
C(55)	0.8339(5)	0.3054(4)	0.4147(4)	1.3(2)
C(56)	0.8869(4)	0.2358(4)	0.4067(4)	1.1(2)
C(57)	1.0768(6)	0.3581(6)	0.6628(4)	2.2(3)
C(58)	0.8008(6)	0.4618(5)	0.5032(5)	2.1(3)
B	0.8520(5)	0.1277(5)	0.3118(4)	1.1(2)
F(1)	0.9553(8)	0.3827(7)	0.1739(7)	1.9(4)
F(1A)	0.9586(8)	0.3609(8)	0.1483(7)	2.1(4)
F(2)	0.7948(8)	0.3788(8)	0.1515(8)	2.5(4)
F(2A)	0.7811(8)	0.3568(7)	0.1143(7)	2.4(4)
F(3)	0.8165(9)	0.2982(7)	0.0211(7)	2.7(4)

Table 4.3. (con't) Final Positional and Isotropic Thermal Parameters for [Co(TC-3,3)]BAr′₄, **2a′**.[a]

atom	x	y	z	B(eq) Å^{2b}
F(3A)	0.8599(9)	0.2906(7)	0.0201(6)	2.5(4)
F(4)	0.5190(8)	-0.1199(7)	-0.0234(7)	1.2(3)
F(4A)	0.5270(9)	-0.0536(8)	-0.0948(7)	1.8(3)
F(4B)	0.5184(11)	-0.0972(10)	-0.0606(9)	2.2(4)
F(5)	0.6599(8)	-0.0833(6)	-0.1151(6)	2.5(3)
F(5A)	0.5904(16)	-0.0752(12)	-0.1173(12)	5.8(6)
F(6)	0.6522(8)	-0.1537(6)	-0.0343(6)	0.9(2)
F(6A)	0.6571(14)	-0.1368(14)	-0.0672(13)	3.5(4)
F(6B)	0.5819(20)	-0.1419(16)	-0.0289(13)	4.5(5)
F(7)	0.4234(9)	0.0329(10)	0.2701(12)	1.0(2)
F(7A)	0.4078(11)	-0.0138(13)	0.2264(11)	2.6(3)
F(7B)	0.4283(11)	0.0402(11)	0.3038(11)	2.2(6)
F(8)	0.3690(8)	-0.1360(8)	0.2111(8)	1.0(3)
F(8A)	0.3915(10)	-0.1001(11)	0.1882(8)	2.2(4)
F(8B)	0.3682(9)	-0.1516(8)	0.2449(9)	1.8(4)
F(9)	0.3919(9)	-0.0430(11)	0.3592(8)	1.0(4)
F(9A)	0.3732(13)	-0.0895(14)	0.3171(14)	3.2(6)
F(9B)	0.3983(13)	-0.0107(13)	0.3519(11)	2.7(6)
F(10)	0.8668(7)	-0.0581(10)	0.5159(9)	0.7(3)
F(10A)	0.8515(12)	-0.0234(11)	0.5446(10)	2.5(5)
F(10B)	0.8588(13)	-0.0975(14)	0.4804(13)	2.5(6)
F(11)	0.6995(11)	-0.0872(13)	0.5364(9)	0.8(3)
F(11A)	0.6875(12)	-0.1277(14)	0.5096(12)	2.4(6)
F(11B)	0.7476(20)	-0.0484(16)	0.5523(13)	3.9(7)
F(12)	0.7169(14)	-0.2092(9)	0.4176(8)	1.2(4)
F(12A)	0.7755(17)	-0.1778(14)	0.4275(11)	3.0(5)
F(12B)	0.6932(14)	-0.1939(15)	0.4383(13)	2.8(7)
F(13)	0.9500(7)	-0.1816(6)	0.1150(6)	1.9(3)
F(13A)	0.9429(9)	-0.1938(8)	0.1456(8)	3.1(4)
F(14)	1.0918(10)	-0.1528(8)	0.2563(7)	2.9(4)
F(14A)	1.0337(9)	-0.1731(7)	0.2482(7)	2.8(4)
F(15)	1.1185(8)	-0.1312(7)	0.1416(7)	2.2(3)

Table 4.3. (con't) Final Positional and Isotropic Thermal Parameters for [Co(TC-3,3)]BAr′$_4$, **2a′**.^{a}

atom	x	y	z	B(eq) Å^{2b}
F(15A)	1.1319(10)	-0.1376(9)	0.1735(8)	3.3(5)
F(16)	1.3691(5)	0.2351(4)	0.3499(4)	2.5(3)
F(16A)	1.3540(11)	0.2202(10)	0.3072(11)	0.7(4)
F(17)	1.2725(5)	0.3245(4)	0.3270(4)	2.1(3)
F(17A)	1.2633(14)	0.3017(13)	0.2952(13)	0.9(5)
F(18)	1.3118(5)	0.3224(5)	0.4513(4)	2.3(3)
F(18A)	1.3286(18)	0.2912(17)	0.4410(15)	1.9(7)
F(19)	1.0403(12)	0.3993(13)	0.7418(8)	1.3(4)
F(19A)	1.0818(16)	0.4236(14)	0.7390(12)	3.2(6)
F(19B)	1.0480(13)	0.3669(12)	0.7310(10)	2.1(6)
F(20)	1.1823(10)	0.3696(12)	0.6578(9)	2.0(3)
F(20A)	1.1821(8)	0.4167(10)	0.6855(7)	1.1(6)
F(20B)	1.1635(14)	0.4631(14)	0.7033(11)	3.4(6)
F(21)	1.0495(14)	0.2760(14)	0.6755(11)	3.0(6)
F(21A)	1.1248(17)	0.2986(17)	0.6552(11)	3.6(3)
F(21B)	1.0797(11)	0.2582(8)	0.6559(7)	1.1(3)
F(22)	0.6757(9)	0.4069(8)	0.4614(9)	0.9(3)
F(22A)	0.7096(15)	0.4427(13)	0.5097(12)	2.8(5)
F(22B)	0.6981(16)	0.4203(13)	0.4444(12)	2.8(7)
F(23)	0.7787(9)	0.4977(8)	0.5897(7)	1.4(3)
F(23A)	0.8743(10)	0.5621(9)	0.5541(9)	2.2(4)
F(23B)	0.8276(13)	0.5397(11)	0.5883(9)	2.6(4)
F(24)	0.8420(9)	0.5316(8)	0.4845(8)	3.0(3)
F(24A)	0.7895(8)	0.4808(7)	0.4224(7)	2.7(3
C(1S)	0.9567(12)	-0.0433(11)	-0.0160(11)	5.9(6)
C(2S)	0.9372(14)	-0.1470(12)	-0.0747(11)	5.9(6)
C(3S)	0.8663(19)	-0.2153(16)	-0.0977(15)	3.9(7)

^{a}Numbers in parentheses are estimated standard deviations of the last significant figure. See Figure 4.6 for atom labeling scheme. ^{b}B$_{eq}$ = 4/3 [a^{2}β$_{11}$ + b^{2}β$_{22}$ + c^{2}β$_{33}$ +2ab cos(γ)β$_{12}$ + 2ac cos (β)β$_{13}$ + 2bc cos(α)β$_{23}$].

Table 4.4. Final Positional and Isotropic Thermal Parameters for [Co(THF)(TC-3,3)]BPh₄, 3.ᵃ

atom	x	y	z	B(eq) Å^2 ᵇ
Co(1)	0.4021(1)	0.26917(9)	0.80151(9)	1.86(3)
O(1)	0.3541(6)	0.1461(4)	0.6842(4)	2.9(2)
N(1)	0.2252(6)	0.2385(5)	0.7901(5)	1.8(2)
N(2)	0.3623(6)	0.3699(5)	0.7208(5)	1.9(2)
N(3)	0.5891(7)	0.3310(5)	0.8431(5)	2.2(2)
N(4)	0.4520(7)	0.1946(5)	0.9093(5)	2.1(2)
C(1)	0.1706(8)	0.3095(6)	0.7526(6)	1.8(2)
C(2)	0.0504(9)	0.3077(7)	0.7565(7)	2.7(2)
C(3)	-0.0165(9)	0.3762(8)	0.7280(8)	3.4(3)
C(4)	0.0109(10)	0.4647(8)	0.6871(8)	3.6(3)
C(5)	0.119(1)	0.5085(7)	0.6584(7)	3.5(3)
C(6)	0.2230(9)	0.4737(7)	0.6705(7)	3.3(3)
C(7)	0.2517(8)	0.3878(6)	0.7121(6)	1.9(2)
C(8)	0.6618(9)	0.3114(7)	0.9315(7)	2.4(2)
C(9)	0.7999(9)	0.3710(7)	0.9825(7)	3.1(2)
C(10)	0.8940(10)	0.3620(8)	1.0703(8)	3.8(3)
C(11)	0.881(1)	0.2917(9)	1.1349(8)	3.8(3)
C(12)	0.765(1)	0.2144(9)	1.1274(7)	4.2(3)
C(13)	0.6333(10)	0.1860(8)	1.0574(7)	3.3(3)
C(14)	0.5819(9)	0.2275(7)	0.9707(7)	2.5(2)
C(15)	0.1543(9)	0.1518(6)	0.8297(7)	2.5(2)
C(16)	0.2174(9)	0.0682(7)	0.8498(7)	2.9(2)
C(17)	0.3562(9)	0.1096(7)	0.9356(7)	3.0(2)
C(18)	0.4501(8)	0.4357(7)	0.6748(6)	2.5(2)
C(19)	0.5591(9)	0.3931(7)	0.6814(7)	2.7(2)
C(20)	0.6531(9)	0.4016(7)	0.7883(7)	3.0(2)
C(21)	0.2476(9)	0.1232(7)	0.5851(6)	2.9(2)
C(22)	0.2510(10)	0.0292(7)	0.5306(7)	3.3(2)
C(23)	0.3986(10)	0.0451(7)	0.5776(7)	3.4(3)
C(24)	0.4359(9)	0.0852(8)	0.6842(7)	3.5(3)
C(25)	0.3193(5)	0.2802(4)	1.1627(3)	2.502

Table 4.4. (con't.) Final Positional and Isotropic Thermal Parameters for [Co(THF)(TC-3,3)]BPh$_4$, **3**.[a]

atom	x	y	z	B(eq) Å^2[b]
C(26)	0.1984(4)	0.2909(4)	1.1054(4)	2.502
C(27)	0.1905(4)	0.3513(4)	1.0279(4)	2.502
C(28)	0.3035(5)	0.4009(4)	1.0078(3)	2.502
C(29)	0.4244(4)	0.3901(4)	1.0652(4)	2.502
C(30)	0.4323(4)	0.3298(4)	1.1426(4)	2.502
C(31)	0.2279(5)	0.2301(4)	1.3099(4)	2.582
C(32)	0.2651(5)	0.3334(4)	1.3564(4)	2.582
C(33)	0.1902(5)	0.3572(3)	1.4045(4)	2.582
C(34)	0.0781(5)	0.2777(4)	1.4063(4)	2.582
C(35)	0.0409(4)	0.1744(3)	1.3598(4)	2.582
C(36)	0.1158(5)	0.1506(3)	1.3117(4)	2.582
C(37)	0.4816(4)	0.2306(4)	1.3364(4)	2.643
C(38)	0.5322(5)	0.2812(4)	1.4358(4)	2.643
C(39)	0.6640(5)	0.2990(4)	1.4999(3)	2.643
C(40)	0.7452(4)	0.2662(4)	1.4647(3)	2.643
C(41)	0.6947(5)	0.2157(4)	1.3653(4)	2.643
C(42)	0.5629(5)	0.1979(4)	1.3011(3)	2.643
C(43)	0.2593(6)	0.0754(3)	1.2046(4)	2.944
C(44)	0.2851(6)	0.0048(4)	1.2710(3)	2.944
C(45)	0.2360(6)	-0.1033(4)	1.2345(4)	2.944
C(46)	0.1612(6)	-0.1408(3)	1.1317(4)	2.944
C(47)	0.1354(5)	-0.0702(4)	1.0653(3)	2.944
C(48)	0.1845(6)	0.0379(4)	1.1018(4)	2.944
B(1)	0.3225(9)	0.2036(7)	1.2519(7)	1.8(2)

[a]Numbers in parentheses are estimated standard deviations of the last significant figure. See Figure 4.7 for atom labeling scheme. [b]$B_{eq} = 4/3 \, [a^2\beta_{11} + b^2\beta_{22} + c^2\beta_{33} + 2ab \, \cos(\gamma)\beta_{12} + 2ac \, \cos(\beta)\beta_{13} + 2bc \, \cos(\alpha)\beta_{23}]$.

Table 4.5. Final Positional and Isotropic Thermal Parameters for [Co(TC-4,4)]BPh$_4$, **2b**.[a]

atom	x	y	z	B(eq) Å^2 [b]
Co(1)	1.01583(10)	0.32053(8)	0.28712(7)	1.61(2)
Cl(1)	0.4384(3)	0.2465(2)	0.2221(2)	5.77(8)
Cl(2)	0.2345(7)	0.0179(5)	0.4280(5)	7.5(2)
N(1)	1.0629(6)	0.4031(4)	0.3418(4)	1.7(1)
N(2)	1.1654(6)	0.3801(4)	0.1817(4)	1.7(1)
N(3)	0.9949(6)	0.2032(4)	0.2762(4)	1.7(1)
N(4)	0.8386(5)	0.3021(4)	0.3450(4)	1.7(1)
C(1)	1.1587(7)	0.4686(6)	0.2821(5)	2.0(2)
C(2)	1.1915(7)	0.5478(6)	0.3031(6)	2.5(2)
C(3)	1.2891(8)	0.6210(6)	0.2531(6)	2.9(2)
C(4)	1.3880(8)	0.6362(6)	0.1685(7)	3.2(2)
C(5)	1.4115(7)	0.5781(7)	0.1137(6)	3.5(2)
C(6)	1.3417(8)	0.4983(6)	0.1231(6)	2.8(2)
C(7)	1.2247(7)	0.4499(5)	0.1915(5)	1.8(2)
C(8)	0.8746(7)	0.1651(5)	0.3019(5)	1.6(2)
C(9)	0.8422(8)	0.0858(6)	0.2828(6)	2.4(2)
C(10)	0.7267(8)	0.0351(5)	0.3075(6)	2.3(2)
C(11)	0.6066(8)	0.0494(6)	0.3624(6)	2.9(2)
C(12)	0.5747(7)	0.1203(6)	0.4046(6)	2.7(2)
C(13)	0.6499(7)	0.1933(6)	0.3996(5)	2.1(2)
C(14)	0.7816(7)	0.2211(5)	0.3510(5)	1.6(2)
C(15)	0.9988(8)	0.4064(6)	0.4413(5)	2.4(2)
C(16)	0.9002(8)	0.3218(6)	0.5071(5)	2.5(2)
C(17)	0.7667(7)	0.3365(6)	0.4981(5)	2.4(2)
C(18)	0.7667(7)	0.3667(5)	0.3943(5)	2.1(2)
C(19)	1.2131(7)	0.3618(5)	0.0873(5)	2.0(2)
C(20)	1.1225(7)	0.3023(5)	0.0703(5)	2.0(2)
C(21)	1.1261(8)	0.1939(6)	0.1156(5)	2.6(2)
C(22)	1.1058(7)	0.1592(5)	0.2243(5)	2.0(2)
C(23)	0.7951(7)	0.6489(5)	0.2209(5)	1.5(2)
C(24)	0.9207(7)	0.6217(5)	0.1827(5)	2.0(2)
C(25)	0.9425(7)	0.5475(5)	0.1453(5)	2.2(2)

Table 4.5. (con't) Final Positional and Isotropic Thermal Parameters for [Co(TC-4,4)]BPh₄, **2b**.[a]

atom	x	y	z	B(eq) Å^2 [b]
C(26)	0.8419(8)	0.4946(5)	0.1456(5)	2.1(2)
C(27)	0.7158(8)	0.5189(5)	0.1830(5)	2.2(2)
C(28)	0.6961(7)	0.5930(5)	0.2193(5)	1.7(2)
C(29)	0.6497(7)	0.7929(5)	0.2286(5)	2.0(2)
C(30)	0.6558(7)	0.8204(5)	0.1297(6)	2.3(2)
C(31)	0.5659(8)	0.8713(6)	0.0919(6)	2.9(2)
C(32)	0.4621(8)	0.8981(6)	0.1534(8)	3.7(2)
C(33)	0.4502(8)	0.8744(6)	0.2494(7)	3.6(2)
C(34)	0.5428(7)	0.8227(6)	0.2876(6)	2.7(2)
C(35)	0.8923(7)	0.8116(5)	0.2247(5)	1.5(2)
C(36)	0.9096(7)	0.9003(5)	0.1526(5)	1.5(2)
C(37)	1.0182(7)	0.9637(5)	0.1195(5)	2.1(2)
C(38)	1.1159(7)	0.9363(5)	0.1594(5)	2.1(2)
C(39)	1.1028(8)	0.8481(6)	0.2312(6)	2.5(2)
C(40)	0.9945(7)	0.7878(5)	0.2624(5)	2.2(2)
C(41)	0.7176(6)	0.6918(5)	0.3858(5)	1.5(2)
C(42)	0.6566(7)	0.6008(5)	0.4413(5)	2.1(2)
C(43)	0.6102(7)	0.5671(6)	0.5435(5)	2.5(2)
C(44)	0.6230(8)	0.6247(6)	0.5937(6)	2.8(2)
C(45)	0.6822(8)	0.7154(7)	0.5409(6)	3.1(2)
C(46)	0.7288(8)	0.7486(6)	0.4409(6)	2.8(2)
C(47)	0.5792(9)	0.2232(7)	0.1413(6)	3.6(2)
C(48)	0.5784(9)	0.1443(7)	0.1169(7)	3.7(2)
C(49)	0.688(1)	0.1275(8)	0.0549(8)	5.4(3)
C(50)	0.7974(9)	0.1902(7)	0.0171(7)	4.1(3)
C(51)	0.7946(10)	0.2690(9)	0.0420(8)	5.9(3)
C(52)	0.6823(9)	0.2864(7)	0.1072(7)	3.9(3)
C(54)	0.132(2)	-0.042(1)	0.430(1)	12.9(6)
C(55)	0.114(2)	0.041(1)	0.489(2)	14.5(7)
C(57)	0.007(1)	0.0568(8)	0.5364(8)	5.1(2)
B(1)	0.7642(8)	0.7356(6)	0.2662(6)	1.7(2)

Table 4.5. (con't) Final Positional and Isotropic Thermal Parameters for [Co(TC-4,4)]BPh$_4$, **2b**.^{a}

^{a}Numbers in parentheses are estimated standard deviations of the last significant figure. See Figure 4.8 for atom labeling scheme. ^{b}B$_{eq}$ = 4/3 [a$^2\beta_{11}$ + b$^2\beta_{22}$ + c$^2\beta_{33}$ +2ab cos(γ)β_{12} + 2ac cos (β)β_{13} + 2bc cos(α)β_{23}].

Table 4.6. Final Positional and Isotropic Thermal Parameters for [Co(NO)(TC-3,3)], **4a**.[a]

atom	x	y	z	$B(eq)\ \text{Å}^2$ [b]
Co(1)	1.000	0.19820(8)	0.102(3)	2.40(2)
O(1)	1.000	0.4078(5)	0.039(3)	5.0(2)
N(1)	1.0869(3)	0.2356(4)	0.237(3)	3.0(1)
N(2)	1.0860(3)	0.1165(3)	0.009(3)	2.5(1)
N(3)	1.000	0.3183(6)	-0.009(3)	4.1(2)
C(1)	1.1619(4)	0.1901(4)	0.206(3)	2.6(1)
C(2)	1.2358(4)	0.2218(4)	0.282(3)	3.2(1)
C(3)	1.3119(4)	0.1754(5)	0.282(3)	3.5(1)
C(4)	1.3423(4)	0.0863(5)	0.208(3)	3.7(2)
C(5)	1.2996(3)	0.0237(4)	0.109(3)	3.5(1)
C(6)	1.2218(3)	0.0376(4)	0.049(2)	3.1(1)
C(7)	1.1588(3)	0.1113(4)	0.082(3)	2.3(1)
C(8)	1.0761(4)	0.3118(5)	0.361(3)	4.2(2)
C(9)	1.000	0.2934(9)	0.450(3)	5.1(2)
C(10)	1.0787(4)	0.0527(4)	-0.129(3)	3.1(1)
C(11)	1.000	0.0819(6)	-0.212(3)	3.0(2)

[a]Numbers in parentheses are estimated standard deviations of the last significant figure. See Figure 4.9 for atom labeling scheme. [b]$B_{eq} = 4/3\ [a^2\beta_{11} + b^2\beta_{22} + c^2\beta_{33} + 2ab\ \cos(\gamma)\beta_{12} + 2ac\ \cos(\beta)\beta_{13} + 2bc\ \cos(\alpha)\beta_{23}]$.

Table 4.7. Final Positional and Isotropic Thermal Parameters for [Co(NO)(TC-4,4)], **4a**.[a]

atom	x	y	z	B(eq) Å^2 [b]
Co(1)	0.7261(2)	-0.0588(2)	0.4873(2)	1.77(5)
O(1)	0.887(1)	-0.164(1)	0.588(2)	2.9(5)
O(1*)	0.848(3)	-0.187(2)	0.408(4)	3(1)
N(1)	0.582(1)	-0.0954(8)	0.480(1)	2.0(3)
N(2)	0.675(1)	-0.0690(9)	0.288(1)	1.9(3)
N(3)	0.7825(9)	0.0520(9)	0.491(1)	1.6(3)
N(4)	0.7710(10)	-0.0438(9)	0.688(1)	1.7(3)
N(5)	0.824(1)	-0.1397(9)	0.493(2)	2.3(4)
C(1)	0.522(1)	-0.119(1)	0.354(2)	1.9(4)
C(2)	0.421(1)	-0.156(1)	0.335(2)	1.8(4)
C(3)	0.345(1)	-0.180(1)	0.217(2)	2.4(5)
C(4)	0.345(1)	-0.175(1)	0.078(2)	2.7(5)
C(5)	0.426(2)	-0.144(1)	0.028(2)	2.8(5)
C(6)	0.526(1)	-0.111(1)	0.095(1)	2.5(4)
C(7)	0.575(1)	-0.098(1)	0.239(2)	1.6(4)
C(8)	0.840(1)	0.083(1)	0.616(1)	1.7(3)
C(9)	0.900(1)	0.157(1)	0.631(2)	2.1(4)
C(10)	0.958(1)	0.197(1)	0.747(2)	2.5(5)
C(11)	0.975(1)	0.178(1)	0.884(2)	2.5(4)
C(12)	0.936(1)	0.110(1)	0.936(2)	2.3(4)
C(13)	0.875(1)	0.043(1)	0.874(2)	2.4(4)
C(14)	0.827(1)	0.025(1)	0.729(2)	1.7(4)
C(15)	0.541(1)	-0.096(1)	0.607(2)	3.1(5)
C(16)	0.573(2)	-0.171(1)	0.697(2)	3.3(5)
C(17)	0.692(2)	-0.185(1)	0.735(2)	2.7(5)
C(18)	0.759(1)	-0.111(1)	0.789(2)	3.0(5)
C(19)	0.745(1)	-0.055(1)	0.188(1)	2.8(4)
C(20)	0.853(1)	-0.016(1)	0.252(2)	2.9(5)
C(21)	0.848(1)	0.080(1)	0.281(2)	2.8(5)
C(22)	0.767(1)	0.103(1)	0.363(2)	2.4(4)

Table 4.7. (con't) Final Positional and Isotropic Thermal Parameters for [Co(NO)(TC-4,4)], **4a**.[a]

---

[a]Numbers in parentheses are estimated standard deviations of the last significant figure. See Figure 4.10 for atom labeling scheme. [b]$B_{eq} = 4/3 \, [a^2\beta_{11} + b^2\beta_{22} + c^2\beta_{33} + 2ab \cos(\gamma)\beta_{12} + 2ac \cos(\beta)\beta_{13} + 2bc \cos(\alpha)\beta_{23}]$.

Table 4.8. Final Positional and Isotropic Thermal Parameters for [Co(SC$_6$F$_5$)(TC-3,3)],

5a.[a]

atom	x	y	z	B(eq) Å^2 [b]
Co(1)	0.5592(1)	0.1922(2)	0.15541(3)	1.86(3)
S(1)	0.3978(2)	0.3104(4)	0.14941(7)	2.89(7)
F(1)	0.4485(6)	0.5894(7)	0.1140(2)	5.1(2)
F(2)	0.4448(7)	0.6390(8)	0.0511(2)	6.7(2)
F(3)	0.3784(6)	0.4240(8)	0.0103(2)	5.8(2)
F(4)	0.3099(6)	0.1613(8)	0.0344(2)	4.8(2)
F(5)	0.3115(5)	0.1123(8)	0.0966(2)	4.2(2)
N(1)	0.5186(7)	0.0701(10)	0.1900(2)	2.3(2)
N(2)	0.6343(6)	0.2905(9)	0.1889(2)	1.8(2)
N(3)	0.6304(6)	0.2921(10)	0.1217(2)	2.2(2)
N(4)	0.5350(7)	0.0535(9)	0.1225(2)	2.0(2)
C(1)	0.5622(8)	0.097(1)	0.2187(2)	1.8(3)
C(2)	0.5370(8)	0.019(1)	0.2459(3)	2.3(3)
C(3)	0.5824(9)	0.023(1)	0.2767(2)	2.4(3)
C(4)	0.6684(10)	0.101(1)	0.2873(2)	2.4(3)
C(5)	0.7279(8)	0.202(1)	0.2714(2)	2.6(3)
C(6)	0.7135(8)	0.258(1)	0.2411(2)	1.8(3)
C(7)	0.6386(8)	0.222(1)	0.2170(2)	1.7(3)
C(8)	0.6260(8)	0.231(1)	0.0929(3)	2.2(3)
C(9)	0.6712(9)	0.294(1)	0.0656(3)	3.4(3)
C(10)	0.672(1)	0.254(2)	0.0337(3)	3.9(4)
C(11)	0.632(1)	0.126(2)	0.0206(3)	4.7(4)
C(12)	0.588(1)	0.006(2)	0.0359(3)	4.0(4)
C(13)	0.5636(10)	-0.012(1)	0.0673(3)	3.0(3)
C(14)	0.5726(9)	0.084(1)	0.0936(2)	2.0(3)
C(15)	0.4443(10)	-0.059(1)	0.1875(3)	2.8(3)
C(16)	0.3955(9)	-0.074(1)	0.1552(3)	3.0(3)
C(17)	0.4753(10)	-0.086(1)	0.1279(3)	3.1(3)
C(18)	0.6965(8)	0.428(1)	0.1848(3)	2.5(3)
C(19)	0.6576(9)	0.510(1)	0.1561(3)	3.2(3)
C(20)	0.6818(9)	0.439(1)	0.1248(3)	2.8(3)

Table 4.8. (con't) Final Positional and Isotropic Thermal Parameters for [Co(SC$_6$F$_5$)(TC-3,3)], **5a.**[a]

atom	x	y	z	B(eq) Å^2 [b]
C(21)	0.3862(8)	0.348(1)	0.1081(3)	2.2(3)
C(22)	0.4157(9)	0.481(1)	0.0950(3)	3.2(3)
C(23)	0.4145(10)	0.508(1)	0.0626(3)	3.7(4)
C(24)	0.380(1)	0.399(2)	0.0420(3)	3.9(4)
C(25)	0.3452(9)	0.266(1)	0.0541(3)	2.9(3)
C(26)	0.3467(9)	0.246(1)	0.0866(3)	2.8(3)

[a]Numbers in parentheses are estimated standard deviations of the last significant figure. See Figure 4.11 for atom labeling scheme. [b]$B_{eq} = 4/3 \, [a^2\beta_{11} + b^2\beta_{22} + c^2\beta_{33} + 2ab \cos(\gamma)\beta_{12} + 2ac \cos(\beta)\beta_{13} + 2bc \cos(\alpha)\beta_{23}]$.

Table 4.9. Final Positional and Isotropic Thermal Parameters for [Co(SC$_6$F$_5$)(TC-4,4)],

5b.[a]

atom	x	y	z	B(eq) Å^2 [b]
Co(1)	0.9008(1)	0.17089(10)	0.7715(1)	1.99(3)
S(1)	0.7517(3)	0.2538(2)	0.6217(2)	2.64(5)
F(1)	0.5329(6)	0.2905(4)	0.7761(5)	3.3(1)
F(2)	0.3884(6)	0.4812(5)	0.7893(5)	4.0(2)
F(3)	0.4228(7)	0.6718(5)	0.6485(5)	4.6(2)
F(4)	0.6079(7)	0.6697(4)	0.4938(5)	4.1(2)
F(5)	0.7581(6)	0.4807(4)	0.4815(4)	3.6(1)
N(1)	0.8744(8)	0.2945(6)	0.8164(6)	2.3(2)
N(2)	0.8332(8)	0.1095(6)	0.9064(6)	2.2(2)
N(3)	0.9290(8)	0.0437(6)	0.7310(6)	2.3(2)
N(4)	1.1026(8)	0.1522(6)	0.7536(6)	2.7(2)
C(1)	0.803(1)	0.2887(8)	0.9021(7)	2.5(2)
C(2)	0.754(1)	0.3815(8)	0.9327(8)	3.5(3)
C(3)	0.680(1)	0.3932(9)	1.0172(10)	4.7(3)
C(4)	0.633(2)	0.317(1)	1.1000(10)	5.3(4)
C(5)	0.655(1)	0.206(1)	1.1152(9)	5.2(4)
C(6)	0.718(1)	0.1470(9)	1.0538(9)	3.8(3)
C(7)	0.780(1)	0.1784(7)	0.9569(7)	2.4(2)
C(8)	1.055(1)	0.0200(7)	0.6894(7)	2.3(2)
C(9)	1.083(1)	-0.0607(8)	0.6398(8)	3.3(2)
C(10)	1.201(1)	-0.0972(8)	0.5923(9)	3.9(3)
C(11)	1.331(1)	-0.0676(10)	0.5792(9)	4.2(3)
C(12)	1.370(1)	0.009(1)	0.6126(9)	4.3(3)
C(13)	1.297(1)	0.0752(9)	0.6659(9)	3.6(3)
C(14)	1.1576(10)	0.0842(8)	0.7023(8)	2.7(2)
C(15)	0.923(1)	0.3950(8)	0.7631(8)	3.2(2)
C(16)	1.017(1)	0.3889(9)	0.6788(10)	4.7(3)
C(17)	1.171(1)	0.328(1)	0.717(1)	6.7(4)
C(18)	1.188(1)	0.2166(9)	0.7904(9)	4.1(3)
C(19)	0.820(1)	-0.0189(7)	0.7297(7)	2.6(2)
C(20)	0.6889(10)	0.0062(8)	0.7903(9)	3.1(2)

Table 4.9. (con't) Final Positional and Isotropic Thermal Parameters for [Co(SC$_6$F$_5$)(TC-4,4)], **5b.**[a]

atom	x	y	z	B(eq) Å^2 [b]
C(21)	0.713(1)	-0.0396(8)	0.9095(9)	3.3(2)
C(22)	0.839(1)	-0.0068(8)	0.9492(7)	2.7(2)
C(23)	0.6547(10)	0.3776(7)	0.6296(7)	2.3(2)
C(24)	0.5568(10)	0.3825(8)	0.7065(8)	2.5(2)
C(25)	0.479(1)	0.4807(8)	0.7127(8)	2.9(2)
C(26)	0.499(1)	0.5777(8)	0.6418(9)	3.3(3)
C(27)	0.591(1)	0.5754(7)	0.5644(8)	2.9(2)
C(28)	0.667(1)	0.4774(7)	0.5599(7)	2.6(2)
C(29)	1.094(2)	0.298(1)	0.3316(8)	9.2512
C(30)	1.239(1)	0.2666(9)	0.3147(9)	9.2512
C(31)	0.9921(9)	0.3439(9)	0.246(1)	9.2512
C(32)	1.2819(9)	0.2819(9)	0.212(1)	9.2512
C(33)	1.180(2)	0.3281(10)	0.1271(8)	9.2512
C(34)	1.035(1)	0.3591(9)	0.1440(9)	9.2512
C(35)	1.060(3)	0.283(2)	0.413(2)	15.9(9)

[a]Numbers in parentheses are estimated standard deviations of the last significant figure. See Figure 4.12 for atom labeling scheme. [b]$B_{eq} = 4/3 [a^2\beta_{11} + b^2\beta_{22} + c^2\beta_{33} + 2ab \cos(\gamma)\beta_{12} + 2ac \cos(\beta)\beta_{13} + 2bc \cos(\alpha)\beta_{23}]$.

Table 4.10. UV-visible data for Co(III) Tropocoronand Complexes.

complex	λ (nm) {ε M⁻¹ cm⁻¹}					
[Co(TC-3,3)]BPh$_4$, **2a**	338 (16,600)	388 (13,600)	454 (9500)	497 (9800)	544 (25, 300)	574 (9300)
[Co(TC-3,3)]BAr'$_4$, **2a'**	342 (16,200)	389 (12,100)		496 (10,500)	545 (28,300)	
[Co(THF)(TC-3,3)]BPh$_4$, **3**	338 (8700)	400 (10,400)	450(12,000)		545 (5900)	
[CoEt(TC-3,3)][a]		411 (35,700)				801 (10,400)
[Co(NO)(TC-3,3)], **4a**	342 (14,300)	417 (12,000)			547 (4350)	677 (2300)
[Co(SC$_6$F$_5$)(TC-3,3)], **5a**		391 (12,900)	477 (15,300)		573 (7,700)	
[CoCl(TC-3,3)][b]	358 (11,700)	412 (11,400)	488 (6470)		542 (5660)	838 (5010)
[Co(TC-4,4)]BPh$_4$, **2b**		372 (25,400)			532 (10,000)	804 (7800)
[Co(Me)(TC-4,4)][a]		408 (26,400)			762 (4880)	
[Co(COMe)(TC-4,4)][a]		394 (28,600)			600 (7000)	835 (5520)
[Co(NO)(TC-4,4)], **4b**		409 (20,300)	486 (9200)			796 (2400)
[CoCl(TC-4,4)][b]		366 (23,300)	431 (17,900)	554 (7880)		792 (6020)
[Co(SC$_6$F$_5$)(TC-4,4)], **5b**		371 (21,300)	456 (22,600)	561 (7100)	669 (3000)	743 (3600)

[a]Jaynes, B. S.; Ren, T.; Masschelein, A.; Lippard, S. J. *J. Am. Chem. Soc.* **1993**, *115*, 5589-5599 [b]Jaynes, B. S.; Ren, T.; Liu, S.; Lippard, S. J. *J. Am. Chem. Soc.* **1992**, *114*, 9670.

223

Table 4.11. Selected Bond Distances and Angles for Cationic Co(III) Tropocoronands.[a]

	Distances (Å)			Angles (deg)
[Co(TC-3,3)]BAr'4	Co-N1	1.856(5)	N1-Co-N2	82.5(2)
2a'	Co-N2	1.857(5)	N1-Co-N3	175.9(2)
	Co-N3	1.864(4)	N1-Co-N4	97.5(2)
	Co-N4	1.865(5)	N2-Co-N3	96.9(2)
	Co-N$_{avg}$	1.861(5)	N2-Co-N4	173.0(2)
			N3-Co-N4	82.6(2)
[Co(THF)(TC-3,3)]BPh4	Co-N1	1.886(7)	N1-Co-N2	81.8(3)
3	Co-N2	1.879(7)	N1-Co-N3	163.2(3)
	Co-N3	1.887(7)	N1-Co-N4	96.5(3)
	Co-N4	1.892(7)	N2-Co-N3	95.9(3)
	Co-N$_{avg}$	1.886(5)	N2-Co-N4	165.6(3)
	Co-O	2.128(6)	N3-Co-N4	81.7(3)
			O-Co-N1	95.9(3)
			O-Co-N2	98.1(3)
			O-Co-N3	100.9(3)
			O-Co-N4	96.3(3)
[Co(TC-4,4)]BPh4	Co-N1	1.875(6)	N1-Co-N2	83.3(2)
2b	Co-N2	1.889(6)	N1-Co-N3	154.4(2)
	Co-N3	1.836(6)	N1-Co-N4	102.9(3)
	Co-N4	1.859(6)	N2-Co-N3	103.6(2)
	Co-N$_{avg}$	1.86(2)	N2-Co-N4	152.0(2)
			N3-Co-N4	82.7(3)

[a]Numbers in parentheses are estimated standard deviations of the last significant figure. Atoms are labeled as indicated in Figures 4.6-4.8.

**Table 4.12.** Selected Bond Distances and Angles for Cobalt Nitrosyl Tropocoronands.[a]

	Distances (Å)			Angles (deg)
[Co(NO)(TC-3,3)]	Co-N1	1.909(7)	N1-Co-N1*	95.1(4)
4a	Co-N2	1.905(7)	N1-Co-N2	81.9(3)
	Co-N$^{TC}_{avg}$	1.907(2)	N1-Co-N2*	160.0(3)
	Co-N3	1.77(1)	N2-Co-N2*	94.2(4)s
	O1-N3	1.18(1)	N1-Co-N3	98.7(4)
			N2-Co-N3	101.4(3)
			Co-N3-O1	125(1)
[Co(NO)(TC-4,4)]	Co-N1	1.91(1)	N1-Co-N2	81.4(5)
4b	Co-N2	1.92(1)	N1-Co-N3	129.7(5)
	Co-N3	1.93(1)	N1-Co-N4	97.0(5)
	Co-N4	1.93(1)	N1-Co-N5	115.6(6)
	Co-N$^{TC}_{avg}$	1.92(1)	N2-Co-N3	97.5(6)
	Co-N5	1.80(1)	N2-Co-N4	176.6(6)
	O1-N5	1.14(2)	N2-Co-N5	91.6(6)
	O1*-N5	1.23(3)	N3-Co-N4	81.2(5)
			N3-Co-N5	114.7(6)
			N4-Co-N5	91.7(6)
			Co-N1-O1	128(2)
			Co-N1-O1*	136(2)

[a]Numbers in parentheses are estimated standard deviations of the last significant figure. Atoms are labeled as indicated in Figures 4.9 and 4.10.

Table 4.13. Selected Bond Distances and Angles for Cobalt Thiolate Tropocoronands.[a]

		Distances (Å)		Angles (deg)
[Co(SC6F5)(TC-3,3)]	Co-N1	1.890(8)	N1-Co-N2	80.5(4)
5a	Co-N2	1.902(8)	N1-Co-N3	167.0(4)
	Co-N3	1.892(8)	N1-Co-N4	97.4(4)
	Co-N4	1.889(8)	N2-Co-N3	96.0(3)
	Co-N$_{avg}$	1.893(6)	N2-Co-N4	158.0(3)
	Co-S	2.262(3)	N3-Co-N4	81.1(4)
	S-C21	1.77(1)	S-Co-N1	97.6(3)
			S-Co-N2	106.4(3)
			S-Co-N3	95.4(3)
			S-Co-N4	95.6(3)
			Co-S-C21	105.6(3)
[Co(SC6F5)(TC-4,4)]	Co-N1	1.896(9)	N1-Co-N2	81.4(3)
5b	Co-N2	1.900(7)	N1-Co-N3	178.2(3)
	Co-N3	1.906(9)	N1-Co-N4	98.4(4)
	Co-N4	1.910(8)	N2-Co-N3	97.1(3)
	Co-N$_{avg}$	1.903(6)	N2-Co-N4	120.1(3)
	Co-S	2.292(3)	N3-Co-N4	81.5(4)
	S-C23	1.75(1)	S-Co-N1	96.1(2)
			S-Co-N2	123.0(2)
			S-Co-N3	85.6(2)
			S-Co-N4	116.6(2)
			Co-S-C23	107.3(3)

[a]Numbers in parentheses are estimated standard deviations of the last significant figure. Atoms are labeled as indicated in Figures 4.11 and 4.12.
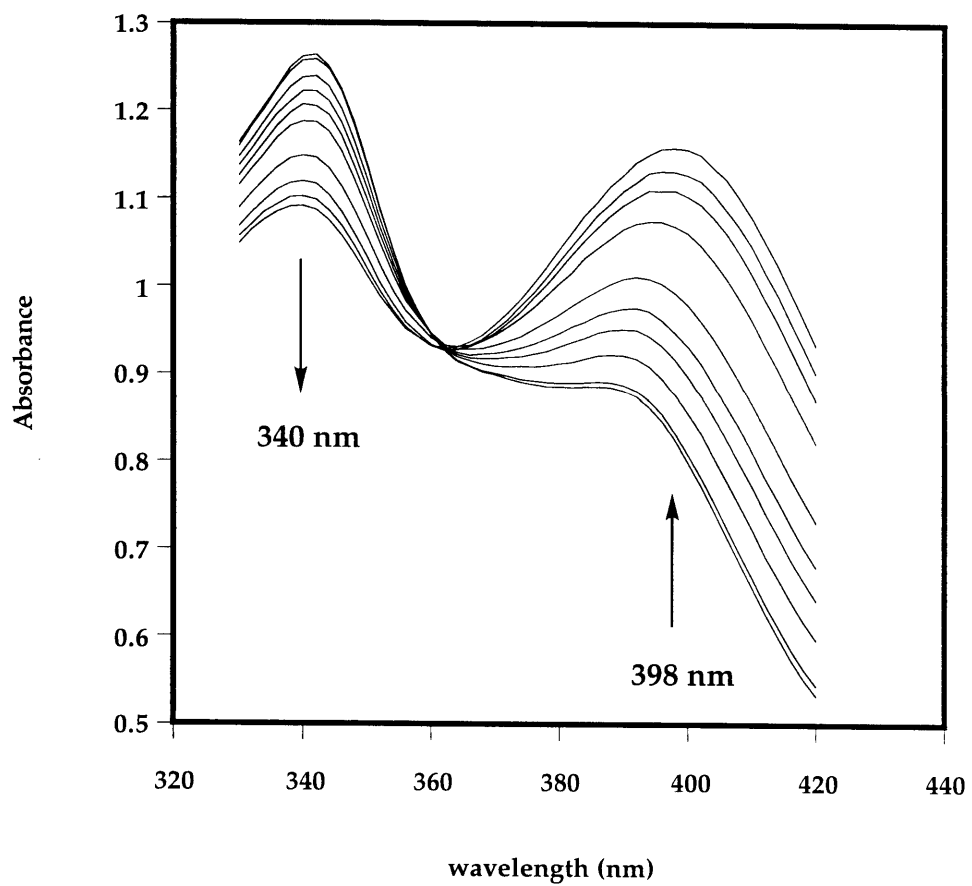
Figure 4.1. Electronic spectral changes observed upon reaction of excess THF with [Co(TC-3,3)]BPh$_4$, **2a**, to form [Co(THF)(TC-3,3)]BPh$_4$, **3**.
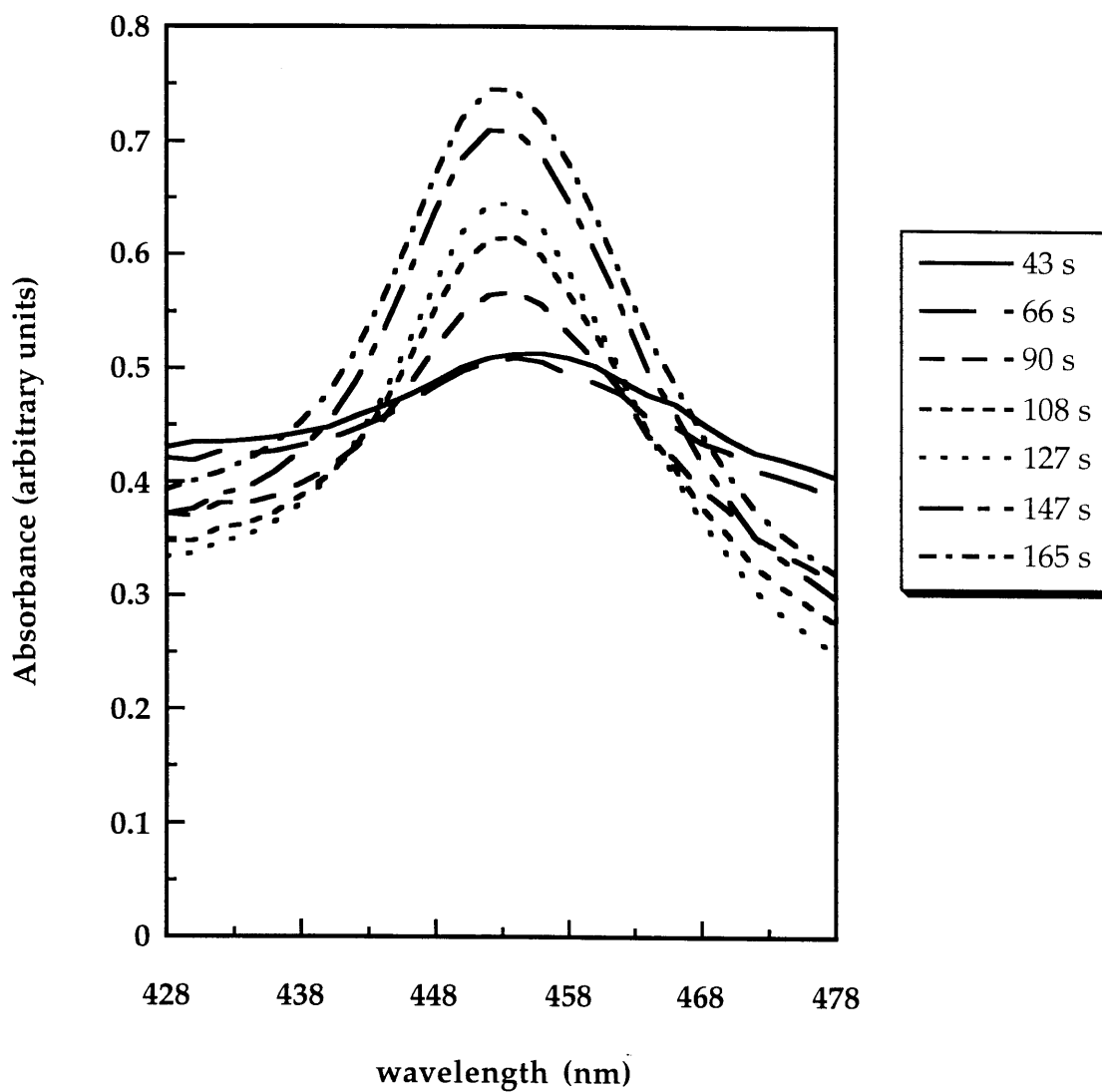
Figure 4.2. Absorbance changes at 452 nm demonstsrating the formation of [Co(TC-3,3)] in less than three minutes upon reaction of [Co(TC-3,3)]$^+$ with PhS$^-$ at -78 °C.
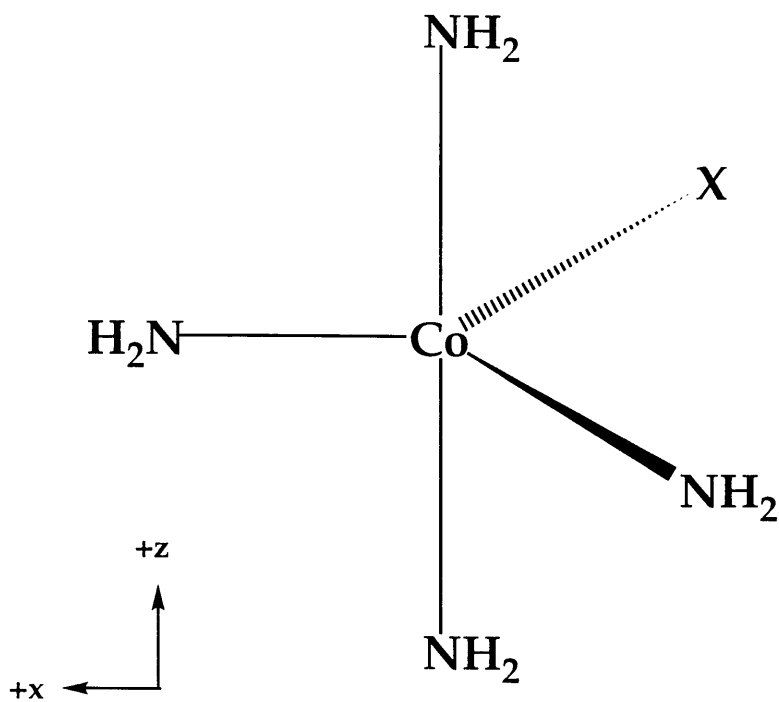
Figure 4.3. Atomic positions for extended Hückel calculations on trigonal bipyramidal [CoX(NH2)4]⁻ systems where X = Cl⁻, SPh⁻, NO⁻.
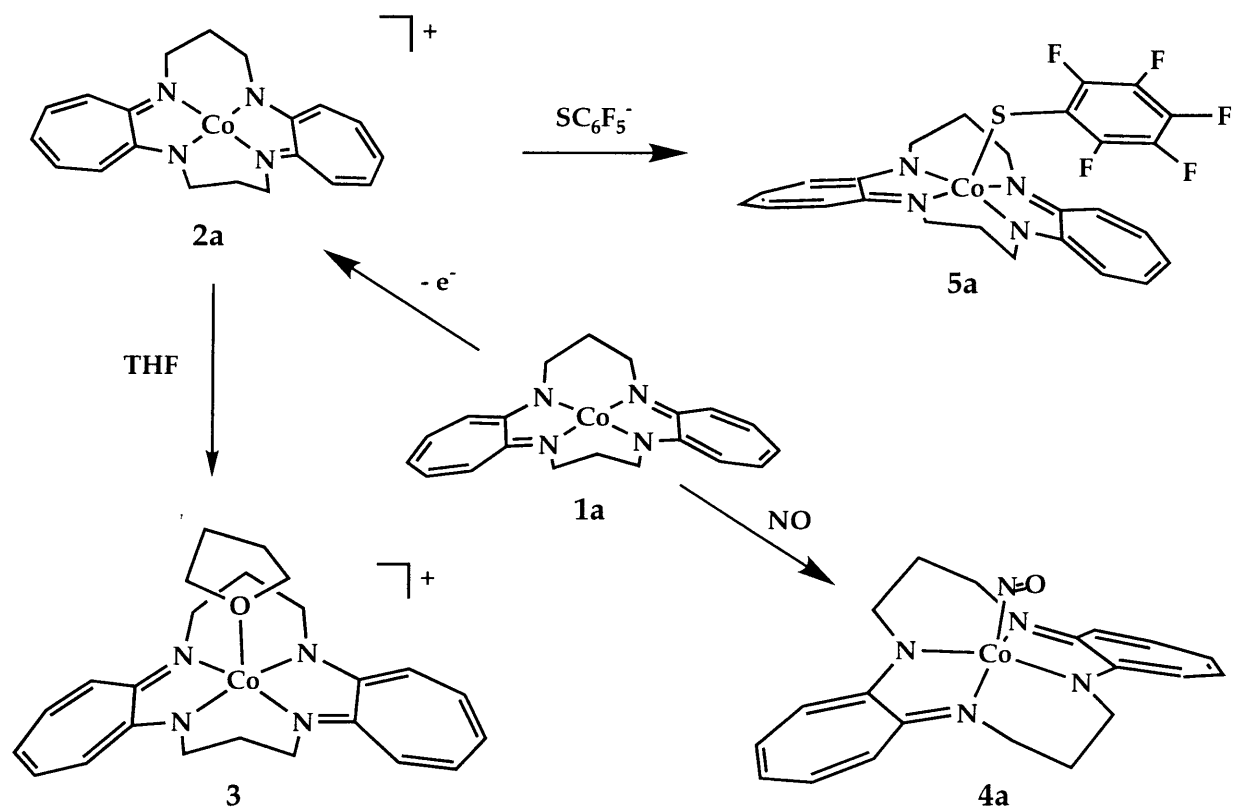
Figure 4.4. Summary of [Co(TC-3,3)] reactivity to form structurally characterized four- and five-coordinate cobalt(III) complexes.
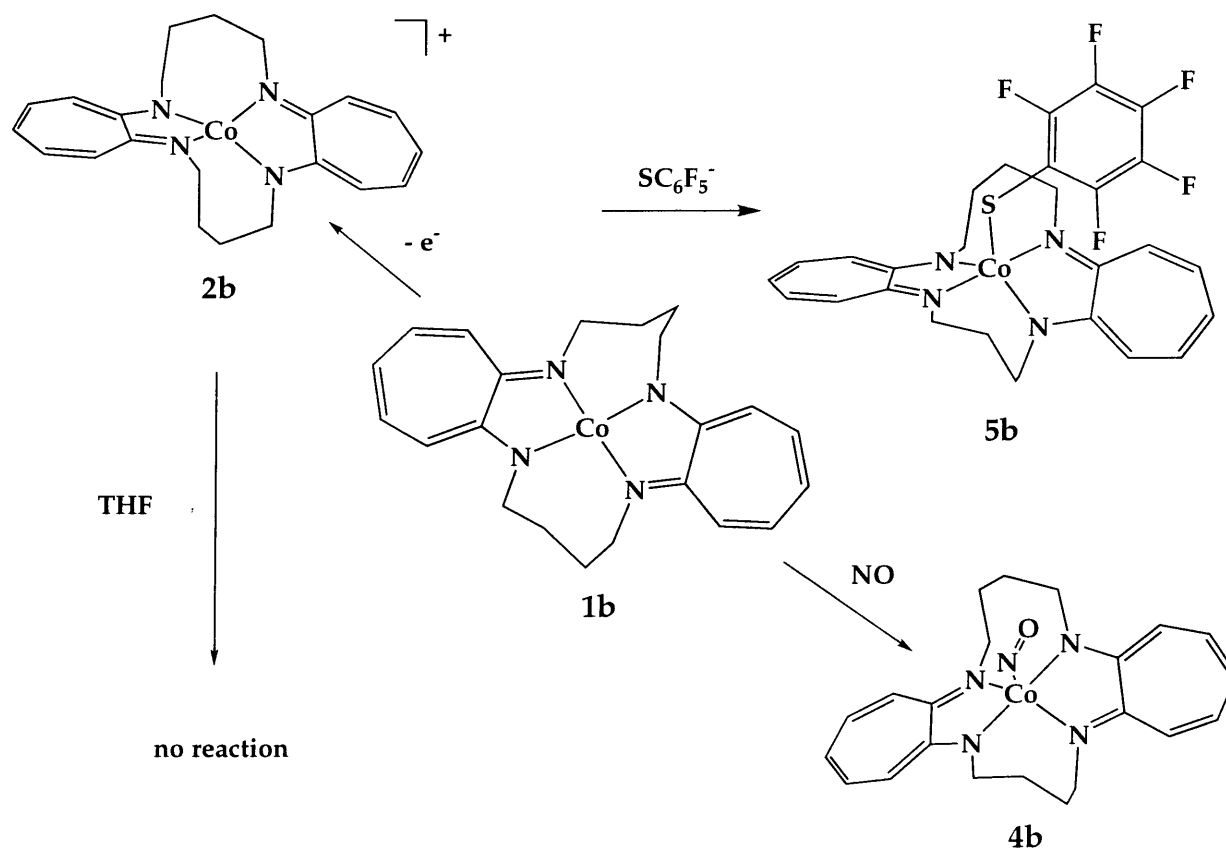
Figure 4.5. Summary of [Co(TC-4,4)] reactivity to form structurally characterized four- and five-coordinate cobalt(III) complexes.
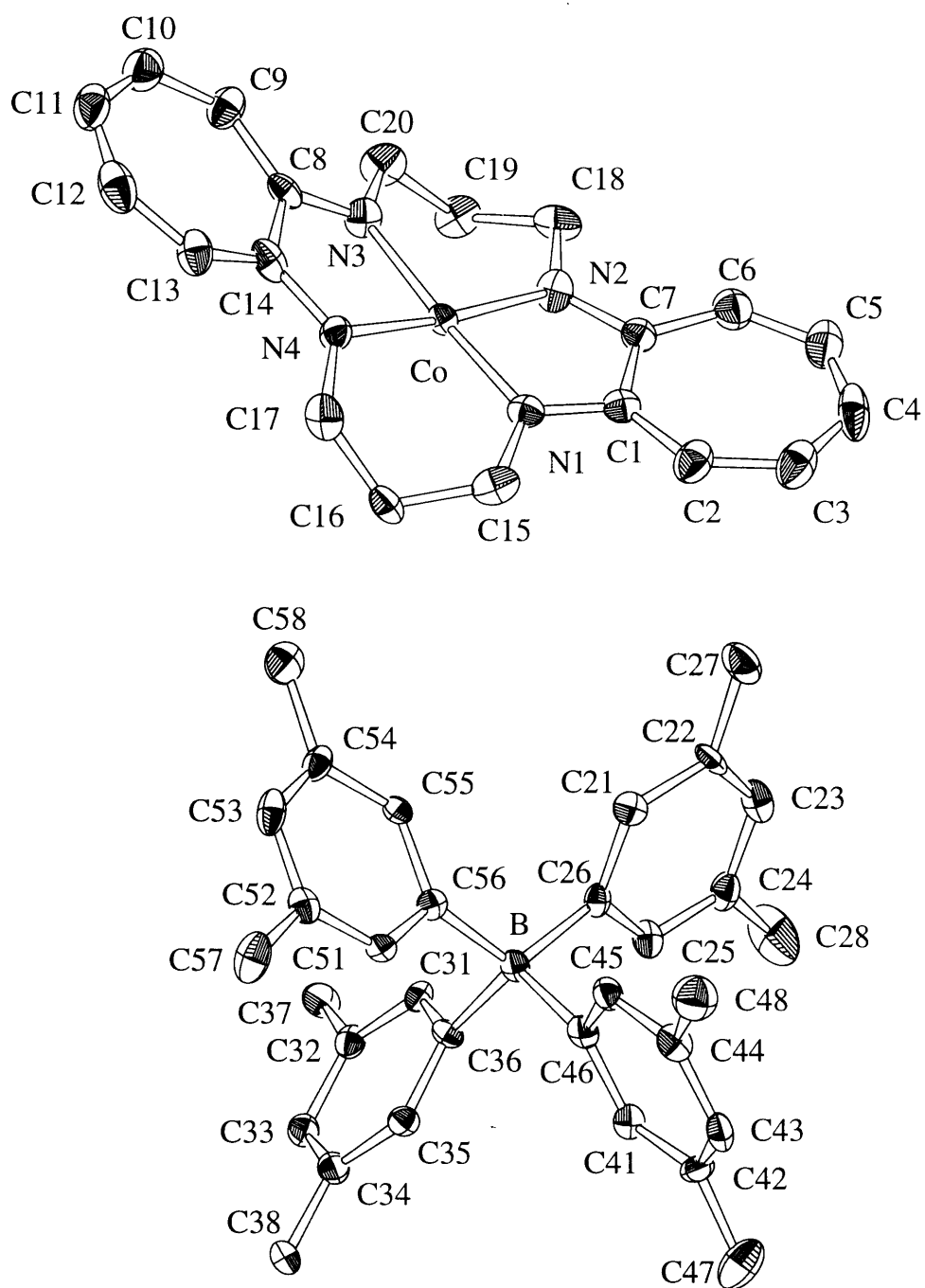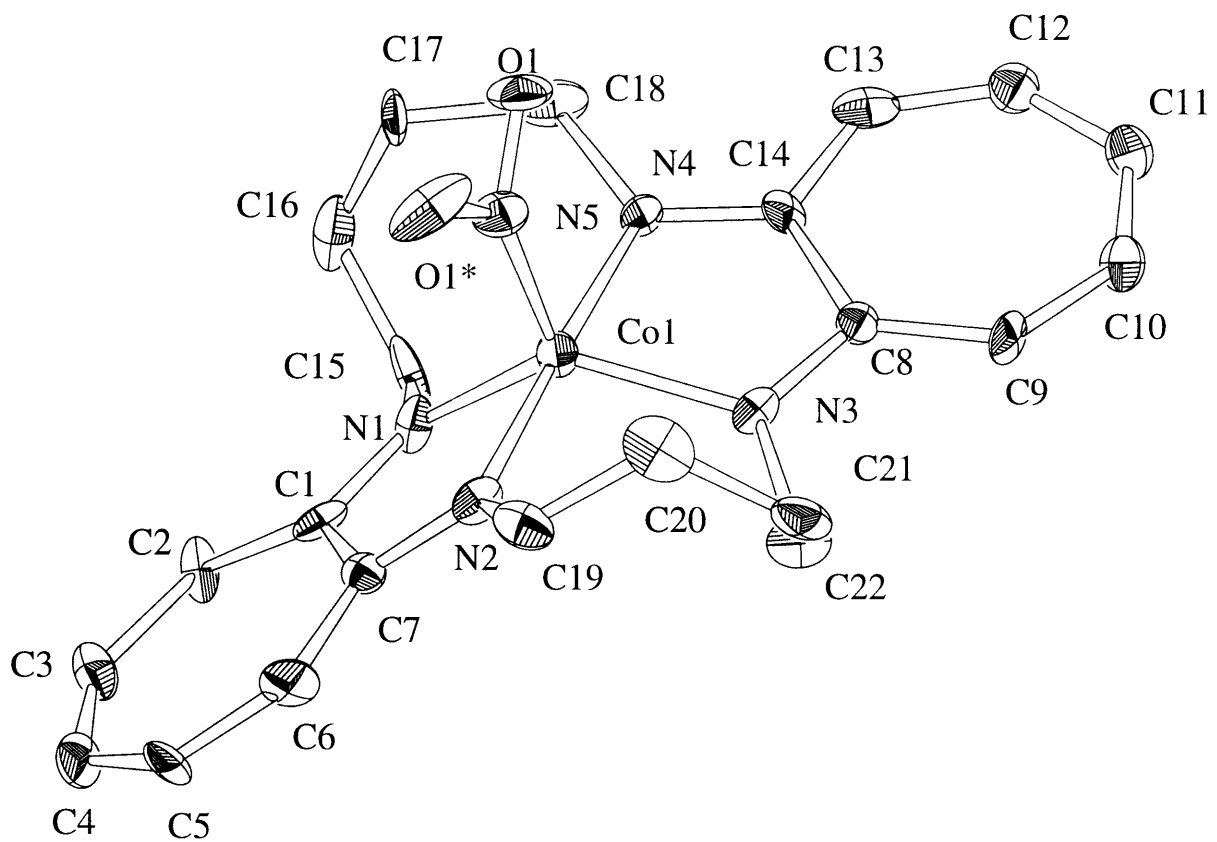
Figure 4.6. ORTEP drawing for [Co(TC-3,3)]BAr′$_4$, **2a′**, showing 40% probability ellipsoids for all non-hydrogen atoms.
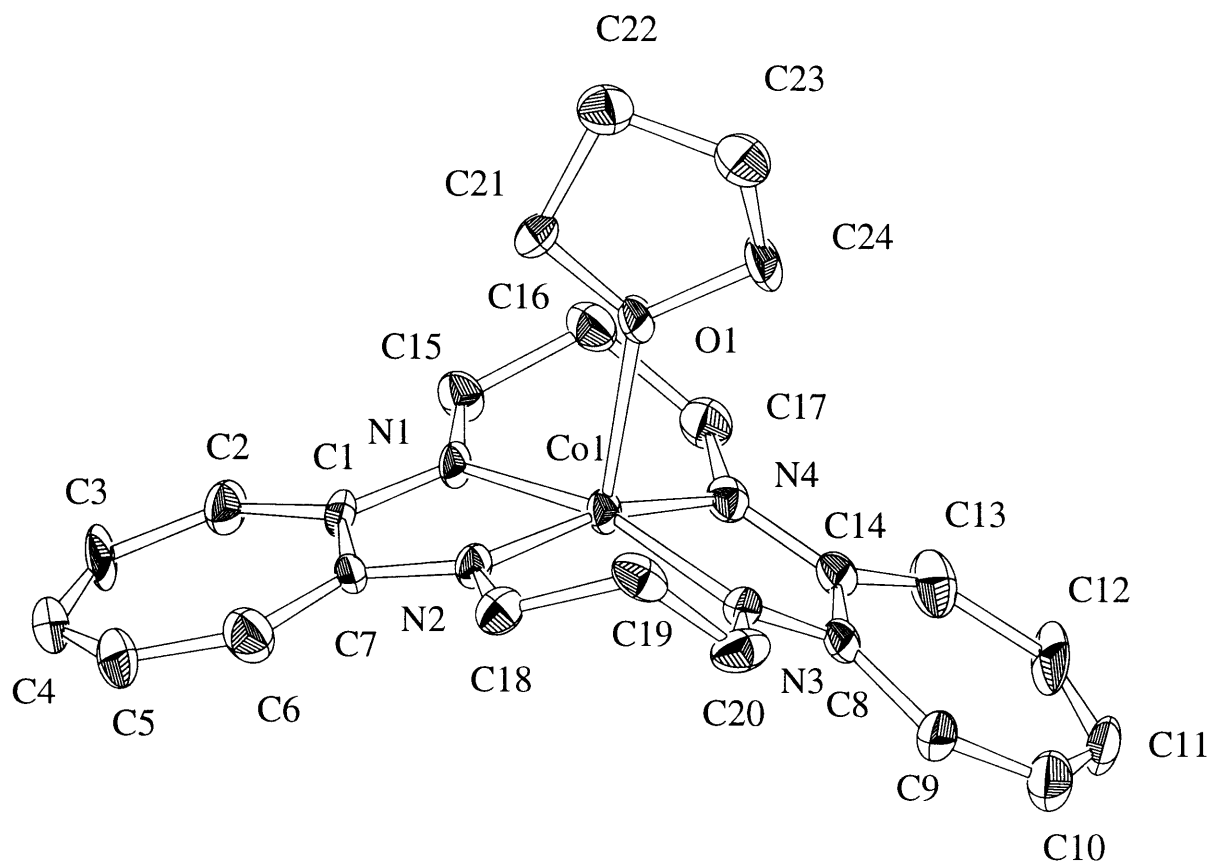
Figure 4.7. ORTEP drawing for [Co(THF)(TC-3,3)]BPh4, **3**, cation showing 40% probability ellipsoids for all non-hydrogen atoms.
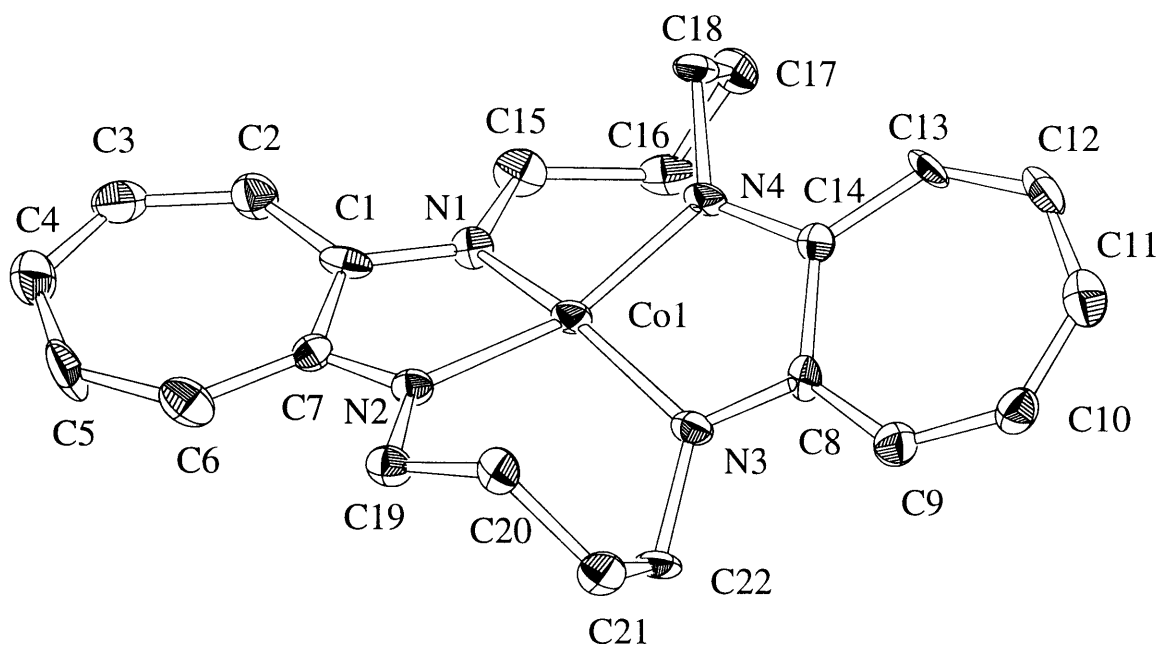
Figure 4.8. ORTEP drawing for [Co(TC-4,4)]BPh4, **2b**, cation showing 40% probability ellipsoids for all non-hydrogen atoms.
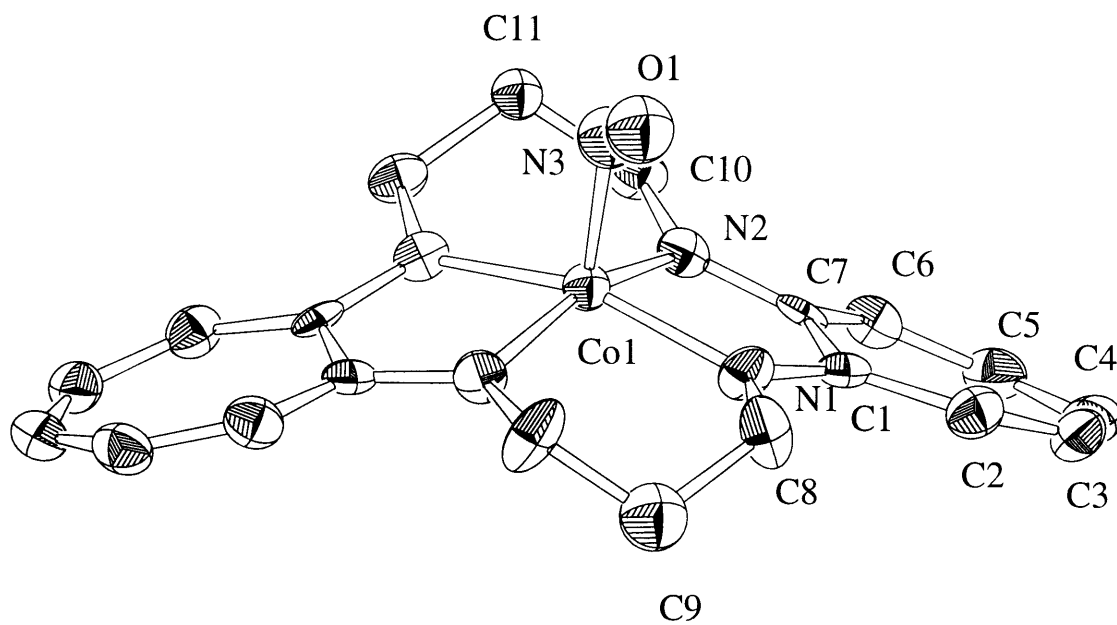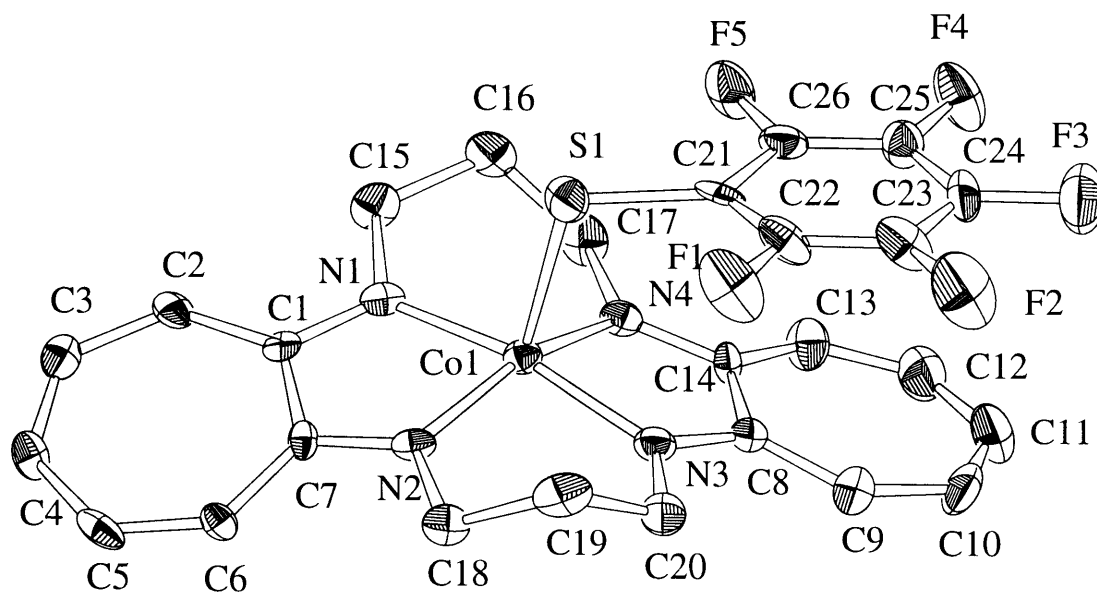
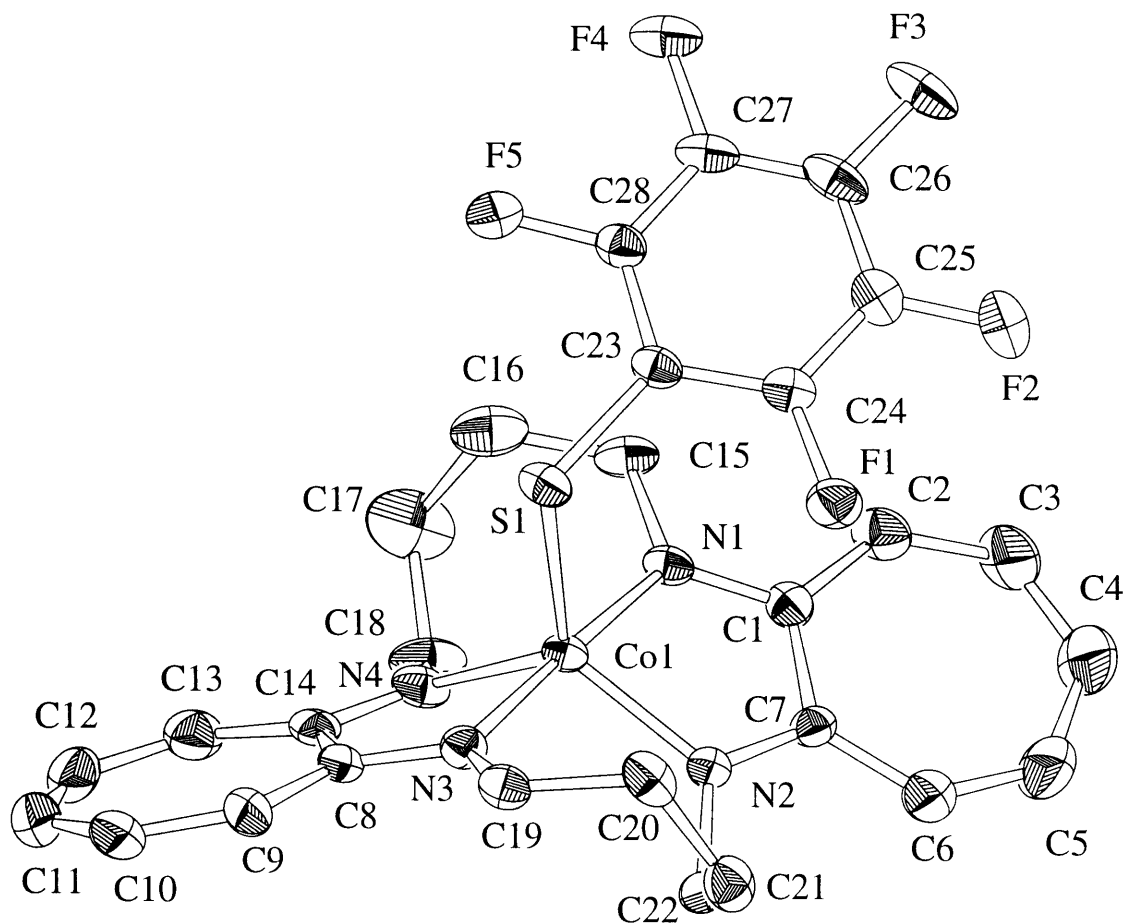**Figure 4.9.** ORTEP drawing for [Co(NO)(TC-3,3)], **4a**, showing 40% probability ellipsoids for all non-hydrogen atoms.

Figure 4.10. ORTEP drawing for [Co(NO)(TC-4,4)], **4b**, showing 40% probability ellipsoids for all non-hydrogen atoms.
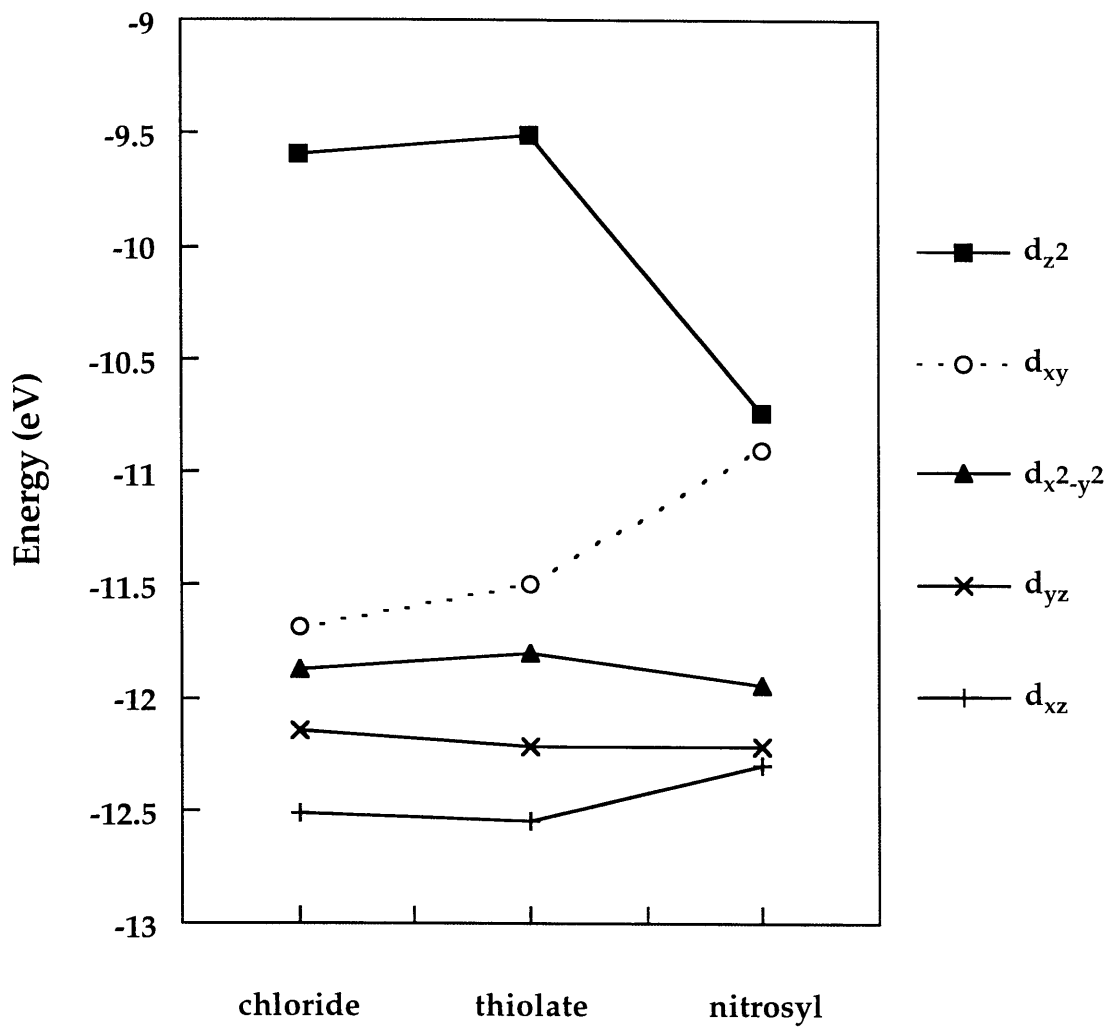
Figure 4.11. ORTEP drawing for [Co(SC5F5)(TC-3,3)], **5a**, showing 40% probability ellipsoids for all non-hydrogen atoms.

Figure 4.12. ORTEP drawing for [Co(SC5F5)(TC-4,4)], **5b**, showing 40% probability ellipsoids for all non-hydrogen atoms.

Figure 4.13. Energies of frontier molecular orbitals for $[CoCl(NH_2)_4]^-$, $[Co(SPh)(NH_2)_4]^-$, and $[Co(NO)(NH_2)_4]^-$ from extended Hückel calculations.
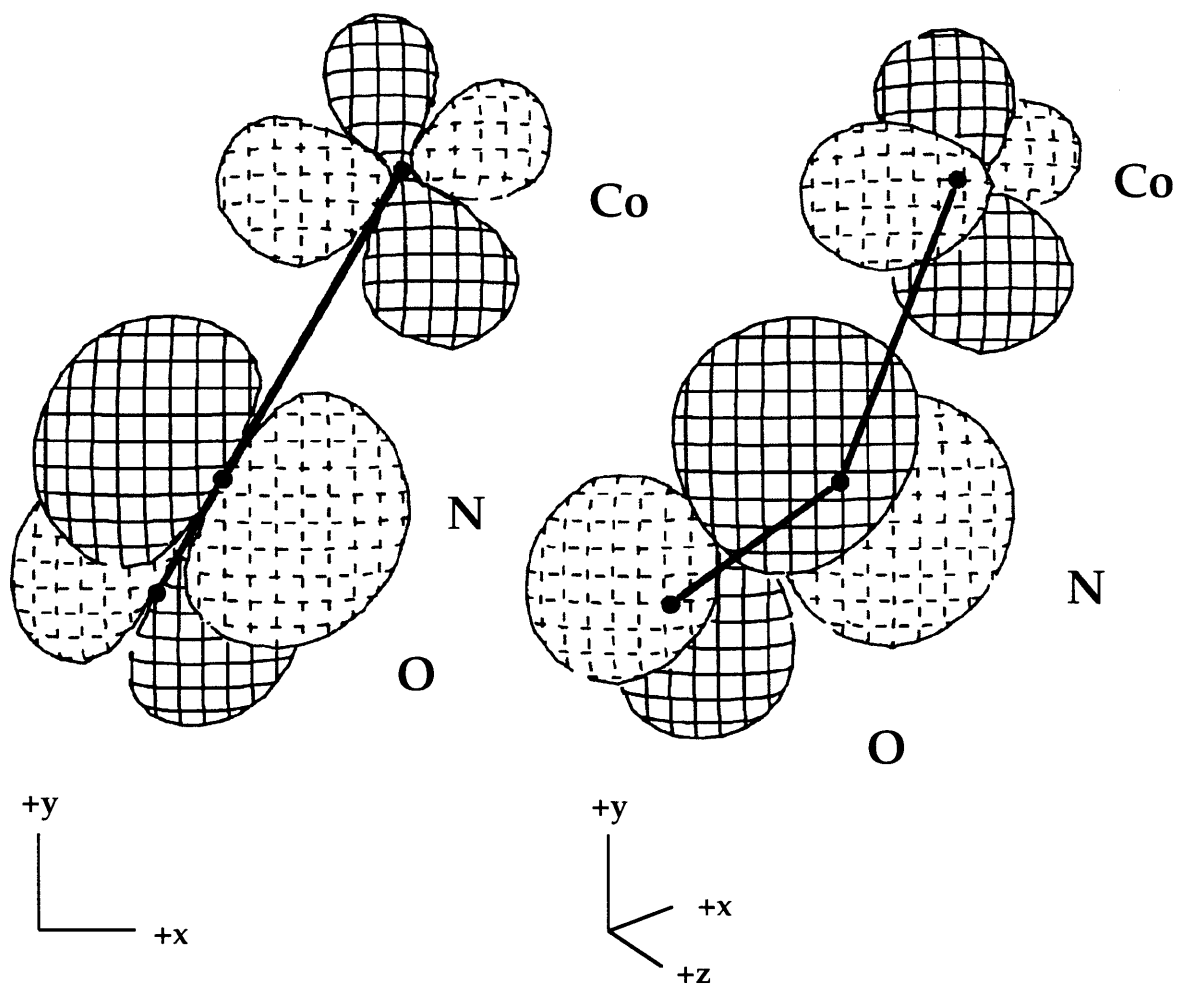
Figure 4.14. Interaction of Co $d_{x^2-y^2}$ orbital with NO π^* orbital in [Co(NO)(TC-4,4)], **4b.**

Biographical Note

The author was born on August 26, 1968 in Ithaca, New York. After residing there for a time and spending several years in Ames, Iowa, her parents settled in Pensacola, Florida, which she considers home. Her teachers in the Escambia County school district encouraged her early and often in all the disciplines, including the sciences. After graduation from Booker T. Washington High School, she majored in chemistry at Cornell University, where she worked in the laboratories of Klaus Theopold and Frank DiSalvo. Following her graduate work at MIT with Steve Lippard, she will be working at Oxford University with Malcolm Green as a NSF/NATO Postdoctoral Fellow.